UNIVERSITY OF ZAGREB

FACULTY OF ELECTRICAL ENGINEERING AND COMPUTING

SVEUČILIŠTE U ZAGREBU

FAKULTET ELEKTROTEHNIKE I RAČUNARSTVA

Nijaz Dizdarević

UNIFIED POWER FLOW CONTROLLER IN ALLEVIATION OF VOLTAGE STABILITY PROBLEM

DOCTORAL THESIS

OBJEDINJENI REGULATOR TOKA SNAGE U IZBJEGAVANJU NESTABILNOSTI NAPONA

DOKTORSKA DISERTACIJA

Zagreb, 2001.

Doctoral dissertation is made in

Department of Power Systems
Faculty of Electrical Engineering and Computing
University of Zagreb
Zagreb, Croatia

and

Department of Electrical Engineering
Electric Power Systems
Royal Institute of Technology
Stockholm, Sweden

Principal Adviser

Professor Sejid Tešnjak, Ph.D.
Department of Power Systems
Faculty of Electrical Engineering and Computing
University of Zagreb
Zagreb, Croatia

Associate Adviser

Prof. Dr. Göran Andersson
Department of Electrical Engineering
Swiss Federal Institute of Technology
Zurich, Switzerland

Doctoral dissertation has … pages

Dissertation no.: …

Doktorska disertacija je izrađena u

Zavodu za visoki napon i energetiku
Fakultet elektrotehnike i računarstva
Sveučilište u Zagrebu
Zagreb, Hrvatska

i

Department of Electrical Engineering
Electric Power Systems
Royal Institute of Technology
Stockholm, Sweden

Mentor

Prof. dr. sc. Sejid Tešnjak, dipl. ing.
Zavod za visoki napon i energetiku
Fakultet elektrotehnike i računarstva
Sveučilište u Zagrebu
Zagreb, Hrvatska

Komentor

Prof. Dr. Göran Andersson
Department of Electrical Engineering
Swiss Federal Institute of Technology
Zurich, Switzerland

Doktorska disertacija ima … stranica

Disertacija br.: …

Members of the committee for evaluation of doctoral dissertation:

1. **Dr.sc. Srđan Babić**
   Associate Professor (retired), FER Zagreb
2. **Dr.sc. Sejid Tešnjak**
   Professor, FER Zagreb
3. **Dr.sc. Göran Andersson**
   Professor, ETH Zürich

Povjerenstvo za ocjenu doktorske disertacije:

1. **Dr.sc. Srđan Babić**
   Izvanredni profesor u mirovini, FER Zagreb
2. **Dr.sc. Sejid Tešnjak**
   Redoviti profesor, FER Zagreb
3. **Dr.sc. Göran Andersson**
   Redoviti profesor, ETH Zürich

Members of the committee for defend of doctoral dissertation:

1. **Dr.sc. Srđan Babić**
   Associate Professor (retired), FER Zagreb
2. **Dr.sc. Sejid Tešnjak**
   Professor, FER Zagreb
3. **Dr.sc. Göran Andersson**
   Professor, ETH Zürich
4. **Dr.sc. Zvonko Benčić**
   Associate Professor, FER Zagreb
5. **Dr.sc. Ljubo Marangunić**
   Associate Professor, FER Zagreb

Povjerenstvo za obranu doktorske disertacije:

1. **Dr.sc. Srđan Babić**
   Izvanredni profesor u mirovini, FER Zagreb
2. **Dr.sc. Sejid Tešnjak**
   Redoviti professor, FER Zagreb
3. **Dr.sc. Göran Andersson**
   Redoviti profesor, ETH Zürich
4. **Dr.sc. Zvonko Benčić**
   Izvanredni professor, FER Zagreb
5. **Dr.sc. Ljubo Marangunić**
   Izvanredni professor, FER Zagreb

Date of defend of doctoral dissertation:
October 12, 2001

Datum obrane doktorske disertacije:
12. listopada 2001. godine

TABLE OF CONTENTS

PREFACE

Alleviation of power system voltage stability by using modern, power electronics based, FACTS device represents main concern of this dissertation. Especially, the Unified Power Flow Controller has been analysed as the FACTS device capable of giving voltage support and/or co-ordinating power flow control action.

The dissertation comes as a result of the research work taken at the Faculty of Electrical Engineering and Computing - University of Zagreb, and at the Department of Electric Power Engineering - Royal Institute of Technology in Stockholm.

Starting in 1991, continuous work on power system steady state and dynamic operation has been conducted at the Faculty of Electrical Engineering and Computing in Zagreb. First under supervision of Professor Srđan Babić during M.S. studies, and then under Professor Sejid Tešnjak during Ph.D. studies, the voltage stability problem has been established as a central issue of the research work. As mentors, both of them largely contributed to appearance of the dissertation and their efforts are thoroughly acknowledged. Many other colleagues are also commended for creating friendly atmosphere at the Department of Power Systems, which helped even in moments when it was not easy to stay calm. The Ministry of Science and Technology of Republic of Croatia have provided financial support to this research. Being essential through the times, it really enabled appearance of this dissertation. Their help is gratefully acknowledged.

From September 1996 to December 1997, the research was carried out at the Royal Institute of Technology in Stockholm. Being a guest PhD student under a guidance of Professor Göran Andersson, I had a privilege to share their highly motivated working atmosphere. Truly acknowledging his trustfulness and support, I gained new experiences by expanding the voltage stability problem with FACTS devices. I also express gratitude to other colleagues who were group members at the time. Stimulating discussions with Dr. Stefan Arnborg, Dr. Mehrdad Ghandhari, Dr. Arnim Herbig, Dr. Denis Lee, and Dr. James Gronquist have certainly helped raising this dissertation. Not to forget the other colleagues for making friendly atmosphere there. Financial support from the Swedish Institute was invaluable and highly appreciated. It enabled my horizons being broadened not only in scientific aspects, but also in numerous sociological ones.

Findings that have come out from the research work at these two institutions are written in this dissertation. The dissertation is divided into ten main Chapters, describing four main parts, namely, introduction, modelling, results, and conclusions. A short description of the Chapters is provided hereafter in order to enable a reader to follow presented material easier.

In Chapter I, introductory guidelines are provided for the voltage stability problem and FACTS devices. Current activities in both fields are noted in an attempt of establishing correlation that has given major motivation for this research. Upon recognition of mutual causalities, the objectives are defined. Sequence of the dissertation is explained along with phases of the thesis elaboration. Main contribution of the dissertation is stated at the end.

Modelling part of the dissertation starts with Chapter II. Multi-machine test system is described with related data given in Appendices. Model of synchronous generator is explained along with excitation system and speed governor - turbine system. Load models are discussed, clearly separating details of the composite load model from the dynamic one with non-linear recovery. The details concerning network modelling are provided at the end.

Chapter III is dedicated to the UPFC. First, general description of the UPFC is given. Then, the UPFC injection model is derived. The control system of the UPFC injection model is proposed. It is capable to support transmission voltage, power flow regulation, series compensation, phase shifting, and damping of electromechanical oscillations. The optimal rating algorithm is addressed. Ways to include the UPFC injection model in load flow procedure are explained.

Upon giving description of the system model and the UPFC model, overall differential and algebraic equations are combined in Chapter IV. First, overall system model is established, and then it is linearised around an operating point. The state and extended Jacobi matrices are defined. So-called the differential-algebraic system model is established.

Modelling part is completed in Chapter V. Sensitivity analysis is introduced to recognise characteristics of the state and extended Jacobi matrices. Based on singular and eigenvalue decompositions, bus, branch and generator participation factors are defined. Parametric and functional sensitivities are derived. Sub-optimal formulation using sensitivities is set either to maximise minimum singular value or to minimise total active power loss in the network.

Numerical results are given within following three chapters. In Chapter VI, results of the UPFC voltage/power flow regulation are described to illustrate capabilities of the UPFC in general steady state operation. Rating powers are first discussed. Then, independent operation of the UPFC shunt and series branch is analysed. At the end, simultaneous three-parameter control of the UPFC injection model is denoted.

In Chapter VII, the UPFC damping control is discussed. The voltage collapse scenarios are based on a slow dynamics response of the system, which is initiated by the three-phase short circuit. Since the disturbance initially induces electromechanical oscillations, possible utilisation of the UPFC in damping control is analysed.

Centrally positioned topic comes out after recognising possible regulating actions of the UPFC. In Chapter VIII, the role of the UPFC in alleviation of the voltage stability problem is explained by using its steady state and dynamic characteristics. The voltage collapse scenarios are analysed from two aspects given by the dynamic load with non-linear recovery, and by the composite one. Critical location and critical operating points are recognised. The UPFC is accordingly situated and initiated to provide adequate support.

In Chapter IX, conclusions are given concerning the voltage stability problem and possible utilisation of the UPFC within established scenarios.

A few directions of future work are provided in Chapter X.

At the end, the dissertation is equipped with appendices, notation, and references that are linked throughout the text. In addition, resume and abstract with keywords are provided in English and Croatian language, according to the rules set by the Faculty of Electrical Engineering and Computing - University of Zagreb.

The material presented in this dissertation is closely related to several technical papers that I have been associated to as an author. Only those papers that are linked, more or less, to the dissertation are listed. Hereafter, list of publications that appeared during this research work is provided in chronological order:

Dizdarević N., Tešnjak S., and Andersson G., "Unified Power Flow Controller in alleviation of voltage stability problem," Project at *Electralis 2001 - International Research to Business Convention for Electricity Professionals: Campus*, Liege, Belgium, March 2001 (in English)

Dizdarević N., "Possible solutions for increasing power transmission capacity by usage of conventional and FACTS controllers," *Round Table of Croatian CIGRE Committee: Voltage conditions in the 400 kV network and stability of Croatian power system*, Cavtat, Croatia, October 2000, pp. 1-23 (in Croatian)

Glavan B., Bakula M., Katić Z., and Dizdarević N., "Analysis of TPP Rijeka dynamic response due to nearby disturbances in the electric power network with aspect on a turbine-generator set protection system," *Proceedings of the 4th International Symposium on Power and Process Plants*, Dubrovnik, Croatia, May 2000, pp. 179-182 (in Croatian)

Dizdarević N., Tešnjak S., and Andersson G., "Power flow regulation by use of UPFC's injection model," *Proceedings of the IEEE Budapest Power Tech '99 Conference*, Budapest, Hungary, August 1999, paper BPT99-367-12 (in English)

Dizdarević N., Tešnjak S., and Andersson G., "Utilising parametric sensitivity of Unified Power Flow Controller during voltage emergency situations," *Proceedings of the 1999 IEEE PES Winter Meeting*, New York, February 1999, pp. 634-639 (in English)

Dizdarević N., Tešnjak S., and Andersson G., "On regulating capabilities of Unified Power Flow Controller during voltage emergency situations," *Proceedings of the 30th North American Power Symposium NAPS'98*, Cleveland, OH, USA, October 1998, pp. 275-282 (in English)

Dizdarević N., Arnborg S., and Andersson G., "Possible alleviation of voltage stability problem by use of Unified Power Flow Controller," *Proceedings of the 32nd Universities Power Engineering Conference UPEC'97*, Manchester, UK, September 1997, pp. 975-978 (in English)

Dizdarević N., Višić I., and Tešnjak S., "Combined dynamic and static approach in voltage collapse analysis," *Proceedings of the 31st Universities Power Engineering Conference UPEC'96*, Iraklio, Crete, Greece, September 1996, pp. 562-565 (in English)

Dizdarević N., Kuterovac Lj., and Tešnjak S., "Stator terms in analysis of synchronous generator air-gap and torsional torques during transmission line three-phase automatic reclosing," *Proceedings of the 31st Universities Power Engineering Conference UPEC'96*, Iraklio, Crete, Greece, September 1996, pp. 180-183 (in English)

Dizdarević N. and Tešnjak S., "A comprehensive approach to dynamic simulation of voltage collapse phenomenon," *Proceedings of the IEEE/KTH Stockholm Power Tech Conference*, Stockholm, Sweden, June 1995, pp. 161-166 (in English)

Dizdarević N. and Tešnjak S., "Contingency selection algorithms in on-line security assessment," *Proceedings of the International Conference on Electrical Engineering ICEE'95*, Taejon, Korea, July 1995, pp. 199-202 (in English)

Babić S. and Dizdarević N., "Load modelling and its effect on power system transient stability studies," *Proceedings of the 2nd Conference of Croatian CIGRE Committee*, Primosten, Croatia, May 1995, pp. 531-538 (in Croatian)

Dizdarević N., Babić S., and Tešnjak S., "Contingency selection algorithms for transmission line overload analysis in on-line security assessment," *Proceedings of the 3rd Electrotechnical and Computer Science Conference ERK'94*, Portorose, Slovenia, September 1994, pp. 307-310 (in English)

Dizdarević N., Babić S., and Tešnjak S., "The influence of excitation system regulation on the transient stability of synchronous generator," *Energija Magazine*, Zagreb, Croatia, no. 42, 1993, pp. 83-88 (in Croatian)

Babić S., Tešnjak S., Dizdarević N., and Glavan B., "Analysis of effects of different synchronous generator excitation systems on transient stability of Istrian electric power system," Proceedings of the 1st Conference of Croatian CIGRE Committee, Zagreb, Croatia, October 1993, pp. 569-578 (in Croatian).

Within the list, some traces of activities in transient stability and load flow contingency analysis are found. They represent basic roots wherefrom this dissertation was originally started. Transient stability is analysed within my B.S. thesis, given as

Dizdarević N., *Transient Stability of Synchronous Generator – A Computer Representation*, B.S. Thesis, University of Zagreb, Faculty of Electrical Engineering and Computing, Dept. Power Systems, Zagreb, Croatia, December 1990.

Load flow contingency analysis is covered in M.S. thesis

Dizdarević N., *Contingency Selection and Analysis Algorithms in Electrical Power Networks*, M.S. Thesis, University of Zagreb, Faculty of Electrical Engineering and Computing, Dept. Power Systems, Zagreb, Croatia, February 1994.

Motivation for choosing power system voltage stability as the research topic of the dissertation came out from combining these two theses. In the B.S. thesis, dynamic model of a single-machine infinite-bus test system is established, whereas in the M.S. thesis steady state load flow computational procedures are covered. Then, the intention for combining generator model with load flows initiated research activities on dynamic simulation of multi-machine test system. Main concern has been found in the voltage stability problem from a dynamic viewpoint. The UPFC has come along.

The primary motivation has been to combine these elements within a common frame, and to provide their comprehensive treatment. Hopefully, it is found in this dissertation.

Zagreb, June 2001

Nijaz Dizdarević

I. INTRODUCTION

I.1 OVERVIEW OF POWER SYSTEM VOLTAGE STABILITY PROBLEM

The voltage stability problem with voltage collapse as its final consequence is an emerging phenomenon in planning and operation of modern power systems. The increase in utilisation of existing power systems may get the system operating closer to voltage stability boundaries making it subject to the risk of voltage collapse. This possibility in association with several incidents throughout the world have given major impetus for analysing the problem with increased interest in modelling of generation, transmission and distribution/load equipment of electric power systems.

Fast advances in computer analysis of power systems have enabled appearance of extensive knowledge related to general power system control and stability. Many general guides [160-161] and books [8, 10, 18, 115, 232, 360, 378-380, 393] cover modelling issues in depth. Some of them directly concern the voltage stability problem [191, 356, 357, 376]. Useful definitions of terms related to stability are provided within several taxonomies [9, 139, 188].

A large number of scientists and engineers have been attracted by the voltage stability problem. Their attention has resulted with a number of papers being published in magazines and conference proceedings. Extensive bibliography [5] treats the most referenced ones among them. Hereafter, the papers that have been used during the research work are overviewed.

Voltage stability phenomena have been comprehensively treated from the early beginnings [23, 70, 72, 198, 386]. Dynamic simulation of power system is recognised as one of the most important tools of its assessment [26, 47, 64, 84, 91, 184, 199, 201, 257, 275, 314, 347, 350, 384]. It enables different studies of co-ordinated control to be carried out [27-28, 34, 66-67, 73, 274, 385, 387, 395].

Load behaviour is recognised as one of the main driving forces of the voltage collapse. Bibliography [157] covers main references, which are related either to modelling techniques [108, 158, 249, 288-290] or to field measurements and identification [24, 87, 130, 176, 399]. Several models of a dynamic load with non-linear recovery are extensively used to denote restorative intention [38-39, 137-138, 140-141, 172, 175, 177, 208, 219, 247, 298, 301-302, 397]. The dynamic load represents a composite load as it is seen from a high-voltage network bus. Usually, response of this composite load is dominated by a behaviour of an LTC transformer [46, 76, 277, 296, 332, 402, 408], an induction motor load [37, 44, 173, 297, 318, 383, 400, 403], and thermostatically controlled load [36, 191, 356-357].

The other important driving force is related to a limited reactive power production of synchronous generators [280-282, 291, 322]. Constraints are mostly imposed by a rotor thermal stress [169-170, 200]. Over-excitation limiters are modelled in order to enable a decrease of generator excitation voltage [2, 113, 122-123, 156, 191, 253-254].

For computational purposes, combined static and dynamic power system model is established to provide a basis for a voltage security assessment [82, 211, 286-287, 306, 329-331]. Many different types of predictive indices come out from the combined model. Majority of them has a theoretical background, while just a few are practically applied [53, 83, 93, 119-121, 180, 213, 334, 346, 349, 382]. Some comparisons exist as well [45, 56]. Lately, as a de-regulated market sets the rules in the field, computations of the maximum loading point, available transfer capacity, different security margins and distances appear as a basis for indices [49-51, 81, 92, 147, 182, 203, 342, 377]. Indices based on eigenvalue analysis [105-106, 187, 189, 216, 220, 233, 258, 295, 359, 392], and singular value analysis [192-197, 210, 230, 338, 361-363] do not only predict severity of the problem, but open a way toward a general sensitivity analysis. Methods aimed for sensitivity analysis of power system are established [98-99, 116, 276, 407]. A small-disturbance impact to the combined model results with a sensitivity of an operating point during time domain trajectory [317, 368-375]. Sensitivities are also evaluated with respect to transfer margin and contingencies, or in control purposes [25, 30-31, 231]. Several other computational issues are raised from the combined model. Convergence at the limits, singularity and bifurcation points are just a few to be named [1, 4, 6, 20, 35, 42, 86, 102, 285, 321, 381].

Computational procedures find the applications either within various planning stages of voltage stability endangered power system [61, 162, 164, 250-251, 398], or within development phases of different countermeasures [65, 97, 155, 190, 259, 353, 355, 358]. Several protection schemes are developed and implemented [40, 60, 68, 163, 167, 248]. Undervoltage load shedding is considered as the most affordable solution for the problem with a low level of occurrence probability and a high level of consequences [13-17, 351, 354].

Future trends in the field are certainly dominated by de-regulated market conditions and transmission system open access [32, 166, 202, 320]. A challenge also appears within operating grid issues related to a new FACTS technology.

I.2 OVERVIEW OF FACTS DEVICES

Since the rapid development of power electronics has made it possible to design power electronic equipment of high rating for high voltage systems, the voltage stability problem resulting from transmission system may be, at least partly, improved by use of the equipment well-known as FACTS-controllers. A number of papers treats development status of this technology from the early years up to date [88, 90, 142-146, 209, 333, 343-344, 405]. So far, only one book thoroughly covers component and system wise aspects of the FACTS technology [145]. The de-regulation (restructuring) of power networks will probably imply new loading conditions and new power flow situations. Lately, some concerns are raised as to show FACTS capabilities in open access environment [57, 148, 320, 406]. This is certainly an additional reason to face the FACTS.

Analysis of a power system with embedded FACTS-controllers calls for development of adequate models [41, 75, 85, 154, 236]. Models largely depend on a type of the analysis, which is generally either component or system orientated. In the component orientated analysis, individual physical elements of a FACTS-controller are concerned. On the other side, the system orientated analysis needs answers on achievements that could be possibly gained by using a FACTS-controller. This research work is solely concerned with system wise aspects of the FACTS technology. In general form, system wise aspects are related either to the improvements of security and economics [19, 69, 112, 117, 255, 264, 300, 352], or to the enhancements of transmission network capability [71, 77, 212, 214, 245, 279, 294]. Mostly, the analysis is dominantly concentrated either on a power flow regulation [29, 62, 89, 103-104, 107, 114, 132, 134-136, 218, 227, 234, 262-263, 266-267, 299, 310-311, 401], or on a damping method of electromechanical oscillations [48, 52, 63, 74, 94, 109-111, 118, 265, 268-273, 303, 389].

As a modern FACTS-controller capable for providing simultaneous voltage support and co-ordinated control action, the Unified Power Flow Controller is chosen. Conceptual solution at an idea level is first established [124-129, 325], and then followed by its, one and the only, physical application in a real power system [237-238, 304-305, 312-313, 328]. In addition to this installation, several real time laboratory models are developed [79-80, 168, 204, 252]. Several other utilities have application plans [95, 159, 305]

The Unified Power Flow Controller is composed of two mutually coupled branches, shunt and series one. There is a large experience in the field related to the individual applications either of the shunt branch [3, 21, 58, 152, 183, 207, 217, 235, 323-324, 327, 335, 348, 404], or of the series one [55, 133, 179, 205-206, 240, 242-243, 283, 307-308, 345, 366, 394]. Being adequately coupled, they form a new device, which needs a new computer model as well. Several different models are developed depending on whether the analysis is component or system wise [11-12, 59, 100-101, 178, 181, 186, 224, 228, 241, 256, 284, 309, 336, 339, 367, 391]. Models enable simulation of various case studies [33, 150-151, 215, 226, 229, 261, 292, 316, 325-326, 340-341, 364, 396]. Again, the system wise analysis is dominantly related either to a load flow control [7, 174, 225, 244], or to an oscillation damping method [149, 185, 221-222, 239, 246, 337, 388, 390].

In order to deal with the voltage stability problem, the solutions with FACTS-controllers must provide voltage support and/or appropriately co-ordinated control actions. Apart from several larger rating prototypes of Static Var Generator as an improved version of Static Var Compensator [22, 43, 96, 131, 365], no other modern FACTS-controller application has been considered to help solve the voltage stability problem. The Unified Power Flow Controller is considered to be a new impetus.

I.3 OBJECTIVES OF THE DISSERTATION

The thesis goal is defined as to show how it is possible to alleviate the voltage stability problem by using the Unified Power Flow Controller (UPFC), modern power electronics based FACTS device. The UPFC in its general form can provide simultaneous, real-time control of all basic power system parameters (transmission voltage, impedance and phase angle), and dynamic compensation of ac system.

Besides satisfying conditions set by power flow regulation and damping of electromechanical oscillations, it also provides voltage support to the system, and helps voltage unstable situations being solved.

Therefore, a work on this dissertation has been launched aiming to fulfil following general objectives:

- Set a comprehensive explanation of voltage stability problem and mechanism of voltage collapse in a multi-machine power system,
- Develop analytical methods useful in the problem solving by early recognition of impending voltage collapse within combined dynamic and static approach, and
- Develop preventative measures and actions using adequate FACTS-controllers (especially Unified Power Flow Controller, UPFC) to alleviate the problem and increase transmission throughput.

I.4 SEQUENCE OF THE DISSERTATION

In the elaboration of the thesis, a research work on computer analysis of power system stability has been carried out. In order to analyse dynamic phenomena, a FORTRAN computer program for mid-term time domain simulation of multi-machine power system is developed, combining dynamic and static aspects of analysis. It is primarily focused on off-line simulation of voltage emergency situations using differential-algebraic model of power system. Besides, parallel work on more complex multi-machine model of practical power system appeared using commercially available software that helped having own in-house developed program tested and verified. Eventually, the program could be installed in a control centre serving for voltage security evaluation of a power system.

There have been several phases in the elaboration.

In the first phase, the computer program for time domain simulation has been made. It has featured different generator models with generic excitation and speed governor - turbine control systems, models of static and dynamic loads, induction motors, LTCs, transmission lines and buses... Computational methods that have been included comprised fast de-coupled transient load flow along with Gauss-Seidel and Jacobi load flows, sparse matrix techniques, and 4^{th}-order Runge-Kutta method of solving differential equations by using constant step-size integration.

In the second phase, the static aspects of the linearised differential-algebraic power system model have been included and applied at snap-shots along time domain system trajectory. Concerned properties of the state and extended Jacobi matrices are useful in general stability analysis (singular and eigenvalue decomposition, sensitivity analysis, and participation factors). While the static aspects are very helpful in recognition of the voltage stability problem, modern means of voltage support are sought for should they be applied thereafter.

Thus, the third phase of the elaboration has been initiated turning out the need for FACTS device modelling. The UPFC injection model has been established along with appropriate control system. While the static aspects help the voltage stability problem being recognised through the matrix decompositions, the UPFC, heart and soul of the dissertation, represents a source of voltage support and power flow control.

Afterwards, the UPFC has been studied concerning its capability to help the voltage stability problem solved. Combined dynamic and static approach is used to analyse the control system of the UPFC injection model. The injection model enables three parameters to be simultaneously controlled, namely the shunt reactive power, Q_{conv1}, and the magnitude, r, and angle, γ, of the injected series voltage. It fulfils functions of reactive shunt compensation, voltage regulation, line power flow regulation, series compensation, PAR/QBT phase shifting, and damping of electromechanical oscillations meeting multiple control objectives.

I.5 CONTRIBUTION OF THE DISSERTATION

Benefits of the proposed methodology are explored by analysing a multi-machine test system using in-house developed computer program. According to the established general objectives, it is possible to point out the main contribution and achievements of the dissertation as it follows:

- Development of differential-algebraic model of multi-machine power system useful in time-domain simulation with combined dynamic and static elements of analysis in order to study dynamic phenomena of mid-term transient periods of decreased voltage security level,

- Development of the UPFC injection model with adequate control system in order to define the role of the device and its regulation capabilities useful in voltage stability problem, as well as to define methodology of rating, locating and timing of the UPFC action with simultaneous three-parameter control, and

- Development of methodology aimed to recognise critical points of power system operation using matrix decompositions and functions characteristic for appearance and evolution of voltage stability problem, as well as to compute their sensitivities with respect to the load parameters and the UPFC set of control parameters.

II. SYSTEM MODELLING

II.1 MULTI-MACHINE TEST SYSTEM

The benefits of the UPFC and its injection model with several types of control strategies contributing to alleviation of the voltage stability problem are explored by analysing simple 6-machine, 400 kV 20(22)-bus test system (Fig. II.1). It is inspired by the one often used in CIGRÉ reports [62]. It has 20 buses when the UPFC is not included and 22 buses when it is included in the system. Additional 4 buses are introduced when two composite loads are modelled. Data are given in Appendices.

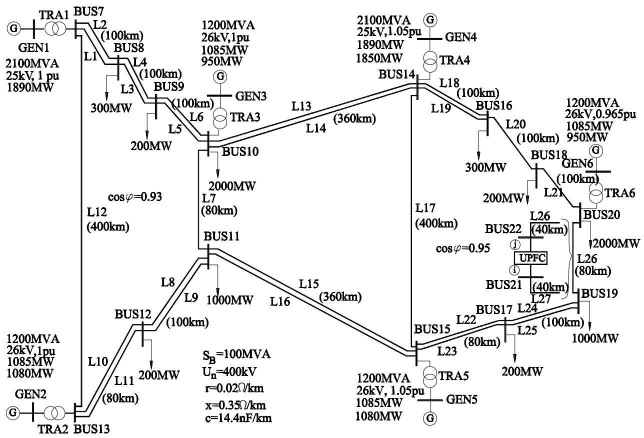

Fig. II.1. Multi-machine test system

The system is comprised of two main areas (left and right-hand one). Six generators are located in the system being divided equally in two main areas. The loads are located in both of them. They are of two types, the static ZIP type or the dynamic one. Dynamic load model is either a composite or a non-linear recovery one. Static parts of the loads are constant current in active power and constant impedance in reactive one. The UPFC is located in the middle of the line 26, which initially connects buses 19 and 20 with dynamic load models applied. During voltage collapse scenarios these loads are shown to have the largest contribution to instability due to their dynamics. Following simple logic, the UPFC is located nearby these loads to help voltage stability problem solved. Furthermore, the UPFC is used to control power flows in steady state as well. The task is considered to be typical in removing a constraint that limits possible power transfer.

II.2 GENERATOR MODELLING

Dynamics of synchronous generator is represented by appropriate transient model [10, 160]. It is estimated that sub-transient phenomena do not have larger impact on a voltage collapse scenario. Thus, the transient effects are accounted for, while the sub-transient ones are neglected. In order to be included in the load flow computational procedure, it is necessary to introduce generator internal bus (Fig. II.2), with the voltage vector $\overline{E'_i}$ behind the admittance *1/(r+jx'_d)*, where *r* denotes stator resistance, and x'_d d-axis transient reactance.

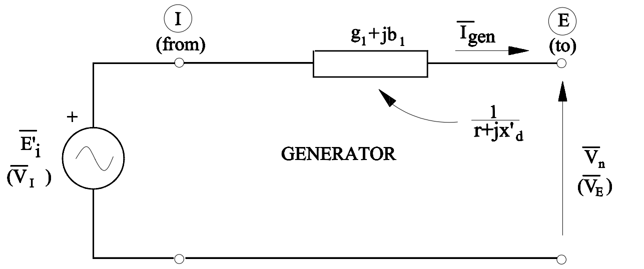

Fig. II.2 Generator model in load flow computations

The vector diagram of the generator model reveals a need for a correction of internal voltage at the I-bus due to pole saliency (Fig. II.3). Whenever there is a difference in d and q-axis transient reactances, the voltage $\overline{E'_i}$ should be eventually corrected with the term $\left(x'_q - x'_d\right) I_q^{gen}$, resulting with the voltage $\overline{E'}_{gen}$.

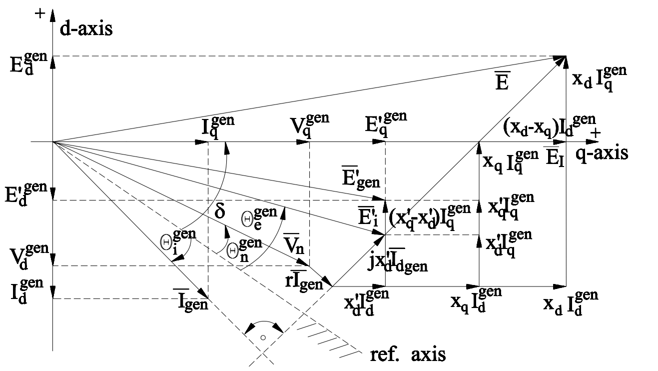

Fig. II.3 Vector diagram of generator model

After decomposition of the voltage $\overline{E'}_{gen}$ into d and q-axis components, differential equations are written for its variables E'_d and E'_q, belonging to the two-axis transient E'-model of synchronous generator. If superscript ^{gen} is omitted due to simplification, the d-q decomposition of the key variables is given as $\overline{V}_n = V_d + jV_q$, $\overline{E'}_{gen} = E'_d + jE'_q$, and $\overline{I}_{gen} = I_d + jI_q$.

Since the stator voltage equations in this model are the algebraic ones, the differential equations describing dynamics of synchronous generator are given as

$$\frac{d\delta}{dt} = \omega - 1, \tag{II.1}$$

$$\frac{d\omega}{dt} = \frac{T_m}{\tau_j} - \frac{E'_d I_d + E'_q I_q - (x'_q - x'_d) I_d I_q}{\tau_j} - \frac{D(\omega - 1)}{\tau_j}, \tag{II.2}$$

$$\frac{dE'_q}{dt} = \frac{E_{FD} - E_I}{\tau'_{d0}} = \frac{E_{FD} - E'_q + (x_d - x'_d) I_d}{\tau'_{d0}}, \tag{II.3}$$

$$\frac{dE'_d}{dt} = -\frac{E'_d + (x_q - x'_q) I_q}{\tau'_{q0}}, \tag{II.4}$$

where δ denotes angle between referent and q-axis, ω rotor speed, E'_d and E'_q d and q-axis components of the voltage $\overline{E}'_{gen}$, T_m mechanical torque, I_d and I_q d and q-axis components of the generator current $\overline{I}_{gen}$, D damping coefficient, τ_j constant proportional to the generator inertia, τ'_{d0} and τ'_{q0} transient time constants of open circuits in d and q-axis, E_{FD} excitation voltage, and E_I q-axis component of induced voltage $\overline{E}$.

The algebraic equations that describe generator voltage relations are given as

$$E'_d - V_d - rI_d - x'_d I_q - \left(x'_q - x'_d\right) I_q = 0\,, \tag{II.5}$$

$$E'_q - V_q - rI_q + x'_d I_d = 0\,, \tag{II.6}$$

$$V_d - V_n \sin(\Theta_n - \delta) = 0\,, \tag{II.7}$$

$$V_q - V_n \cos(\Theta_n - \delta) = 0\,, \tag{II.8}$$

where V_d and V_q denote d and q-axis components of the terminal voltage $\overline{V}_n$ with magnitude V_n and angle Θ_n.

Concerning control systems, the generators are equipped with an excitation system (1 state variable) including over-excitation limiter (OEL, 1 state variable), and a speed governor - turbine system (4 state variables).

The excitation system [10, 161, 191] is modelled in a very simplified way (Fig. II.4).

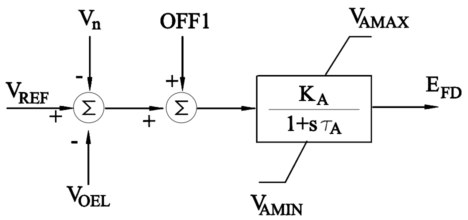

Fig. II.4 Model of excitation system

Only one differential equation describes corresponding dynamics of the model

$$\frac{dE_{FD}}{dt} = \frac{K_A(V_{REF} - V_n - V_{OEL} + OFF1) - E_{FD}}{\tau_A}\,, \tag{II.9}$$

where E_{FD} denotes excitation voltage as state variable, K_A and τ_A gain and time constant of the linear regulator limited by maximum, V_{AMAX}, and minimum, V_{AMIN}, values, V_{REF} referent voltage set-point, V_n magnitude of generator terminal voltage, V_{OEL} output voltage from the OEL, and *OFF1* offset value that allows initial values of voltages V_{REF} and V_n to be equalised.

In voltage stability analysis of the systems where the problem except from transmission part arises also from the generator regulation circuits, it is necessary to include the over-excitation limiter (OEL) [2, 113, 122-123, 156, 253-254] in the model (Fig. II.5).

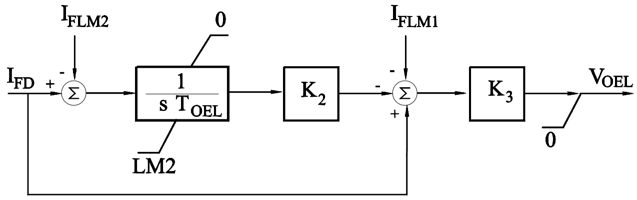

Fig. II.5 Model of over-excitation limiter

In a simple form, the OEL differential equation is given as

$$\frac{dV_{OEL}}{dt} = \frac{(I_{FD} - I_{FLM2})K_2 K_3}{T_{OEL}}\,, \tag{II.10}$$

where V_{OEL} denotes output voltage from the OEL, I_{FD} excitation current, I_{FLM2} continuos operation limit of the excitation current, K_2 and K_3 gains, and T_{OEL} time constant.

The algebraic equation belonging to the OEL is given as

$$E'_q - \left(x_d - x'_d\right) I_d - I_{FD} = 0\,, \tag{II.11}$$

where x_d denotes d-axis synchronous reactance.

By approximate reasoning, the maximum allowable excitation current in continuous operation, I_{FLM2}, could be defined according to the operating diagrams of generator with a round rotor (Fig. II.6), and a rotor with salient poles (Fig. II.7).

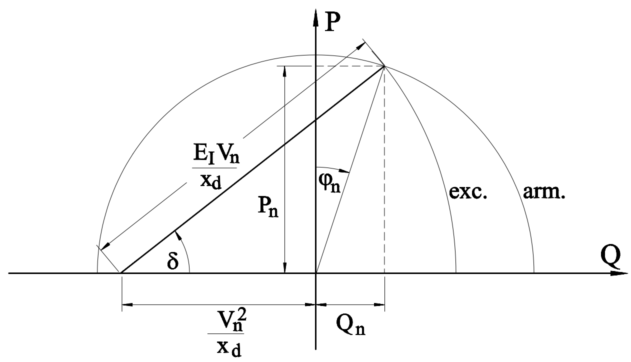

Fig. II.6 Operating diagram of a generator with round rotor

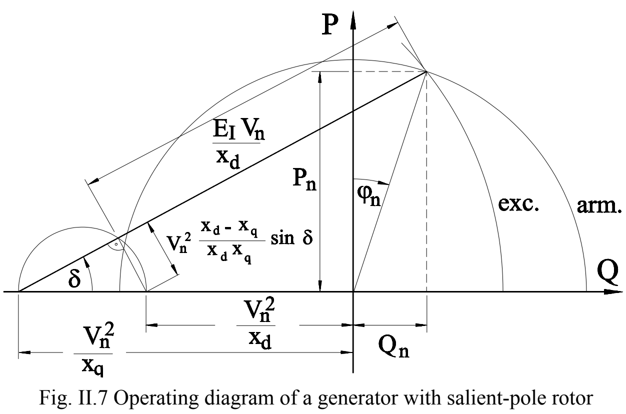

Fig. II.7 Operating diagram of a generator with salient-pole rotor

The q-axis component, $\overline{E}_I$, of the induced voltage $\overline{E}$ is set to be equal to the maximum value I_{FLM2} due to initial steady state conditions of the model.

For the generator with a round rotor, the E_I is defined as

$$E_I = \frac{x_d}{V_n}\sqrt{P_n^2 + \left(Q_n + \frac{V_n^2}{x_d}\right)^2}\ , \tag{II.12}$$

where P_n and Q_n denote nominal active and reactive power.

For the generator with salient poles, the E_I is

$$E_I = \frac{x_d}{V_n}\left[\frac{P_n}{\sin\delta_n} - V_n^2\left(\frac{x_d - x_q}{x_d x_q}\right)\cos\delta_n\right]. \tag{II.13}$$

The angle δ_n in (II.13) is computed as

$$\delta_n = arc\,tg\,\frac{P_n}{Q_n + \frac{V_n^2}{x_q}}\ . \tag{II.14}$$

The speed governor - turbine system [10, 191] is represented according to its general model (Fig. II.8).

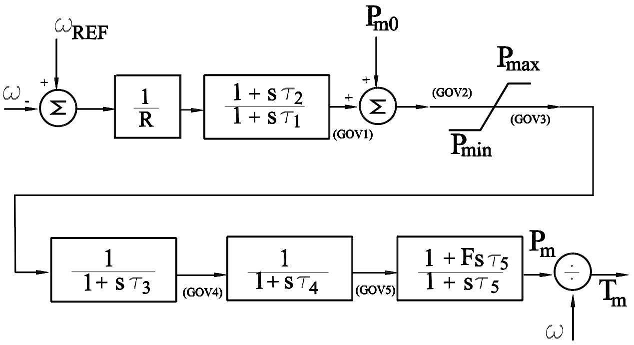

Fig. II.8 Model of speed governor - turbine system

There are four differential equations describing the model

$$\begin{aligned}\frac{dGOV1}{dt} &= \frac{\omega_{REF} - \omega}{\tau_1 R} - \frac{GOV1}{\tau_1} - \frac{\tau_2}{\tau_1 R \tau_j}T_m + \\ &+ \frac{\tau_2}{\tau_1 R \tau_j}\left[E_d^{'} I_d + E_q^{'} I_q - (x_q^{'} - x_d^{'})I_d I_q\right] + \\ &+ \frac{\tau_2 D}{\tau_1 R \tau_j}(\omega - 1)\end{aligned} \tag{II.15}$$

$$\frac{dGOV4}{dt} = \frac{GOV3 - GOV4}{\tau_3} = \frac{P_{m0} + GOV1 - GOV4}{\tau_3}\ , \tag{II.16}$$

$$\frac{dGOV5}{dt} = \frac{GOV4 - GOV5}{\tau_4}\ , \tag{II.17}$$

$$\begin{aligned}\frac{dT_m}{dt} &= \frac{GOV5}{\omega\tau_5} - \frac{T_m}{\tau_5} + \frac{F}{\tau_4}\frac{GOV4 - GOV5}{\omega} - \frac{T_m^2}{\omega\tau_j} + \\ &+ \frac{T_m}{\omega\tau_j}\left[E_d^{'} I_d + E_q^{'} I_q - \left(x_q^{'} - x_d^{'}\right)I_d I_q\right] + \\ &+ \frac{T_m D}{\tau_j}\left(1 - \frac{1}{\omega}\right)\end{aligned}\ , \tag{II.18}$$

where *GOV1*, *GOV4*, *GOV5*, and T_m denote state variables, P_{m0} and ω_{REF} referent power and rotor speed set-points, R droop, P_{MAX} and P_{MIN} power limits, τ_1 to τ_5 time constants, and F constant determining aggregate type (hydro/turbo).

II.3 LOAD MODELLING

The loads are often considered to be driving forces of the voltage stability problem. Therefore, special attention should be paid to load modelling considering its contribution to a voltage collapse scenario. After being shortly disturbed, e.g. with three-phase short circuit cleared by line outage, permanently decreased voltage magnitude level appears in the system as a consequence. By mid-term recovery process of re-establishing initial power consumption, the loads bring generators under over-excitation limiting conditions and/or cause transmission system being incapable of requested power delivery.

In order to compare a level of their contribution to the voltage collapse scenario, two different types of dynamic load model are used:

- Composite load model, and
- Dynamic load model with non-linear recovery.

II.3.A Composite load model

Looking from a high-voltage side (HV bus), there is an LTC transformer as the first element in composite load model (Fig. II.9). Tap changer is located at the HV primary side controlling the voltage magnitude of the secondary low-voltage side (LV bus). Reactive power compensation is provided at the LV bus by a fixed shunt capacitor bank (SHUNT CAP). Equivalent impedance of a distribution feeder, Z_{eq}, is located between the LV bus and a load one (LOAD bus). The LOAD bus has induction motor load (IM), thermostatically controlled load (TCL), and static load (SL) connected on itself [191, 356-357].

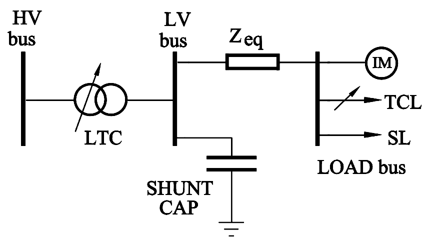

Fig. II.9 Composite load model

LTC transformer

As a starting point in LTC transformer modelling [46, 76, 277, 296, 332, 402, 408], standard π model is used (Fig. II.10). That model contains an ideal transformer with a tap ratio, t_r, and an admittance π scheme. The tap ratio could be constant or changeable. Admittance $\overline{y}_T$ depends on a short circuit voltage, u_k, whereas admittance $\overline{y}_0$ is function of a no-load current i_0. Admittance scheme is placed at the opposite side of the one with voltage regulation.

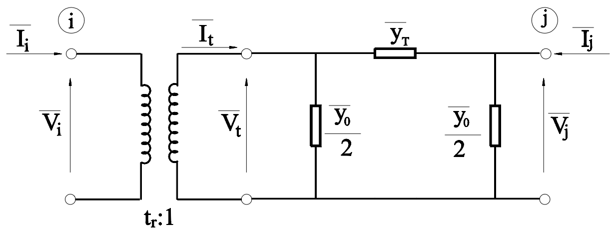

Fig. II.10 Transformer model

Starting with the expression for the tap ratio t_r

$$t_r = \frac{V_i}{V_t} = \frac{I_t}{I_i}, \tag{II.19}$$

where the current $\overline{I}_t$ is defined as

$$\overline{I}_t = \left(\overline{V}_t - \overline{V}_j\right)\overline{y}_T + \overline{V}_t \frac{\overline{y}_0}{2}, \tag{II.20}$$

the expressions for currents $\overline{I}_i$ and $\overline{I}_j$ as functions of voltages $\overline{V}_i$ and $\overline{V}_j$ are given as

$$\overline{I}_i = \overline{V}_i\left[\frac{\overline{y}_T}{t_r} + \frac{\overline{y}_T}{t_r}\left(\frac{1}{t_r} - 1\right) + \frac{\overline{y}_0}{2}\frac{1}{t_r^2}\right] - \overline{V}_j\frac{\overline{y}_T}{t_r}, \tag{II.21}$$

$$\overline{I}_j = -\overline{V}_i\frac{\overline{y}_T}{t_r} + \overline{V}_j\left[\frac{\overline{y}_T}{t_r} + \overline{y}_T\left(1 - \frac{1}{t_r}\right) + \frac{\overline{y}_0}{2}\right]. \tag{II.22}$$

As it is necessary to include transformer model in appropriate load flow algorithm, (II.21-22) give a basis for obtaining the equivalent π scheme (Fig. II.11).

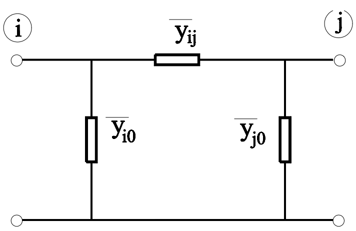

Fig. II.11 Equivalent π scheme

The impact of the ideal transformer is included within the elements of the scheme. The elements of the equivalent π scheme are

$$\overline{y}_{ij} = \frac{\overline{y}_T}{t_r}, \tag{II.23}$$

$$\overline{y}_{i0} = \frac{\overline{y}_T}{t_r}\left(\frac{1}{t_r} - 1\right) + \frac{\overline{y}_0}{2}\frac{1}{t_r^2}, \tag{II.24}$$

$$\overline{y}_{j0} = \overline{y}_T\left(1 - \frac{1}{t_r}\right) + \frac{\overline{y}_0}{2} \tag{II.25}$$

This scheme could be used to represent LTC transformer as well. In this case, each tap change causes necessary re-computation of admittance matrices due to changed parameter values.

In order to avoid re-computation, transformer model with injected currents or powers is used instead (Fig. II.12).

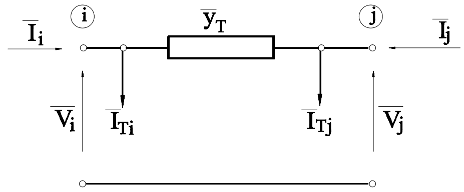

Fig. II.12 Transformer model with injected currents

Transformer is represented with a 4-pole element, where the admittance $\overline{y}_T$ has constant value, and the injected currents depend on the tap ratio. Due to a shunt character of the injected currents, they could be modelled as additional load powers at buses.

The currents $\overline{I}_i$ and $\overline{I}_j$ are defined as

$$\overline{I}_i = \left(\overline{V}_i - \overline{V}_j\right)\overline{y}_T + \overline{I}_{Ti}, \tag{II.26}$$

$$\overline{I}_j = \left(\overline{V}_j - \overline{V}_i\right)\overline{y}_T + \overline{I}_{Tj}. \tag{II.27}$$

By equalising (II.26-27) with (II.21-22), the injected currents are obtained as

$$\overline{I}_{Ti} = \overline{V}_i\left(-1 + \frac{1}{t_r^2}\right)\overline{y}_T + \overline{V}_j\left(1 - \frac{1}{t_r}\right)\overline{y}_T, \tag{II.28}$$

$$\overline{I}_{Tj} = \overline{V}_i\left(1 - \frac{1}{t_r}\right)\overline{y}_T. \tag{II.29}$$

By applying standard expressions for apparent power

$$\overline{S}_{Ti} = \overline{V}_i\overline{I}_{Ti}^*, \tag{II.30}$$

$$\overline{S}_{Tj} = \overline{V}_j\overline{I}_{Tj}^*, \tag{II.31}$$

the transformer model with injected powers is obtained (Fig. II.13).

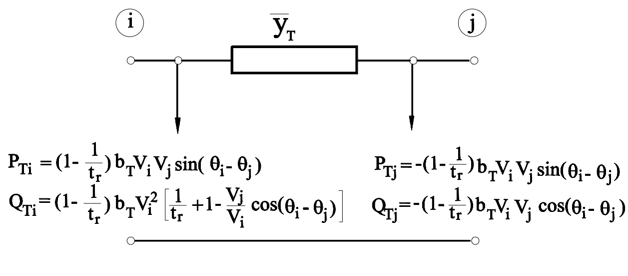

Fig. II.13 Transformer model with injected powers

Further on, the injected powers appear as

$$P_{Ti} = \left(1 - \frac{1}{t_r}\right) b_T V_i V_j \sin\left(\Theta_i - \Theta_j\right), \tag{II.32}$$

$$Q_{Ti} = \left(1 - \frac{1}{t_r}\right) b_T V_i^2\left[\frac{1}{t_r} + 1 - \frac{V_j}{V_i}\cos\left(\Theta_i - \Theta_j\right)\right], \tag{II.33}$$

$$P_{Tj} = -\left(1 - \frac{1}{t_r}\right) b_T V_i V_j \sin\left(\Theta_i - \Theta_j\right), \tag{II.34}$$

$$Q_{Tj} = -\left(1 - \frac{1}{t_r}\right) b_T V_i V_j \cos\left(\Theta_i - \Theta_j\right). \tag{II.35}$$

In order to allow the tap ratio, t_r, being variable, it is necessary to introduce a model of a scheme serving for voltage regulation of the secondary side (Fig. II.14).

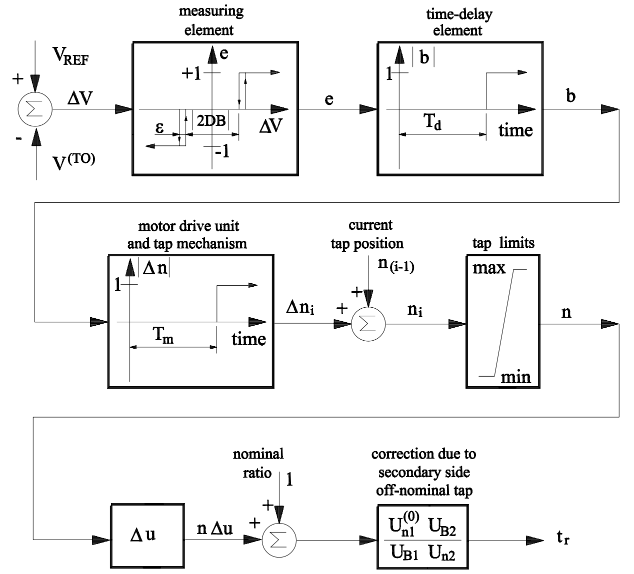

Fig. II.14 Voltage regulation by LTC transformer scheme

In the LTC scheme [76, 356-357], voltage regulation is carried out using voltage magnitude $V^{(TO)}$ of the transformer secondary j-side. The scheme contains models of measuring element, time-delay element, motor drive unit, tap mechanism, tap limits, and a correction due to initially off-nominal tap position at the secondary side.

The voltage difference, ΔV, given as

$$\Delta V = V_{REF} - V^{(TO)}, \tag{II.36}$$

serves as input for the measuring element, which is characterised by dead-band, DB, and directional sensitivity tolerance, ε.

The output of the measuring element, e, is defined as

$$e = \begin{cases} 0 \quad for \quad -DB \le \Delta V \le +DB \\ 0 \quad for \quad \Delta V \le (DB+\varepsilon),\ \Delta V\ increases \\ 0 \quad for \quad \Delta V \ge -(DB+\varepsilon),\ \Delta V\ decreases \\ +1\ for \quad \Delta V > (DB+\varepsilon),\ \Delta V\ increases \\ +1\ for \quad \Delta V > DB,\ \Delta V\ decreases \\ -1\ for \quad \Delta V < -(DB+\varepsilon),\ \Delta V\ decreases \\ -1\ for \quad \Delta V < -DB,\ \Delta V\ increases \end{cases}. \tag{II.37}$$

The time delay element is characterised by the time delay constant, T_d, defined with two values ($T_{d1} > T_{d2}$) as

$$T_d = \begin{cases} T_{d1} \quad for\ the\ first\ tap\ move \\ T_{d2} \quad for\ the\ subsequent\ ones \end{cases}. \tag{II.38}$$

The output of the time delay element, b, is defined as

$$b = \begin{cases} 0 \quad for \quad t \le T_d,\ e = arbitrary \\ +1\ for \quad t > T_d,\ e = +1 \\ -1\ for \quad t > T_d,\ e = -1 \end{cases}. \tag{II.39}$$

The output of the time delay element is the input of the motor drive unit and tap changer mechanism. They are characterised by time constant T_m, while the output, Δn, is defined as

$$\Delta n = \begin{cases} 0 \quad for \quad t \le T_m,\ b = arbitrary \\ +1\ for \quad t > T_m,\ b = -1 \\ -1\ for \quad t > T_m,\ b = +1 \end{cases}. \tag{II.40}$$

According to the voltage regulation scheme, the tap position, n_i, that should be achieved in the next step, is obtained by adding eventual tap change Δn_i to the current tap position $n_{(i-1)}$, as given in

$$n_i = n_{(i-1)} + \Delta n_i\ . \tag{II.41}$$

After passing through the tap limiter, the tap position should be transferred to the tap ratio basis. It is made possible by multiplying the requested tap position with expected per unit change, Δu, which equals to ($n\ \Delta u$). That value is added to the nominal ratio (set equal to 1), and the result is corrected by the off-nominal ratio due to initially off-nominal tap position at the secondary side. The final expression for the tap ratio, t_r, is given as

$$t_r = (1 + n\Delta u)\frac{U_{n1}^{(0)} U_{B2}}{U_{B1} U_{n2}}, \tag{II.42}$$

where U_{B1} and U_{B2} denote primary and secondary side base voltages, and U_{n1} and U_{n2} primary and secondary side nominal voltages. Primary side off-nominal conditions are set through the initial position defined with $n_{(i-1)}$.

Shunt capacitor bank

In order to decrease reactive power flow through the high-voltage system, the shunt reactive compensation is provided locally at the LV bus (Fig. II.9), by using fixed shunt capacitor bank [356-357]. In general, there is an option, especially in HV system, to have a shunt reactor connected as well.

If load consumption in the system increases, bus voltage magnitudes decrease. In due time, shunt capacitor banks should be switched on to increase the voltages. On the other side, if load consumption is small, line shunt capacitances could increase voltage magnitudes above acceptable values. Then, shunt reactors should be switched on to increase inductive load consume, and decrease voltages. In general load flow problem, in the beginning of the analysis it is not known whether reactive compensation devices should be switched on or off. The answer to that question is obtained by iterative procedure.

The most important parameter of the shunt capacitor bank from this load model is its nominal reactive power, Q_{SHn}, given in Mvar at nominal bus voltage magnitude (1 pu). The reactive power Q_{SHn} is positive for inductive load, and negative for capacitive one. By using system base power, S_B, given in MVA, the per unit value of the shunt susceptance, b_{SH}, is defined as

$$b_{SH} = \frac{-Q_{SHn}}{S_B}. \tag{II.43}$$

The shunt susceptance, b_{SH}, is positive for capacitive load, and negative for inductive one.

Distribution equivalent impedance

In order to represent low-voltage sub-transmission and distribution system in the composite load model (Fig. II.9), the equivalent impedance of lumped distribution feeders and transformers, Z_{eq}, is located between the LV bus and the load one [356-357].

Induction motor

The induction motor is represented by using its transient dynamic model. Appropriate differential and algebraic equations are included in the system model.

As a starting point in derivation of the transient dynamic model [37, 44, 173, 297, 318, 356, 383, 400, 403], standard impedance scheme of induction motor is used (Fig. II. 15).

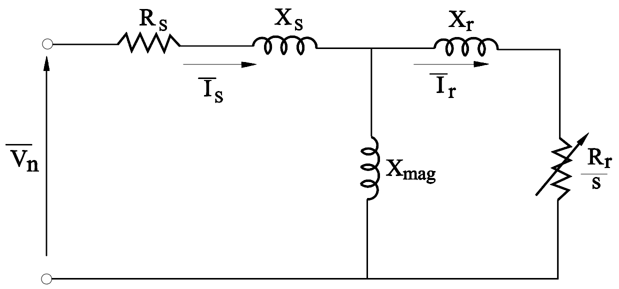

Fig. II.15 Standard impedance scheme of induction motor

Parameters R_S and R_r represent stator and rotor resistances, X_S and X_r stator and rotor leakage reactances, X_{mag} magnetising reactance, and s motor slip. Motor bus voltage is denoted by $\overline{V}_n$, while $\overline{I}_S$ and $\overline{I}_r$ denote stator and rotor currents.

In order to compute initial steady state operating point of the system with induction motors included, first it is necessary to define initial equivalent impedance $R_m(s)+jX_m(s)$. It is valid only for steady state (Fig. II.16), and helps motor power consumption being computed.

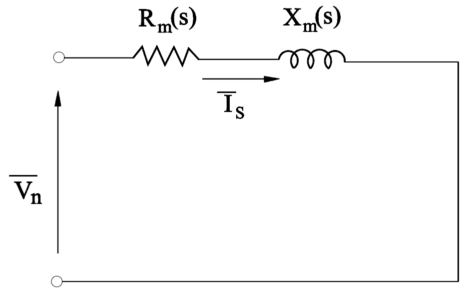

Fig. II.16 Initial steady state equivalent impedance

The equivalent impedance depends on induction motor slip, and should be computed according to following expression

$$R_m(s) + jX_m(s) = (R_S + jX_S) + \frac{jX_{mag}\left(\frac{R_r}{s} + jX_r\right)}{\frac{R_r}{s} + j(X_{mag} + X_r)}. \tag{II.44}$$

After some elaboration, it results with the expressions

$$R_m(s) = R_S + \frac{1}{s}\frac{X_{mag}^2 R_r}{\left(\frac{R_r}{s}\right)^2 + (X_{mag} + X_r)^2}, \tag{II.45}$$

$$X_m(s) = X_S + \frac{\frac{X_{mag}R_r^2}{s^2} + X_{mag}X_r(X_{mag} + X_r)}{\left(\frac{R_r}{s}\right)^2 + (X_{mag} + X_r)^2}. \tag{II.46}$$

The current $\overline{I}_S$, which flows through the impedance $R_m(s)+jX_m(s)$, is defined as

$$\overline{I}_S = \frac{\overline{V}_n}{R_m(s) + jX_m(s)}. \tag{II.47}$$

Consequently, the apparent electric power is defined as

$$\overline{S} = \overline{V}_n \overline{I}_S^* = \frac{V_n^2}{R_m(s) - jX_m(s)}. \tag{II.48}$$

Further elaboration gives active and reactive power as

$$P_{emot} = \frac{R_m(s)}{R_m^2(s) + X_m^2(s)} V_n^2, \tag{II.49}$$

$$Q_{emot} = \frac{X_m(s)}{R_m^2(s) + X_m^2(s)} V_n^2. \tag{II.50}$$

The powers (II.49-50) are given in per unit values with motor nominal power S_{nmot} as a basis. Before being included in the load flow computation, the powers should be multiplied by S_{nmot}/S_B introducing the system base power S_B as common reference.

In order to compute a complete set of motor variables valid for initial steady state operating point, the series equivalent scheme is used (Fig. II.17).

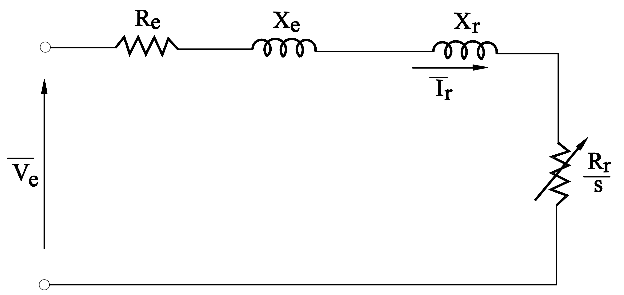

Fig. II.17 Series equivalent scheme of induction motor

The equivalent series resistance, R_e, and reactance, X_e, are derived from

$$R_e + jX_e = \frac{jX_{mag}(R_S + jX_S)}{R_S + j(X_S + X_{mag})}, \tag{II.51}$$

and given as

$$R_e = \frac{R_S X_{mag}^2}{R_S^2 + (X_S + X_{mag})^2}, \tag{II.52}$$

$$X_e = \frac{R_S^2 X_{mag} + X_S^2 X_{mag} + X_{mag}^2 X_S}{R_S^2 + (X_S + X_{mag})^2}. \tag{II.53}$$

If the equivalent voltage $\overline{V}_e$ is defined as

$$\begin{aligned}\overline{V}_e &= \overline{V}_n \frac{jX_{mag}}{R_S + j(X_S + X_{mag})} = \\ &= \overline{V}_n \left[\frac{X_{mag}(X_S + X_{mag})}{R_S^2 + (X_S + X_{mag})^2} + j \frac{R_S X_{mag}}{R_S^2 + (X_S + X_{mag})^2} \right]\end{aligned}, \tag{II.54}$$

the rotor current $\overline{I}_r$ results as

$$\overline{I}_r = \frac{\overline{V}_e}{\left(R_e + \frac{R_r}{s}\right) + j(X_e + X_r)}. \tag{II.55}$$

Hereby, the electromagnetic torque, T_e, developed by the motor is defined as

$$\begin{aligned}T_e &= \frac{P_{sh}}{\omega_m} = \frac{P_{ag}}{\omega_{0S}} = \frac{R_r}{s\omega_{0S}} I_r^2 = \\ &= \frac{R_r}{s\omega_{0S}} \frac{V_e^2}{\left(R_e + \frac{R_r}{s}\right)^2 + (X_e + X_r)^2}\end{aligned}, \tag{II.56}$$

where P_{sh} denotes motor shaft power or the mechanical power given to the motor load, P_{ag} motor air-gap power or the power that is transferred through the air-gap from stator to rotor, ω_{0S} per unit value of stator frequency that is equal to $(2\pi f)/(2\pi f_0) = \omega_S/\omega_0$, and ω_m per unit value of the rotor speed that is equal to $(1\text{-}s)\omega_{0S}$.

The shaft power, P_{sh}, is regarded as a difference between the air-gap power, P_{ag}, and the rotor power loss, P_{rloss}. It is computed as

$$P_{sh} = P_{ag} - P_{r\,loss} = \frac{R_r}{s} I_r^2 - R_r I_r^2 = \frac{1-s}{s} R_r I_r^2. \tag{II.57}$$

Thus, the electromagnetic torque, T_e, developed by the motor, could be defined as

$$\begin{aligned}T_e &= \frac{P_{sh}}{\omega_m} = \frac{P_{ag}}{\omega_{0S}} = \frac{(1-s)R_r}{s\omega_m} I_r^2 = \\ &= \frac{(1-s)R_r}{s\omega_m} \frac{V_e^2}{\left(R_e + \frac{R_r}{s}\right)^2 + (X_e + X_r)^2}\end{aligned}. \tag{II.58}$$

Point of maximum electromagnetic torque in a well-known motor slip-torque characteristic is achieved when the load impedance becomes equal to the circuit impedance

$$\frac{R_r}{s} = \sqrt{R_e^2 + (X_e + X_r)^2}. \tag{II.59}$$

Maximum point is defined by following characteristic values of torque T_{emax} and slip s_{Temax}

$$T_{e\max} = \frac{1}{\omega_{0S}} \frac{0.5V_e^2}{R_e + \sqrt{R_e^2 + (X_e + X_r)^2}}, \tag{II.60}$$

$$s_{Te\max} = \frac{R_r}{\sqrt{R_e^2 + (X_e + X_r)^2}}. \tag{II.61}$$

The initial steady state value of motor slip, s, is derived from (II.56) by establishing following quadratic equation

$$as^2 + bs + c = 0, \tag{II.62}$$

where coefficients a, b, and c, are given as

$$a = \omega_{0S} T_e \left[R_e^2 + (X_e + X_r)^2\right], \tag{II.63}$$

$$b = 2R_e R_r \omega_{0S} T_e - R_r V_e^2, \tag{II.64}$$

$$c = \omega_{0S} T_e R_r^2. \tag{II.65}$$

At the initial steady state operating point, it is assumed that ω_{0S} is equal to 1, which makes the motor slip being one of the roots of (II.62).

Mechanical load torque of the motor, T_m, is defined according to

$$T_m = T_{m0}\left[A\left(\frac{\omega_m}{\omega_{m0}}\right)^2 + B\left(\frac{\omega_m}{\omega_{m0}}\right) + C + D\left(\frac{\omega_m}{\omega_{m0}}\right)^{am}\right], \tag{II.66}$$

where T_{m0} is a value of the load torque at the speed ω_{m0}, A, B, and C are appropriate coefficients of quadratic, linear and constant term, while D and am define initial value of the torque.

The exact solution for the initial steady state operating point of the system with induction motors included is obtained iteratively (Fig. II.18). In the sequence, the motor initialisation is followed by the load flow procedure, which calls for the motor adjustment. Upon satisfying iterative difference in motor electric powers, the base case is completed as the motors are concerned.

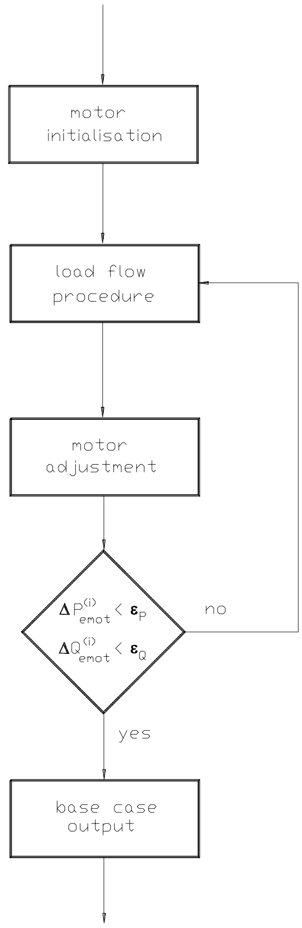

Fig. II.18 Iterative procedure for determination of exact initial steady state operating point

Motor initialisation and adjustment have rather similar sequence. First, the set of parameters (R_e, X_e, s_{Temax}, V_e^2, T_{emax}) is computed. Then, the second one (T_m, T_e, a, b, c, s) is determined. Using the value of the motor slip s, the motor speed ω_m is calculated. If the difference of the value of the motor speed ω_m from two consecutive iterations is larger then the value of pre-established threshold (e.g. 1.e-6), the procedure is taken backward to the evaluation of the second set of the parameters. Iterative procedure is stopped when the value of ω_m from two consecutive iterations becomes small enough. Afterwards, the third set of parameters ($R_m(s)$, $X_m(s)$, P_{emot}, Q_{emot}) is computed. The active, P_{emot}, and reactive, Q_{emot}, power of the motor are necessary inputs for the initial load flow procedure. The powers are considered as the bus load injections. They are added to the load powers of the other loads at the same bus.

The whole procedure is stopped when the changes ΔP_{emot} and ΔQ_{emot} between two consecutive iterations satisfy pre-established thresholds ε_P and ε_Q.

Having the initial steady state operating point determined, the analysis is focused on the transient dynamic model of the induction motor (Fig. II.19). Within dynamic load flow model, besides terminal connection bus (E, external) the induction motor needs additional internal bus (I) as well. At the internal bus, the transient voltage $\overline{E}'_{mot}$ is set to adjust for dynamic behaviour of the motor.

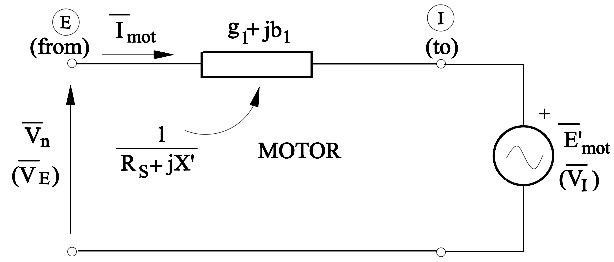

Fig. II.19 Dynamic load flow representation of induction motor

The admittance g_1+jb_1, between external and internal bus, is given by the inverse of the motor impedance R_S+jX'. According to the standard impedance scheme of the induction motor (Fig. II.15), parameter R_S represents stator resistance. Reactance X' depends on stator reactance X_S and a parallel combination of the magnetising reactance X_{mag}, and the rotor reactance X_r. It is computed as

$$X' = X_S + \frac{X_{mag} X_r}{X_{mag} + X_r} \tag{II.67}$$

The transient voltage $\overline{E}'_{mot}$ is defined as

$$\overline{E}'_{mot} = \overline{V}_n - (R_S + jX')\overline{I}_{mot}, \tag{II.68}$$

where $\overline{V}_n$ denotes terminal bus voltage, and $\overline{I}_{mot}$ motor current drawn from the network.

Corresponding vector diagram is set according to the decomposition into d and q-axis (Fig. II.20).

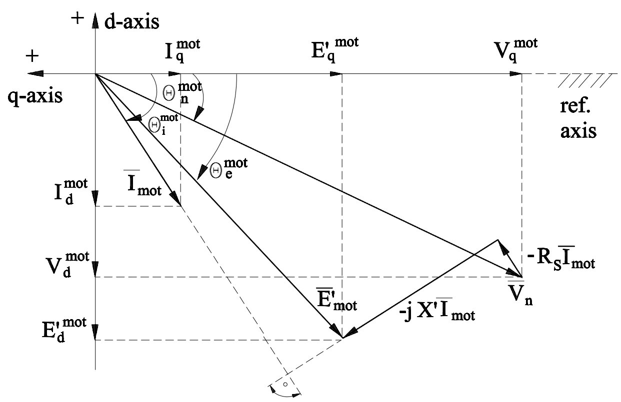

Fig. II.20 Vector diagram of induction motor

It is assumed that the q-axis leads the d-axis for 90°, while the angles are negative. Therefore, neglecting the superscript ^{mot} in motor d-q components, the key variables are decomposed as $\overline{V}_n = V_d - jV_q$, $\overline{E}'_{mot} = E_d' - jE_q'$, and $\overline{I}_{mot} = I_d - jI_q$.

The d and q-axis components are given as

$$V_d = V_n \sin\Theta_n , \tag{II.69}$$
$$V_q = V_n \cos\Theta_n , \tag{II.70}$$
$$E_d' = E_{mot}' \sin\Theta_e , \tag{II.71}$$
$$E_q' = E_{mot}' \cos\Theta_e , \tag{II.72}$$
$$I_d = \frac{1}{R_S^2 + X'^2}\left[R_S\left(V_d - E_d'\right) - X'\left(V_q - E_q'\right)\right], \tag{II.73}$$
$$I_q = \frac{1}{R_S^2 + X'^2}\left[R_S\left(V_q - E_q'\right) + X'\left(V_d - E_d'\right)\right]. \tag{II.74}$$

Basic differential equation, which describes electrical dynamics of the transient model, is given as

$$\frac{d\overline{E}'_{mot}}{dt} = -j\omega_{0S} s\overline{E}'_{mot} - \frac{1}{T_0'}\left[\overline{E}'_{mot} - j(X - X')\overline{I}_{mot}\right], \tag{II.75}$$

where the reactance X is defined as

$$X = X_S + X_{mag} , \tag{II.76}$$

and the constant T_0' as

$$T_0' = \frac{X_r + X_{mag}}{\omega_{0S} R_r} . \tag{II.77}$$

Per unit value of the frequency ω_{0S} at the bus where the motor is connected to the system is variable. Since it is computed depending on the bus voltage angle change as

$$\omega_{0S} = 1 + \frac{d\Theta_n}{dt} , \tag{II.78}$$

the constant T_0' should be recomputed in each time step.

After d and q-axis decomposition, (II.75) becomes

$$\frac{dE_q'}{dt} = (\omega_{0S} - \omega_m)E_d' - \frac{E_q'}{T_0'} - \frac{X - X'}{T_0'} I_d , \tag{II.79}$$
$$\frac{dE_d'}{dt} = -(\omega_{0S} - \omega_m)E_q' - \frac{E_d'}{T_0'} + \frac{X - X'}{T_0'} I_q . \tag{II.80}$$

Motor shaft dynamics is defined as

$$\frac{d\omega_m}{dt} = \frac{T_e - T_m}{2H} , \tag{II.81}$$

where H denotes motor inertia constant, and T_e and T_m electromagnetic and mechanical torques.

The electromagnetic torque, T_e, is computed as

$$T_e = \left(E_d' I_d + E_q' I_q\right)/\omega_{0S} , \tag{II.82}$$

whereas the mechanical torque, T_m, is defined by (II.66).

Besides these three differential equations (II.79-81), the transient model of the induction motor includes four algebraic equations as well. They are derived from (II.73-74, II.69-70), and are given as

$$-X'E_q' + R_S E_d' + \left(R_S^2 + X'^2\right)I_d - R_S V_d + X'V_q = 0 , \tag{II.83}$$
$$R_S E_q' + X'E_d' + \left(R_S^2 + X'^2\right)I_q - X'V_d - R_S V_q = 0 , \tag{II.84}$$
$$V_d - V_n \sin\Theta_n = 0 , \tag{II.85}$$
$$V_q - V_n \cos\Theta_n = 0 . \tag{II.86}$$

Differential (II.79-81) and algebraic (II.83-86) equations of the induction motor transient model are included in the overall system model when the motors are present in the system.

Thermostatically controlled load

At the LOAD bus, the composite load model includes a thermostatically controlled load (TCL). The TCL represents aggregated thermal heating consumes supplied from the bus [36, 191, 356-357]. The active load power of the TCL depends on a conductance G (linearly), and on a bus voltage magnitude V_n (quadratic) as

$$P_{eTCL}(G, V_n) = GV_n^2 . \tag{II.87}$$

Generally, when the bus voltage magnitude is decreased, the conductance G is increased through temperature feedback control (Fig. II.21). Actually, by sudden drop in voltage, the consumed active power is decreased. Then the TCL stays switched-on longer and increases its active power consumption by increasing conductance G.

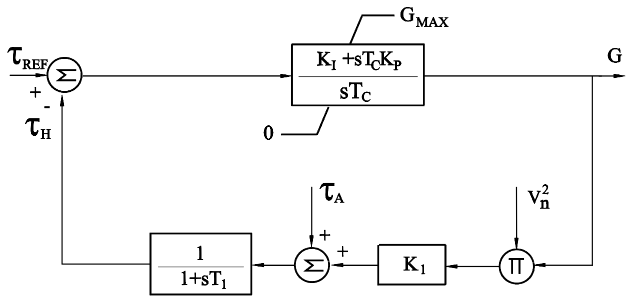

Fig. II.21 Thermostatically controlled load model

The leading branch of the model is of proportional-integral type defined by gains K_P and K_I, respectively, and integral time constant T_C. Maximum conductance value, G_{MAX}, depends on a minimum acceptable bus voltage magnitude.

As the input in the PI term, a temperature change appears. It is a difference between the referent temperature τ_{REF} and the temperature of heated space τ_H. Besides on the lag term defined by the time constant T_1, the heated space temperature τ_H depends on the ambient temperature τ_A and the term proportional to the active power consumption $K_1 G V_n^2$. In that feedback term, the gain K_1 adjusts for the initial steady state value of the active power and is given as

$$K_1 = \frac{\tau_{REF} - \tau_A}{G_0 V_{n0}^2} \quad [°C / pu], \tag{II.88}$$

where subscript $_0$ denotes initial steady state value of conductance and bus voltage magnitude. Time constants T_C and T_I are much larger than the others in the system due to a longer regulation mechanism of space heating.

Finally, the TCL load model is described by two differential equations

$$\frac{d\tau_H}{dt} = -\frac{\tau_H}{T_1} + \frac{K_1}{T_1} G V_n^2 + \frac{\tau_A}{T_1}, \tag{II.89}$$

$$\begin{aligned} \frac{dG}{dt} &= \left(\frac{K_P}{T_1} - \frac{K_I}{T_C}\right)\tau_H - \frac{K_P K_1}{T_1} G V_n^2 + \\ &+ \frac{\tau_{REF} K_I}{T_C} - \frac{K_P \tau_A}{T_1} \end{aligned}. \tag{II.90}$$

The model does not have any of algebraic equations that should be included in the overall system model.

Static load

At the LOAD bus, besides induction motor and thermostatically controlled load there is a part of the total load which is considered to be static in nature (SL). Static load power depends on the bus voltage magnitude, V_n, and eventually on the change of the bus frequency Δf [157-158, 191]. The active power of the static load is defined as

$$\begin{aligned} P_S(V_n, \Delta f) = P_L^0 \Bigg\{ &\left[K_{pz}\left(\frac{V_n}{V_{n0}}\right)^2 + K_{pi}\left(\frac{V_n}{V_{n0}}\right) + K_{pp} \right] + \\ &+ \left[K_{p1}\left(\frac{V_n}{V_{n0}}\right)^{n_{pv1}} \left(1 + n_{pf1}\Delta f\right) \right] + \\ &+ \left[K_{p2}\left(\frac{V_n}{V_{n0}}\right)^{n_{pv2}} \left(1 + n_{pf2}\Delta f\right) \right] \Bigg\} \end{aligned} \tag{II.91}$$

where P_L^0 denotes active power demand at the bus voltage magnitude V_{n0} at initial steady state, K_{pz}, K_{pi}, and K_{pp} proportionality coefficients for voltage dependent part of the power, and K_{p1}, n_{pv1}, and n_{pf1} (respectively 2) proportionality coefficients of voltage/frequency dependent parts. The coefficients should satisfy following relationship

$$K_{pz} = 1 - \left(K_{pi} + K_{pp} + K_{p1} + K_{p2}\right). \tag{II.92}$$

This type of the static load is commonly known as ZIP load model. Similar expressions are valid for reactive power of the static load.

II.3.B Dynamic load model with non-linear recovery

The aggregate first-order non-linear recovery type of the dynamic load model is introduced in the voltage collapse scenario. This load model expresses load dynamics in terms of its steady state and transient characteristics [13-17, 137, 140-141, 176, 298]. As seen from HV bus, it is aimed to represent load recovery process influenced by LTC transformers and TCL loads (mid to long-term) and induction motors (short-term).

Basic differential equation of active power load is given as

$$T_P \frac{dP_d}{dt} + P_d = P_S(V_n) + k_P(V_n)\frac{dV_n}{dt}, \tag{II.93}$$

where P_d denotes consumed dynamic active power with time constant T_P of its recovery process, and P_S static active power characteristic dependable on bus voltage magnitude V_n.

Voltage dependable function $k_P(V_n)$ is usually defined as

$$k_P(V_n) = k_P V_n^{\alpha-1}. \tag{II.94}$$

Basic differential equation (II.93) is rather inconvenient for usage in numerical integration procedures. Therefore, the other formulation is established by introducing new state variable of the load active power, x_P, given as

$$x_P = T_P P_d - T_P P_t(V_n), \tag{II.95}$$

where active power transient function $P_t(V)$ is defined as

$$P_t(V) = \frac{1}{T_P}\int_0^V k_P(V)dV + P_t(0). \tag{II.96}$$

The derivative of the state variable, dx_P/dt, is defined as

$$\begin{aligned} \frac{dx_P}{dt} &= T_P \frac{dP_d}{dt} - T_P \frac{1}{T_P} k_P(V_n)\frac{dV_n}{dt} = \\ &= P_S(V_n) - P_d \end{aligned}. \tag{II.97}$$

Since the consumed dynamic active power, P_d, could be defined from (II.95-96) as

$$P_d(x_P, V_n) = \frac{x_P}{T_P} + P_t(V_n) = \frac{x_P}{T_P} + \frac{k_P V_n^{\alpha}}{\alpha T_P}, \tag{II.98}$$

the derivative dx_P/dt, from (II.97), becomes dependable only on x_P and V_n as

$$\frac{dx_P}{dt} = -\frac{x_P}{T_P} + P_S(V_n) - P_t(V_n) = = -\frac{x_P}{T_P} + P_S(V_n) - \frac{k_P V_n^{\alpha}}{\alpha T_P} \quad . \tag{II.99}$$

The state variable, x_P, from (II.95), and its corresponding derivative dx_P/dt, from (II.99), are used to describe first-order non-linear load recovery. The recovery appears after a bus voltage magnitude change caused difference between consumed dynamic active power and static power.

There are two properties in time response of a consumed dynamic load active power due to a voltage change. They are defined as initial and final changes.

The initial change, ΔP_{d0}, is computed as

$$\Delta P_{d0} = P_d(t_{0-}) - P_d(t_{0+}) = P_t(V_{n0-}) - P_t(V_{n0+}) = = \frac{k_P\left(V_{n0-}^{\alpha} - V_{n0+}^{\alpha}\right)}{\alpha T_P} \quad , \tag{II.100}$$

where V_{n0-} and V_{n0+} denote values of bus voltage magnitude before and immediately after a disturbance.

The final change, $\Delta P_{d\infty}$, appears after load recovery has finished. It is computed as

$$\Delta P_{d\infty} = P_d(t_{0-}) - P_d(t_{\infty}) = P_S(V_{n0-}) - P_S(V_{n\infty}) \ , \tag{II.101}$$

where V_{n0-} and $V_{n\infty}$ denote initial and final values of the bus voltage magnitude V_n.

At the initial steady state operating point, the derivative dx_P/dt is equal to zero. It makes the consumed dynamic load active power, P_d, being equal to the static power $P_S(V)$

$$\frac{dx_P}{dt} = 0 \quad \Rightarrow \quad P_d = P_S(V_n) \ , \tag{II.102}$$

with the state variable x_P computed as

$$x_P = T_P P_S(V_n) - T_P P_t(V_n) \ . \tag{II.103}$$

Similarly to (II.93-103), relations belonging to load reactive power are established as well, defining corresponding state variable x_Q and its derivative dx_Q/dt.

In the voltage collapse scenario, the steady state characteristic of the load dynamics is expressed by constant active and reactive load power, whereas the transient load characteristic corresponds to constant impedance.

II.4 NETWORK MODELLING

Network bus equations for active and reactive power depend on whether there is a generator or motor connected at the bus. Actually, it is possible to set bus equations in a general form that is independent of generator/motor connection, but if the generator/motor algebraic equations should be included in dynamic system, the network bus equations differ mutually for generating/motor and non-generating/motor buses.

Network bus equations in the general form [10, 18, 191, 378-380] are defined for bus k ($k=1$ to n_{BUS}) as it follows

$$P_k(\Theta, V) = \sum_{m=1}^{n} P_{km} = = \sum_{m=1}^{n} \left(G_{km} V_k V_m \cos\Theta_{km} + B_{km} V_k V_m \sin\Theta_{km}\right) \tag{II.104}$$

$$Q_k(\Theta, V) = \sum_{m=1}^{n} Q_{km} = = \sum_{m=1}^{n} \left(G_{km} V_k V_m \sin\Theta_{km} - B_{km} V_k V_m \cos\Theta_{km}\right) \tag{II.105}$$

where n denotes total number of network and internal generator/motor buses, n_{BUS}, n_{GEN}, and n_{MOT}, given as $n=n_{BUS}+n_{GEN}+n_{MOT}$. The terms G_{km} and B_{km} denote elements of the bus admittance matrix $[Y] = [G] + j[B]$, with generator/motor internal admittance included.

In order to have the generator/motor algebraic equations included in (II.104-105), the d and q-axis components of the terminal generator/motor voltage and current are used. The active and reactive power flows from external to internal bus are given for generator as

$$P_{EI} = G_{EI} V_E V_I \cos\Theta_{EI} + B_{EI} V_E V_I \sin\Theta_{EI} - G_{EI} V_E^2 = = -\left(V_d I_d + V_q I_q\right) \tag{II.106}$$

$$Q_{EI} = G_{EI} V_E V_I \sin\Theta_{EI} - B_{EI} V_E V_I \cos\Theta_{EI} + B_{EI} V_E^2 = = -\left(V_d I_q - V_q I_d\right) \tag{II.107}$$

and similarly for motor as

$$P_{EI} = +\left(V_d I_d + V_q I_q\right) \tag{II.108}$$

$$Q_{EI} = +\left(V_d I_q - V_q I_d\right). \tag{II.109}$$

Therefore, the network bus equations (II.104-105) are rewritten for generator bus ($k=E$) as

$$P_E(\Theta, V) = \sum_{m=1}^{n} P_{Em} - P_{EI} - \left(V_d I_d + V_q I_q\right) \tag{II.110}$$

$$Q_E(\Theta, V) = \sum_{m=1}^{n} Q_{Em} - Q_{EI} - \left(V_d I_q - V_q I_d\right) \tag{II.111}$$

and for motor bus as

$$P_E(\Theta, V) = \sum_{m=1}^{n} P_{Em} - P_{EI} + \left(V_d I_d + V_q I_q\right) \tag{II.112}$$

$$Q_E(\Theta, V) = \sum_{m=1}^{n} Q_{Em} - Q_{EI} + \left(V_d I_q - V_q I_d\right). \tag{II.113}$$

If there are no further bus power injections, the bus network equations are written in algebraic form as

$$P_k(\Theta,V)=0\,, \tag{II.114}$$
$$Q_k(\Theta,V)=0\,. \tag{II.115}$$

Generally, due to eventually bus connected dynamic recovery loads, static loads, TCL loads, shunt capacitors/inductors, and transformers, the algebraic bus network equations (II.114-115) are written as

$$\begin{aligned}&P_k(\Theta,V)+P_d(x_P,V)+P_S(V,\Delta f)+\\&+P_{eTCL}(G,V)+P_{Ti\ or\ j}(\Theta,V,t_r)=0\end{aligned}\,, \tag{II.116}$$

and

$$\begin{aligned}&Q_k(\Theta,V)+Q_d(x_Q,V)+Q_S(V,\Delta f)+\\&+Q_{SH}(b_{SH},V)+Q_{Ti\ or\ j}(\Theta,V,t_r)=0\end{aligned}\,. \tag{II.117}$$

The algebraic bus network equations (II.116-117) have additional terms in both active and reactive powers when the UPFC is included in the system. The UPFC is modelled by using its injection model with active and reactive powers injected at terminal buses from both sides.

III. THE UPFC MODEL

III.1 GENERAL DESCRIPTION OF THE UPFC

The UPFC can provide simultaneous control of all basic power system parameters (transmission voltage, impedance and phase angle) and dynamic compensation of ac system. The controller can fulfil functions of reactive shunt compensation, series compensation and phase shifting meeting multiple control objectives.

From a functional perspective [124-129], the objectives are met by applying boosting transformer injected voltage and exciting transformer reactive current (Fig. III.1). The injected voltage is inserted by using series transformer. Its output value is added to the network bus voltage from the shunt side, and is controllable both in magnitude and angle. The reactive current is drawn or supplied by using shunt transformer.

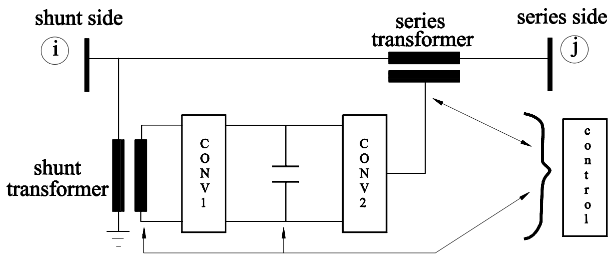

Fig. III.1 The UPFC device circuit arrangement

Besides transformers, the general structure of the UPFC contains also two "back to back" AC to DC voltage source converters operated from a common DC link capacitor. First converter (CONV1) is connected in shunt and the second one (CONV2) in series with the line. The shunt converter (CONV1) is primarily used to provide active power demand of the series converter (CONV2) through a common DC link.

Since the converters are operated from a DC link, they exchange only active power and there is no reactive power flow between them. It means that reactive power could be controlled independently at both converters. Therefore, there are three variables between two of the UPFC buses, which can be controlled simultaneously. Generally, such a structure enables voltage control from the shunt side, and independent active and reactive power flow control from the series side.

III.2 THE INJECTION MODEL OF THE UPFC

Functional structure of the UPFC results with appropriate electric circuit arrangement [265-273]. The series converter output voltage is injected in series with the line and acts as an AC voltage source (Fig. III.2). The reactance x_S describes a reactance seen from terminals of the series transformer and is equal to

$$x_S = x_k r_{\max}^2 \left(S_B / S_{conv\ 2n} \right), \tag{III.1}$$

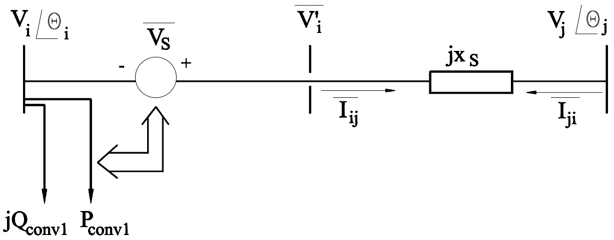

Fig. III.2 The UPFC electric circuit arrangement

where x_k denotes a series transformer reactance, r_{max} maximum per unit value of injected voltage magnitude, S_B system base power, and S_{conv2n} nominal rating power of the series converter. The current flowing through the injected voltage source, $\overline{I}_{ij}$, is the transmission line current from the series side. Therefore, the nominal rating power S_{conv2n} is determined as a product of the maximum injected voltage and the maximum line current at which power flow control is still provided. The voltage source exchanges active power with shunt converter (CONV1), whereas reactive power of the shunt converter, Q_{conv1}, could be controlled independently, or, as it is explained later on, according to its remaining capacity after satisfying demand for active power.

The UPFC injection model [266-267] is derived enabling three parameters to be simultaneously controlled. They are namely the shunt reactive power, Q_{conv1}, and the magnitude, r, and angle, γ, of the injected series voltage $\overline{V}_S$. The injected voltage $\overline{V}_S$ is added to the shunt side network bus voltage $\overline{V}_i$ according to a general vector diagram of the UPFC steady state operation (Fig. III.3).

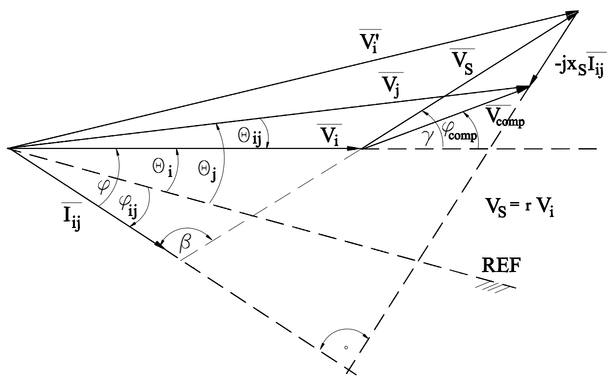

Fig. III.3 General vector diagram of the UPFC steady state operation

The injected voltage $\overline{V}_S$ is defined as

$$\overline{V}_S = r\overline{V}_i e^{j\gamma} = rV_i e^{j(\Theta_i+\gamma)} = V_S e^{j(\Theta_i+\gamma)}, \tag{III.2}$$

where the shunt side bus voltage is given as $\overline{V}_i = V_i e^{j\Theta_i}$, and the voltage source magnitude as $V_S = rV_i$. Therefore, the UPFC parameter r, which defines magnitude of injected voltage, is given as

$$r = \frac{V_S}{V_i}, \qquad \text{(III.3)}$$

and has a value in the range $0 \le r \le r_{\max}$, whereas the angle γ is fully controlled in the range $0 \le \gamma < 2\pi$.

In order to derive the UPFC injection model, first it is necessary to consider the series voltage source (Fig. III.4).

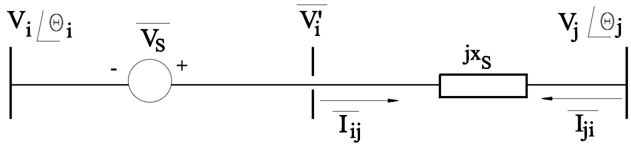

Fig. III.4 Series voltage source

The series voltage source is described in a form of a vector diagram (Fig. III.5), where the voltage $\overline{V}_i'$ is defined as

$$\overline{V}_i' = \overline{V}_i + \overline{V}_S, \qquad \text{(III.4)}$$

and the current $\overline{I}_{ij}$ as

$$\overline{I}_{ij} = \frac{\overline{V}_i' - \overline{V}_j}{jx_S}. \qquad \text{(III.5)}$$

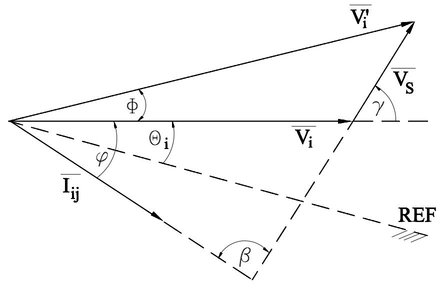

Fig. III.5 Vector diagram of series voltage source

In the next step, the series voltage source is transformed to the Norton equivalent (Fig. III.6), having current, $\overline{I}_S$, and susceptance, b_S, instead of voltage, $\overline{V}_S$, and reactance, x_S.

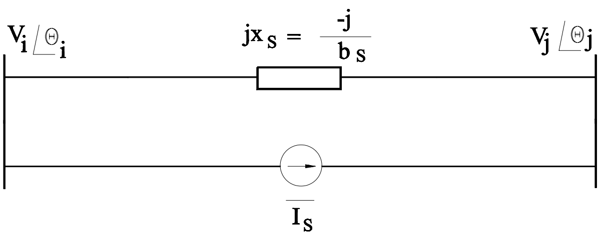

Fig. III.6 Transformed series voltage source

The current $\overline{I}_S$ is defined as

$$\overline{I}_S = \frac{\overline{V}_S}{jx_S} = jb_S\overline{V}_S, \qquad \text{(III.6)}$$

where the susceptance b_S has negative value ($b_S \le 0$) and is equal to $b_S = -1/x_S$.

Transformed series voltage source enables introduction of the bus power injections into the buses (Fig. III.7).

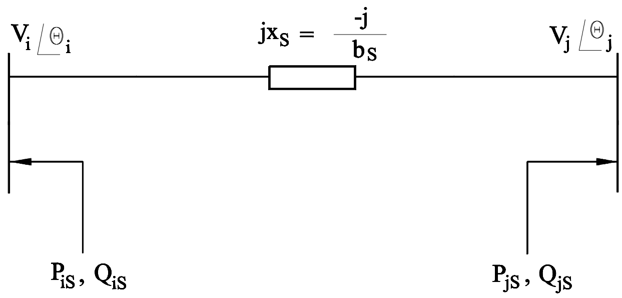

Fig. III.7 Transformed series voltage source with bus power injections

The injections are obtained using current $\overline{I}_S$ and bus voltages $\overline{V}_i$ and $\overline{V}_j$ as

$$\overline{S}_{iS} = \overline{V}_i\left(-\overline{I}_S\right)^* \quad ; \quad \overline{S}_{jS} = \overline{V}_j\left(\overline{I}_S\right)^*, \qquad \text{(III.7)}$$

where a load bus power has a negative sign, and a source bus power positive one. By using (III.7, III.6, III.2), the bus power injection $\overline{S}_{iS}$ is obtained as

$$\begin{aligned}\overline{S}_{iS} &= \overline{V}_i\left(-jb_S\overline{V}_S\right)^* = \overline{V}_i\left(-jb_S r\overline{V}_i e^{j\gamma}\right)^* = \\ &= rb_S V_i^2 \sin\gamma + jrb_S V_i^2 \cos\gamma\end{aligned}, \qquad \text{(III.8)}$$

and the bus power injection $\overline{S}_{jS}$ as

$$\begin{aligned}\overline{S}_{jS} &= \overline{V}_j\left(jb_S\overline{V}_S\right)^* = \overline{V}_j\left(jb_S r\overline{V}_i e^{j\gamma}\right)^* = \\ &= -rb_S V_i V_j \sin\left(\Theta_i - \Theta_j + \gamma\right) - \\ &\quad - jrb_S V_i V_j \cos\left(\Theta_i - \Theta_j + \gamma\right)\end{aligned} \qquad \text{(III.9)}$$

Afterwards, the series voltage source is coupled with the shunt part of the UPFC (Fig. III.8).

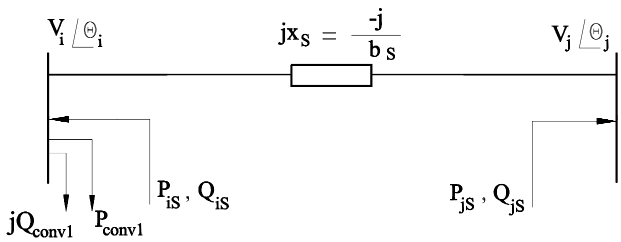

Fig. III.8 Coupling of the UPFC series branch with the shunt one

Having branches of the UPFC coupled, the bus power injections of the UPFC are formed (Fig. III.9), and defined as

$$P_{Si} = -\mathrm{Re}\left(\overline{S}_{iS}\right) + \mathrm{Re}\left(\overline{S}_{conv1}\right), \qquad \text{(III.10)}$$

$$Q_{Si} = -\mathrm{Im}\left(\overline{S}_{iS}\right) + \mathrm{Im}\left(\overline{S}_{conv1}\right), \qquad \text{(III.11)}$$

$$P_{Sj} = -\mathrm{Re}\left(\overline{S}_{jS}\right), \qquad \text{(III.12)}$$

$$Q_{Sj} = -\mathrm{Im}\left(\overline{S}_{jS}\right). \qquad \text{(III.13)}$$

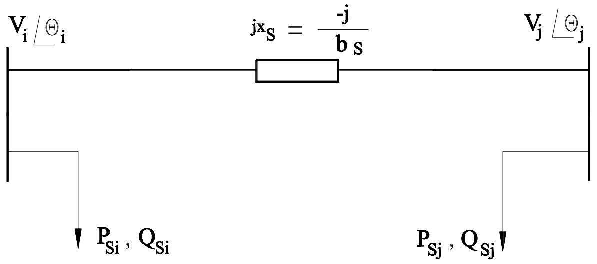

Fig. III.9 Bus power injections of the UPFC

In order to define the bus power injections of the UPFC at the i-side, it is necessary to have the apparent power of the shunt converter $\overline{S}_{conv1}$ defined.

The UPFC shunt and series converters mutually exchange only active power, whereas reactive power is controlled independently at both sides. It is written as

$$P_{conv1} = P_{conv2}\,, \tag{III.14}$$

$$Q_{conv1} = independently\ controlled\,. \tag{III.15}$$

Therefore, the active power of the shunt converter, P_{conv1}, could be computed from the expression for the apparent power of the series converter, $\overline{S}_{conv2}$, which is given as

$$\overline{S}_{conv2} = \overline{V}_S \overline{I}_{ij}^{*} = r\overline{V}_i e^{j\gamma}\left(\frac{\overline{V}_i - \overline{V}_j}{jx_S}\right)^{*} =$$

$$= -rb_S V_i V_j \sin(\Theta_{ij} + \gamma) + rb_S V_i^2 \sin\gamma + \tag{III.16}$$

$$+ j\left[rb_S V_i V_j \cos(\Theta_{ij} + \gamma) - rb_S V_i^2 \cos\gamma - r^2 b_S V_i^2\right]$$

Finally, the bus power injections of the UPFC (III.10-13) are obtained as it follows

$$P_{Si} = -rb_S V_i V_j \sin(\Theta_{ij} + \gamma), \tag{III.17}$$

$$Q_{Si} = -rb_S V_i^2 \cos\gamma + Q_{conv1}, \tag{III.18}$$

$$P_{Sj} = rb_S V_i V_j \sin(\Theta_{ij} + \gamma), \tag{III.19}$$

$$Q_{Sj} = rb_S V_i V_j \cos(\Theta_{ij} + \gamma). \tag{III.20}$$

Having the bus power injections of the UPFC obtained, there is the UPFC injection model completed (Fig. III.10).

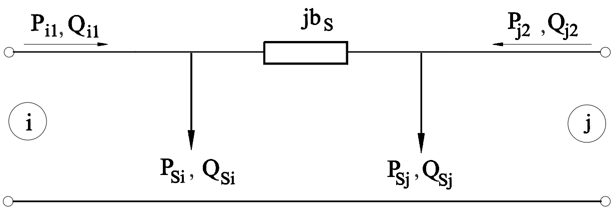

Fig. III.10 The UPFC injection model

Besides the bus power injections, it is very useful to have expressions for power flows from both sides of the UPFC injection model defined. At the UPFC shunt side, the active and reactive power flows are given as

$$P_{i1} = -rb_S V_i V_j \sin(\Theta_{ij} + \gamma) - b_S V_i V_j \sin\Theta_{ij}\,, \tag{III.21}$$

$$Q_{i1} = -rb_S V_i^2 \cos\gamma + Q_{conv1} - b_S V_i^2 + b_S V_i V_j \cos\Theta_{ij}\,, \tag{III.22}$$

whereas at the series side they are

$$P_{j2} = +rb_S V_i V_j \sin(\Theta_{ij} + \gamma) + b_S V_i V_j \sin\Theta_{ij}\,, \tag{III.23}$$

$$Q_{j2} = +rb_S V_i V_j \cos(\Theta_{ij} + \gamma) - b_S V_j^2 + b_S V_i V_j \cos\Theta_{ij}\,. \tag{III.24}$$

The UPFC injection model is thereby defined by the constant series branch susceptance, b_S, which is included in the system bus admittance matrix *[B]*, and the bus power injections P_{Si}, Q_{Si}, P_{Sj}, and Q_{Sj}. If there is a control objective to be achieved, the bus power injections are modified through changes of the UPFC parameters r, γ, and Q_{conv1}. Therefore, it is necessary to establish appropriate control system of the injection model which could govern the system to a pre-defined operating point by changing the set of the UPFC control parameters (r, γ, Q_{conv1}).

III.3 INJECTION MODEL CONTROL SYSTEM

The UPFC injection model needs a control system to be operated in a system-wise manner. In general, the control system, as it is proposed here, is of de-coupled single-input single-output proportional-integral type (Fig. III.11).

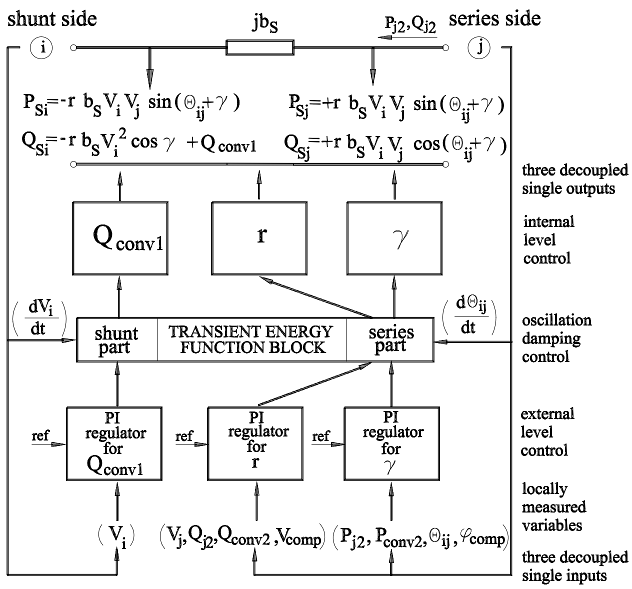

Fig. III.11 General form of the UPFC injection model control system

The selection of input/output signals depends on the predetermined control mode, which could be changed during the simulation.

Upon the basis of the general form, the control system is expanded to include more detailed representation of the regulation procedure (Fig. III.12).

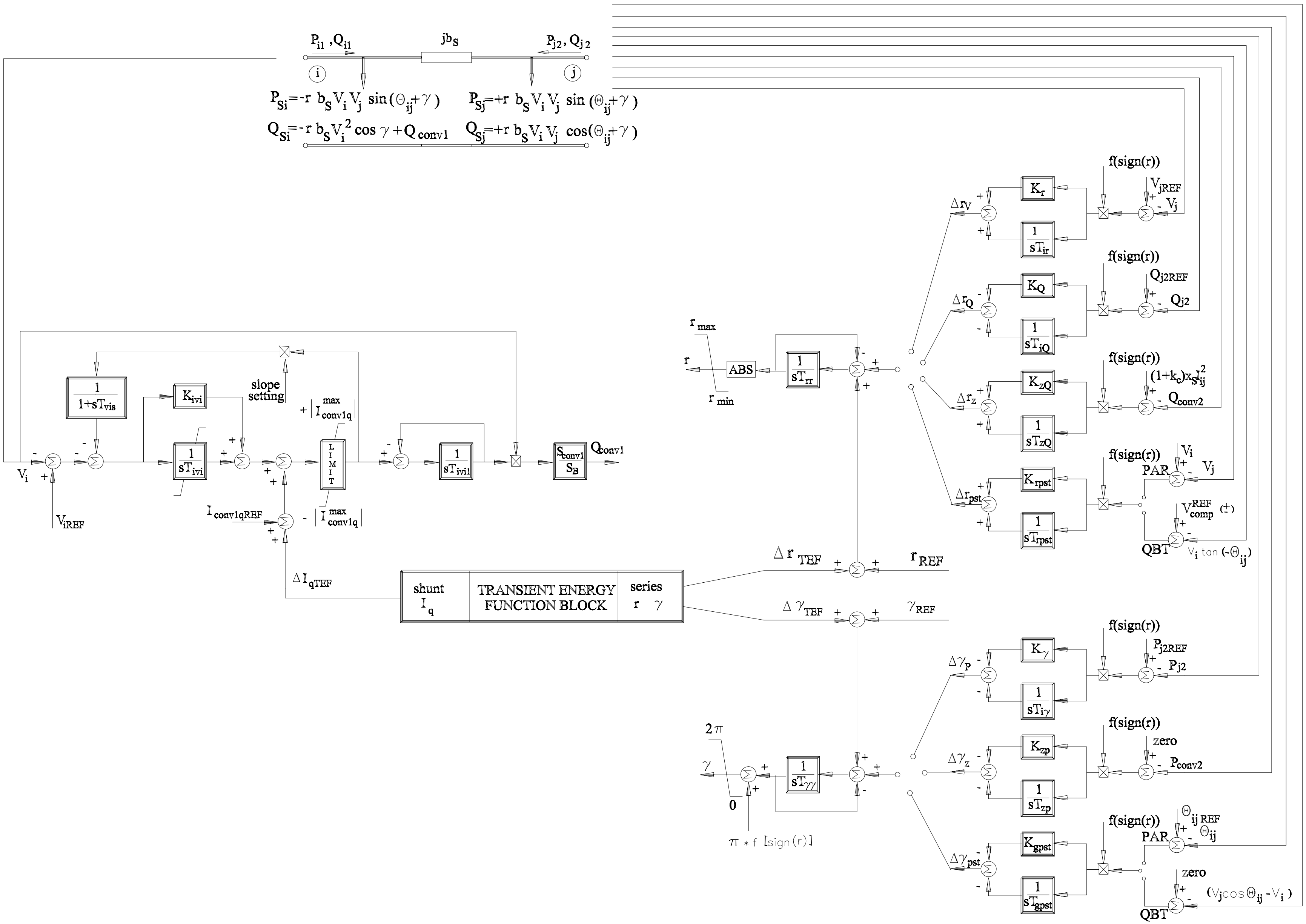

Fig. III.12 Detailed form of the UPFC injection model control system

At the external level, following locally measured variables of the UPFC are controlled:

- *by changing Q_{conv1}*
  - shunt side bus voltage magnitude, V_i,

- *by changing r*
  - series side bus voltage magnitude, V_j,
  - reactive power flow into series side bus, Q_{j2},
  - reactive power requirement of the series side converter CONV2, Q_{conv2}, or
  - compensating voltage magnitude, V_{comp}, and

- *by changing γ*
  - active power flow into the series side bus, P_{j2},
  - active power requirement of the series side converter CONV2, P_{conv2},
  - bus voltage angle difference, Θ_{ij}, or
  - compensating voltage angle, φ_{comp}.

In the model, the shunt side could be controlled only in the voltage mode, $V_i \leftrightarrow Q_{conv1}$, emphasising that Q_{conv1} represents reactive power loading of the shunt converter.

The series side could be controlled through the $r \Leftrightarrow \gamma$ pair in several different modes:

- bus voltage magnitude and active power flow, $V_j \Leftrightarrow P_{j2}$,
- reactive and active power flows, $Q_{j2} \Leftrightarrow P_{j2}$,
- series compensation, $Q_{conv2} \Leftrightarrow P_{conv2}(=0)$,
- phase shifting of Phase Angle Regulator (PAR) type, $V_j\,(=V_i) \Leftrightarrow \Theta_{ij}$, and
- phase shifting of Quadrature Booster Transformer (QBT) type, $V_{comp} \Leftrightarrow \varphi_{comp}(=\pi/2)$.

The variables are chosen to satisfy general $V \leftrightarrow Q$ and $\Theta \leftrightarrow P$ de-coupling. Therefore, the control system enables the UPFC injection model to participate in several different modes of operation fully utilising its versatile regulating capabilities.

III.4 OPERATING MODES OF THE UPFC

Generally, the UPFC participates in transmission voltage support at the shunt side and in power flow regulation at the series side. At the series side, bus voltage magnitude could be controlled as well, enabling voltage support at both sides of the UPFC during voltage emergency situations. Then, the angle γ, as the third parameter, could be used to fulfil a functional objective by simultaneous three-parameter control.

III.4.A Transmission voltage support

Bus voltage magnitudes could be supported at both sides of the UPFC. At the series side, voltage V_j is supported through the r-loop with appropriate adjustment of the angle γ. At the shunt side, the V_i-feedback enables support through the Q_{conv1}-loop.

If device losses are neglected, the active power requirement is equal for both converters (III.14, III.16)

$$\begin{aligned} P_{conv1} = P_{conv2} &= \mathrm{Re}\left(\overline{V}_S \overline{I}_{ij}^*\right) = \\ &= -rb_S V_i V_j \sin\left(\theta_{ij} + \gamma\right) + rb_S V_i^2 \sin\gamma \end{aligned} \quad . \qquad \text{(III.25)}$$

Thereby, the minimum nominal rating power S_{conv1n} of the shunt converter is given as a maximum active power demanded by the injected series voltage source

$$S_{conv1n} = \max\left|P_{conv1}(r,\gamma)\right| \, . \qquad \text{(III.26)}$$

Since the rating MVA capacity is not always fully utilised, there usually remains some capacity available for producing reactive power Q_{conv1}, and thereby for controlling the shunt side bus voltage magnitude V_i. The impact of the Q_{conv1} comes through the shunt side bus reactive power injection Q_{Si} of the UPFC injection model (Fig. III.10), which is given as

$$Q_{Si} = -rb_S V_i^2 \cos\gamma + Q_{conv1} \; . \qquad \text{(III.27)}$$

Thus, during the simulation it is necessary to check for the maximum available reactive power capacity max $|Q_{conv1}|$ (Fig. III.13), given as

$$\max\left|Q_{conv1}\right| = \sqrt{S_{conv1n}^2 - P_{conv1}^2(r,\gamma)} \; . \qquad \text{(III.28)}$$

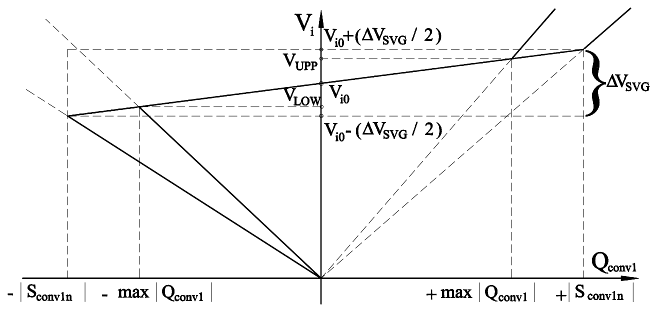

Fig. III.13 Maximum reactive power capacity of shunt converter

Maximum reactive power capacity is less or equal to the minimum nominal rating power of the shunt converter, depending on an active power loading level. If the active power loading level is zeroed, the slope of the voltage regulation characteristic is defined by the value ΔV_{SVG} corresponding to the range of doubled value of rating power S_{conv1n}. If the active power loading level is larger than zero, the controllable voltage range becomes $V_{LOW} \leq V_i \leq V_{UPP}$ due to decreased reactive power capability.

Generally, in the steady state operation the reactive power Q_{conv1} is found in the range

$$-\max\left|Q_{conv1}\right| \leq Q_{conv1} \leq +\max\left|Q_{conv1}\right| \, . \qquad \text{(III.29)}$$

However, in the model it is supposed that the thermal limits are set due to the total current flow through the shunt converter instead of the power flow. Therefore, the limiting conditions are accounted for by using reactive current

I_{conv1q} with certain transient short-term overload capability (Fig. III.14), which results with

$$-\left|I^{\max}_{conv1q}\right| \le I_{conv1q} \le +\left|I^{\max}_{conv1q}\right|, \quad \text{(III.30)}$$

where $I^{\max}_{conv1q}$ denotes maximum reactive current capability of the shunt converter [58, 323, 324, 328, 335].

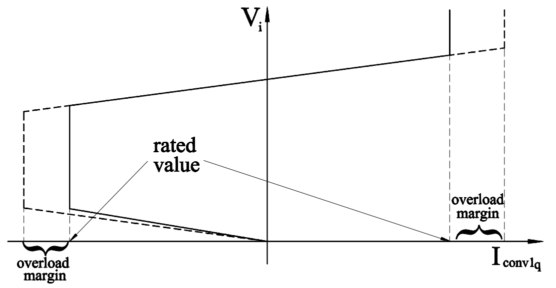

Fig. III.14. Short-term overload capability of shunt converter

A large part of attention should be paid to a proper computation of the maximum current conditions.

The total current of the shunt converter, $\bar{I}_{conv1}$, is given as

$$\bar{I}_{conv1} = I_{conv1p} + jI_{conv1q}, \quad \text{(III.31)}$$

where I_{conv1p} denotes the active part of the total current, and I_{conv1q} the reactive one.

Since the active part is demanded by the series voltage source, there is only the reactive part to be modified freely within allowed range.

The actual magnitude of the total current I_{conv1} is thereby defined as

$$I_{conv1} = \sqrt{I^2_{conv1p} + I^2_{conv1q}} = \frac{\sqrt{P^2_{conv1} + Q^2_{conv1}}}{V_i} = \frac{S_{conv1}}{V_i}, \quad \text{(III.32)}$$

where S_{conv1} denotes the actual value of the shunt converter apparent power whose active power is given by (III.25) and reactive power freely controlled within allowed range.

Since the nominal rating power S_{conv1n} is defined according to (III.26), the nominal rating current I_{conv1n} is computed as

$$I_{conv1n} = \frac{S_{conv1n}}{V_{inom}}, \quad \text{(III.33)}$$

where V_{inom} denotes per unit value of the shunt side bus voltage magnitude at which the nominal rating power S_{conv1n} results with the nominal rating current I_{conv1n}.

Thereby, the maximum reactive current capability of the shunt converter, $I^{\max}_{conv1q}$, is given as

$$I^{\max}_{conv1q} = \sqrt{I^2_{conv1n} - I^2_{conv1p}}. \quad \text{(III.34)}$$

The overload margin enables usage of the shunt converter overload in the transient short-term periods (Fig. III.14). The limiting action (Fig. III.15), depends on the current overload level, x, which is given as

$$x = \frac{I_{conv1}}{I_{conv1n}}. \quad \text{(III.35)}$$

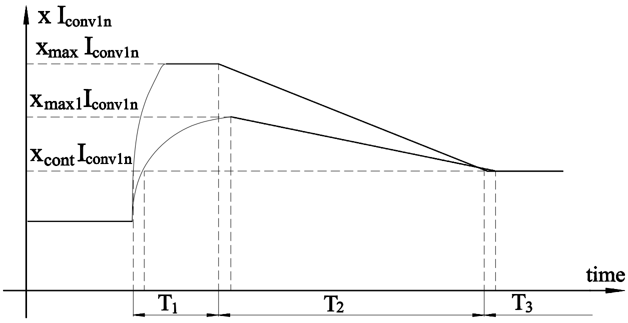

Fig. III.15 Limiting action in short-term overload of shunt converter

If the continuous operation limit is defined by x_{cont}, and the maximum short-term limit by x_{max}, then the overload level x is allowed to be in the range $x_{cont}<x\le x_{max}$ for the time span T_1. After the time T_1, the overload level x is linearly decreased from achieved maximum value x_{max1} down to the continuous limit x_{cont} in the time span T_2, according to

$$x = x_{\max 1} - \frac{x_{\max 1} - x_{cont}}{T_2}(t - T_1), \quad \text{(III.36)}$$

where t denotes time variable which takes zero value when the current overload appears. If the overload is linearly decreased to the continuous operation limit, the overloading capability is blocked for the next T_3 time span. If the overload level x is included in the consideration of the maximum reactive current $I^{\max}_{conv1q}$, equation (III.34) becomes

$$I^{\max}_{conv1q} = \sqrt{(xI_{conv1n})^2 - I^2_{conv1p}}. \quad \text{(III.37)}$$

Whenever the demanded active current I_{conv1p} is larger than the nominal rating current I_{conv1}, the maximum reactive current $I^{\max}_{conv1q}$ is zeroed, disabling thereby any reactive power support from Q_{conv1}.

By setting appropriate V_i-feedback control in an SVG manner (Fig. III.16), the reactive current I_{conv1q} (consequently Q_{conv1}) keeps the shunt side bus voltage magnitude V_i at the referent value V_{iREF} whenever there is enough remaining reactive capacity $I^{\max}_{conv1q}$ in the shunt converter.

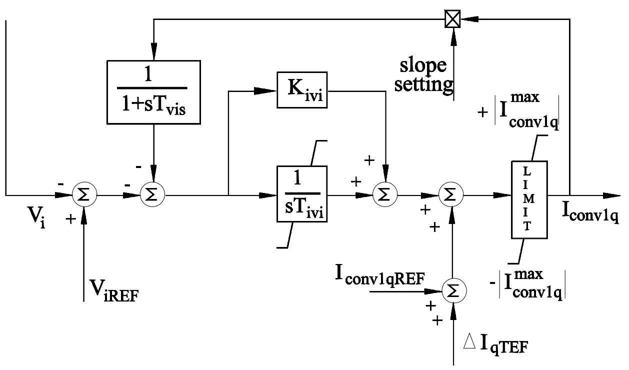

Fig. III.16 The UPFC shunt side control system

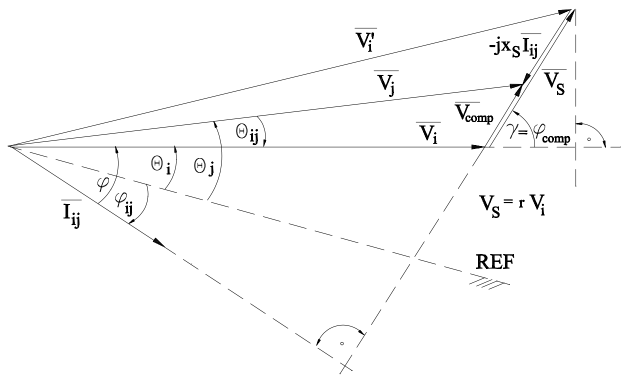

Fig. III.17 Series compensation mode of the UPFC

The UPFC shunt side control system is based on a proportional-integral type with gain K_{ivi} and time constant T_{ivi}. The voltage V_i regulation characteristic is given as

$$V_i = V_{i0} + \frac{\Delta V_{SVG} V_{inom}}{2 S_{conv1n}} I_{conv1q} \,, \qquad \text{(III.38)}$$

where $(\Delta V_{SVG} V_{inom})/(2 S_{conv1n})$ denotes slope setting of the characteristic which acts after T_{vis} lagging. The reference value of the reactive current, $I_{conv1qREF}$, is set at the initial steady state operating point, and is modified with damping output ΔI_{qTEF} during period with electromechanical oscillations.

III.4.B Power flow regulation

At the series side of the UPFC, priority is given to power flow control. The active, P_{j2}, and reactive, Q_{j2}, power flow into the j-bus of the UPFC are defined according to (III.23-24). The active power flow is controlled through the γ-loop, and the reactive power flow through the r-loop. Control system is of proportional-integral type with corresponding gains and time constants. Since the magnitude r is supposed to be non-negative, at each time when it hits zero value trying to cross to a negative range, the angle γ gets π rad added, keeping the absolute value of the magnitude r. Function *f(sign(r))* serves to adjust for these changes.

Instead of the reactive power flow control at the series side, it is possible to control bus voltage magnitude V_j through the r-loop. Thereby, the UPFC could give voltage support at both sides simultaneously. This is considered to be the most useful property during voltage emergency situations.

III.4.C Series compensation

Setting the angle γ in a position that results with

$$\gamma = \pi / 2 - \varphi \,, \qquad \text{(III.39)}$$

the series compensation mode of the UPFC injection model is attained. In that case (Fig. III.17), the vectors $\overline{V}_S$ and $\overline{V}_{comp}$ are co-linear and perpendicular to the current $\overline{I}_{ij}$.

Therefore, following relation holds

$$V_i \sin\gamma = V_j \sin\left(\Theta_{ij} + \gamma\right) , \qquad \text{(III.40)}$$

which makes the active power of the series converter, P_{conv2} from (III.25), equal to zero. It comes out that if the active power P_{conv2} is kept at zero value through the γ-loop, the characteristic ($V \Leftrightarrow I$) perpendicular form of the vector diagram is obtained.

The r-loop is controlled by feedback of the reactive power of the series converter Q_{conv2}. From (III.5), the current $\overline{I}_{ij}$ is generally defined as

$$\overline{I}_{ij} = \left(\overline{V}'_i - \overline{V}_j\right) / jx_S = \left[(P_{conv2} + jQ_{conv2}) / \overline{V}_S \right]^* . \qquad \text{(III.41)}$$

Since the magnitude V_S is equal to rV_i, this expression is rather inconvenient to be employed during simulation of transient periods due to division by parameter r, which could take zero value. To be used in the series compensation mode solely, following relations are applied instead

$$I_{ij} = \sqrt{P_{i1}^2 + (Q_{i1} - Q_{conv1})^2} \,/ V_i \,, \qquad \text{(III.42)}$$

$$\varphi = \Theta_i + arctg[-(Q_{i1} - Q_{conv1}) / P_{i1}] . \qquad \text{(III.43)}$$

The injected series voltage $\overline{V}_S$ is given as

$$\overline{V}_S = \overline{V}_{comp} + jx_S \overline{I}_{ij} \,. \qquad \text{(III.44)}$$

If (III.44) is multiplied by $\overline{I}_{ij}^*$, it results with

$$\overline{V}_S \overline{I}_{ij}^* = \overline{V}_{comp} \overline{I}_{ij}^* + jx_S I_{ij}^2 \,. \qquad \text{(III.45)}$$

If the proportionality factor k_c is defined as

$$k_c = \frac{V_{comp}}{x_S I_{ij}} \,, \qquad \text{(III.46)}$$

then due to zero value of the active power P_{conv2}, equation (III.45) is written as

$$jQ_{conv2} = jk_c x_S I_{ij}^2 + jx_S I_{ij}^2 \,. \tag{III.47}$$

More conveniently, equation (III.47) is written as

$$(1+k_c)x_S I_{ij}^2 - Q_{conv2} = 0 \,. \tag{III.48}$$

Using (III.48) as a basic equation in the *r*-loop, the voltage magnitude V_{comp} is adjusted by setting proportionality factor k_c at appropriate value. If the factor k_c is set to zero, then the series voltage magnitude V_S is equal to $x_S I_{ij}$, whereas the bus voltage angles from both sides of the UPFC are equal ($\Theta_i = \Theta_j$). Thereby, the reactance x_S between buses *i* and *j* is fully compensated. Having $k_c<0$ ($k_c>0$), the total reactance between buses *i* and *j* is made to be inductive (capacitive) with respect to the current I_{ij}.

III.4.D Phase shifting

Phase shifting mode of the UPFC could be achieved operating it either as the Phase Angle Regulator (PAR) or the Quadrature Booster Transformer (QBT).

In the PAR operation, the bus voltage magnitudes V_i and V_j should be set equal (Fig. III.18).

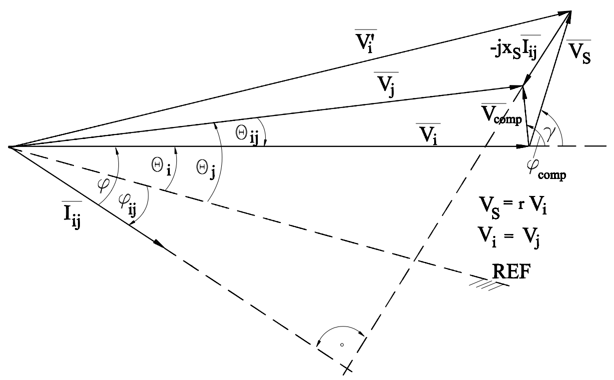

Fig. III.18 Phase angle regulator (PAR) mode of the UPFC

The equalisation of the magnitudes is imposed through the *r*-loop, by setting

$$V_i - V_j = 0 \,. \tag{III.49}$$

Then, the UPFC bus voltage angle difference Θ_{ij}, which is equal to Θ_i-Θ_j, is set equal to the predetermined referent value Θ_{ijREF} through the γ-loop. By changing referent value Θ_{ijREF}, the PAR phase shifting operation mode is applied.

In the QBT operation, the voltage $\overline{V}_{comp}$ should be set perpendicular to the shunt side bus voltage $\overline{V}_i$ (Fig. III.19).

Thus, the angle γ is set at the position defined by

$$\varphi_{comp}^{REF} - \varphi_{comp} = 0; \quad \varphi_{comp}^{REF} = \pi/2 \; or \; 3\pi/2. \tag{III.50}$$

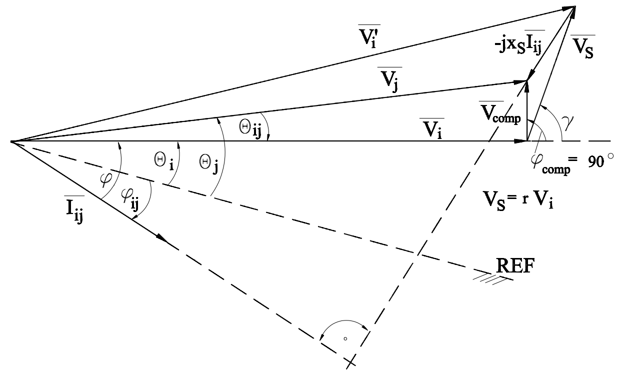

Fig. III.19 Quadrature booster transformer (QBT) mode of the UPFC

Concerning the magnitude of the voltage $\overline{V}_{comp}$, following relation should be satisfied

$$V_{comp} = \sqrt{V_i^2 + V_j^2 - 2V_iV_j\cos\Theta_{ij}} \,. \tag{III.51}$$

Accordingly, the angle of the voltage $\overline{V}_{comp}$ is defined by

$$\varphi'_{comp} = arc\cos\left[\left(V_j\cos\Theta_{ij} - V_i\right)/V_{comp}\right], \tag{III.52}$$

where

$$\begin{array}{l} for\ (\Theta_{ij} \le 0) \;\Rightarrow\; \varphi_{comp} = \varphi'_{comp} \\ for\ (\Theta_{ij} > 0) \;\Rightarrow\; \varphi_{comp} = 2\pi - \varphi'_{comp} \end{array} . \tag{III.53}$$

Therefore, in the QBT mode the *r*-loop is controlled to hold

$$V_{comp}^{REF} - V_i\tan(-\Theta_{ij}) = 0\,, \tag{III.54}$$

whereas the γ-loop holds

$$V_j\cos\Theta_{ij} - V_i = 0 \,. \tag{III.55}$$

In (III.54), the referent value V_{comp}^{REF} is allowed to be positive or negative, defining whether the angle φ_{comp} is equal to $\pi/2$ or $3\pi/2$.

III.4.E Damping of electromechanical oscillations

Besides the regulators, the control system incorporates a strategy for damping of electromechanical oscillations induced by large disturbances, e.g. three-phase short circuit. The strategy is of take-over type and is based on a transient energy function (TEF), using time derivatives of local variables from both sides of the UPFC [109-111, 265, 268-269]. The shunt part of the transient energy function block uses information from dV_i/dt, whereas the series part from $d\Theta_{ij}/dt$.

The control law for the shunt part is based on the function $\dot{v}_{sh}$, which is given as

$$\dot{v}_{sh} = -\frac{Q_{conv1}}{V_i}\frac{dV_i}{dt} \le 0\,, \tag{III.56}$$

where Q_{conv1} is positive when flowing out of the bus.

The output of the TEF-I_q shunt part is defined according to

$$\Delta I_{qTEF} = k_l\left(gain\left|\frac{dV_i}{dt}\right|\right)k_k\,, \tag{III.57}$$

where k_l is defined as

$$k_l = \begin{cases} +1; & if\ [(k_k = -1)\ or\ (k_k = +1)] \\ 0; & if\ (k_k = 0) \end{cases}, \tag{III.58}$$

and k_k as

$$k_k = \begin{cases} -1; & if\left[\left(\frac{dV_i}{dt} < -\varepsilon\right) and\ \ (Q_{conv\ 1} > 0)\right] \\ +1; & if\left[\left(\frac{dV_i}{dt} > +\varepsilon\right) and\ \ (Q_{conv\ 1} < 0)\right] \\ 0; & if\left(-\varepsilon \le \frac{dV_i}{dt} \le +\varepsilon\right) \end{cases}. \tag{III.59}$$

The control law for the series part is based on the function $\dot{v}_{ser}$, which is given as

$$\dot{v}_{ser} = P_{Sj}\frac{d\Theta_{ij}}{dt} = rb_sV_iV_j\sin(\Theta_{ij}+\gamma)\frac{d\Theta_{ij}}{dt} \le 0\,, \tag{III.60}$$

where $b_s<0$.

The output of the TEF-(r,γ) series part is defined as

$$\begin{aligned} \Delta r_{TEF} &= \left(r_{\max}\ gain\left|\frac{d\Theta_{ij}}{dt}\right|\right)k_j \\ \Delta\gamma_{TEF} &= \left(k_i\frac{\pi}{2} - \Theta_{ij}\right)k_j \end{aligned}, \tag{III.61}$$

where k_j is given as

$$k_j = \begin{cases} +1; & if\ [(k_i = -1)\ or\ (k_i = +1)] \\ 0; & if\ (k_i = 0) \end{cases}, \tag{III.62}$$

and k_i as

$$k_i = \begin{cases} -1; & if\left[\left(\frac{d\Theta_{ij}}{dt} < -\varepsilon\right) and\ \left(\sin(\Theta_{ij}+\gamma) > 0\right)\right] \\ +1; & if\left[\left(\frac{d\Theta_{ij}}{dt} > +\varepsilon\right) and\ \left(\sin(\Theta_{ij}+\gamma) < 0\right)\right] \\ 0; & if\left(-\varepsilon \le \frac{d\Theta_{ij}}{dt} \le +\varepsilon\right) \end{cases}. \tag{III.63}$$

Within the dissertation, pre-established voltage collapse scenarios include dynamic phenomena induced by three-phase short circuit. The disturbance is neutralised by outage of the faulted line. As a consequence, electromechanical oscillations arise which could be effectively damped by the UPFC using TEF method. Since the voltage stability problem is considered to be the main issue of the dissertation, the attention is only marginally paid to the damping capability of the UPFC. The damping capability is concerned to give broader rather than deeper insight to the UPFC application. The analytical activities are directed dominantly toward voltage support capability.

III.4.F Optimal rating of the UPFC

Operation of the UPFC demands proper power rating of the series and shunt branches. The rating should enable the UPFC carrying out pre-defined regulation tasks without becoming overloaded. Therefore, the algorithm for optimal rating of the UPFC [266-267] is employed here to give an initial estimate on minimum nominal dimensioning which satisfies pre-defined power flow objective (Fig. III.20).

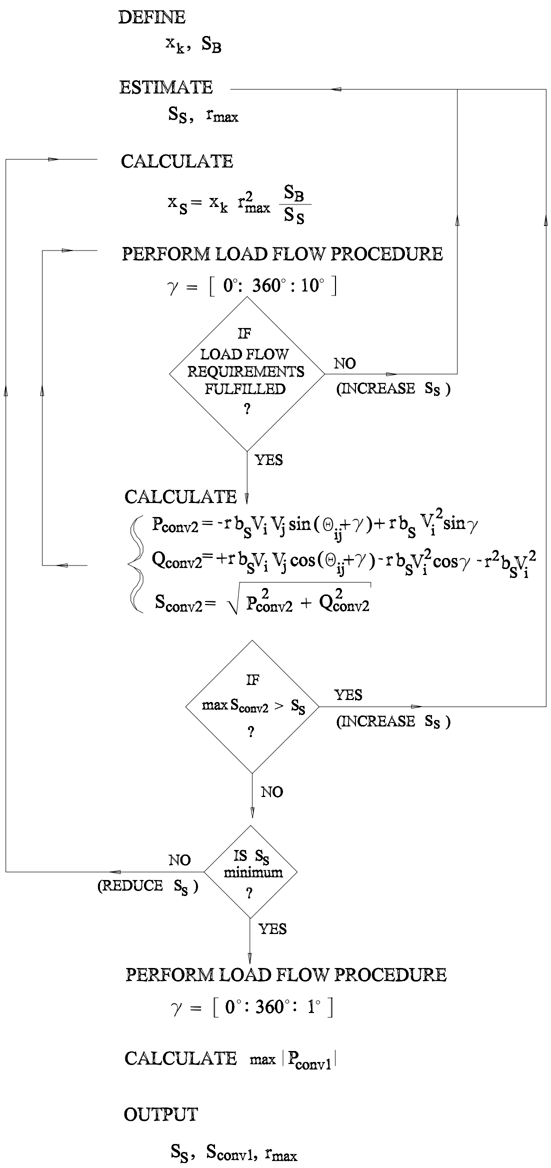

Fig. III.20 Algorithm for optimal rating of the UPFC

The algorithm starts with definition of the series transformer short circuit reactance, x_k, and the system base power, S_B. Then, the initial estimation is given for the series converter rating power, S_S, and the maximum magnitude of the injected series voltage, r_{max}. Computation of the UPFC reactance seen from the terminals of the series transformer, x_S, is followed with its inclusion in all relevant system bus admittance matrices.

Load flows are computed changing the angle γ between 0° and 360° in steps of 10°, with the magnitude r kept at its maximum value r_{max}. Such a rotational change of the UPFC parameter influences active and reactive power flows in the system. Obviously, the largest impact is given to the power flowing through the line where the UPFC is installed. Therefore, the regulation of the active and reactive power flow through the series branch of the UPFC could be set as initial pre-defined objective to be achieved within the UPFC steady state operation. Then, the load flow procedure is performed to check whether the pre-defined objective is achieved with satisfactorily estimated parameters. If the load flow requirements are not satisfied at any of the operating points of the rotational change, it is necessary to get back in the algorithm, again estimate S_S and r_{max}, and perform new rotational change of the UPFC within the load flow procedure. This loop is performed until the load flow requirements are completely fulfilled for each operating point. Upon fulfilment of the requirements, the active, reactive, and apparent power of the series converter are calculated for each step change in the angle γ.

Having the load flow requirements fulfilled and the series converter powers calculated, it is checked whether the maximum value of the series converter apparent power, max S_{conv2}, is larger than the initially estimated power S_S. If max S_{conv2} is larger than S_S, it is necessary to increase power S_S and start the loop again until this condition is satisfied. If max S_{conv2} is not larger than the power S_S, it is necessary to check whether the power S_S is at an acceptable minimum level. If not, the value of S_S is reduced and the loop is started all over again. The acceptable minimum is achieved when two consecutive iterations do not differ more than a pre-established tolerance.

Having the power S_S minimised, the load flow procedure is performed with smaller step of rotational change of the angle γ (1°), calculating maximum absolute value of the series/shunt converter active power, max $|P_{conv1}|$. The value given by max $|P_{conv1}|$ is considered to be minimal criteria for dimensioning shunt converter rating power, whereas the power S_S represents series converter rating power as a function of the maximum magnitude r_{max}.

Described algorithm is based on a steady state load flow procedure. The series branch of the UPFC is dimensioned according to the power flow regulation objective, whereas the shunt one just to satisfy active power demand from the series branch.

If a dynamic load flow procedure with voltage-dependent loads is introduced instead of the steady state one, the rating powers could be different due to changes in bus voltage magnitudes.

If a damping of electromechanical oscillations is of larger concern, then the series branch could be dimensioned with larger magnitude r_{max}, and increased value of the series converter rating power S_{conv2n}.

If the voltage stability problem is of concern, then the shunt branch could be dimensioned with increased value of the shunt converter rating power S_{conv1n}. Thereby, the voltage support capability is increased by having larger maximum value of the shunt converter reactive power, Q_{conv1}, remained upon satisfying active power demand from the series branch.

Therefore, described algorithm serves only as the initial estimation of the UPFC dimensioning, followed by further thorough analysis when the other operational aspects are of concern.

III.4.G Inclusion of the UPFC in load flow procedure

The UPFC is modelled by using its injection model with active and reactive powers injected at terminal buses from both sides. Generally, its inclusion in the load flow procedure has an impact on the network equations written for i and j-bus due to the load power injections P_{Si}, Q_{Si}, P_{Sj}, and Q_{Sj} (Fig. III.10). Therefore, for the UPFC incidental buses the algebraic bus network equations (II.116-117) are rewritten as

$$\begin{aligned} & P_k(\Theta,V)+P_d(x_P,V)+P_S(V,\Delta f)+ \\ & +P_{eTCL}(G,V)+P_{Ti\,or\,j}(\Theta,V,t_r)+ \ , \\ & +P_{Si\,or\,j}(\Theta,V,r,\gamma,I_{conv1q})=0 \end{aligned} \tag{III.64}$$

$$\begin{aligned} & Q_k(\Theta,V)+Q_d(x_Q,V)+Q_S(V,\Delta f)+ \\ & +Q_{SH}(b_{SH},V)+Q_{Ti\,or\,j}(\Theta,V,t_r)+ \ . \\ & +Q_{Si\,or\,j}(\Theta,V,r,\gamma,I_{conv1q})=0 \end{aligned} \tag{III.65}$$

The algebraic bus network equations (III.64-65) have additional terms in both active and reactive powers. It means that four of the network equations are influenced when the UPFC is included in the system.

The equations for the bus incidental with the UPFC shunt i and series j-bus with no other elements connected are stated as

$$\begin{aligned} P_i(\Theta,V) &= \sum_{m=1}^{n}(G_{im}V_iV_m\cos\Theta_{im}+B_{im}V_iV_m\sin\Theta_{im})- \\ & -rb_SV_iV_j\sin(\Theta_{ij}+\gamma) \end{aligned} \tag{III.66}$$

$$\begin{aligned} Q_i(\Theta,V) &= \sum_{m=1}^{n}(G_{im}V_iV_m\sin\Theta_{im}-B_{im}V_iV_m\cos\Theta_{im})- \\ & -rb_SV_i^2\cos\gamma+Q_{conv1} \end{aligned} \tag{III.67}$$

$$P_j(\Theta,V)=\sum_{m=1}^{n}\left(G_{jm}V_jV_m\cos\Theta_{jm}+B_{jm}V_jV_m\sin\Theta_{jm}\right)+ \\ +rb_SV_iV_j\sin(\Theta_{ij}+\gamma) \tag{III.68}$$

$$Q_j(\Theta,V)=\sum_{m=1}^{n}\left(G_{jm}V_jV_m\sin\Theta_{jm}-B_{jm}V_jV_m\cos\Theta_{jm}\right)+ \\ +rb_SV_iV_j\cos(\Theta_{ij}+\gamma) \tag{III.69}$$

In equation (III.67), the term Q_{conv1} equals to (I_{conv1q} V_i S_{conv1n} / S_B), enabling the current I_{conv1q} to be set as a parameter.

Since the Newton-Raphson load flow procedure [18, 191, 356] employs partial derivatives of the network equations with respect to the voltage angles, Θ, and magnitudes, V, there are at most 16 positions in the Jacobian matrix to be concerned due to the UPFC injection model.

These positions are filled with on and off-diagonal terms given as

on-diagonal terms

$$\frac{\partial P_i}{\partial\Theta_i}=-\sum_{\substack{m=1\\m\neq i}}^{n}\left(G_{im}V_iV_m\sin\Theta_{im}-B_{im}V_iV_m\cos\Theta_{im}\right)- \\ -rb_SV_iV_j\cos(\Theta_{ij}+\gamma) \tag{III.70}$$

$$\frac{\partial P_i}{\partial V_i}=\sum_{\substack{m=1\\m\neq i}}^{n}\left(G_{im}V_m\cos\Theta_{im}+B_{im}V_m\sin\Theta_{im}\right)+2G_{ii}V_i- \\ -rb_SV_j\sin(\Theta_{ij}+\gamma) \tag{III.71}$$

$$\frac{\partial Q_i}{\partial\Theta_i}=\sum_{\substack{m=1\\m\neq i}}^{n}\left(G_{im}V_iV_m\cos\Theta_{im}+B_{im}V_iV_m\sin\Theta_{im}\right) \tag{III.72}$$

$$\frac{\partial Q_i}{\partial V_i}=\sum_{\substack{m=1\\m\neq i}}^{n}\left(G_{im}V_m\sin\Theta_{im}-B_{im}V_m\cos\Theta_{im}\right)-2B_{ii}V_i- \\ -2rb_SV_i\cos\gamma+I_{conv1q}\frac{S_{conv1n}}{S_B} \tag{III.73}$$

$$\frac{\partial P_j}{\partial\Theta_j}=-\sum_{\substack{m=1\\m\neq j}}^{n}\left(G_{jm}V_jV_m\sin\Theta_{jm}-B_{jm}V_jV_m\cos\Theta_{jm}\right)- \\ -rb_SV_iV_j\cos(\Theta_{ij}+\gamma) \tag{III.74}$$

$$\frac{\partial P_j}{\partial V_j}=\sum_{\substack{m=1\\m\neq j}}^{n}\left(G_{jm}V_m\cos\Theta_{jm}+B_{jm}V_m\sin\Theta_{jm}\right)+2G_{jj}V_j+ \\ +rb_SV_i\sin(\Theta_{ij}+\gamma) \tag{III.75}$$

$$\frac{\partial Q_j}{\partial\Theta_j}=\sum_{\substack{m=1\\m\neq j}}^{n}\left(G_{jm}V_jV_m\cos\Theta_{jm}+B_{jm}V_jV_m\sin\Theta_{jm}\right)+ \\ +rb_SV_iV_j\sin(\Theta_{ij}+\gamma) \tag{III.76}$$

$$\frac{\partial Q_j}{\partial V_j}=\sum_{\substack{m=1\\m\neq j}}^{n}\left(G_{jm}V_m\sin\Theta_{jm}-B_{jm}V_m\cos\Theta_{jm}\right)-2B_{jj}V_j+ \\ +rb_SV_i\cos(\Theta_{ij}+\gamma) \tag{III.77}$$

off-diagonal terms

$$\frac{\partial P_i}{\partial\Theta_j}=G_{ij}V_iV_j\sin\Theta_{ij}-B_{ij}V_iV_j\cos\Theta_{ij}+ \\ +rb_SV_iV_j\cos(\Theta_{ij}+\gamma) \tag{III.78}$$

$$\frac{\partial P_i}{\partial V_j}=G_{ij}V_i\cos\Theta_{ij}+B_{ij}V_i\sin\Theta_{ij}- \\ -rb_SV_i\sin(\Theta_{ij}+\gamma) \tag{III.79}$$

$$\frac{\partial Q_i}{\partial\Theta_j}=-G_{ij}V_iV_j\cos\Theta_{ij}-B_{ij}V_iV_j\sin\Theta_{ij} \tag{III.80}$$

$$\frac{\partial Q_i}{\partial V_j}=G_{ij}V_i\sin\Theta_{ij}-B_{ij}V_i\cos\Theta_{ij} \tag{III.81}$$

$$\frac{\partial P_j}{\partial\Theta_i}=-G_{ji}V_iV_j\sin\Theta_{ij}-B_{ji}V_iV_j\cos\Theta_{ij}+ \\ +rb_SV_iV_j\cos(\Theta_{ij}+\gamma) \tag{III.82}$$

$$\frac{\partial P_j}{\partial V_i}=G_{ji}V_j\cos\Theta_{ij}-B_{ji}V_j\sin\Theta_{ij}+ \\ +rb_SV_j\sin(\Theta_{ij}+\gamma) \tag{III.83}$$

$$\frac{\partial Q_j}{\partial\Theta_i}=-G_{ji}V_iV_j\cos\Theta_{ij}+B_{ji}V_iV_j\sin\Theta_{ij}- \\ -rb_SV_iV_j\sin(\Theta_{ij}+\gamma) \tag{III.84}$$

$$\frac{\partial Q_j}{\partial V_i}=-G_{ji}V_j\sin\Theta_{ij}-B_{ji}V_j\cos\Theta_{ij}+ \\ +rb_SV_j\cos(\Theta_{ij}+\gamma) \tag{III.85}$$

As it is seen from (III.70-85), the actual number of the concerned positions is smaller than 16. This happens because the UPFC reactive load power injection Q_{Si} depends on V_i, and does not depend on Θ_i, Θ_j, and V_j. Thus, at the three of the positions, it is not necessary to provide the corrections, namely $\partial Q_i/\partial\Theta_i$, $\partial Q_i/\partial\Theta_j$, and $\partial Q_i/\partial V_j$. It makes total of 13 positions to be concerned due to the impact of the UPFC injection model.

The UPFC injection model is included in the differential-algebraic model of the system through its impact on the Jacobian matrix.

IV. DIFFERENTIAL-ALGEBRAIC MODEL

IV.1 OVERALL SYSTEM MODEL

The voltage stability problem is analysed from two aspects, a large disturbance (dynamic) aspect and a small disturbance (static) one. The large disturbance aspect is orientated towards the appearance of a three-phase short circuit and addresses post-contingency system response. The small signal aspect investigates the stability of an operating point and needs development of linearised model.

It is supposed that the system has following set of differential-algebraic equations [35, 82, 191, 287-288, 301-302]

$$\frac{dx}{dt} = f(x, y, p)\,, \tag{IV.1}$$

$$0 = g(x, y, p)\,, \tag{IV.2}$$

where x denotes state variables, y algebraic variables, p arbitrary parameters, f differential equations, and g algebraic ones.

By using models described in previous Chapters, differential and algebraic equations of the system in general are given as follows

generator differential equations (gde)

$$\frac{d\delta}{dt} = \omega - 1 \tag{IV.3}$$

$$\frac{d\omega}{dt} = \frac{T_m}{\tau_j} - \frac{E_d^{'} I_d + E_q^{'} I_q - (x_q^{'} - x_d^{'}) I_d I_q}{\tau_j} - \frac{D(\omega - 1)}{\tau_j} \tag{IV.4}$$

$$\frac{dE_q^{'}}{dt} = \frac{E_{FD} - E_I}{\tau'_{d0}} = \frac{E_{FD} - E_q^{'} + (x_d - x_d^{'}) I_d}{\tau'_{d0}} \tag{IV.5}$$

$$\frac{dE_d^{'}}{dt} = -\frac{E_d^{'} + (x_q - x_q^{'}) I_q}{\tau'_{q0}} \tag{IV.6}$$

$$\frac{dE_{FD}}{dt} = \frac{K_A (V_{REF} - V_n - V_{OEL} + OFF1) - E_{FD}}{\tau_A} \tag{IV.7}$$

$$\begin{aligned} \frac{dGOV1}{dt} &= \frac{\omega_{REF} - \omega}{\tau_1 R} - \frac{GOV1}{\tau_1} - \frac{\tau_2}{\tau_1 R \tau_j} T_m + \\ &+ \frac{\tau_2}{\tau_1 R \tau_j} \left[E_d^{'} I_d + E_q^{'} I_q - (x_q^{'} - x_d^{'}) I_d I_q \right] + \\ &+ \frac{\tau_2 D}{\tau_1 R \tau_j} (\omega - 1) \end{aligned} \tag{IV.8}$$

$$\frac{dGOV4}{dt} = \frac{GOV3 - GOV4}{\tau_3} = \frac{P_{m0} + GOV1 - GOV4}{\tau_3} \tag{IV.9}$$

$$\frac{dGOV5}{dt} = \frac{GOV4 - GOV5}{\tau_4} \tag{IV.10}$$

$$\begin{aligned} \frac{dT_m}{dt} &= \frac{GOV5}{\omega \tau_5} - \frac{T_m}{\tau_5} + \frac{F}{\tau_4} \frac{GOV4 - GOV5}{\omega} - \frac{T_m^2}{\omega \tau_j} + \\ &+ \frac{T_m}{\omega \tau_j} \left[E_d^{'} I_d + E_q^{'} I_q - \left(x_q^{'} - x_d^{'} \right) I_d I_q \right] + \\ &+ \frac{T_m D}{\tau_j} \left(1 - \frac{1}{\omega}\right) \end{aligned} \tag{IV.11}$$

$$\frac{dV_{OEL}}{dt} = \frac{(I_{FD} - I_{FLM2}) K_2 K_3}{T_{OEL}} \tag{IV.12}$$

motor differential equations (mde)

$$\frac{dE_q^{'}}{dt} = (\omega_{0S} - \omega_m) E_d^{'} - \frac{E_q^{'}}{T_0^{'}} - \frac{X - X'}{T_0^{'}} I_d \tag{IV.13}$$

$$\frac{dE_d^{'}}{dt} = -(\omega_{0S} - \omega_m) E_q^{'} - \frac{E_d^{'}}{T_0^{'}} + \frac{X - X'}{T_0^{'}} I_q \tag{IV.14}$$

$$\begin{aligned} \frac{d\omega_m}{dt} &= \left\{ \left(E_d^{'} I_d + E_q^{'} I_q \right) - \right. \\ &\left. - \omega_{0S} T_{m0} \left[A \left(\frac{\omega_m}{\omega_{m0}} \right)^2 + B \left(\frac{\omega_m}{\omega_{m0}} \right) + C + D \left(\frac{\omega_m}{\omega_{m0}} \right)^{am} \right] \right\} \Big/ (2H\omega_{0S}) \end{aligned} \tag{IV.15}$$

differential equation of dynamic non-linear recovery active power load (dyn$_p$)

$$\frac{dx_P}{dt} = -\frac{x_P}{T_P} + P_S(V_n) - \frac{k_P V_n^{\alpha}}{\alpha T_P} = P_S(V_n) + P_k(\Theta, V) \tag{IV.16}$$

differential equation of dynamic non-linear recovery reactive power load (dyn$_q$)

$$\frac{dx_Q}{dt} = -\frac{x_Q}{T_Q} + Q_S(V_n) - \frac{k_Q V_n^{\alpha}}{\alpha T_Q} = Q_S(V_n) + Q_k(\Theta, V) \tag{IV.17}$$

differential equations of thermostatically controlled load (tcl)

$$\frac{d\tau_H}{dt} = -\frac{\tau_H}{T_1} + \frac{K_1}{T_1} G V_n^2 + \frac{\tau_A}{T_1} \tag{IV.18}$$

$$\begin{aligned} \frac{dG}{dt} &= \left(\frac{K_P}{T_1} - \frac{K_I}{T_C} \right) \tau_H - \frac{K_P K_1}{T_1} G V_n^2 + \\ &+ \frac{\tau_{REF} K_I}{T_C} - \frac{K_P \tau_A}{T_1} \end{aligned} \tag{IV.19}$$

active power network algebraic equations (nae_p)

$$0 = P_k(\Theta,V) + P_d(x_P,V) + P_S(V,\Delta f) + \\ + P_{eTCL}(G,V) + P_{Ti\,or\,j}(\Theta,V,t_r) + \\ + P_{Si\,or\,j}(\Theta,V,r,\gamma,I_{conv1q}) \tag{IV.20}$$

reactive power network algebraic equations (nae_q)

$$0 = Q_k(\Theta,V) + Q_d(x_Q,V) + Q_S(V,\Delta f) + \\ + Q_{SH}(b_{SH},V) + Q_{Ti\,or\,j}(\Theta,V,t_r) + \\ + Q_{Si\,or\,j}(\Theta,V,r,\gamma,I_{conv1q}) \tag{IV.21}$$

generator algebraic equations (gae)

$$0 = E_d' - V_d - rI_d - x_d' I_q - (x_q' - x_d')I_q \tag{IV.22}$$

$$0 = E_q' - V_q - rI_q + x_d' I_d \tag{IV.23}$$

$$0 = V_d - V_n \sin(\Theta_n - \delta) \tag{IV.24}$$

$$0 = V_q - V_n \cos(\Theta_n - \delta) \tag{IV.25}$$

$$0 = E_q' - (x_d - x_d')I_d - I_{FD} \tag{IV.26}$$

motor algebraic equations (mae)

$$0 = -X'E_q' + R_S E_d' + (R_S^2 + X'^2)I_d - R_S V_d + X'V_q \tag{IV.27}$$

$$0 = R_S E_q' + X'E_d' + (R_S^2 + X'^2)I_q - X'V_d - R_S V_q \tag{IV.28}$$

$$0 = V_d - V_n \sin\Theta_n \tag{IV.29}$$

$$0 = V_q - V_n \cos\Theta_n \tag{IV.30}$$

From differential and algebraic equations (IV.3-30), it is concluded that the vector of the state variables is defined as

$$x = [\,\delta, \omega, E_q', E_d', E_{FD}, GOV1, GOV4, GOV5, \\ T_m, V_{OEL}, E_q', E_d', \omega_m, x_P, x_Q, \tau_H, G]^{\tau}, \tag{IV.31}$$

whereas the vector of the algebraic variables is

$$y = [\,\Theta_{1\ldots n}, V_{1\ldots n}, I_d, I_q, V_d, V_q, I_{FD}, I_d, I_q, V_d, V_q]^{\tau}. \tag{IV.32}$$

It is supposed that the UPFC has an impact to the differential-algebraic model only through its load flow part described by the network equations. Due to fast responses of its control loops, it is assumed that the UPFC differential equations should not be necessarily included in the model.

Within the network equations given by (IV.20-21), some modifications are introduced to adjust for the variables that do not appear in steady state load flow, but give additional insight in the dynamics.

The modifications are introduced to include d and q-axis components of generator voltage and current in equation sensitivity.

The network equations, written for the generator external bus, are modified as

$$0 = \sum_{m=1}^{n} P_{Em} - G_{EI}V_E V_I \cos\Theta_{EI} - B_{EI}V_E V_I \sin\Theta_{EI} + \\ + G_{EI}V_E^2 - V_d I_d - V_q I_q \tag{IV.33}$$

$$0 = \sum_{m=1}^{n} Q_{Em} - G_{EI}V_E V_I \sin\Theta_{EI} + B_{EI}V_E V_I \cos\Theta_{EI} - \\ - B_{EI}V_E^2 - V_d I_q + V_q I_d \tag{IV.34}$$

Similarly, the network equations, written for the motor external bus, are modified as

$$0 = \sum_{m=1}^{n} P_{Em} - G_{EI}V_E V_I \cos\Theta_{EI} - B_{EI}V_E V_I \sin\Theta_{EI} + \\ + G_{EI}V_E^2 + V_d I_d + V_q I_q \tag{IV.35}$$

$$0 = \sum_{m=1}^{n} Q_{Em} - G_{EI}V_E V_I \sin\Theta_{EI} + B_{EI}V_E V_I \cos\Theta_{EI} - \\ - B_{EI}V_E^2 + V_d I_q - V_q I_d \tag{IV.36}$$

Modified network equations, written for bus k with dynamic non-linear recovery loads, are given as

$$0 = P_k(\Theta,V) + \frac{x_P}{T_P} + \frac{k_P V_n^{\alpha}}{\alpha T_P}, \tag{IV.37}$$

$$0 = Q_k(\Theta,V) + \frac{x_Q}{T_Q} + \frac{k_Q V_n^{\alpha}}{\alpha T_Q}. \tag{IV.38}$$

Modified active power network equation, written for bus k with thermostatically controlled load, is given as

$$0 = P_k(G,\Theta,V) = \sum_{i=1}^{n} P_{ki}' + GV_k^2 = \sum_{i=1}^{n} P_{ki}, \tag{IV.39}$$

where in the first case the shunt conductance G is accounted separately from the term P'_{kk}, whereas in the second case it is accounted in the term P_{kk} through its position in the k-th diagonal term of the bus conductance matrix *[G]*.

IV.2 LINEARISED SYSTEM MODEL

By linearising (IV.1-2) around an operating point, the set of the linearised equations appears in general form as

$$\Delta\frac{dx}{dt} = f_x\Delta x + f_y\Delta y + f_p\Delta p, \tag{IV.40}$$

$$0 = g_x\Delta x + g_y\Delta y + g_p\Delta p. \tag{IV.41}$$

More particularly, by linearising the system of equations (IV.3-30), following particular form appears as *linearised generator differential equations (gde)*

$$\Delta\frac{d\delta}{dt}=\Delta\omega \tag{IV.42}$$

$$\begin{aligned}\Delta\frac{d\omega}{dt}&=-\frac{D}{\tau_j}\Delta\omega-\frac{I_q}{\tau_j}\Delta E_q^{'}-\frac{I_d}{\tau_j}\Delta E_d^{'}+\frac{1}{\tau_j}\Delta T_m-\\&-\frac{E_d^{'}-(x_q^{'}-x_d^{'})I_q}{\tau_j}\Delta I_d-\frac{E_q^{'}-\left(x_q^{'}-x_d^{'}\right)I_d}{\tau_j}\Delta I_q\end{aligned} \tag{IV.43}$$

$$\Delta\frac{dE_q^{'}}{dt}=-\frac{1}{\tau_{d0}^{'}}\Delta E_q^{'}+\frac{1}{\tau_{d0}^{'}}\Delta E_{FD}+\frac{(x_d-x_d^{'})}{\tau_{d0}^{'}}\Delta I_d \tag{IV.44}$$

$$\Delta\frac{dE_d^{'}}{dt}=-\frac{1}{\tau_{q0}^{'}}\Delta E_d^{'}-\frac{(x_q-x_q^{'})}{\tau_{q0}^{'}}\Delta I_q \tag{IV.45}$$

$$\Delta\frac{dE_{FD}}{dt}=-\frac{1}{\tau_A}\Delta E_{FD}-\frac{K_A}{\tau_A}\Delta V_{OEL}-\frac{K_A}{\tau_A}\Delta V_n \tag{IV.46}$$

$$\begin{aligned}\Delta\frac{dGOV1}{dt}&=\left(\frac{\tau_2 D}{\tau_1 R\tau_j}-\frac{1}{\tau_1 R}\right)\Delta\omega+\frac{\tau_2 I_q}{\tau_1 R\tau_j}\Delta E_q^{'}+\\&+\frac{\tau_2 I_d}{\tau_1 R\tau_j}\Delta E_d^{'}-\frac{1}{\tau_1}\Delta GOV1-\frac{\tau_2}{\tau_1 R\tau_j}\Delta T_m+\\&+\frac{\tau_2\left[E_d^{'}-(x_q^{'}-x_d^{'})I_q\right]}{\tau_1 R\tau_j}\Delta I_d+\\&+\frac{\tau_2\left[E_q^{'}-\left(x_q^{'}-x_d^{'}\right)I_d\right]}{\tau_1 R\tau_j}\Delta I_q\end{aligned} \tag{IV.47}$$

$$\Delta\frac{dGOV\,4}{dt}=\frac{1}{\tau_3}\Delta GOV\,1-\frac{1}{\tau_3}\Delta GOV\,4 \tag{IV.48}$$

$$\Delta\frac{dGOV\,5}{dt}=\frac{1}{\tau_4}\Delta GOV\,4-\frac{1}{\tau_4}\Delta GOV\,5 \tag{IV.49}$$

$$\begin{aligned}\Delta\frac{dT_m}{dt}&=\left\{-\frac{GOV\,5}{\tau_5\omega^2}-\frac{F\,GOV\,4}{\tau_4\omega^2}+\frac{F\,GOV\,5}{\tau_4\omega^2}+\frac{T_m^2}{\tau_j\omega^2}-\right.\\&-\frac{T_m}{\tau_j\omega^2}\left[E_d^{'}I_d+E_q^{'}I_q-\left(x_q^{'}-x_d^{'}\right)I_d I_q\right]+\\&\left.+\frac{T_m D}{\tau_j\omega^2}\right\}\Delta\omega+\frac{T_m I_q}{\omega\tau_j}\Delta E_q^{'}+\frac{T_m I_d}{\omega\tau_j}\Delta E_d^{'}+\\&+\frac{F}{\tau_4\omega}\Delta GOV\,4+\left(\frac{1}{\omega\tau_5}-\frac{F}{\omega\tau_4}\right)\Delta GOV\,5+\\&+\left\{-\frac{1}{\tau_5}-\frac{2T_m}{\omega\tau_j}+\frac{1}{\omega\tau_j}\left[E_d^{'}I_d+E_q^{'}I_q-\right.\right.\\&\left.\left.-\left(x_q^{'}-x_d^{'}\right)I_d I_q\right]+\frac{D}{\tau_j}\left(1-\frac{1}{\omega}\right)\right\}\Delta T_m+\\&+\frac{T_m}{\omega\tau_j}\left[E_d^{'}-\left(x_q^{'}-x_d^{'}\right)I_q\right]\Delta I_d+\\&+\frac{T_m}{\omega\tau_j}\left[E_q^{'}-\left(x_q^{'}-x_d^{'}\right)I_d\right]\Delta I_q\end{aligned} \tag{IV.50}$$

$$\Delta\frac{dV_{OEL}}{dt}=\frac{K_2K_3}{T_{OEL}}\Delta I_{FD} \tag{IV.51}$$

linearised motor differential equations (mde)

$$\begin{aligned}\Delta\frac{dE_q^{'}}{dt}&=-\frac{1}{T_0^{'}}\Delta E_q^{'}+(\omega_{0S}-\omega_m)\Delta E_d^{'}-\\&-E_d^{'}\Delta\omega_m-\frac{X-X'}{T_0^{'}}\Delta I_d\end{aligned} \tag{IV.52}$$

$$\begin{aligned}\Delta\frac{dE_d^{'}}{dt}&=-(\omega_{0S}-\omega_m)\Delta E_q^{'}-\frac{1}{T_0^{'}}\Delta E_d^{'}+\\&+E_q^{'}\Delta\omega_m+\frac{X-X'}{T_0^{'}}\Delta I_q\end{aligned} \tag{IV.53}$$

$$\begin{aligned}\Delta\frac{d\omega_m}{dt}&=\frac{I_q}{2H\omega_{0S}}\Delta E_q^{'}+\frac{I_d}{2H\omega_{0S}}\Delta E_d^{'}-\\&-\frac{T_{m0}}{2H}\left(\frac{2A\omega_m}{\omega_{m0}^2}+\frac{B}{\omega_{m0}}+\frac{am\,D\,\omega_m^{am-1}}{\omega_{m0}^{am}}\right)\Delta\omega_m+\\&+\frac{E_d^{'}}{2H\omega_{0S}}\Delta I_d+\frac{E_q^{'}}{2H\omega_{0S}}\Delta I_q\end{aligned} \tag{IV.54}$$

linearised differential equation of dynamic non-linear recovery active power load (dyn_p)

$$\begin{aligned}\Delta\frac{dx_P}{dt}&=-\frac{1}{T_P}\Delta x_P-\frac{k_P V_n^{\alpha-1}}{T_P}\Delta V_n+\Delta P_S(V_n)=\\&=\Delta P_S(V_n)+\frac{\partial P_k(\Theta,V)}{\partial\Theta}\Delta\Theta+\frac{\partial P_k(\Theta,V)}{\partial V}\Delta V\end{aligned} \tag{IV.55}$$

linearised differential equation of dynamic non-linear recovery reactive power load (dyn_q)

$$\begin{aligned}\Delta\frac{dx_Q}{dt}&=-\frac{1}{T_Q}\Delta x_Q-\frac{k_Q V_n^{\alpha-1}}{T_Q}\Delta V_n+\Delta Q_S(V_n)=\\&=\Delta Q_S(V_n)+\frac{\partial Q_k(\Theta,V)}{\partial\Theta}\Delta\Theta+\frac{\partial Q_k(\Theta,V)}{\partial V}\Delta V\end{aligned} \tag{IV.56}$$

linearised differential equations of thermostatically controlled load (tcl)

$$\Delta\frac{d\tau_H}{dt}=-\frac{1}{T_1}\Delta\tau_H+\frac{K_1}{T_1}V_n^2\Delta G+\frac{2K_1}{T_1}GV_n\Delta V_n \tag{IV.57}$$

$$\begin{aligned}\Delta\frac{dG}{dt}&=\left(\frac{K_P}{T_1}-\frac{K_I}{T_C}\right)\Delta\tau_H-\frac{K_PK_1}{T_1}V_n^2\Delta G-\\&-\frac{2K_PK_1}{T_1}GV_n\Delta V_n\end{aligned} \tag{IV.58}$$

linearised active power network algebraic equations (nae_p)

$$\begin{aligned}0&=\Delta P_k(\Theta,V)+\Delta P_S(V,\Delta f)+\Delta P_{Ti\,or\,j}(\Theta,V,t_r)+\\&+\Delta P_{Si\,or\,j}\left(\Theta,V,r,\gamma,I_{conv1q}\right)\end{aligned} \tag{IV.59}$$

linearised reactive power network algebraic equations (nae_q)

$$0=\Delta Q_k(\Theta,V)+\Delta Q_S(V,\Delta f)+\Delta Q_{Ti\,or\,j}(\Theta,V,t_r)+ \\ +\Delta Q_{Si\,or\,j}(\Theta,V,r,\gamma,I_{conv1q}) \quad \text{(IV.60)}$$

linearised generator algebraic equations (gae)

$$0=\Delta E_d^{'}-r\Delta I_d-x_q^{'}\Delta I_q-\Delta V_d \quad \text{(IV.61)}$$

$$0=\Delta E_q^{'}+x_d^{'}\Delta I_d-r\Delta I_q-\Delta V_q \quad \text{(IV.62)}$$

$$0=V_n\cos(\Theta_n-\delta)\Delta\delta-V_n\cos(\Theta_n-\delta)\Delta\Theta_n- \\ -\sin(\Theta_n-\delta)\Delta V_n+\Delta V_d \quad \text{(IV.63)}$$

$$0=-V_n\sin(\Theta_n-\delta)\Delta\delta+V_n\sin(\Theta_n-\delta)\Delta\Theta_n- \\ -\cos(\Theta_n-\delta)\Delta V_n+\Delta V_q \quad \text{(IV.64)}$$

$$0=\Delta E_q^{'}-\left(x_d-x_d^{'}\right)\Delta I_d-\Delta I_{FD} \quad \text{(IV.65)}$$

linearised motor algebraic equations (mae)

$$0=-X'\Delta E_q^{'}+R_S\Delta E_d^{'}+\left(R_S^2+X'^2\right)\Delta I_d- \\ -R_S\Delta V_d+X'\Delta V_q \quad \text{(IV.66)}$$

$$0=R_S\Delta E_q^{'}+X'\Delta E_d^{'}+\left(R_S^2+X'^2\right)\Delta I_q- \\ -X'\Delta V_d-R_S\Delta V_q \quad \text{(IV.67)}$$

$$0=-V_n\cos\Theta_n\Delta\Theta_n-\sin\Theta_n\Delta V_n+\Delta V_d \quad \text{(IV.68)}$$

$$0=V_n\sin\Theta_n\Delta\Theta_n-\cos\Theta_n\Delta V_n+\Delta V_q \quad \text{(IV.69)}$$

Due to the modifications introduced in (IV.33-39), linearised equations for buses with connected generators, motors, dynamic loads with non-linear recovery or thermostatically controlled loads are introduced.

The linearised network equations written for the generator external bus are modified as

$$0=\frac{\partial\sum_{m=1}^{n}P_{Em}}{\partial\Theta}\Delta\Theta+\frac{\partial\sum_{m=1}^{n}P_{Em}}{\partial V}\Delta V+ \\ +(G_{EI}V_EV_I\sin\Theta_{EI}-B_{EI}V_EV_I\cos\Theta_{EI})\Delta\Theta_E- \\ -[(G_{EI}V_I\cos\Theta_{EI}+B_{EI}V_I\sin\Theta_{EI})-2G_{EI}V_E]\Delta V_E- \\ -V_d\Delta I_d-V_q\Delta I_q-I_d\Delta V_d-I_q\Delta V_q \quad \text{,(IV.70)}$$

$$0=\frac{\partial\sum_{m=1}^{n}Q_{Em}}{\partial\Theta}\Delta\Theta+\frac{\partial\sum_{m=1}^{n}Q_{Em}}{\partial V}\Delta V- \\ -(G_{EI}V_EV_I\cos\Theta_{EI}+B_{EI}V_EV_I\sin\Theta_{EI})\Delta\Theta_E- \\ -[(G_{EI}V_I\sin\Theta_{EI}-B_{EI}V_I\cos\Theta_{EI})+2B_{EI}V_E]\Delta V_E+ \\ +V_q\Delta I_d-V_d\Delta I_q-I_q\Delta V_d+I_d\Delta V_q \quad \text{.(IV.71)}$$

Similarly, the linearised network equations written for the motor external bus are modified as

$$0=\frac{\partial\sum_{m=1}^{n}P_{Em}}{\partial\Theta}\Delta\Theta+\frac{\partial\sum_{m=1}^{n}P_{Em}}{\partial V}\Delta V+ \\ +(G_{EI}V_EV_I\sin\Theta_{EI}-B_{EI}V_EV_I\cos\Theta_{EI})\Delta\Theta_E- \\ -[(G_{EI}V_I\cos\Theta_{EI}+B_{EI}V_I\sin\Theta_{EI})-2G_{EI}V_E]\Delta V_E+ \\ +V_d\Delta I_d+V_q\Delta I_q+I_d\Delta V_d+I_q\Delta V_q \quad \text{,(IV.72)}$$

$$0=\frac{\partial\sum_{m=1}^{n}Q_{Em}}{\partial\Theta}\Delta\Theta+\frac{\partial\sum_{m=1}^{n}Q_{Em}}{\partial V}\Delta V- \\ -(G_{EI}V_EV_I\cos\Theta_{EI}+B_{EI}V_EV_I\sin\Theta_{EI})\Delta\Theta_E- \\ -[(G_{EI}V_I\sin\Theta_{EI}-B_{EI}V_I\cos\Theta_{EI})+2B_{EI}V_E]\Delta V_E- \\ -V_q\Delta I_d+V_d\Delta I_q+I_q\Delta V_d-I_d\Delta V_q \quad \text{.(IV.73)}$$

Linearised network equations for the bus k with dynamic loads with non-linear recovery are given as

$$0=\frac{1}{T_P}\Delta x_P+\frac{k_PV_n^{\alpha-1}}{T_P}\Delta V_n+ \\ +\frac{\partial P_k(\Theta,V)}{\partial\Theta}\Delta\Theta+\frac{\partial P_k(\Theta,V)}{\partial V}\Delta V \quad , \quad \text{(IV.74)}$$

$$0=\frac{1}{T_Q}\Delta x_Q+\frac{k_QV_n^{\alpha-1}}{T_Q}\Delta V_n+ \\ +\frac{\partial Q_k(\Theta,V)}{\partial\Theta}\Delta\Theta+\frac{\partial Q_k(\Theta,V)}{\partial V}\Delta V \quad . \quad \text{(IV.75)}$$

Linearised active power network equation for the bus k with thermostatically controlled load is given as

$$0=V_k^2\Delta G+\frac{\partial\sum_{i=1}^{n}P_{ki}}{\partial\Theta}\Delta\Theta+\frac{\partial\sum_{i=1}^{n}P_{ki}}{\partial V}\Delta V\ , \quad \text{(IV.76)}$$

where the shunt conductance G is accounted in the term P_{kk} through its position in the k-th diagonal term of the bus conductance matrix *[G]*. This approach enables the differential $[\partial(GV_k^2)/\partial V_k]\Delta V_k$ to be included within the third term of (IV.76).

IV.3 MATRIX FORMATION

Linearisation procedure, in general form given by (IV.40-41) and in more particular form by (IV.42-76), results with formation of the extended Jacobian matrix J_{EXT} as

$$J_{EXT} = \left[\begin{array}{c|cc} f_x & \multicolumn{2}{c}{f_y} \\ \hline g_x & g_{y1} & g_{y2} \\ & g_{y3} & g_{y4} \end{array}\right], \tag{IV.77}$$

where the ordinary Jacobian load flow matrix g_{y1} is a part of the major sub-matrix g_y. The sub-matrix g_y is composed of four minor sub-matrices due to the additional algebraic equations which bring additional generator/motor algebraic variables.

Detailed form of (IV.77) is given as it follows in (IV.78). Linearised generator differential and algebraic equations are supposed to have 9 and 4 variables, respectively. If the OEL were activated, then there would be 10 and 5 variables, respectively. Null entries, denoted as [0], suggest that there are many minor sub-matrices without any numerical value other than zero. It opens a way for utilisation of sparse matrix methods with expected decrease in computational burden. The sub-matrix $[J]_{LF}$ denotes a position of the ordinary steady state Jacobian matrix within the larger matrix extended with dynamic terms. Major sub-matrices are easily corresponded between (IV.77) and (IV.78).

The extended Jacobian matrix, J_{EXT}, is used in computations on the system, which is given as

$$\begin{bmatrix} \Delta \dfrac{dx}{dt} \\ 0 \end{bmatrix} = \left[\begin{array}{c|c} f_x & f_y \\ \hline g_x & g_y \end{array}\right] \begin{bmatrix} \Delta x \\ \Delta y \end{bmatrix}. \tag{IV.79}$$

Besides on the extended Jacobian matrix, the analysis is carried out on the system state matrix as well. By eliminating the vector of algebraic variables, Δy, following system is obtained

$$\Delta \frac{dx}{dt} = A_S \Delta x\,, \tag{IV.80}$$

where the state matrix A_S is given as

$$A_S = \left[f_x - \left(f_y g_y^{-1} g_x \right) \right]. \tag{IV.81}$$

Matrices J_{EXT} and A_S are used in sensitivity analysis aimed to show critical issues in the voltage stability problem.

Sensitivity analysis is introduced in its general sense within issues such as singular and eigenvalue decomposition, and parametric and functional sensitivities. These issues result with characteristic indices and participation factors, which help the voltage stability problem being recognised.

$$\begin{array}{c} \\ gde \\ mde \\ dyn_P \\ dyn_Q \\ tcl \\ nae_p + nae_q \\ gae \\ mae \end{array}
\begin{array}{c}
\begin{array}{cccccccc} gde & mde & dyn_P & dyn_Q & tcl & nae_p + nae_q & gae & mae \end{array} \\
\left[\begin{array}{ccccc|c|cc}
\begin{bmatrix}[9x9] & & \\ & \ddots & \\ & & [9x9]\end{bmatrix} & [0] & [0] & [0] & [0] & & \begin{bmatrix}[9x4] & & \\ & \ddots & \\ & & [9x4]\end{bmatrix} & [0] \\
[0] & \begin{bmatrix}[3x3] & & \\ & \ddots & \\ & & [3x3]\end{bmatrix} & [0] & [0] & [0] & [0] & [0] & \begin{bmatrix}[3x4] & & \\ & \ddots & \\ & & [3x4]\end{bmatrix} \\
[0] & [0] & \begin{bmatrix}[1x1] & & \\ & \ddots & \\ & & [1x1]\end{bmatrix} & [0] & [0] & & [0] & [0] \\
[0] & [0] & [0] & \begin{bmatrix}[1x1] & & \\ & \ddots & \\ & & [1x1]\end{bmatrix} & [0] & & [0] & [0] \\
[0] & [0] & [0] & [0] & \begin{bmatrix}[2x2] & & \\ & \ddots & \\ & & [2x2]\end{bmatrix} & & [0] & [0] \\
\hline
[0] & [0] & & & & [J]_{LF} & & \\
\begin{bmatrix}[4x9] & & \\ & \ddots & \\ & & [4x9]\end{bmatrix} & [0] & [0] & [0] & [0] & & \begin{bmatrix}[4x4] & & \\ & \ddots & \\ & & [4x4]\end{bmatrix} & [0] \\
[0] & \begin{bmatrix}[4x3] & & \\ & \ddots & \\ & & [4x3]\end{bmatrix} & [0] & [0] & [0] & & [0] & \begin{bmatrix}[4x4] & & \\ & \ddots & \\ & & [4x4]\end{bmatrix}
\end{array}\right]
\end{array} \tag{IV.78}$$

V. SENSITIVITY ANALYSIS

V.1 SINGULAR AND EIGENVALUE DECOMPOSITION

Singular and eigenvalue decomposition of the matrices J_{EXT} and A_S provide an approach to a voltage stability assessment. The procedures for obtaining critical singular and eigenvalues (σ_n and λ_n), the associated left and right critical vectors (u_n, v_n, and f_n, e_n), and the participation factors are well established in the field. Due to that fact, these issues are covered here in a rather general and introductory sense.

V.1.A Singular value decomposition

Assuming that A is real and quadratic (n x n) matrix, as it is used in the analysis throughout the dissertation, then it could be decomposed [192-197, 338, 361-363] as

$$A = U\ \Sigma\ V^{\tau} = \sum_{i=1}^{n} \sigma_i u_i v_i^{\tau}\ , \tag{V.1}$$

where U denotes matrix whose columns are composed of left singular vectors u_i, V matrix of right singular vectors v_i, and Σ diagonal matrix whose entries are singular values σ_i.

The singular values are usually ordered as $\sigma_1 \geq \sigma_2 \geq \ldots \geq \sigma_n \geq 0$, where σ_n denotes minimum singular value. Minimum singular value is considered to be one of the critical indices in the voltage stability problem.

The singular vectors are orthonormal satisfying following general relation

$$u_i^{\tau} u_j = \delta_{ij} = \begin{cases} 0 & for \quad i \neq j \\ 1 & for \quad i = j \end{cases} . \tag{V.2}$$

Similar relation is valid for $v_i^{\tau} v_j$, as well.

In the fast procedure of the minimum singular value and corresponding singular vectors computation, following general relations are used

$$A\, v_n = \sigma_n u_n\, , \tag{V.3}$$

$$u_n^{\tau} A = \sigma_n v_n^{\tau} \quad or \quad A^{\tau} u_n = \sigma_n v_n\, . \tag{V.4}$$

Then, the fast computational procedure is given in symbolic steps as it follows

(Initialising part for the first iteration)

1. Initial guess for the vector $v_n^{(1)}$ in the first iteration,
2. Computing the second norm of the vector $v_n^{(1)}$,
3. Normalisation of the vector $v_n^{(1)}$,

(Iterative part for the subsequent iterations)

4. Solving $A^{\tau} u_n^{(i)} = v_n^{(i)}$ in the i-th iteration,
5. Computing the second norm of the vector $u_n^{(i)}$,
6. Normalisation of the vector $u_n^{(i)}$,
7. Estimating $\sigma_n^{'(i)} = 1 / SNRM2(u_n^{(i)})$,
8. Convergence checking in $\sigma_n^{'(i)}$,
9. Solving $A v_n^{(i+1)} = u_n^{(i)}$ in the $(i+1)$-th iteration,
10. Computing the second norm of the vector $v_n^{(i+1)}$,
11. Normalisation of the vector $v_n^{(i+1)}$,
12. Estimating $\sigma_n^{''(i)} = 1 / SNRM2(v_n^{(i+1)})$,
13. Convergence checking in $\sigma_n^{''(i)}$,
14. Exit from iterative part when convergence is achieved (difference from two consecutive iterations smaller than a pre-established threshold).

Besides fast computational procedure, the other methods resulting in complete singular value decomposition are used as well in order to check validity of results.

Upon defining the way of computing singular value decomposition, the problem is stated so as to reflect the system given by (IV.79). If the problem is given by

$$A\, x = b\, , \tag{V.5}$$

then the solution x, depending on input b, is achieved as

$$\begin{aligned} x &= A^{-1} b = \left(U\ \Sigma\ V^{\tau} \right)^{-1} b = \sum_{i=1}^{n} \frac{v_i u_i^{\tau}}{\sigma_i} b \approx \\ &\approx \left(\sigma_n^{-1} v_n \right) \left(u_n^{\tau} b \right) \end{aligned} , \tag{V.6}$$

assuming that $\sigma_{n-1} >> \sigma_n$, which holds especially in the vicinity of the critical point.

If the problem and the solution, as given by (V.5-6), are applied to a more particular steady state power flow problem, the previous relations appear as

$$J_{LF} \begin{bmatrix} \Delta\Theta \\ \Delta V \end{bmatrix} = \begin{bmatrix} \Delta P \\ \Delta Q \end{bmatrix}, \tag{V.7}$$

where the steady state load flow Jacobian matrix, J_{LF}, is decomposed as

$$J_{LF} = U\, \Sigma\, V^{\tau}\, . \tag{V.8}$$

The inverse of the matrix J_{LF} then appears as

$$\begin{aligned} J_{LF}^{-1} &= \left(U\, \Sigma\, V^{\tau} \right)^{-1} = V\ \Sigma^{-1}\ U^{\tau} \approx \\ &\approx \sigma_n^{-1} v_n u_n^{\tau} \end{aligned} . \tag{V.9}$$

By introducing (V.9) in (V.7), the solution is given as

$$\begin{bmatrix}\Delta\Theta\\ \Delta V\end{bmatrix} = \sigma_n^{-1} v_n u_n^\tau \begin{bmatrix}\Delta P\\ \Delta Q\end{bmatrix}. \quad \text{(V.10)}$$

By stating that the right singular vector, v_n, indicates sensitive voltage angles and magnitudes, and the left singular vector, u_n, the most sensitive direction for changes of active and reactive power injections, following relations are introduced

$$\begin{bmatrix}\Delta\Theta\\ \Delta V\end{bmatrix} = \sigma_n^{-1} v_n , \quad \text{(V.11)}$$

$$\begin{bmatrix}\Delta P\\ \Delta Q\end{bmatrix} = u_n . \quad \text{(V.12)}$$

If this approach is applied to the extended load flow Jacobian matrix J_{EXT}, then singular value decomposition results with the right and left singular vectors that correspond to the minimum singular value as well. By correlating entries within these vectors to the steady state power flow algebraic equations, further dynamics insight is provided to the assumptions introduced in (V.11-12) valid for the algebraic variables. If the approach is applied to the state matrix A_S, the insight is given to the state variables.

Minimum singular value presents an index of impending voltage collapse, but also warns on voltage security level of the system. In order to maximise minimum singular value and by that to increase voltage security of the system, its sensitivity with respect to the parameters (r, γ, I_{conv1q}) of the UPFC injection model calls for being explained.

If following relation between σ_n, u_n, v_n, and J_{EXT}

$$J_{EXT}\ v_n = \sigma_n u_n \quad \text{(V.13)}$$

is first differentiated with respect to parameter p, and then pre-multiplied by u_n^τ , it gives

$$u_n^\tau \frac{\partial J_{EXT}}{\partial p} v_n + u_n^\tau J_{EXT} \frac{\partial v_n}{\partial p} = u_n^\tau \frac{\partial \sigma_n}{\partial p} u_n + u_n^\tau \sigma_n \frac{\partial u_n}{\partial p} . \quad \text{(V.14)}$$

By using following relations

$$u_n^\tau J_{EXT} = \sigma_n v_n^\tau \quad and \quad u_n^\tau u_n = 1 , \quad \text{(V.15)}$$

the sensitivity of minimum singular value with respect to the parameter p is obtained from (V.14) as

$$\frac{\partial \sigma_n}{\partial p} = u_n^\tau \frac{\partial J_{EXT}}{\partial p} v_n + \sigma_n \left(v_n^\tau \frac{\partial v_n}{\partial p} - u_n^\tau \frac{\partial u_n}{\partial p} \right). \quad \text{(V.16)}$$

Due to orthonormality, the singular vector u_n, and similarly the vector v_n, satisfies following relation

$$\frac{\partial u_i^\tau}{\partial p} u_i = u_i^\tau \frac{\partial u_i}{\partial p} = 0 . \quad \text{(V.17)}$$

Therefore, the minimum singular value sensitivity is obtained from (V.16) as

$$\frac{\partial \sigma_n}{\partial p} = u_n^\tau \frac{\partial J_{EXT}}{\partial p} v_n . \quad \text{(V.18)}$$

The sensitivity, given by (V.18), is defined with respect to an arbitrary parameter p, but the control set of the UPFC parameters (r, γ, I_{conv1q}) is used here.

Partial derivatives $\partial J_{EXT}/\partial p$ from (V.18) are defined by differentiating its appropriate terms belonging to the equations (III.70-85) with respect to the parameters (r, γ, I_{conv1q}).

Partial derivatives $\partial J_{EXT}/\partial r$ are given as

on-diagonal terms

$$\frac{\partial}{\partial r}\left(\frac{\partial P_i}{\partial \Theta_i}\right) = -\, b_S V_i V_j \cos(\Theta_{ij} + \gamma) \quad \text{(V.19)}$$

$$\frac{\partial}{\partial r}\left(\frac{\partial P_i}{\partial V_i}\right) = -b_S V_j \sin(\Theta_{ij} + \gamma) \quad \text{(V.20)}$$

$$\frac{\partial}{\partial r}\left(\frac{\partial Q_i}{\partial \Theta_i}\right) = 0 \quad \text{(V.21)}$$

$$\frac{\partial}{\partial r}\left(\frac{\partial Q_i}{\partial V_i}\right) = -2 b_S V_i \cos\gamma \quad \text{(V.22)}$$

$$\frac{\partial}{\partial r}\left(\frac{\partial P_j}{\partial \Theta_j}\right) = -b_S V_i V_j \cos(\Theta_{ij} + \gamma) \quad \text{(V.23)}$$

$$\frac{\partial}{\partial r}\left(\frac{\partial P_j}{\partial V_j}\right) = b_S V_i \sin(\Theta_{ij} + \gamma) \quad \text{(V.24)}$$

$$\frac{\partial}{\partial r}\left(\frac{\partial Q_j}{\partial \Theta_j}\right) = b_S V_i V_j \sin(\Theta_{ij} + \gamma) \quad \text{(V.25)}$$

$$\frac{\partial}{\partial r}\left(\frac{\partial Q_j}{\partial V_j}\right) = b_S V_i \cos(\Theta_{ij} + \gamma) \quad \text{(V.26)}$$

off-diagonal terms

$$\frac{\partial}{\partial r}\left(\frac{\partial P_i}{\partial \Theta_j}\right) = b_S V_i V_j \cos\left(\Theta_{ij} + \gamma\right) \quad \text{(V.27)}$$

$$\frac{\partial}{\partial r}\left(\frac{\partial P_i}{\partial V_j}\right) = -b_S V_i \sin\left(\Theta_{ij} + \gamma\right) \quad \text{(V.28)}$$

$$\frac{\partial}{\partial r}\left(\frac{\partial Q_i}{\partial \Theta_j}\right) = 0 \quad \text{(V.29)}$$

$$\frac{\partial}{\partial r}\left(\frac{\partial Q_i}{\partial V_j}\right) = 0 \quad \text{(V.30)}$$

$$\frac{\partial}{\partial r}\left(\frac{\partial P_j}{\partial \Theta_i}\right) = b_S V_i V_j \cos\left(\Theta_{ij} + \gamma\right) \quad \text{(V.31)}$$

$$\frac{\partial}{\partial r}\left(\frac{\partial P_j}{\partial V_i}\right)=b_S V_j \sin\left(\Theta_{ij}+\gamma\right) \qquad (V.32)$$

$$\frac{\partial}{\partial r}\left(\frac{\partial Q_j}{\partial \Theta_i}\right)=-b_S V_i V_j \sin\left(\Theta_{ij}+\gamma\right) \qquad (V.33)$$

$$\frac{\partial}{\partial r}\left(\frac{\partial Q_j}{\partial V_i}\right)=b_S V_j \cos\left(\Theta_{ij}+\gamma\right) \qquad (V.34)$$

Partial derivatives $\partial J_{EXT}/\partial\gamma$ are given as

on-diagonal terms

$$\frac{\partial}{\partial \gamma}\left(\frac{\partial P_i}{\partial \Theta_i}\right)=rb_S V_i V_j \sin(\Theta_{ij}+\gamma) \qquad (V.35)$$

$$\frac{\partial}{\partial \gamma}\left(\frac{\partial P_i}{\partial V_i}\right)=-rb_S V_j \cos(\Theta_{ij}+\gamma) \qquad (V.36)$$

$$\frac{\partial}{\partial \gamma}\left(\frac{\partial Q_i}{\partial \Theta_i}\right)=0 \qquad (V.37)$$

$$\frac{\partial}{\partial \gamma}\left(\frac{\partial Q_i}{\partial V_i}\right)=2rb_S V_i \sin\gamma \qquad (V.38)$$

$$\frac{\partial}{\partial \gamma}\left(\frac{\partial P_j}{\partial \Theta_j}\right)=rb_S V_i V_j \sin(\Theta_{ij}+\gamma) \qquad (V.39)$$

$$\frac{\partial}{\partial \gamma}\left(\frac{\partial P_j}{\partial V_j}\right)=rb_S V_i \cos(\Theta_{ij}+\gamma) \qquad (V.40)$$

$$\frac{\partial}{\partial \gamma}\left(\frac{\partial Q_j}{\partial \Theta_j}\right)=rb_S V_i V_j \cos(\Theta_{ij}+\gamma) \qquad (V.41)$$

$$\frac{\partial}{\partial \gamma}\left(\frac{\partial Q_j}{\partial V_j}\right)=-rb_S V_i \sin(\Theta_{ij}+\gamma) \qquad (V.42)$$

off-diagonal terms

$$\frac{\partial}{\partial \gamma}\left(\frac{\partial P_i}{\partial \Theta_j}\right)=-rb_S V_i V_j \sin\left(\Theta_{ij}+\gamma\right) \qquad (V.43)$$

$$\frac{\partial}{\partial \gamma}\left(\frac{\partial P_i}{\partial V_j}\right)=-rb_S V_i \cos\left(\Theta_{ij}+\gamma\right) \qquad (V.44)$$

$$\frac{\partial}{\partial \gamma}\left(\frac{\partial Q_i}{\partial \Theta_j}\right)=0 \qquad (V.45)$$

$$\frac{\partial}{\partial \gamma}\left(\frac{\partial Q_i}{\partial V_j}\right)=0 \qquad (V.46)$$

$$\frac{\partial}{\partial \gamma}\left(\frac{\partial P_j}{\partial \Theta_i}\right)=-rb_S V_i V_j \sin\left(\Theta_{ij}+\gamma\right) \qquad (V.47)$$

$$\frac{\partial}{\partial \gamma}\left(\frac{\partial P_j}{\partial V_i}\right)=rb_S V_j \cos\left(\Theta_{ij}+\gamma\right) \qquad (V.48)$$

$$\frac{\partial}{\partial \gamma}\left(\frac{\partial Q_j}{\partial \Theta_i}\right)=-rb_S V_i V_j \cos\left(\Theta_{ij}+\gamma\right) \qquad (V.49)$$

$$\frac{\partial}{\partial \gamma}\left(\frac{\partial Q_j}{\partial V_i}\right)=-rb_S V_j \sin\left(\Theta_{ij}+\gamma\right) \qquad (V.50)$$

Partial derivative $\partial J_{EXT}/\partial I_{conv1q}$ is given for one and the only non-zero term

on-diagonal term

$$\frac{\partial}{\partial I_{conv\,1q}}\left(\frac{\partial Q_i}{\partial V_i}\right)=\frac{S_{conv\,1n}}{S_B} \qquad (V.51)$$

There are only four entries in the left and right singular vectors actively participating in computation of the sensitivity (V.18) with respect to *r* and *γ*, and one entry with respect to I_{conv1q}. Due to largely sparse matrix $\partial J_{EXT}/\partial p$, computational burden is significantly decreased.

V.1.B Eigenvalue decomposition

When all eigenvalues are distinct, real and quadratic (*n* x *n*) matrix *A* could be decomposed [106, 187, 189, 191, 393] as

$$A = E\ \Lambda\ F^{\tau} = \sum_{i=1}^{n} \lambda_i e_i f_i^{\tau}\ , \qquad (V.52)$$

where *E* denotes matrix whose columns are composed of the right eigenvectors e_i, *F* matrix of the left eigenvectors f_i, and *Λ* diagonal matrix whose entries are eigenvalues λ_i.

The squares of the singular values σ_i of matrix *A* are equal to the eigenvalues λ_i of $A^{\tau}A$ or AA^{τ} as it follows

$$\Sigma^2(A)=\Lambda\left(A^{\tau}A\right)=\Lambda\left(AA^{\tau}\right). \qquad (V.53)$$

Combining properties of the singular value decomposition (V.1) with (V.52-53), the eigenvalue decompositions of $A^{\tau}A$, or AA^{τ} are given as

$$A^{\tau}A = V\left(\Sigma^{\tau}\Sigma\right)V^{\tau}\ , \qquad (V.54)$$

$$AA^{\tau} = U\left(\Sigma\Sigma^{\tau}\right)U^{\tau}\ . \qquad (V.55)$$

This shows that the eigenvectors of $A^{\tau}A$, or AA^{τ} are equal to the right and left singular vectors. Thereby, if *A* is real and symmetric matrix, the absolute vales of the eigenvalues are identical to the singular values

$$|\lambda_i(A)|=\sigma_i(A). \qquad (V.56)$$

The eigenvalues may be complex or real. As one of the critical indices in the voltage stability problem, the eigenvalue whose real part crosses from negative to positive half-plane is concerned.

The left and right eigenvectors of *A* corresponding to different eigenvalues are orthonormal satisfying following general relation

$$f_i^{\tau}e_j=\delta_{ij}=\begin{cases}0 & for\quad i\neq j\\ 1 & for\quad i=j\end{cases}. \qquad (V.57)$$

Similar relation is valid for $e_i^{\tau}f_j$, as well.

The fast procedure of the minimum absolute eigenvalue and corresponding eigenvectors computation employs following general relations

$$A\,e_n = \lambda_n e_n\,, \qquad \text{(V.58)}$$

$$A^\tau f_n = \lambda_n f_n\,. \qquad \text{(V.59)}$$

The fast computational procedure is given as

(e_n part)

1. Initial guess for the vector $e_n^{(1)}$ in the first iteration,
2. Computing the second norm of the vector $e_n^{(1)}$,
3. Normalisation of the vector $e_n^{(1)}$,
    4. Solving $Ae_n^{(i+1)} = e_n^{(i)}$ in the i-th iteration,
    5. Computing the second norm of the vector $e_n^{(i+1)}$,
    6. Normalisation of the vector $e_n^{(i+1)}$,
    7. Estimating $\lambda_n^{'(i)} = 1/SNRM2(e_n^{(i+1)})$,
    8. Convergence checking in $\lambda_n^{'(i)}$,
    9. Either solution achieved in e_n part, or get back to 4

(f_n part)

10. Initial guess for vector $f_n^{(1)}$ ($=e_n$) in the first iteration,
    11. Solving $A^\tau f_n^{(i+1)} = f_n^{(i)}$ in the $(i+1)$-th iteration,
    12. Computing the second norm of vector $f_n^{(i+1)}$,
    13. Normalisation of vector $f_n^{(i+1)}$,
    14. Estimating $\lambda_n^{''(i)} = 1/SNRM2(f_n^{(i+1)})$,
    15. Convergence checking in $\lambda_n^{''(i)}$,
    16. Either solution achieved in f_n part, or get back to 11

17. Exit from iterative part when convergence is achieved (difference from two consecutive iterations smaller than a pre-established threshold).

Besides fast computational procedure, the other methods resulting in complete eigenvalue decomposition are used as well.

Similarly to singular value decomposition applied to the problem (V.5), the eigenvalue decomposition gives the solution x, depending on input b, as

$$\begin{aligned} x &= A^{-1}b = \left(E\ \Lambda\ F^\tau\right)^{-1} b = \sum_{i=1}^{n} \frac{e_i f_i^\tau}{\lambda_i} b \approx \\ &\approx \left(\lambda_n^{-1} e_n\right)\left(f_n^\tau b\right) \end{aligned}, \qquad \text{(V.60)}$$

assuming that $|\lambda_{n-1}| >> |\lambda_n|$, which holds especially in the vicinity of the critical point.

With respect to the particular steady state power flow problem (V.7), the steady state load flow Jacobian matrix, J_{LF}, is decomposed as

$$J_{LF} = E\,\Lambda\,F^\tau = E\,\Lambda\,E^{-1}\,. \qquad \text{(V.61)}$$

The inverse of the matrix J_{LF} then appears as

$$\begin{aligned} J_{LF}^{-1} &= \left(E\ \Lambda\ F^\tau\right)^{-1} = E\ \Lambda^{-1}\ F^\tau \approx \\ &\approx \lambda_n^{-1} e_n f_n^\tau \end{aligned}. \qquad \text{(V.62)}$$

By introducing (V.62) in (V.60), the solution is given as

$$\begin{bmatrix}\Delta\Theta \\ \Delta V\end{bmatrix} = \lambda_n^{-1} e_n f_n^\tau \begin{bmatrix}\Delta P \\ \Delta Q\end{bmatrix}. \qquad \text{(V.63)}$$

By reasoning similarly to (V.11-12), following relations are introduced

$$\begin{bmatrix}\Delta\Theta \\ \Delta V\end{bmatrix} = \lambda_n^{-1} e_n\,, \qquad \text{(V.64)}$$

$$\begin{bmatrix}\Delta P \\ \Delta Q\end{bmatrix} = f_n\,. \qquad \text{(V.65)}$$

This approach is applied to the extended load flow Jacobian matrix, J_{EXT}, and the state matrix, A_S, as well.

Concerning sensitivity of critical eigenvalue [216, 220, 233, 258, 295, 359, 392], if following relation between λ_n, e_n, and J_{EXT}

$$J_{EXT}\ e_n = \lambda_n e_n \qquad \text{(V.66)}$$

is first differentiated with respect to parameter p, and then pre-multiplied by f_n^τ, it gives

$$f_n^\tau \frac{\partial J_{EXT}}{\partial p} e_n + f_n^\tau J_{EXT} \frac{\partial e_n}{\partial p} = f_n^\tau \frac{\partial \lambda_n}{\partial p} e_n + f_n^\tau \lambda_n \frac{\partial e_n}{\partial p}\,. \qquad \text{(V.67)}$$

By using relation

$$f_n^\tau J_{EXT} = \lambda_n f_n^\tau\,, \qquad \text{(V.68)}$$

the sensitivity of critical eigenvalue with respect to the parameter p is obtained from (V.67) as

$$\frac{\partial \lambda_n}{\partial p} = \frac{f_n^\tau \dfrac{\partial J_{EXT}}{\partial p} e_n}{f_n^\tau e_n}\,. \qquad \text{(V.69)}$$

If the sensitivity, given by (V.69), is defined with respect to the control set of the UPFC parameters (r, γ, I_{conv1q}), it leads to a very similar approach that is used in the case of the singular value sensitivity.

V.1.C Participation factors

The sensitivity analysis, as seen from the viewpoint of singular and eigenvalue decomposition, contributes to find appropriate location and action of the UPFC. The UPFC has rather unique capability of simultaneous series control of branch power flow and shunt control of bus voltage magnitude. By correlating branch and bus participation factors obtained from the matrix decompositions [195], it is possible to recognise location of its installation where appropriate regulation characteristics could be extensively used during voltage emergency situations.

Branch participation factors

Due to different models, branch participation factors are defined for transmission lines and transformers separately.

Transmission line is represented by π model (Fig. V.1). It has a series admittance g_l+jb_l, and two shunt ones $jb_c/2$.

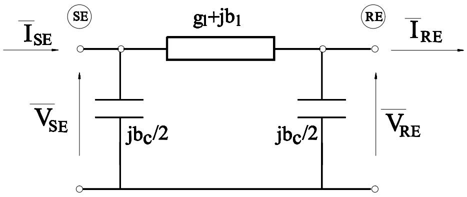

Fig. V.1 Transmission line π model

Apparent power at the sending end of the line model, $\overline{S}_{SE}$, is given as

$$\begin{aligned}\overline{S}_{SE} &= P_{SE} + jQ_{SE} = \overline{V}_{SE}\overline{I}_{SE}^{*} = \\ &= \overline{V}_{SE}\left[(g_l + jb_l)\left(\overline{V}_{SE} - \overline{V}_{RE}\right) + j\frac{b_c}{2}\overline{V}_{SE}\right]^{*} = \\ &= \left[V_{SE}^2 g_l - V_{SE}V_{RE}(g_l\cos\Theta_{SR} + b_l\sin\Theta_{SR})\right] + \\ &+ j\left[-V_{SE}^2\left(b_l + \frac{b_c}{2}\right) + V_{SE}V_{RE}(b_l\cos\Theta_{SR} - g_l\sin\Theta_{SR})\right]\end{aligned} \qquad (V.70)$$

where Θ_{SR} denotes angle difference (Θ_{SE} - Θ_{RE}).

At the receiving end of the line model, the apparent power $\overline{S}_{RE}$ is given as

$$\begin{aligned}\overline{S}_{RE} &= P_{RE} + jQ_{RE} = \overline{V}_{RE}\overline{I}_{RE}^{*} = \\ &= \overline{V}_{RE}\left[(g_l + jb_l)\left(\overline{V}_{SE} - \overline{V}_{RE}\right) - j\frac{b_c}{2}\overline{V}_{RE}\right]^{*} = \\ &= \left[-V_{RE}^2 g_l + V_{SE}V_{RE}(g_l\cos\Theta_{SR} - b_l\sin\Theta_{SR})\right] + \\ &+ j\left[V_{RE}^2\left(b_l + \frac{b_c}{2}\right) - V_{SE}V_{RE}(b_l\cos\Theta_{SR} + g_l\sin\Theta_{SR})\right]\end{aligned} \qquad (V.71)$$

Active and reactive power losses on a transmission line are defined using (V.70-71) as it follows

$$\begin{aligned}P_{loss}^{line} &= P_{SE} - P_{RE} = \\ &= g_l\left(V_{SE}^2 + V_{RE}^2\right) - 2g_l V_{SE}V_{RE}\cos\Theta_{SR}\end{aligned}, \qquad (V.72)$$

$$\begin{aligned}Q_{loss}^{line} &= Q_{SE} - Q_{RE} = \\ &= -\left(b_l + \frac{b_c}{2}\right)\left(V_{SE}^2 + V_{RE}^2\right) + 2b_l V_{SE}V_{RE}\cos\Theta_{SR}\end{aligned} \qquad .(V.73)$$

By linearising (V.72) with respect to the set of variables (Θ_{SE}, Θ_{RE}, V_{SE}, V_{RE}), which is given as

$$\begin{aligned}\Delta P_{loss}^{line} = &\frac{\partial P_{loss}^{line}}{\partial \Theta_{SE}}\Delta\Theta_{SE} + \frac{\partial P_{loss}^{line}}{\partial \Theta_{RE}}\Delta\Theta_{RE} + \\ &+ \frac{\partial P_{loss}^{line}}{\partial V_{SE}}\Delta V_{SE} + \frac{\partial P_{loss}^{line}}{\partial V_{RE}}\Delta V_{RE}\end{aligned}, \qquad (V.74)$$

the differential change of the active power loss appears as

$$\begin{aligned}\Delta P_{loss}^{line} = 2g_l\{&[V_{SE}V_{RE}\sin(\Theta_{SE} - \Theta_{RE})](\Delta\Theta_{SE} - \Delta\Theta_{RE}) + \\ &+ [V_{SE} - V_{RE}\cos(\Theta_{SE} - \Theta_{RE})]\Delta V_{SE} + \\ &+ [V_{RE} - V_{SE}\cos(\Theta_{SE} - \Theta_{RE})]\Delta V_{RE}\}\end{aligned} \qquad .(V.75)$$

Similarly reasoning, the differential change of the reactive power loss from (V.73) is given as

$$\begin{aligned}\Delta Q_{loss}^{line} = -\{&[2V_{SE}V_{RE}b_l\sin(\Theta_{SE} - \Theta_{RE})](\Delta\Theta_{SE} - \Delta\Theta_{RE})\} + \\ &+ \left\{\left[-2V_{SE}\left(b_l + \frac{b_c}{2}\right) + 2V_{RE}b_l\cos(\Theta_{SE} - \Theta_{RE})\right]\Delta V_{SE}\right\} + \\ &+ \left\{\left[-2V_{RE}\left(b_l + \frac{b_c}{2}\right) + 2V_{SE}b_l\cos(\Theta_{SE} - \Theta_{RE})\right]\Delta V_{RE}\right\}\end{aligned} \qquad .(V.76)$$

Differential change in transformer reactive power loss is based on its model with injected powers (Fig. II.13). Due to the assumptions set in the model, there is no active power loss since the series branch of the transformer model has only a susceptance. For the sake of this analysis, the model has been adjusted to account for changed direction of current/power at the receiving end (Fig. V.2)

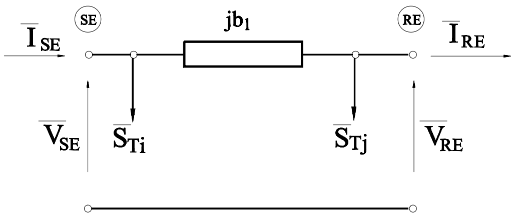

Fig. V.2 Transformer injection model

Thereby, the apparent power at the sending end of the transformer model, $\overline{S}_{SE}$, is given as

$$\begin{aligned}\overline{S}_{SE} = &\left[\left(1 - \frac{1}{t_r}\right)b_l V_{SE}V_{RE}\sin\Theta_{SR} - b_l V_{SE}V_{RE}\sin\Theta_{SR}\right] + \\ &+ j\left\{b_l\left(1 - \frac{1}{t_r}\right)\left[V_{SE}^2\left(1 + \frac{1}{t_r}\right) - V_{SE}V_{RE}\cos\Theta_{SR}\right] + \right. \\ &\left. + b_l V_{SE}V_{RE}\cos\Theta_{SR} - b_l V_{SE}^2\right\}\end{aligned} \qquad .(V.77)$$

At the receiving end of the transformer model, the apparent power $\overline{S}_{RE}$ is given as

$$\begin{aligned}\overline{S}_{RE} &= \left[\left(1-\frac{1}{t_r}\right)b_l V_{SE} V_{RE} \sin\Theta_{SR} - b_l V_{SE} V_{RE} \sin\Theta_{SR}\right] + \\ &+ j\left[\left(1-\frac{1}{t_r}\right)b_l V_{SE} V_{RE} \cos\Theta_{SR} - b_l V_{SE} V_{RE} \cos\Theta_{SR} + b_l V_{RE}^2\right]\end{aligned} \quad (V.78)$$

Then, the active and reactive power losses on a transformer are defined using (V.77-78) as it follows

$$P_{loss}^{tra} = P_{SE} - P_{RE} = 0\,, \quad (V.79)$$

$$\begin{aligned}Q_{loss}^{tra} &= Q_{SE} - Q_{RE} = \\ &= -b_l\left[\left(\frac{V_{SE}}{t_r}\right)^2 + V_{RE}^2\right] + 2b_l \frac{V_{SE}}{t_r} V_{RE} \cos\Theta_{SR}\end{aligned}\,. \quad (V.80)$$

By linearising (V.80) with respect to the set of variables (Θ_{SE}, Θ_{RE}, V_{SE}, V_{RE}) similarly as it is done in (V.74), the differential change of the reactive power loss is given as

$$\begin{aligned}\Delta Q_{loss}^{tra} &= -\left\{\left[2b_l \frac{V_{SE}}{t_r} V_{RE} \sin(\Theta_{SE}-\Theta_{RE})\right](\Delta\Theta_{SE}-\Delta\Theta_{RE})\right\} + \\ &+ \left\{\left[-2b_l \frac{V_{SE}}{t_r^2} + 2b_l \frac{V_{RE}}{t_r}\cos(\Theta_{SE}-\Theta_{RE})\right]\Delta V_{SE}\right\} + \\ &+ \left\{\left[-2b_l V_{RE} + 2b_l \frac{V_{SE}}{t_r}\cos(\Theta_{SE}-\Theta_{RE})\right]\Delta V_{RE}\right\}\end{aligned} \quad .(V.81)$$

Differential changes of the losses (V.75-76, V.81) are considered as branch participation factors. They depend on the set of variables ($\Delta\Theta_{SE}$, $\Delta\Theta_{RE}$, ΔV_{SE}, ΔV_{RE}). In order to compute branch participation factors, this set is replaced with four corresponding variables given by (V.11) for singular value decomposition, or (V.64) for eigenvalue decomposition of the extended Jacobian matrix J_{EXT}. Symbolically written, the set of changes ($\Delta\Theta$, ΔV) becomes replaced with another set given by ($\sigma_n^{-1} v_n$) for singular value decomposition, or ($\lambda_n^{-1} e_n$) for eigenvalue decomposition.

Branch participation factors enable recognition of network branches that have higher participation in the power losses during voltage collapse scenario. Thereby, they point out an area where relieving actions should be taken from a series power flow aspect.

Bus participation factors

Bus participation factors concern algebraic variables of bus voltage angles and magnitudes, (Θ, V), within the extended Jacobian matrix J_{EXT}.

If singular value decomposition is used, the participation of algebraic variables (Θ, V) in the voltage stability problem is reflected through corresponding variables given by (V.11-12). Having computed minimum singular value and associated singular vectors, the entries of the vectors indicate buses with higher participation during voltage collapse. Similar reasoning applies for eigenvalue decomposition as well.

Bus participation factors enable recognition of network buses that have higher participation in voltage decline. Thereby, they point out buses where relieving actions should be taken from a shunt voltage support aspect.

Generator participation factors

Generator participation factors concern state variables of generators within the state matrix A_S. The participation of the state variables in the voltage stability problem is reflected through corresponding variables computed within singular or eigenvalue decomposition (critical values and associated vectors). The approach is similar to the one previously applied to the bus participation factors. Also, similar approach could be applied to the other power system elements having state variables. Having computed critical value and associated vectors, the entries of the vectors indicate generator state variables with higher participation during voltage collapse.

Generator participation factors enable recognition of generators that have higher participation in the scenario. Thereby, they point out generators where relieving actions should be taken from an operational aspect.

V.2 PARAMETRIC SENSITIVITY

It is supposed earlier (IV.1-2) that the differential-algebraic model of the system has following set of equations

$$\frac{dx}{dt} = f(x,y,p)\,, \quad (V.82)$$

$$0 = g(x,y,p)\,, \quad (V.83)$$

where x and y denote state and algebraic variables, p parameters, f and g differential and algebraic equations.

By linearising (V.82-83) around an operating point, the set of the linearised equations appears in general form as

$$\Delta\frac{dx}{dt} = f_x\Delta x + f_y\Delta y + f_p\Delta p\,, \quad (V.84)$$

$$0 = g_x\Delta x + g_y\Delta y + g_p\Delta p\,. \quad (V.85)$$

At any equilibrium point, the system (V.82-83) becomes

$$0 = f(x,y,p)\,, \quad (V.86)$$

$$0 = g(x,y,p)\,. \quad (V.87)$$

Therefore, linearisation of the system at any equilibrium point results with

$$0 = f_x \Delta x + f_y \Delta y + f_p \Delta p \, , \tag{V.88}$$
$$0 = g_x \Delta x + g_y \Delta y + g_p \Delta p \, . \tag{V.89}$$

From (V.88-89), differentials Δx and Δy are obtained as

$$\Delta x = -f_x^{-1}\left(f_y \Delta y + f_p \Delta p\right), \tag{V.90}$$
$$\Delta y = -g_y^{-1}\left(g_x \Delta x + g_p \Delta p\right). \tag{V.91}$$

By introducing (V.91) in (V.90), differential Δx becomes

$$\Delta x = -f_x^{-1}\left[-f_y g_y^{-1}\left(g_x \Delta x + g_p \Delta p\right) + f_p \Delta p\right]. \tag{V.92}$$

Rearranging (V.92), differential Δx becomes dependent only on Δp, as it follows in

$$\Delta x = A_S^{-1}\left(f_y g_y^{-1} g_p - f_p\right)\Delta p \, , \tag{V.93}$$

where A_S is the state matrix given as

$$A_S = \left[f_x - \left(f_y g_y^{-1} g_x\right)\right]. \tag{V.94}$$

By introducing (V.93) in (V.91), differential Δy becomes dependent on Δp as well

$$\Delta y = -g_y^{-1}\left[g_x A_S^{-1}\left(f_y g_y^{-1} g_p - f_p\right) + g_p\right]\Delta p \, . \tag{V.95}$$

Thereby, parametric sensitivities of state and algebraic variables with respect to arbitrary parameters [98-99, 276] are defined from (V.93, V.95) as

$$\frac{\partial x}{\partial p} = A_S^{-1}\left(f_y g_y^{-1} g_p - f_p\right), \tag{V.96}$$
$$\frac{\partial y}{\partial p} = -g_y^{-1}\left[g_x A_S^{-1}\left(f_y g_y^{-1} g_p - f_p\right) + g_p\right]. \tag{V.97}$$

Parametric sensitivities $\partial x/\partial p$ and $\partial y/\partial p$ give a natural measure of the sensitivity of the solution $(x(p),y(p))$ at an operating point. In order to relate these parametric sensitivities to stability, singular value decomposition of the inverse state matrix A_S^{-1} is used first as

$$A_S^{-1} = \left(U \, \Sigma \, V^{\tau}\right)^{-1} = V \, \Sigma^{-1} \, U^{\tau} \approx \sigma_n^{-1} v_n u_n^{\tau} \, . \tag{V.98}$$

Then, projected parametric sensitivity of state variables is written as

$$\frac{\partial x}{\partial p} = \sigma_n^{-1} v_n u_n^{\tau}\left(f_y g_y^{-1} g_p - f_p\right). \tag{V.99}$$

Projection of $\partial x/\partial p$ onto the particular (minimum) singularsubspace of critical interest gives good information for selecting the most influential parameters critical to minimum singular value σ_n.

Furthermore [210, 230], if measure of projected parametric sensitivity onto a particular singularsubspace of interest, m_{pps}, is defined as

$$m_{pps}^{\tau} = u_n^{\tau}\left(f_y g_y^{-1} g_p - f_p\right), \tag{V.100}$$

then the projected parametric sensitivity (V.99) becomes

$$\frac{\partial x}{\partial p} = \sigma_n^{-1} v_n m_{pps}^{\tau} \, . \tag{V.101}$$

Matrices f_x, f_y, g_x, and g_y are defined in Chapter IV as parts of the differential-algebraic model. In addition, it is necessary to define matrices f_p and g_p in order to compute parametric sensitivities. Among suitable parameters, the set of UPFC control parameters (r, γ, I_{conv1q}) is concerned.

In that case, matrix f_p is equal to zero because differential equations of the UPFC control system are not included in the differential-algebraic model. Certainly, this enables some further simplification of the expressions defining the sensitivities.

Matrix g_p is obtained as a three-column matrix (g_r, g_γ, $g_{Iconv1q}$) by differentiating network equations (III.66-69) with respect to the set (r, γ, I_{conv1q}). Therefore, column vectors g_r and g_γ have four non-zero entries, whereas $g_{Iconv1q}$ has one non-zero entry.

Non-zero entries of the column vector g_r are given as

$$g_r^{(P_i)} = -b_S V_i V_j \sin(\Theta_{ij} + \gamma) \, , \tag{V.102}$$
$$g_r^{(P_j)} = b_S V_i V_j \sin(\Theta_{ij} + \gamma) \, , \tag{V.103}$$
$$g_r^{(Q_i)} = -b_S V_i^2 \cos\gamma \, , \tag{V.104}$$
$$g_r^{(Q_j)} = b_S V_i V_j \cos(\Theta_{ij} + \gamma) \, . \tag{V.105}$$

Non-zero entries of the column vector g_γ are given as

$$g_\gamma^{(P_i)} = -r b_S V_i V_j \cos(\Theta_{ij} + \gamma) \, , \tag{V.106}$$
$$g_\gamma^{(P_j)} = r b_S V_i V_j \cos(\Theta_{ij} + \gamma) \, , \tag{V.107}$$
$$g_\gamma^{(Q_i)} = r b_S V_i^2 \sin\gamma \, , \tag{V.108}$$
$$g_\gamma^{(Q_j)} = -r b_S V_i V_j \sin(\Theta_{ij} + \gamma) \, . \tag{V.109}$$

Non-zero entry of the column vector $g_{Iconv1q}$ is given as

$$g_{Iconv1q}^{(Q_i)} = V_i \frac{S_{conv1n}}{S_B} \, . \tag{V.110}$$

By similar reasoning, matrices f_p and g_p are defined for any other arbitrary parameter p. Especially load models from Chapter II are evaluated for their characteristics being considered as parameters. Thereby, following set of parameters appears given as $p = [T_{m0}, (P_L^0)_{DL}, (Q_L^0)_{DL}, \tau_{REF}, t_r, b_{shu}, (P_L^0)_{SL}, (Q_L^0)_{SL}]$, where T_{m0} denotes value of the motor load torque at the speed ω_{m0}, $(P_L^0)_{DL}$ and $(Q_L^0)_{DL}$ static parts of the initial active and reactive power demands of dynamic loads with non-linear recovery, τ_{REF} referent temperature of the TCL load model, t_r transformer ratio, b_{shu} susceptance of the shunt capacitor, and $(P_L^0)_{SL}$, $(Q_L^0)_{SL}$ static parts of the initial active and reactive power demands of static loads.

For parameter T_{m0}, corresponding entries of f_p and g_p are given as

$$f_p = -\left[A\left(\frac{\omega_m}{\omega_{m0}}\right)^2 + B\left(\frac{\omega_m}{\omega_{m0}}\right) + C + D\left(\frac{\omega_m}{\omega_{m0}}\right)^{am} \right] \Big/ (2H) , \tag{V.111}$$

$$g_p = 0 . \tag{V.112}$$

For parameter $(P_L^0)_{DL}$, and similarly $(Q_L^0)_{DL}$, corresponding entries of f_p and g_p are given in a simplified way as

$$f_p = \left\{ \left[K_{pz}\left(\frac{V_n}{V_{n0}}\right)^2 + K_{pi}\left(\frac{V_n}{V_{n0}}\right) + K_{pp} \right] \right\} , \tag{V.113}$$

$$g_p = 0 . \tag{V.114}$$

For parameter τ_{REF}, corresponding entries of f_p and g_p are given as

$$f_p = K_I / T_C , \tag{V.115}$$

$$g_p = 0 . \tag{V.116}$$

For parameter t_r, corresponding entries of f_p and g_p are given as

$$f_p = 0 , \tag{V.117}$$

$$g_p = \begin{cases} \dfrac{\partial P_i}{\partial t_r} = \dfrac{1}{t_r^2} b_T V_i V_j \sin\Theta_{ij} \\ \dfrac{\partial P_j}{\partial t_r} = -\dfrac{1}{t_r^2} b_T V_i V_j \sin\Theta_{ij} \\ \dfrac{\partial Q_i}{\partial t_r} = \dfrac{2}{t_r^3} b_T V_i^2 - \dfrac{1}{t_r^2} b_T V_i V_j \cos\Theta_{ij} \\ \dfrac{\partial Q_j}{\partial t_r} = -\dfrac{1}{t_r^2} b_T V_i V_j \cos\Theta_{ij} \end{cases} . \tag{V.118}$$

For parameter b_{shu}, corresponding entries of f_p and g_p are given as

$$f_p = 0 , \tag{V.119}$$

$$g_p = \left\{ \frac{\partial Q_i}{\partial b_{shu}} = -V_i^2 \right. . \tag{V.120}$$

For parameter $(P_L^0)_{SL}$, and similarly $(Q_L^0)_{SL}$, corresponding entries of f_p and g_p are given in a simplified way as

$$f_p = 0 , \tag{V.121}$$

$$g_p = \left\{ \frac{\partial P_i}{\partial P_L^0} = \left[\left[K_{pz}\left(\frac{V_n}{V_{n0}}\right)^2 + K_{pi}\left(\frac{V_n}{V_{n0}}\right) + K_{pp} \right] \right] \right\} . \tag{V.122}$$

V.3 FUNCTIONAL SENSITIVITY

Besides parametric sensitivity, at snapshots of time domain simulations it is also possible to evaluate sensitivity of a function with respect to arbitrary parameters. Throughout the dissertation, this type of sensitivity is called functional sensitivity. Total reactive power production of generators [368-376] and total active power loss [319] are considered as appropriate functions in the voltage stability problem and in the power flow regulation problem, respectively.

Total reactive power production of generators

The sensitivity of a scalar quantity $\eta(x,y)$ to parameter p is obtained as a system-wide indicator [368-376], given by

$$\frac{\partial \eta}{\partial p} = -\begin{bmatrix} f_p^\tau & g_p^\tau \end{bmatrix} \left(J_{EXT}^\tau\right)^{-1} \begin{bmatrix} \partial \eta / \partial x \\ \partial \eta / \partial y \end{bmatrix} , \tag{V.123}$$

$$\frac{\partial \eta}{\partial p} = -\begin{bmatrix} \dfrac{\partial \eta^\tau}{\partial x} & \dfrac{\partial \eta^\tau}{\partial y} \end{bmatrix} \left(J_{EXT}\right)^{-1} \begin{bmatrix} f_p \\ g_p \end{bmatrix} . \tag{V.124}$$

In the voltage stability problem, the scalar quantity $\eta(x,y)$ is represented by the total reactive power production of the generators Q_G^Σ, given as

$$Q_G^\Sigma = \sum_{i=1}^{n_{GEN}} Q_{Gi} = \sum_{i=1}^{n_{GEN}} \left(V_{di} I_{qi} - V_{qi} I_{di} \right) . \tag{V.125}$$

From (V.125), it is seen that the entries of $\partial\eta/\partial x$ and $\partial\eta/\partial y$ for the total reactive power production are given as

$$\frac{\partial \eta}{\partial x} = 0 , \tag{V.126}$$

$$\frac{\partial \eta}{\partial y} = \left(-V_{qi} ; V_{di} ; I_{qi} ; -I_{di} \right) . \tag{V.127}$$

Arbitrary parameter p is represented by the static parts of the initial active, $(P_L^0)_{DL}$, and reactive, $(Q_L^0)_{DL}$, power demands of dynamic loads with non-linear recovery. The static parts are based on the ones given by (II.91) with slight simplifying modifications

$$P_S(V) = P_L^0 \left(V_i / V_i^0 \right)^\beta , \tag{V.128}$$

$$Q_S(V) = Q_L^0 \left(V_i / V_i^0 \right)^\beta . \tag{V.129}$$

The entries of f_p and g_p are obtained based on (V.113-114).

This functional sensitivity involves the inverse of the extended Jacobian matrix J_{EXT}. Therefore, it has larger magnitudes as the critical point is approached with abrupt change to opposite sign as it is crossed. The appearance of the critical point represents a reliable sign of impending voltage unstable situation and could trigger voltage support from the UPFC.

Total active power loss

For being considered in the power flow regulation problem, the total active power loss [319] is formulated as

$$P_{loss}(\Theta,V) = \sum_{m=1}^{n} V_m \sum_{k=1}^{n} V_k G_{mk} \cos\Theta_{mk} \ . \tag{V.130}$$

Since the loss minimisation is of concern, in the solution of the problem min $P_{loss}(x, y, p)$, the sensitivity $(d\, P_{loss} / d\, p)$ is to be computed.

Change in the loss, ΔP_{loss}, is expressed as

$$\Delta P_{loss}(x,y,p) = \frac{\partial P_{loss}}{\partial x}^{\tau} \Delta x + \frac{\partial P_{loss}}{\partial y}^{\tau} \Delta y + \frac{\partial P_{loss}}{\partial p}^{\tau} \Delta p \tag{V.131}$$

Differentials Δx and Δy, with respect to Δp, are computed from (V.93) and (V.95), respectively. The partial derivatives are given as follows

$$\frac{\partial P_{loss}}{\partial x} = 0 \quad ; \quad \frac{\partial P_{loss}}{\partial p} = 0 \quad and$$
$$\frac{\partial P_{loss}}{\partial y} = \begin{cases} \dfrac{\partial P_{loss}}{\partial \Theta_m} = -2\displaystyle\sum_{\substack{k=1\\k\neq m}}^{n} V_m V_k G_{mk} \sin\Theta_{mk} \\ \dfrac{\partial P_{loss}}{\partial V_m} = 2\displaystyle\sum_{k=1}^{n} V_k G_{mk} \cos\Theta_{mk} \end{cases} . \tag{V.132}$$

Finally, the sensitivity $(d\, P_{loss} / d\, p)$ is expressed as

$$\frac{dP_{loss}}{dp}^{\tau} = -\frac{\partial P_{loss}}{\partial y}^{\tau} g_y^{-1}\left[g_x A_S^{-1}\left(f_y g_y^{-1} g_p - f_p\right) + g_p\right] . \tag{V.133}$$

The set of UPFC control parameters (r, γ, I_{conv1q}) is used for evaluating f_p and g_p according to (V.102-110).

V.4 SUB-OPTIMAL FORMULATION USING SENSITIVITIES

If the objectives are set as either to minimise the total active power loss or to maximise minimum singular value, a simple sub-optimal formulation is proposed through the objective functions [349]. The objective functions address minimisation of the squares of the deviations, including additional penalty term that corresponds to the control variables.

The objective function in the power loss case is given as

$$\begin{aligned} F_{loss} &= \frac{1}{2}\left(\frac{P_{loss}^{set} - P_{loss}}{\Delta P_{loss}^{\max}}\right)^2 + \\ &+ \frac{1}{2}\sum_{k=1}^{3} w_{p_k}\left(\frac{\Delta p_k}{\Delta p_k^{\max}}\right)^2 = \\ &= \frac{1}{2}\left(\frac{P_{loss}^{set} - P_{loss}^{0} - \sum_{k=1}^{3}\frac{dP_{loss}}{dp_k}\Delta p_k}{\Delta P_{loss}^{\max}}\right)^2 + \\ &+ \frac{1}{2}\sum_{k=1}^{3} w_{p_k}\left(\frac{\Delta p_k}{\Delta p_k^{\max}}\right)^2 \end{aligned} , \tag{V.134}$$

where P_{loss}^{0} denotes base case loss, P_{loss}^{set} desired value of the loss (decreased), Δ^{max} maximum permitted deviation of a variable, p_k (k = 1, 2, 3) one of the UPFC control parameters, and w_{pk} its participation factor.

The first term in (V.134) is aimed to bring the loss close to desired lower value, whereas the second one ensures this to be done with minimum control effort.

In order to minimise F_{loss} with respect to the set of UPFC control parameters Δp_k, it is stated that

$$A\Delta p = B \ , \tag{V.135}$$

where A is a 3x3 matrix of type $\partial F_{loss} / \partial \Delta p_k$ for k = 1, 2, 3, and B is a residual 3x1 vector.

The entries of the matrix A are given as

$$\begin{aligned} A_{kk} &= \frac{\left(\dfrac{dP_{loss}}{dp_k}\right)^2}{\left(\Delta P_{loss}^{\max}\right)^2} + \frac{w_{p_k}}{\left(\Delta p_k^{\max}\right)^2}; \\ A_{kl} &= \frac{\dfrac{dP_{loss}}{dp_k}\dfrac{dP_{loss}}{dp_l}}{\left(\Delta P_{loss}^{\max}\right)^2} \end{aligned} , \tag{V.136}$$

whereas the ones of the vector B as

$$B_k = \frac{P_{loss}^{set} - P_{loss}^{0}}{\left(\Delta P_{loss}^{\max}\right)^2}\frac{dP_{loss}}{dp_k} . \tag{V.137}$$

Solution of equation (V.135) gives a control movement Δp_k determining the change in the UPFC parameters to decrease total power system loss.

Similar formulation of the problem appears in the case of maximising minimum singular value σ_n within the function given as

$$
\begin{aligned}
F_{\sigma_n} &= \frac{1}{2}\left(\frac{\sigma_n^{set} - \sigma_n}{\Delta\sigma_n^{\max}}\right)^2 + \\
&+ \frac{1}{2}\sum_{k=1}^{3} w_{p_k}\left(\frac{\Delta p_k}{\Delta p_k^{\max}}\right)^2 = \\
&= \frac{1}{2}\left(\frac{\sigma_n^{set} - \sigma_n^0 - \sum\limits_{k=1}^{3}\frac{d\sigma_n}{dp_k}\Delta p_k}{\Delta\sigma_n^{\max}}\right)^2 + \\
&+ \frac{1}{2}\sum_{k=1}^{3} w_{p_k}\left(\frac{\Delta p_k}{\Delta p_k^{\max}}\right)^2
\end{aligned} \quad . \tag{V.138}
$$

Further procedure leads to a similar form of matrix A and vector B, differing only in the main variable (σ_n) which should be increased to a pre-set value.

VI. NUMERICAL RESULTS ON THE UPFC VOLTAGE/POWER FLOW REGULATION

At the first instance, possible benefits of the UPFC injection model are investigated within voltage/power flow regulation problem on the multi-machine test system. By using appropriate control system of the model it is made possible to control simultaneously three transmission system variables depending on the regulation mode (bus voltage magnitude, power flow, series compensation, and phase shifting). Before tackling voltage/power flow regulation problem, dimensioning procedure is addressed. By describing achieved results it is shown that the UPFC could be useful transmission system controller in steady state operation of power system. Furthermore, its injection model with proposed control system help in recognising each of potential operating modes.

VI.1 INITIAL RATING POWERS OF THE UPFC

In order to analyse impact of the UPFC to voltage/power flow regulation problem, first it is necessary to estimate rating powers of transformers and converters.

Initial dimensioning procedure is described in subsection III.4.F. It considers the system in its steady state without any system dynamics. Therefore, its basis is a steady state load flow computation, where the loads have constant values and are independent on bus voltage magnitudes.

According to the algorithm for optimal rating of the UPFC (Fig. III.20), the results concerning r_{max}, S_S, and max$|P_{conv1}|$ are given in Table VI.1. Powers S_S and max$|P_{conv1}|$ are obtained after optimising procedure is made with respect to the maximum magnitude of the injected series voltage r_{max} (Fig. VI.1).

Table VI.1 Rating powers of the UPFC according to algorithm for optimal rating (Fig. III.20)

r_{max} (pu)	S_S (pu)	max $\|P_{conv1}\|$ (pu)
0.01	0.032	0.0316
0.02	0.066	0.0639
0.03	0.100	0.0974
0.04	0.135	0.1320
0.05	0.172	0.1678
0.06	0.211	0.2048
0.07	0.252	0.2432
0.08	0.294	0.2829
0.09	0.339	0.3240
0.10	0.385	0.3666
0.11	0.433	0.4108
0.12	0.484	0.4566
0.13	0.536	0.5042
0.14	0.591	0.5537
0.15	0.649	0.6050
0.16	0.709	0.6585
0.17	0.771	0.7141
0.18	0.836	0.7720
0.19	0.904	0.8322
0.20	0.974	0.8951
0.21	1.047	0.9608
0.22	1.123	1.0294
0.23	/	/

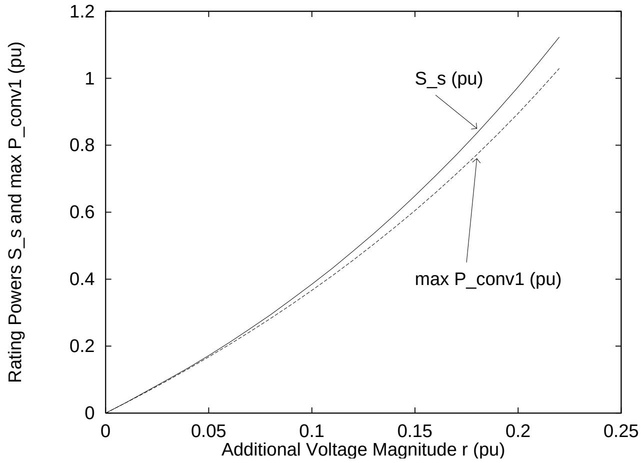

Fig. VI.1 Rating powers with respect to maximum magnitude

The powers are given in pu (1 pu = 100 MVA). The series transformer reactance x_k is set at 0.1 pu, and the system base power is 100 MVA. The results are obtained for the range of r_{max} values between the lowest 0.01 pu and the highest 0.22 pu for which the load flows have convergent solution.

The powers appear correspondingly in approximate range between 3 MVA and 112 MVA. Larger values of r_{max} increase discrepancy between the powers due to appearance of reactive power at the series side. For the value of r_{max} equal to 0.15 pu, the corresponding powers S_S and max$|P_{conv1}|$ are equal to 64.9 MVA and 60.5 MW, respectively. That value of r_{max} is usually estimated to be acceptable for voltage/power flow control purposes and is used hereafter. Smaller values would be inadequate due to decreased control regions, whereas the larger ones due to increased voltage excursions and many non-convergent cases.

Approximate value of power ratings equal to 65 MVA is questioned due to a necessity of the UPFC usage in operating modes other than series power flow regulation. By subsequent repetitions of voltage/power flow control, oscillations damping, and voltage stability support, it is concluded that nominal ratings S_{conv1n} and S_{conv2n} should be equal to 185 MVA for r_{max} equal to 0.15 pu in order to satisfy voltage and damping criteria as well. Rating power of the shunt side S_{conv1n} is increased due to voltage control allowance, whereas rating power of the series side S_{conv2n} due to damping overload allowance. This makes nominal ratings nearly 3 times larger than initial ones equal to 65 MVA for series power flow regulation solely. Reasons for increased ratings are described within subsequent sections and paragraphs concerning voltage and damping issues.

Steady state load flow computations are compared to the approach employing dynamic load flows. Latter approach includes dynamic behaviour of synchronous generators and rotational change of injected series voltage. The rotational change is defined as a rotation of the injected series voltage vector having constant magnitude r = 0.15 pu in the range of angle values γ= [0°: 360°].

The analysis is twofold. In the first case, influence of load voltage dependency to the UPFC power ratings is considered when the UPFC shunt part is inactive in reactive power compensation (I_{conv1q} = 0 pu). In the second case, influence of the UPFC shunt part engagement to the power ratings is analysed when the system has voltage dependent loads (I_{conv1q} = ±0.9 pu).

In the first case (Figs. VI.2-5), system loads are modelled by using static ZIP model either as constant power loads, or with active power part equal to constant current, and reactive one to constant impedance.

Shunt and series converter powers are computed with respect to the angle γ. Concerned converter powers are apparent, active and reactive power.

The results obtained in the first case of dynamic load flow approach with constant loads (Fig. VI.2, Fig. VI.4) are compared to the results from steady state load flows (Table VI.1, Fig. VI.1). In both approaches the loads are set to be independent on bus voltage magnitudes with the UPFC shunt part being inactive in reactive power compensation. Shunt converter reactive power, Q_{conv1}, is equal to zero within the range of the angle γ.

Series converter apparent power has a maximum value of approximately 65 MVA, whereas shunt converter maximum apparent power is slightly less than 60 MVA. Obtained values closely match those computed for the r_{max} equal to 0.15 pu in Table VI.1. Only minor differences exist due to changes of generator terminal voltages caused by excitation systems.

Within the series converter, reactive power requirement, Q_{conv2}, exists in a significant amount. It keeps the apparent power S_{conv2} at higher values when the active power P_{conv2} passes through zero values. At the shunt side, the apparent power S_{conv1} is equal to the absolute value of the active power P_{conv1}. The active powers of both converters are mutually equal.

In the first case of the dynamic load flow approach, the voltage dependency of loads is addressed to compare converter power ratings. In both cases, the UPFC shunt part is inactive in reactive power compensation (Q_{conv1}=0 pu). Both computational procedures start from the same point (r_{max}= 0.15 pu, γ= 0°).

Comparing shunt (Figs. VI.2-3) and series converter powers (Figs. VI.4-5) without and with voltage dependency, it is seen that after being introduced voltage dependency of load causes decreased converter power requirements.

The largest differences appear in the range of the angle γ between 90° and 270°, mostly affecting the active powers P_{conv1} and P_{conv2}. Around γ= 180°, the UPFC series side bus voltage magnitude, V_j, has the lowest values, whereas the UPFC shunt side bus voltage magnitude, V_i, has the highest values. Adjacent to the series side bus there is BUS20 with load twice as larger as the one at BUS19, which is adjacent to the shunt side bus. Decreased bus voltage magnitude V_j also decreases actual power demand of voltage dependent load at BUS20, which overwhelms increase of actual power demand at BUS19. Locally, overall decrease of load power demand imposes less stringent conditions to the converter powers. Therefore, the powers have smaller range of variations and smaller maximum values.

This discussion leads to a conclusion that load characteristics influence maximum values of the converter powers, and at least locally they should be included in dimensioning procedure of the UPFC.

In the second case (Figs. VI.6-9), system loads are voltage dependent and the influence of the UPFC shunt part engagement is of concern.

The power ratings of the UPFC converters are analysed when the shunt converter reactive current, I_{conv1q}, firstly is equal to -0.9 pu capacitive, and secondly to +0.9 pu inductive. Per unit basis of the current is given as the UPFC converter nominal power instead of the system base power. It means that 1 pu of the I_{conv1q} produces 185 Mvar from the shunt converter when the voltage V_i is equal to 1 pu, and there is no active power requirement from the series side. Computational procedures start from different operating points due to the opposite values of the I_{conv1q}, but with the same settings of the series branch (r_{max}= 0.15 pu, γ= 0°).

Shunt (Figs. VI.6-7) and series converter powers (Figs. VI.8-9) are compared with respect to the initial capacitive and inductive engagements of the UPFC shunt converter. It is seen that maximum values of the apparent powers S_{conv1} and S_{conv2} do not differ significantly within both aspects.

The shunt converter is highly loaded due to the initial reactive power. The series converter loading is rather similar to the loading in the previous analysis (Fig. VI.5) with the shunt part being inactive in reactive power compensation.

It leads to a conclusion that initial loading of the shunt converter does not impact significantly the maximum loading of the series converter. Certainly, in case that a larger voltage sensitive load is located adjacent to the shunt side it is necessary to pay attention to the load impact as it is done in the previous case.

Only minor differences are noticed in the powers due to voltage sensitivity of loads. If the shunt converter is loaded capacitively, the UPFC shunt side bus voltage magnitude is somewhat increased causing slightly increased values of the apparent power S_{conv1}. If the UPFC shunt converter is loaded inductively, the voltage is decreased causing lower values of the S_{conv1}. Dominant portion of the shunt apparent power S_{conv1} is the reactive power Q_{conv1}. The values of the S_{conv2} appear in a very similar range. Characteristic of the P_{conv2} is slightly lowered in inductive operation mode of the shunt converter.

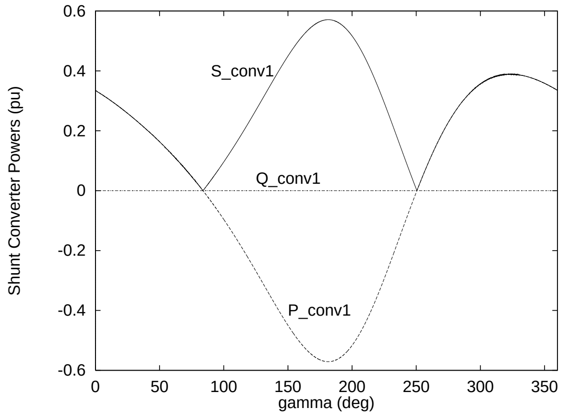

Fig. VI.2 Shunt converter powers with respect to the angle γ
(first case with constant loads)

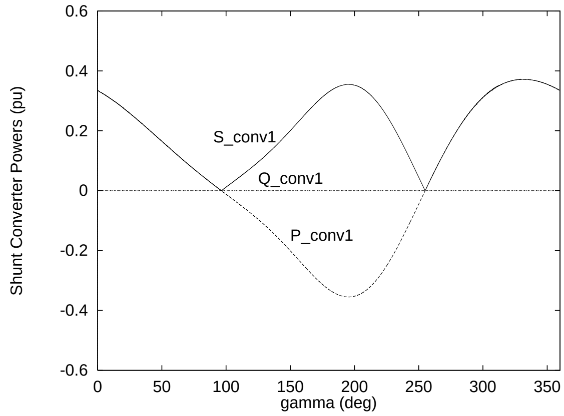

Fig. VI.3 Shunt converter powers with respect to the angle γ
(first case with voltage dependent loads)

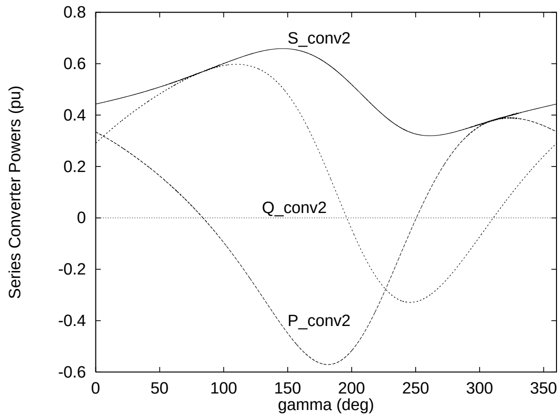

Fig. VI.4 Series converter powers with respect to the angle γ
(first case with constant loads)

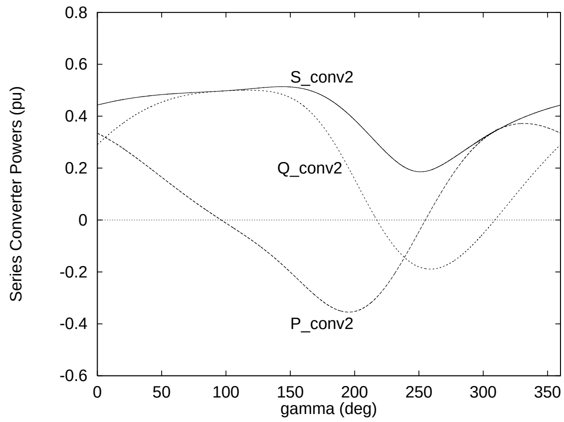

Fig. VI.5 Series converter powers with respect to the angle γ
(first case with voltage dependent loads)

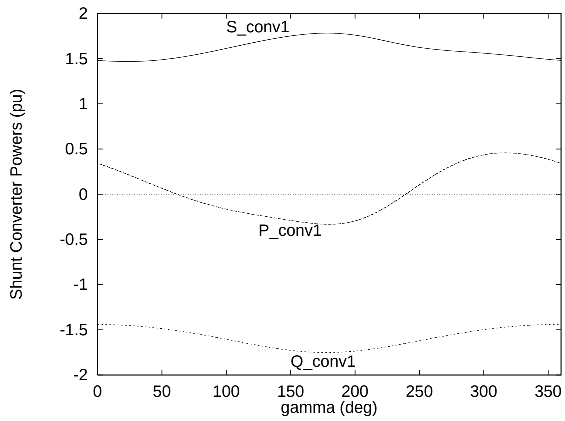

Fig. VI.6 Shunt converter powers with respect to the angle γ
(second case with I_{conv1q} = -0.9 pu)

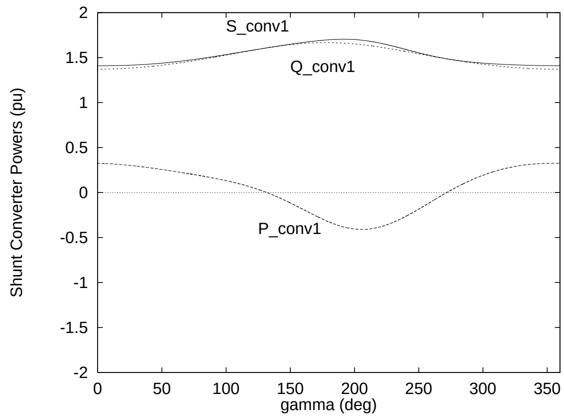

Fig. VI.7 Shunt converter powers with respect to the angle γ
(second case with I_{conv1q} = +0.9 pu)

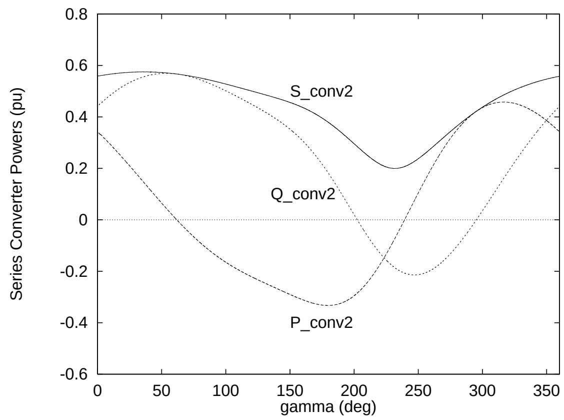

Fig. VI.8 Series converter powers with respect to the angle γ
(second case with I_{conv1q} = -0.9 pu)

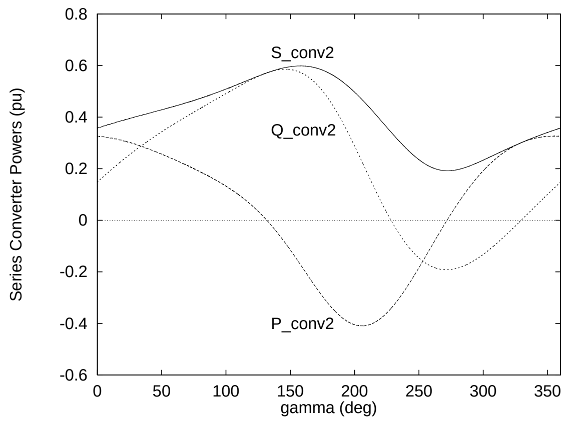

Fig. VI.9 Series converter powers with respect to the angle γ
(second case with I_{conv1q} = +0.9 pu)

VI.2 VOLTAGE CONTROL OF THE UPFC SHUNT SIDE

In order to analyse impact of the UPFC to voltage control problem, the reactive power compensation of the UPFC shunt side is addressed hereafter.

Having the UPFC series part inactive (r = 0 pu), the voltage control of the shunt part is applied solely, according to the considerations given in subsection III.4.A.

The converter rating powers S_{conv1n} and S_{conv2n} are set equal to 185 MVA, with 35% of short-term overload capability of the shunt converter. Limiting action is defined by the time constants T_1=T_2=5 s, and T_3=10 s (Fig. III.15). Continuous operation limit is set equal to x_{cont}=1 pu. The slope setting is defined using the value of the ΔV_{SVG} equal to zero (no slope). The time constants and gain of the shunt side voltage control model are given as T_{vis}=0.5 s, T_{ivi}=0.02 s, and K_{ivi}=5 (Fig. III.16). The loads are modelled by static ZIP model that has active power part equal to constant current, and reactive one to constant impedance.

The simulations start from a steady state operating point given by V_i = 0.9516 pu, where the UPFC is at no-load conditions. The sequence of changes of the referent voltage V_{iREF} is defined as step-up→step-back→step-down→step-back, finishing at the initial point. The values of the step changes are [0.96 pu; 0.94 pu], [0.97 pu; 0.93 pu], [0.98 pu; 0.92 pu], and [0.99 pu; 0.91 pu].

The variables of the UPFC shunt side, V_i, Q_{conv1}, and I_{conv1q}, define initial voltage control range with limiting conditions employed.

Time responses of the UPFC shunt side bus voltage magnitude, V_i, depict that it is freely controlled in the approximate range of ±0.025 pu (Fig. VI.10). Outside of that range the limiting conditions are activated.

Maximum overload limiting conditions are set through the UPFC shunt side reactive current as I_{conv1q} = ±1.35 pu on the shunt converter nominal power base 185 MVA. The time responses of the I_{conv1q} depict that from the 35% maximum limit the overload is ramped down to the continuous operating limit defined by I_{conv1q} = ±1.00 pu (Fig. VI.11).

In the same time, the UPFC shunt side reactive power Q_{conv1} depends not only on the I_{conv1q}, but on the bus voltage magnitude V_i as well (Fig. VI.12). The reactive power Q_{conv1} is given on the system basis 100 MVA. This is the reason for not having the Q_{conv1} at the exact value of 250 MVA (35% overload limit), and 185 MVA (continuous operation limit), but at closely related values.

If the power ratings S_{conv1n} and S_{conv2n} would be defined equal to 65 MVA, as it is given by the initial optimal dimensioning algorithm which accounts only for series power flow regulation, then the magnitude V_i could be freely controlled in significantly smaller range of ±0.010 pu. That comes out from the time responses of the reactive power Q_{conv1}, and the reactive current I_{conv1q}, where only the first sequence of V_{iREF} step changes [0.96 pu; 0.94 pu] could be satisfied. For the other changes, the overloading could appear afterwards. The range of ±0.010 pu in that case is considered to be inadequate from the voltage control perspective. Since it is estimated that the voltage control range of ±0.025 pu suits the voltage criterion better than the range ±0.010 pu, the rating power of the UPFC shunt converter is increased roughly 3 times in comparison with the ratings given by the initial optimal algorithm.

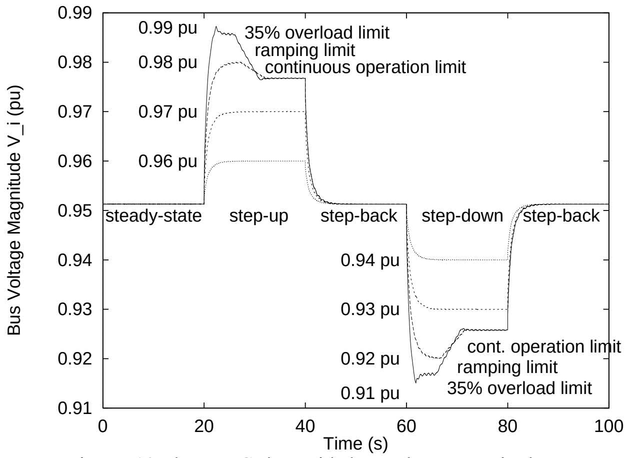

Fig. VI.10 The UPFC shunt side bus voltage magnitude V_i - voltage control mode-

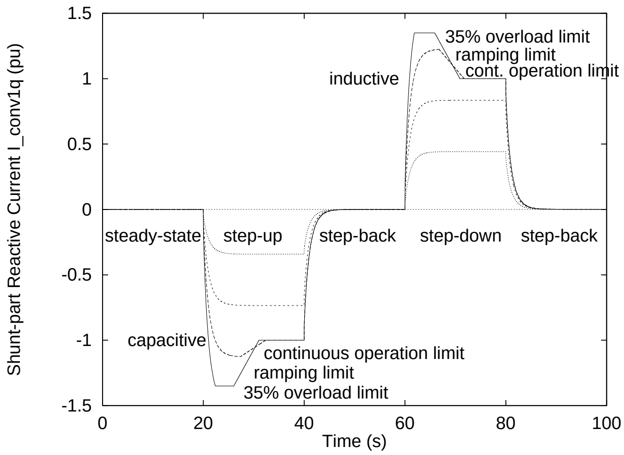

Fig. VI.11 The UPFC shunt side reactive current I_{conv1q} - voltage control mode-

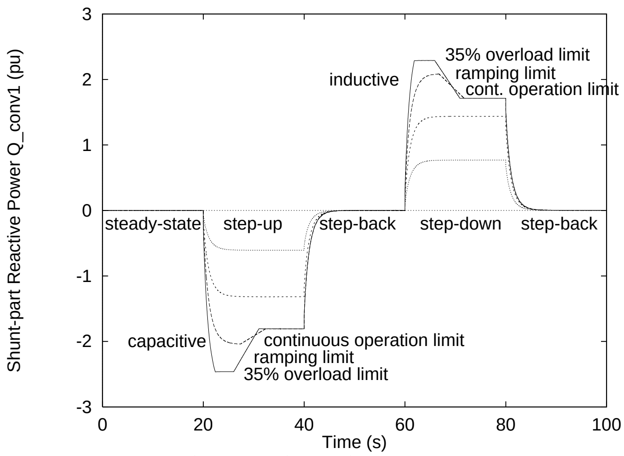

Fig. VI.12 The UPFC shunt side reactive power Q_{conv1} - voltage control mode-

Control and system characteristics are evaluated as the second issue within the UPFC shunt side voltage control. The variables of the UPFC shunt side, V_i, Q_{conv1}, and I_{conv1q}, are employed again. The impact of the slope setting is analysed by computing the characteristics with the values of the ΔV_{SVG} equal to 0%, 5%, and 10%. The overloading capability is disabled here and the rest of the parameters are the same as previously.

Operating points at the control characteristics are computed by keeping the UPFC shunt part in the constant voltage regulation mode while changing active and reactive power demand of the system loads. The system characteristic is computed by keeping the UPFC shunt part in the voltage regulation mode while changing the referent voltage V_{iREF}.

In the $V_i = f\ (Q_{conv1})$ domain (Fig. VI.13), the system characteristic is computed for the initial referent voltage V_{iREF} set equal to the voltage V_i from the no-load steady state operating point of the UPFC. Control characteristics are computed for 3 different values of ΔV_{SVG} (0%, 5%, and 10%). The same results are shown in the $V_i = f\ (I_{conv1q})$ domain (Fig. VI.14). Corresponding general characteristics are described in subsection III.4.A (Figs. III.13-14).

It is clearly seen that within allowed limits of the current I_{conv1q} ($\pm$1 pu), the voltage magnitude V_i is controlled depending on the slope setting. By increasing the slope setting above 0%, the voltage magnitude V_i is no longer equal to the referent voltage V_{iREF}.

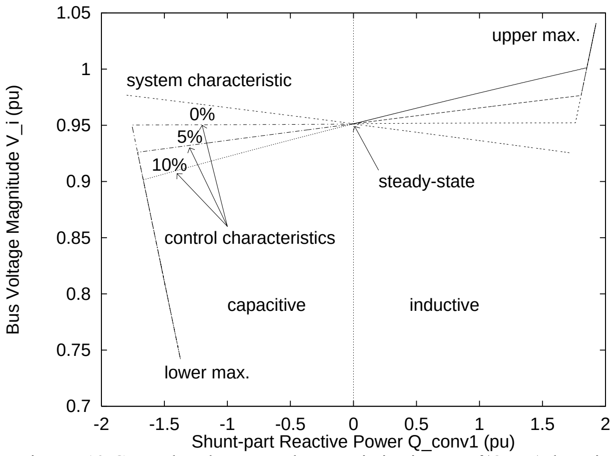

Fig. VI.13 Control and system characteristics in $V_i = f(Q_{conv1})$ domain

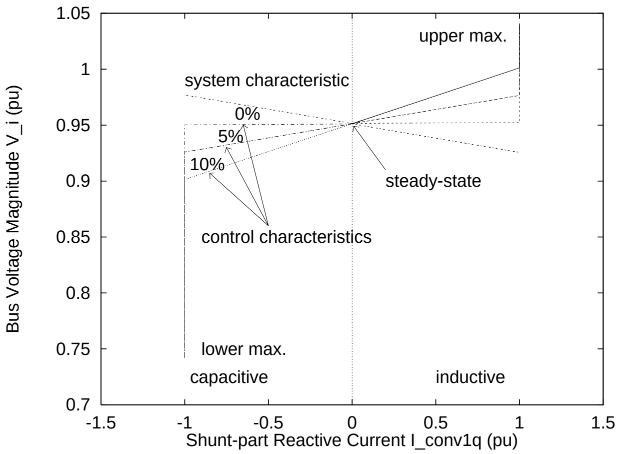

Fig. VI.14 Control and system characteristics in $V_i = f(I_{conv1q})$ domain

At the limits, the current I_{conv1q} becomes constant, whereas the reactive power Q_{conv1} linearly changed due to changes of the voltage magnitude V_i. In the capacitive region of the limiting conditions, maximum reactive power decreases with increased value of the ΔV_{SVG}.

Having the slope setting increased, an operating point at a crossing of the control and system characteristics becomes easier to achieve.

As the third issue within the UPFC shunt side voltage control, the trajectory of the operating point is evaluated showing well-defined capability of the UPFC shunt side control system (Fig. III.16).

The results are depicted in the $V_i = f\ (I_{conv1q})$ domain (Fig. VI.15). Control characteristic is computed by setting ΔV_{SVG} equal to 5%. The trajectory is defined by employing the step changes of the referent voltage V_{iREF} equal to [0.99 pu; 0.91 pu], with the other parameters being the same as previously.

The simulation starts from the steady state operating point by stepping-up the referent voltage V_{iREF} to 0.99 pu. Due to the slope of the control characteristic introduced by ΔV_{SVG} = 5%, the voltage magnitude V_i is lower than the V_{iREF} at the end of the step-up. The step-back brings the operating point back to the initial starting point.

The same happens with the step-down of the V_{iREF} to 0.91 pu, when the V_i becomes higher than the V_{iREF}. The step-back again brings the operating point back to the initial starting point.

The trajectory of the operating point is always situated nearly to the system characteristic showing appropriate settings of the gains and time constants within the UPFC shunt side control system.

In comparison with the first issue discussed within this section where ΔV_{SVG} is equal to 0%, the range of allowable values of V_{iREF} is here as large as $\pm$0.050 pu, but the controllable region is left unchanged, $\pm$0.025 pu. The difference is in easier achievement of the operating point at the crossing point of the characteristics.

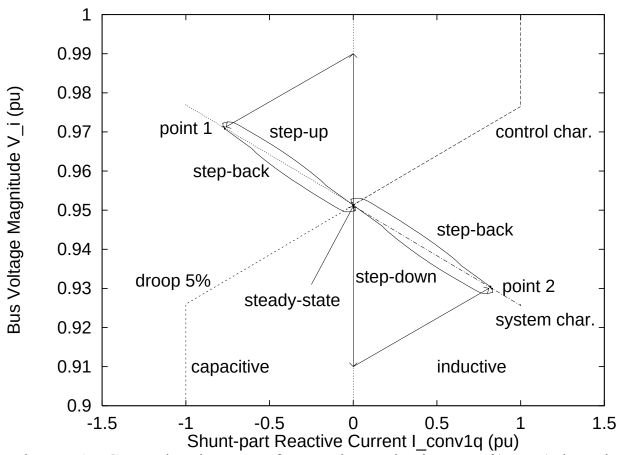

Fig. VI.15 Control trajectory of operating point in $V_i = f(I_{conv1q})$ domain

VI.3 POWER FLOW CONTROL OF THE UPFC SERIES SIDE

In order to analyse impact of the UPFC to the power flow regulation problem, the capability of the UPFC series side is addressed hereafter.

Having the UPFC shunt part inactive (I_{conv1q} = 0 pu), the power flow control of the series part is applied solely, according to the considerations given in subsection III.4.B.

Series power flow regulation is viewed from two aspects concerning type of the UPFC parameter changes, namely rotational change and step change.

VI.3.A Rotational change

The rotational change is defined as a rotation of the injected series voltage vector $\overline{V}_S$ having constant magnitude *r* in the full circular range of angle values γ = [0°: 360°], (Fig. VI.16). The starting point of the injected series voltage vector is defined by (r; γ) = (0.15 pu; 0°), and the ending point by (0.00 pu; 0°). Upon completion of a full circle of the angle γ, the magnitude *r* is changed in rather small steps of 0.001 pu implying conditions similar to the ones valid for continuous operation. The results are written for the values of the magnitude *r* equal to 100%, 80%, 60%, 40%, 20%, and 0% (actually 0.001 pu) of the maximum value r_{max} = 0.15 pu, and for the values of the angle γ equal to 0°, 90°, 180°, 270°, and 360°.

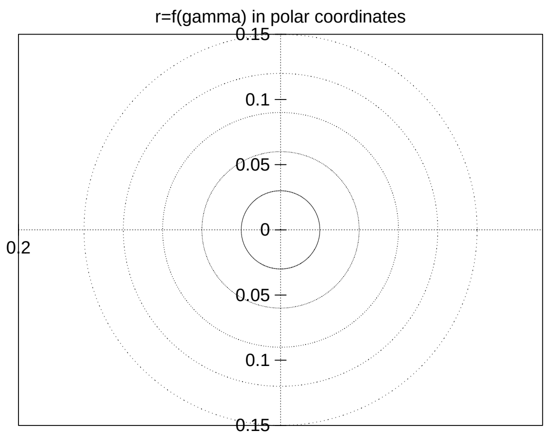

Figure VI.16 Rotational change in polar co-ordinates $r = f(\gamma)$

The converter rating powers S_{conv1n} and S_{conv2n} are set equal to 185 MVA, without any short-term overload capability of the shunt converter. The loads are modelled by static ZIP model that has active power part equal to constant current, and reactive one to constant impedance.

Dependence of the UPFC shunt and series side bus voltage magnitudes, V_i and V_j, with respect to the rotational change in (r, γ) pair is analysed (Fig. VI.17-19). The third parameter, Q_{conv1}, and thereby V_i, is not controlled in this case. It is shown that the voltage magnitudes have opposite direction of changes. Since neither of the buses is voltage controlled, one of them has magnitude increased when the

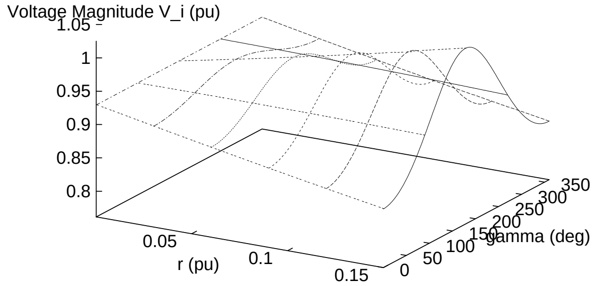

Figure VI.17 Shunt side bus voltage magnitude in $V_i = f(r, \gamma)$ domain

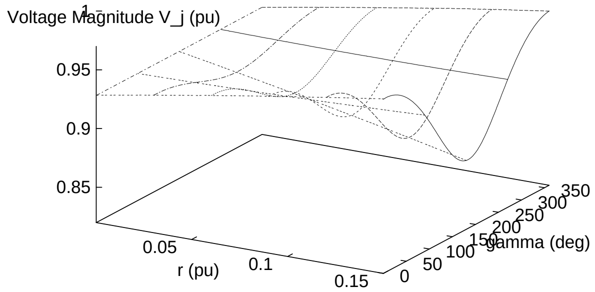

Figure VI.18 Series side bus voltage magnitude in $V_j = f(r, \gamma)$ domain

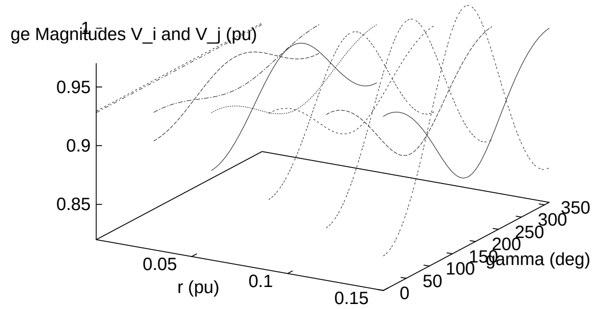

Figure VI.19 Shunt and series side bus voltage magnitudes in $(V_i, V_j) = f(r, \gamma)$ domain

other one is decreased, and vice versa. Similar effect could be found in transformer operation in a network with a low level of short circuit capacity. The distortion becomes more pronounced whenever larger values are given to the magnitude *r*. As it is seen, it would be necessary to have the operating region voltage limited due to low bus voltage magnitude values.

The operating region of the UPFC series side is computed with respect to the active and reactive power flows. Active power flow at the series side, P_{j2}, and reactive power flow at the series and shunt side, Q_{j2} and Q_{i1}, are defined with respect to the angle γ (Figs. VI.20-22).

Dependence of the active power flow P_{j2} on the angle γ depicts the region of possible active power flows at the series side. With the UPFC in no-load conditions, the active power P_{j2} is equal to -2.25 pu, whereas maximum change in both directions is equal to ±1.05 pu. It means that by inserting the maximum value of the magnitude *r* (0.15 pu), the active power P_{j2} could be changed by maximum 105 MW in each direction if the angle γ is appropriately adjusted. The maximum active power flow conditions appear around 70° and 250°, being displaced by approximately 180°.

Dependence of the reactive power flows Q_{j2} and Q_{i1} on the angle γ are given as well. The reactive power flow Q_{j2} has maximum changes equal to +2.10/-1.9 pu from a no-load conditions given by the flow -0.40 pu. Maximum changes of the reactive power flow Q_{i1} are equal to +1.70/-2.3 pu from a no-load conditions of +0.30 pu. Generally, if the maximum magnitude r is inserted having the angle γ at appropriate value, the reactive power flows could be changed by approximately 200 Mvar in each direction. The maximum reactive power flows appear around 170° and 350°, being displaced by approximately 180°.

Active and reactive power flows are 90° phase-displaced.

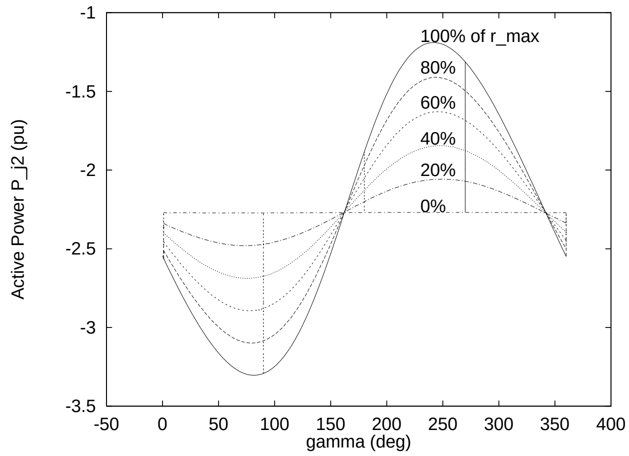

Figure VI.20 Active power flow at the UPFC series side $P_{j2} = f(\gamma)$

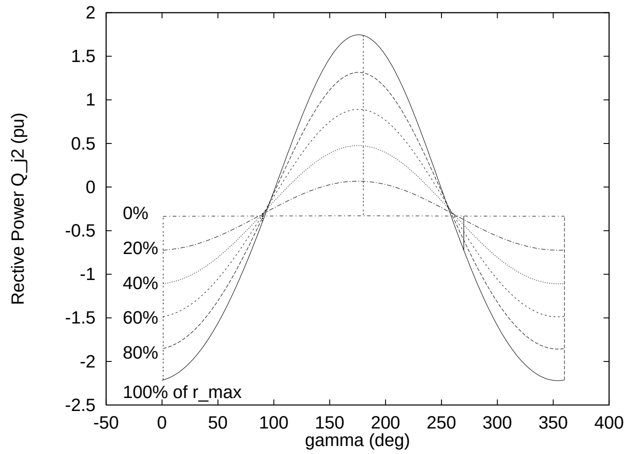

Figure VI.21 Reactive power flow at the UPFC series side $Q_{j2} = f(\gamma)$

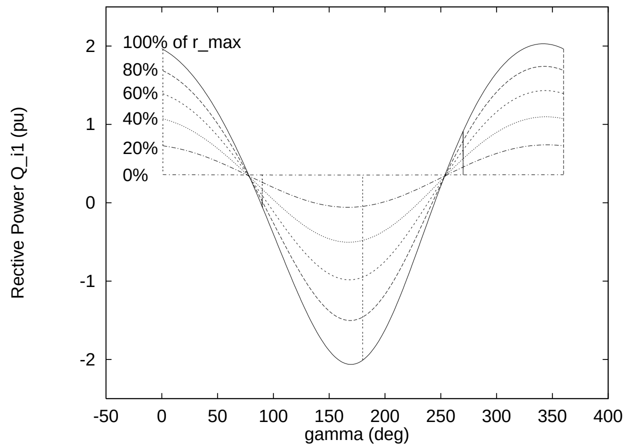

Figure VI.22 Reactive power flow at the UPFC shunt side $Q_{i1} = f(\gamma)$

Previously mentioned variables are also shown in $Q_{j2} = f(P_{j2})$ and $Q_{i1} = f(P_{j2})$ domains (Figs. VI.23-24). In both cases, the diagrams that are obtained have approximately circular characteristics. They are not properly rounded due to non-linearity in the load characteristics and due to impact of generator regulation circuits.

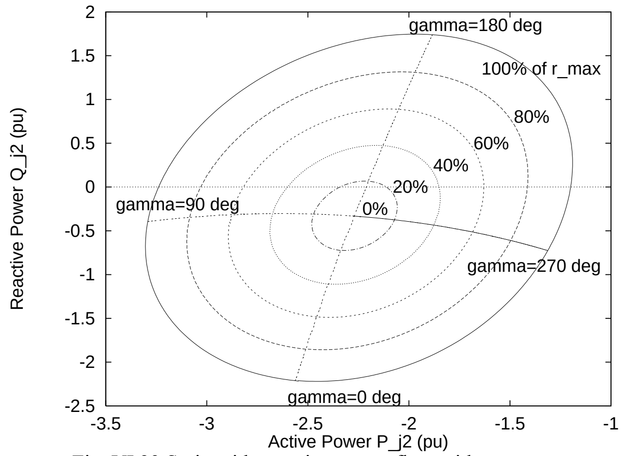

Fig. VI.23 Series side reactive power flow with respect to the active power flow $Q_{j2} = f(P_{j2})$

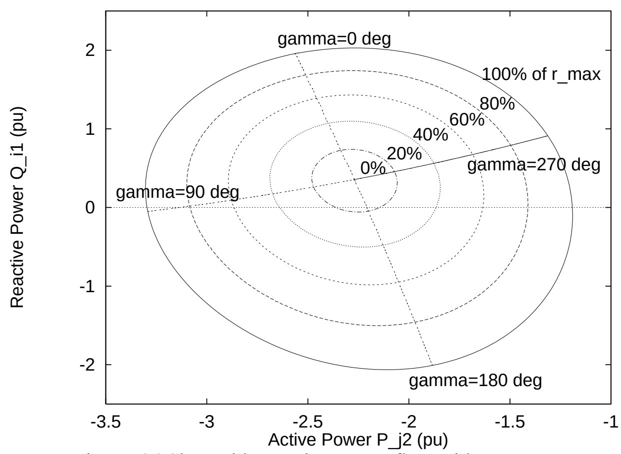

Fig. VI.24 Shunt side reactive power flow with respect to the active power flow $Q_{i1} = f(P_{j2})$

The same case of the rotational (r, γ) change is also shown in $V_j = f(P_{j2})$ and $V_i = f(P_{j2})$ domains (Figs. VI.25-26). In the first case the UPFC series side bus voltage magnitude is given with respect to the active power flow at the series side, whereas in the second case dependence of the shunt side bus voltage magnitude is given.

Diagrams show the range of the active power flow P_{j2} that could be achieved with respect to the bus voltage magnitudes within the rotational change. It is seen that the bus voltage magnitude V_j has values in the range between 0.88 pu and 0.97 pu with no-load conditions given at 0.93 pu (maximum changes -0.05/+0.04 pu). The bus voltage magnitude V_i has quite similar no-load conditions, but with larger operating range between 0.85 pu and 1.02 pu (maximum changes -0.08/+0.09 pu).

In both cases, minimum and maximum values of the bus voltage magnitudes appear at the angle γ equal to 0º and 180°. Along this vertical voltage change, the active power flow is controlled in a rather limited range (±0.35 pu).

Along horizontal voltage change (90° and 270°), the flow of active power P_{j2} has the widest controllable range (±1.05 pu). It shows that the active power flow control could be achieved much easier by controlling the bus voltage angle difference than by controlling bus voltage magnitudes.

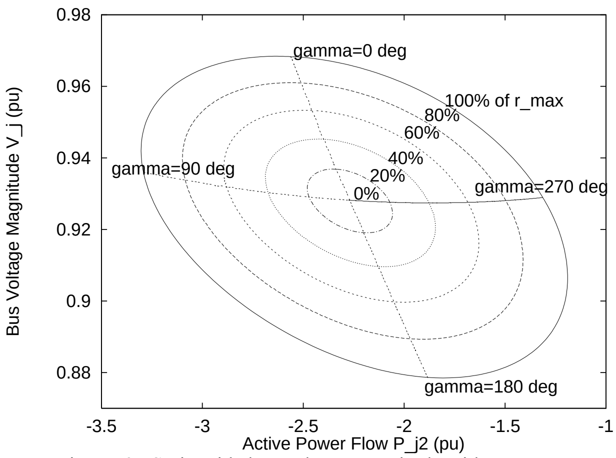

Fig. VI.25 Series side bus voltage magnitude with respect to the active power flow at the series side $V_j = f(P_{j2})$

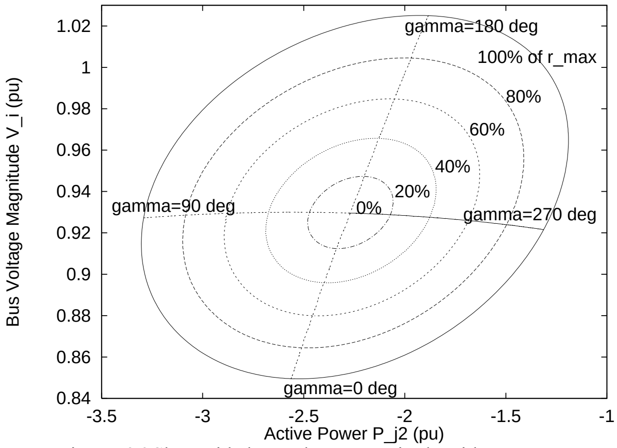

Fig. VI.26 Shunt side bus voltage magnitude with respect to the active power flow at the series side $V_i = f(P_{j2})$

The same rotational change is used to analyse behaviour of the minimum singular value σ_n of the extended Jacobi matrix (Fig. VI.27). Besides, the sensitivities of the minimum singular value with respect to the magnitude r, and the angle γ, $\partial\sigma_n/\partial r$ and $\partial\sigma_n/\partial\gamma$, are evaluated (Figs. VI.28-29). The analysis of the minimum singular value is considered in subsection V.1.A.

The minimum singular value is small in value, and moreover numerically changes within rather small range. This is the reason for its distorted appearance within smaller values of the magnitude r. Larger values of the magnitude r impose larger changes, and thereby the computation is done numerically easier.

Maximum value of the minimum singular value is of concern here. It is seen that the maximum value appears around the angle γ equal to 300°. Around the same value of the angle γ, the sensitivity $\partial\sigma_n/\partial\gamma$ has nearly zero value, whereas the sensitivity $\partial\sigma_n/\partial r$ comes at the negative minimum. This fact is employed within the sub-optimal formulation, which maximises the minimum singular value.

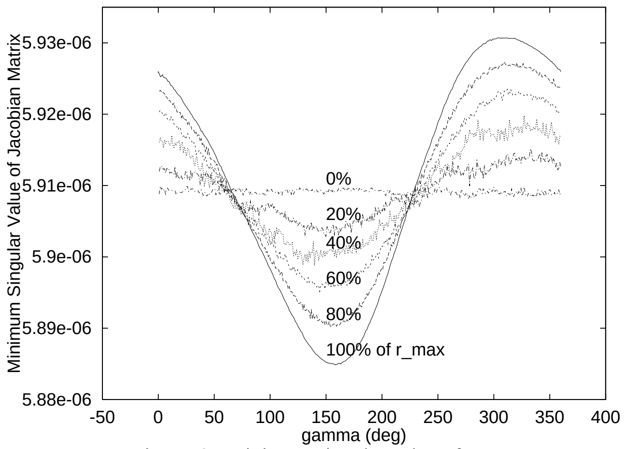

Fig. VI.27 Minimum singular value of J_{EXT} given in γ domain, $\sigma_n = f(\gamma)$

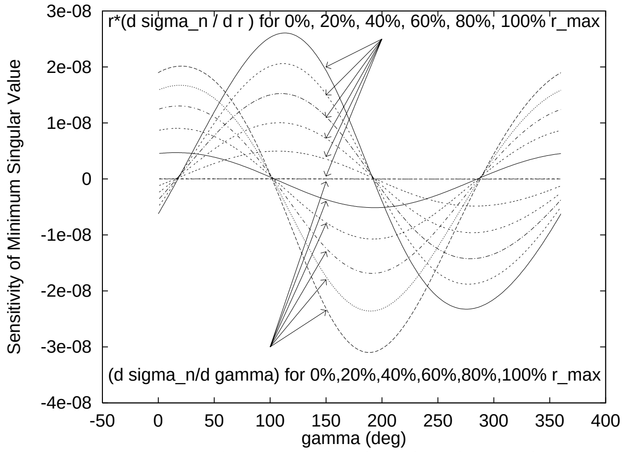

Fig. VI.28 Sensitivities of minimum singular value of J_{EXT} with respect to (r, γ) given in γ domain, $(\partial\sigma_n/\partial r, \partial\sigma_n/\partial\gamma) = f(\gamma)$

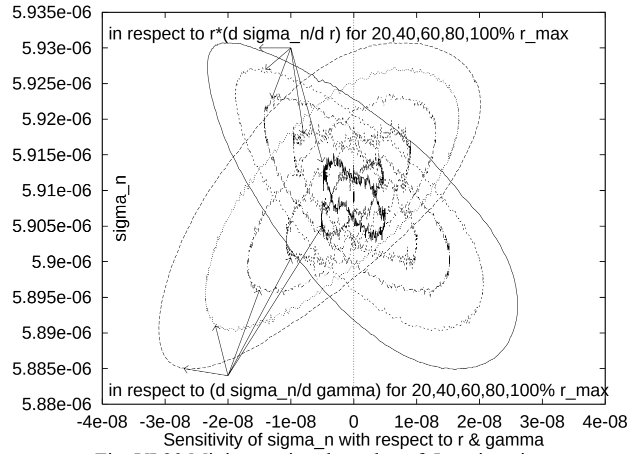

Fig. VI.29 Minimum singular value of J_{EXT} given in $(\partial\sigma_n/\partial r, \partial\sigma_n/\partial\gamma)$ domain, $\sigma_n = f(\partial\sigma_n/\partial r, \partial\sigma_n/\partial\gamma)$

Besides in the analysis of the minimum singular value, the same rotational change is used to analyse behaviour of the total active power loss P_{loss} as well (Fig. VI.30). The sensitivities of the total active power loss with respect to the magnitude r, and the angle γ, dP_{loss}/dr and $dP_{loss}/d\gamma$, are evaluated (Figs. VI.31-32). The analysis of the total active power loss is considered in section V.3.

The total active power loss is changed within approximate range of ±2.5% from a middle level. Larger values of the magnitude r impose larger changes of the P_{loss}.

Minimum value of the total active power loss is of concern here. It is seen that the minimum value appears around the angle γ equal to 180°. Around the same value of the angle γ, the sensitivity $dP_{loss}/d\gamma$ has nearly zero value, whereas the sensitivity dP_{loss}/dr comes at the minimum. Similarly to the previous case, this fact is employed within the sub-optimal formulation, which minimises the total active power loss.

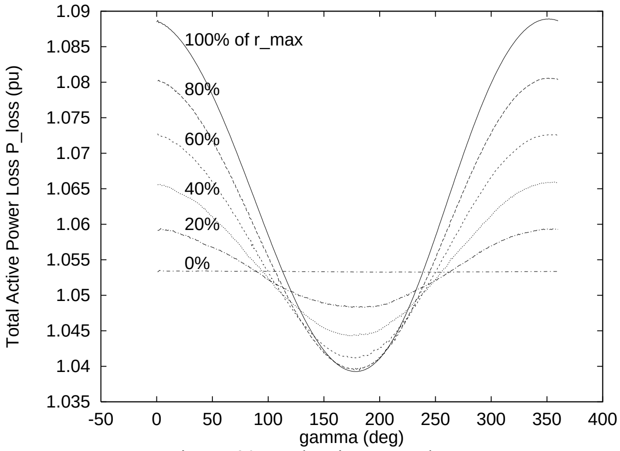

Fig. VI.30 Total active power loss given in γ domain, $P_{loss} = f(\gamma)$

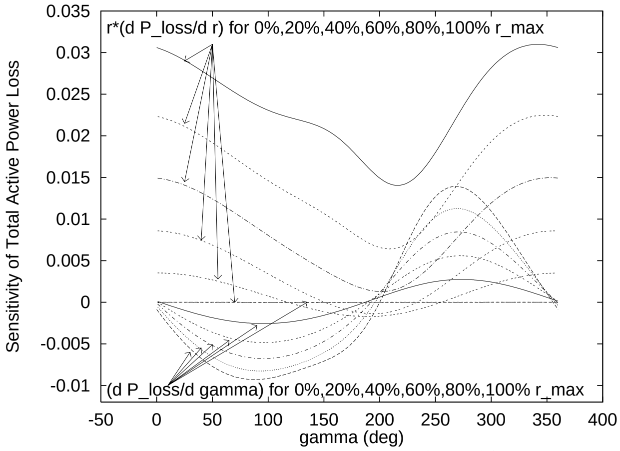

Fig. VI.31 Sensitivities of total active power loss with respect to (r, γ) given in γ domain, $(dP_{loss}/dr, dP_{loss}/d\gamma) = f(\gamma)$

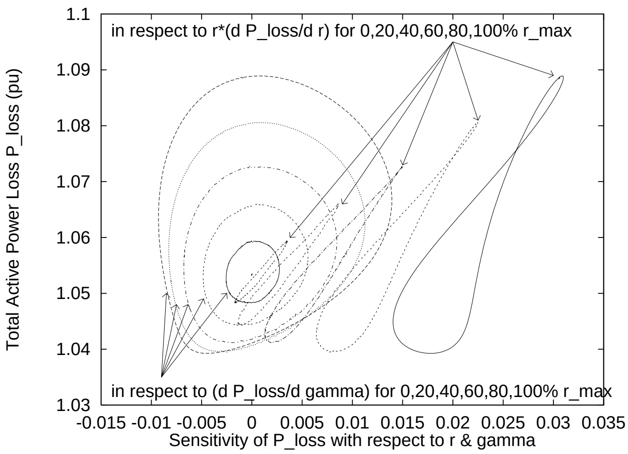

Fig. VI.32 Total active power loss given in $(dP_{loss}/dr, dP_n/d\gamma)$ domain, $P_{loss}=f(dP_{loss}/dr, dP_{loss}/d\gamma)$

VI.3.B Step change

The step change is defined as a change of referent values within the UPFC control system. Parameters of the injected series voltage vector $\overline{V}_S$ are controlled through feedback regulation circuits from the UPFC series side. Two regulation modes are analysed, namely $P_{j2} \Leftrightarrow V_j$ and $P_{j2} \Leftrightarrow Q_{j2}$.

In the first mode, $P_{j2} \Leftrightarrow V_j$, the angle γ is controlled through the feedback of the series side active power flow P_{j2}, whereas the magnitude r through the series side bus voltage magnitude V_j.

In order to achieve adequate time responses of the UPFC, parameters of the PI regulators are adjusted before encountering the problem. The time constants and gains of the series side feedback are given as: P_{j2}-feedback, K_γ=0.05 and $T_{i\gamma}$=0.40 s, and V_j-feedback, K_r=0.02 and T_{ir}=0.30 s, (Fig. III.12). The converter rating powers S_{conv1n} and S_{conv2n} are set equal to 185 MVA. The loads are modelled by static ZIP model having active power part equal to constant current, and reactive one to constant impedance.

The sequence of the step changes is composed of 5 steps. Within each of the steps, one referent value is changed at the time, while the other one is kept constant (Figs. VI.33-35). There are 5 points defined (0-4). Point 0 is defined as a starting point having $r = r_{max}$ = 0.15 pu and γ = 0°. Then, the operation point is driven to the point 1 (P_{j2}; V_j) = (-2.75 pu; 0.95 pu), and further on to the point 2 (-2.75 pu; 0.91 pu), point 3 (-1.75 pu; 0.91 pu), point 4 (-1.75 pu; 0.95 pu), and finally back to the point 1 again.

Trajectory path is shown in the $P_{j2} \Leftrightarrow V_j$ domain (Fig. VI.33). Starting from the operating point 0, it is made possible to move operating point around all four quadrants (0→1→2→3→4→1). The operating point is always kept inside allowed boundaries defined by r_{max}. The straight lines depict the changes of the referent variables, while the curvaceous ones give responses of the variables. It is seen that for the changes of the referent voltage V_{jREF}, the operating point is dominated by the control of the magnitude r. Trajectory path passes through the internal part of the operating region. The magnitude r hits zero value, and adds 180° to the angle γ value. This activates γ control loop, which brings its value at approximately 135° at the point 2. When the changes of the referent value P_{j2REF} appear, the operating point is dominated by the γ control having rather circular trajectory path. These differences appear due to different reaction times of the regulation circuits being disturbed by single step change at the time.

Besides depicting trajectory path in two dimensions, the same case is shown in three dimensions as well (Figs. VI.34-35). Dependence of the angle γ and the magnitude r during the step change scenario is shown respectively to the (P_{j2}, V_j) domain. The γ-dependence has a spiral form, whereas the r-dependence has a conical one. The operating point is found at the surface of the bodies.

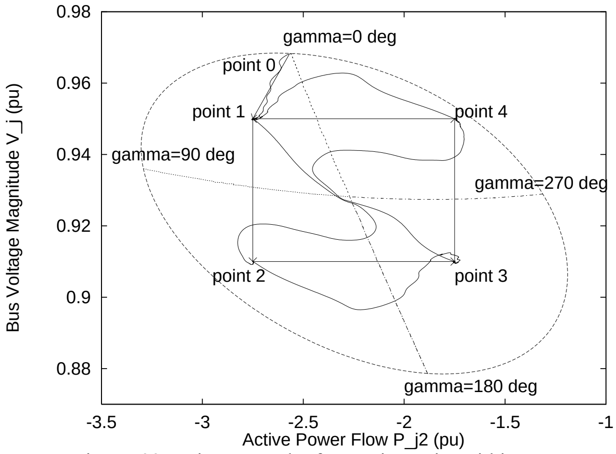

Fig. VI.33 Trajectory path of operating point within step change scenario given in $P_{j2} \Leftrightarrow V_j$ domain

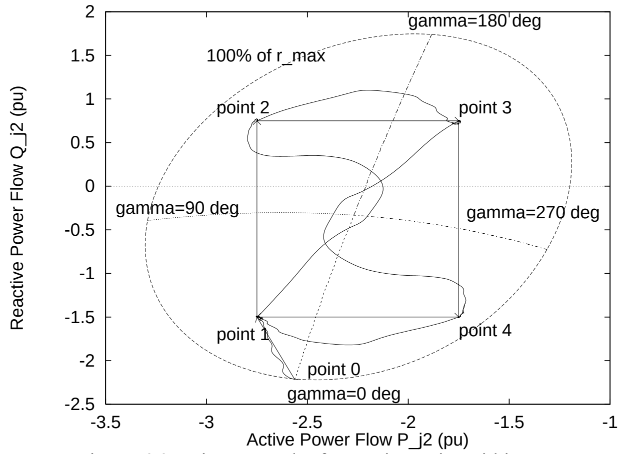

Fig. VI.36 Trajectory path of operating point within step change scenario given in $P_{j2} \Leftrightarrow Q_{j2}$ domain

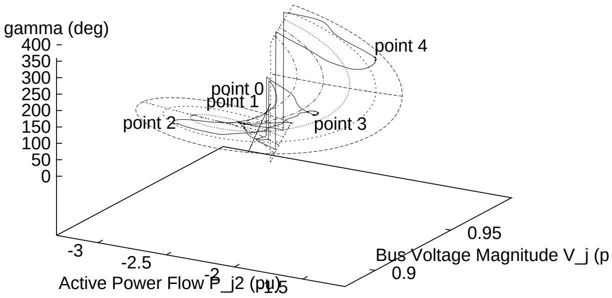

Fig. VI.34 Trajectory path of operating point within step change scenario given in $\gamma = f\,(P_{j2}, V_j)$ domain

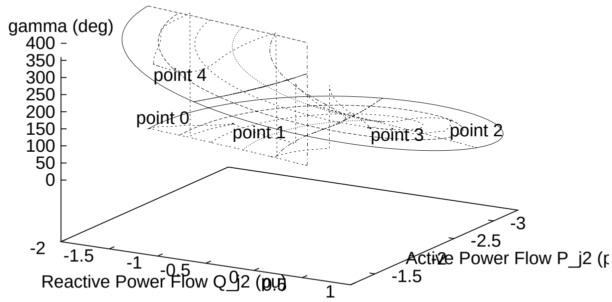

Fig. VI.37 Trajectory path of operating point within step change scenario given in $\gamma = f\,(P_{j2}, Q_{j2})$ domain

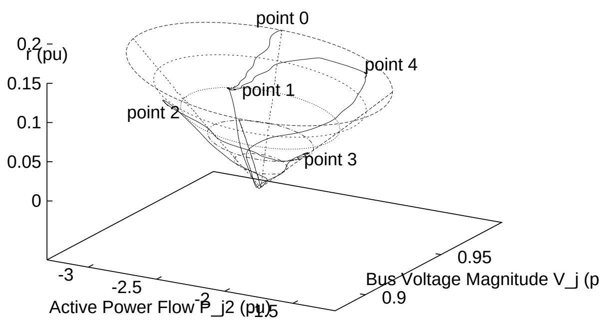

Fig. VI.35 Trajectory path of operating point within step change scenario given in $r = f\,(P_{j2}, V_j)$ domain

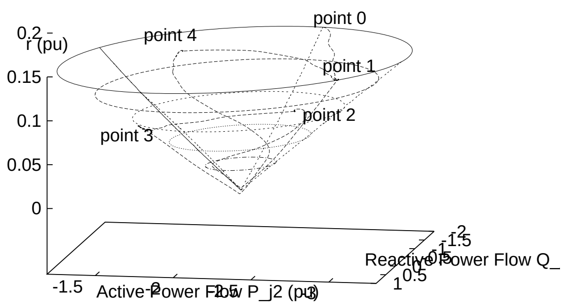

Fig. VI.38 Trajectory path of operating point within step change scenario given in $r = f\,(P_{j2}, Q_{j2})$ domain

In the second mode, $P_{j2} \Leftrightarrow Q_{j2}$, the angle γ is again controlled through the feedback of the series side active power flow P_{j2}, whereas the magnitude r through the series side reactive power flow Q_{j2}, (Figs. VI.36-38).

The time constants and gains of the series side feedback differ from the previous case and are given as: P_{j2}-feedback, K_γ=0.075 and $T_{i\gamma}$=0.40 s, and Q_{j2}-feedback, K_Q=0.000027 and T_{iQ}=15.0 s, (Fig. III.12). The converter rating powers and the load models are the same as in the previous case.

The sequence of the step changes is similar to the previous case. Simulation starts from the point 0 having $r = r_{max}$ = 0.15 pu and γ = 0°. Then, the operating point is driven to the point 1 (P_{j2}; Q_{j2}) = (-2.75 pu; -1.50 pu), and further on to the point 2 (-2.75 pu; 0.75 pu), point 3 (-1.75 pu; 0.75 pu), point 4 (-1.75 pu; -1.50 pu), and finally back to the point 1 again.

Trajectory path is shown in the $P_{j2} \Leftrightarrow Q_{j2}$ domain (Fig. VI.36). Starting from the operating point 0, it is made possible to move operating point around all four quadrants (0→1→2→3→4→1). The operating point is always kept inside allowed boundaries defined by r_{max}. For the changes of the referent reactive power flow Q_{j2REF}, the operating point is dominated by the control of the magnitude r, whereas for the changes of the referent value P_{j2REF}, it is dominated by the γ control.

The same case is shown in three dimensions as well (Figs. VI.37-38). Responses of the angle γ and the magnitude r during the step change scenario are shown respectively to the (P_{j2}, Q_{j2}) domain. The γ-dependence has a spiral form, whereas the r-dependence has a conical one. The operating point is found at the surface of the bodies.

VI.4 SIMULTANEOUS CONTROL OF THE UPFC AT BOTH SIDES

In previous sections, sole operation of either the shunt side or the series side of the UPFC is analysed. Certainly, the UPFC series power flow control needs its shunt part for active power supply, but at the UPFC shunt side its bus voltage magnitude has not been controlled. Hereafter, the simultaneous control of both sides is set in focus.

Simultaneous operation of both sides is viewed from the step change aspect. Having activated the UPFC shunt part in reactive power compensation through bus voltage magnitude control, the series side control is applied in several different modes, namely series power flow control, series compensation, and PAR/QBT phase shifting. Functional sub-optimisation of the total active power loss is given afterwards.

VI.4.A Shunt voltage and series power flow control

In this case, simultaneous control of all three UPFC injection model parameters, (r; γ; Q_{conv1}), is employed. The step change scenario is defined using changes of referent values within the UPFC series side control system, while keeping the bus voltage magnitude of the UPFC shunt side at a constant value. At the series side, the regulation mode $P_{j2} \Leftrightarrow Q_{j2}$ is analysed. In that mode, the angle γ is controlled through the feedback of the series side active power flow P_{j2}, whereas the magnitude r through the series side reactive power flow Q_{j2}. At the shunt side, the bus voltage magnitude V_i is kept constant through Q_{conv1} regulation circuit. This makes simultaneous three parameter control, given as (Q_{j2}; P_{j2}; V_i).

The time constants and gains of the series and shunt side feedback are given as: Q_{j2}-feedback, K_Q=0.05 and T_{iQ}=2.00 s, P_{j2}-feedback, K_γ=0.05 and $T_{i\gamma}$=0.10 s, and V_i-feedback, K_{ivi}=0.50, T_{ivi}=0.02 s, T_{vis}=0.5 s, and ΔV_{SVG}=0, (Fig. III.12). The converter rating powers and the load models are the same as in the previous cases. No overload within the shunt side is allowed.

The sequence of the step changes consists of two disturbance steps and two backward ones. Disturbance steps lead the operating point to opposite directions, while backward ones bring it back to the starting conditions. Initial steady state period is defined by r=0 pu, γ=0°, and V_i being uncontrolled. Then, the sequence is activated to show the series power flow control (Q_{j2}, P_{j2}) by applying step changes in referent values of each PI regulator simultaneously (Figs. VI.39-40). In the same time, the voltage magnitude V_i is kept constant at its initial value (Fig. VI.41). Time responses meet general control criteria showing that the control system parameters are appropriately tuned.

The steady state operating point is defined by (Q_{j2}, P_{j2}, V_i) = (-1.01 pu, -2.93 pu, 0.9516 pu). Thus, the first disturbance step is defined to bring the operating point toward (-0.5 pu, -3.5 pu, 0.9516 pu) through (r, γ, Q_{conv1}) feedback. Having this point achieved the backward step follows to bring the operating point at the initial state given earlier. The second disturbance step forces the operating point to move in different direction given by (-1.5 pu, -2.5 pu, 0.9516 pu). The ending step brings the operating point to the initial value.

It is shown that in addition to the UPFC conventional series power flow regulation (Q_{j2}, P_{j2}), it is also possible to control bus voltage magnitude V_i, whenever there is enough remaining reactive capacity of the shunt converter.

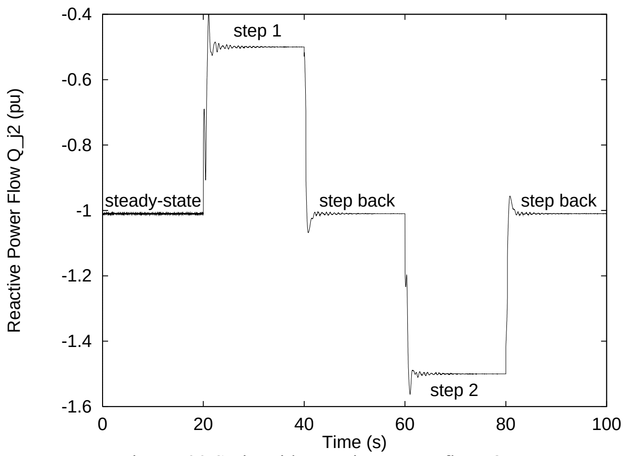

Fig. VI.39 Series side reactive power flow Q_{j2} in simultaneous three parameter control of the UPFC

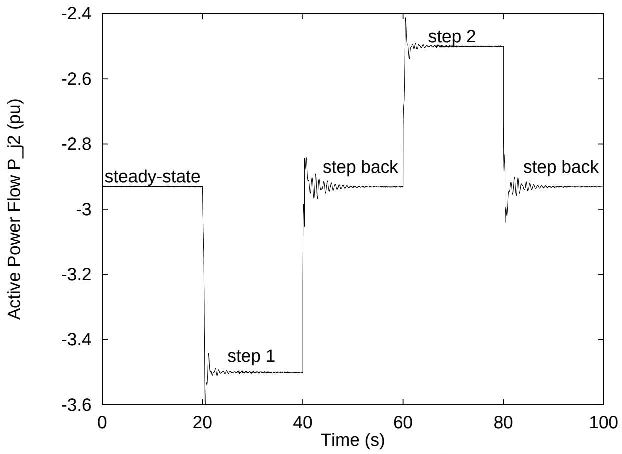

Fig. VI.40 Series side active power flow P_{j2} in simultaneous three parameter control of the UPFC

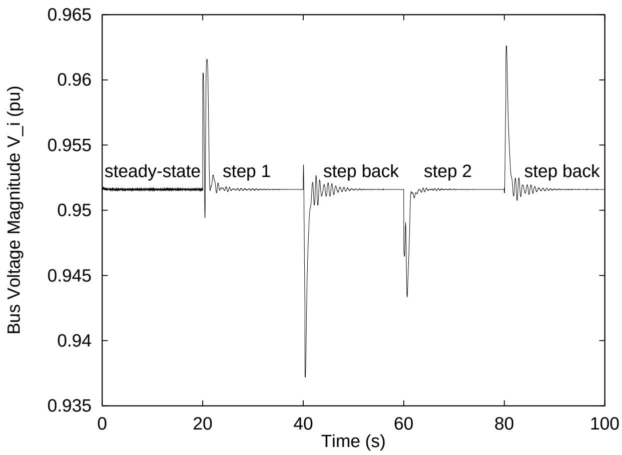

Fig. VI.41 Shunt side bus voltage magnitude V_i in simultaneous three parameter control of the UPFC

At the shunt side, bus voltage magnitude V_i is kept constant through Q_{conv1}-loop. At the series side, the power flows are controlled influencing its bus voltage magnitude V_j. Time response of the magnitudes shows directions of their changes (Fig. VI.42). Since the shunt side bus is voltage controlled, the series side bus has voltage magnitude decreased or increased whenever there is a change in the power flows. Similar effect could be found in transformer operation having one bus voltage controlled. Between the magnitudes, a voltage difference exists due to the series transformer reactance.

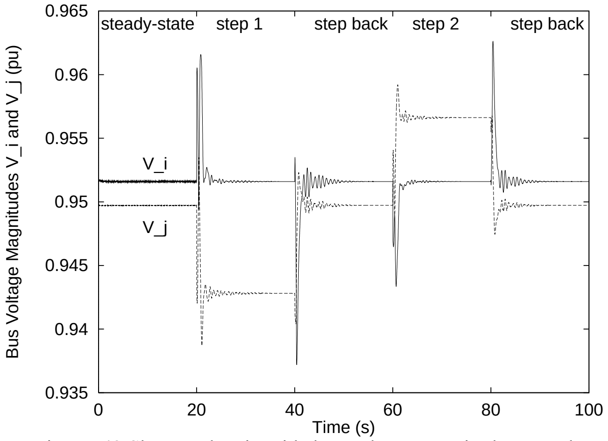

Fig. VI.42 Shunt and series side bus voltage magnitudes V_i and V_j in simultaneous three parameter control of the UPFC

VI.4.B Shunt voltage control and series compensation

In this case, simultaneous three-parameter control is arranged to achieve voltage control at the shunt side and series compensation (SC) at the series side. The series compensation mode is achieved according to the guidelines provided in subsection III.4.C. The γ-loop is controlled to keep the active power P_{conv2} equal to zero, whereas the r-loop is driven through the proportionality factor k_c, which defines type and level of the series compensation.

The time constants and gains of the series and shunt side feedback are given as: Q_{conv2}-feedback, K_{zQ}=0.01 and T_{zQ}=1.50 s, P_{conv2}-feedback, K_{zp}=0.25 and T_{zp}=0.25 s, and V_i-feedback, K_{ivi}=0.50, T_{ivi}=0.02 s, T_{vis}=0.5 s, and ΔV_{SVG}=0, (Fig. III.12). The converter rating powers and the load models are the same as in the previous cases. No overload within the shunt side is allowed.

After initial steady state period, defined by arbitrary values r=0.05 pu, γ=150°, and V_i being uncontrolled, a sequence of steps operates the UPFC in shunt voltage control and series compensation mode.

In the step 1, characteristic perpendicular form of V-I diagram is introduced by forcing the active power of the series converter P_{conv2} to zero (Fig. VI.43). Thus, the angle $(\gamma+\varphi)$ from the vector diagram (Fig. III.17) takes value of 90° in the first step (Fig. VI.44), where the factor k_c is equal to +10 influencing the reactive power Q_{conv2} (Fig. VI.45). In the same time, the shunt side voltage magnitude V_i is controlled at 0.94 pu (Fig. VI.46).

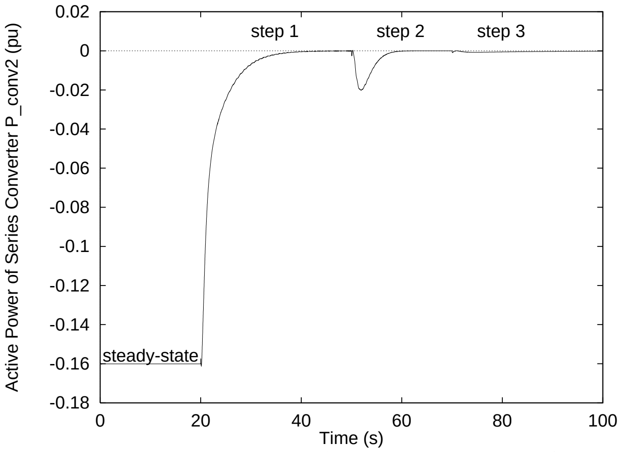

Fig. VI.43 Series converter active power P_{conv2} in SC mode

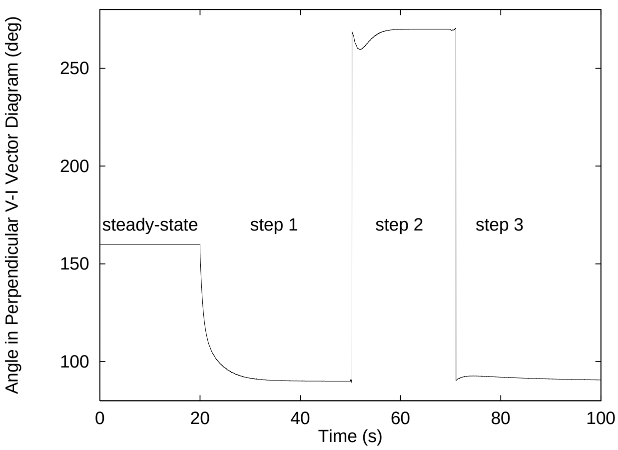

Fig. VI.44 Characteristic angle $(\gamma+\varphi)$ in SC mode

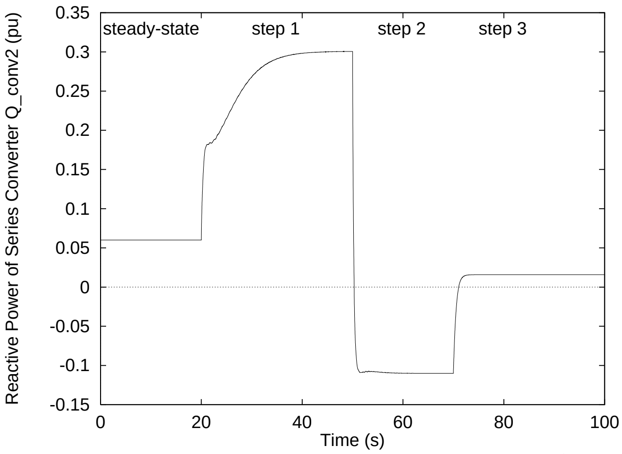

Fig. VI.45 Series converter reactive power Q_{conv2} in SC mode

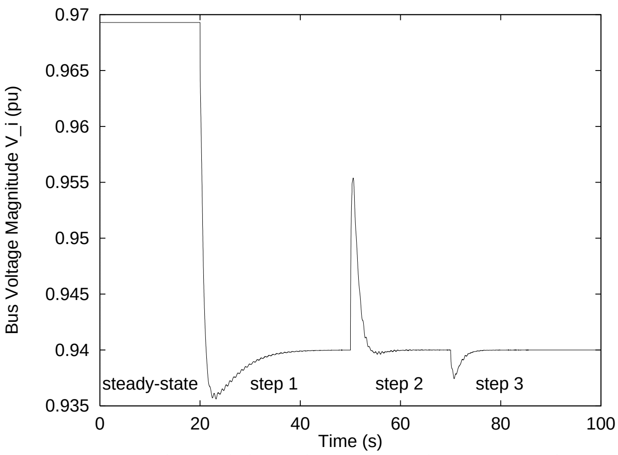

Fig. VI.46 Shunt side bus voltage magnitude V_i in SC mode

In the second step, the UPFC series side is still operated from the series compensation mode, but the change to k_c = -10 forces the angle $(\gamma+\varphi)$ to become 270°. Thereby, the character of the impedance that appears between shunt and series side of the UPFC could be changed upon request (capacitive/inductive). The bus voltage magnitude at the shunt side is still kept constant at 0.94 pu.

In the third step, by setting k_c=0, the voltage vectors $\overline{V_i}$ and $\overline{V_j}$ become equal, neutralising any impedance between the shunt and series side of the UPFC. Therefore, the magnitude V_{comp} becomes equal to zero (Fig. VI.47), whereas the voltage magnitude V_j becomes equal to V_i at 0.94 pu (Fig. VI.48).

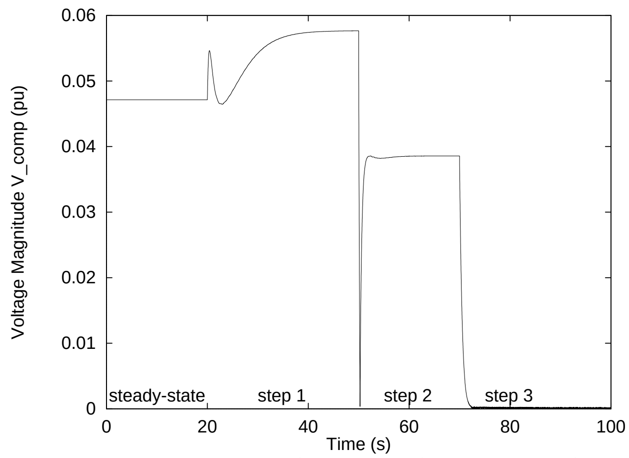

Fig. VI.47 Compensating voltage magnitude V_{comp} in SC mode

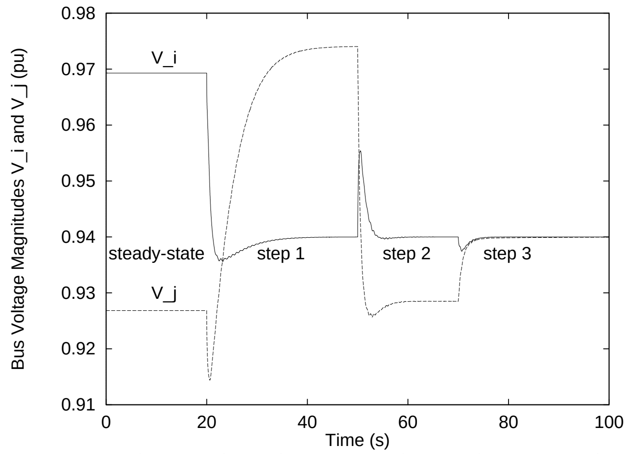

Fig. VI.48 The UPFC bus voltage magnitudes V_i and V_j in SC mode

It is shown that a conventional series compensation mode could be achieved by governing the UPFC within pre-determined conditions of the control system. Moreover, in addition to the UPFC conventional series compensation mode, it is also possible to control bus voltage magnitude V_i, whenever there is enough remaining reactive capacity of the shunt converter.

VI.4.C Shunt voltage control and PAR phase shifting

In this case, simultaneous three-parameter control is arranged to achieve voltage control at the shunt side and PAR phase shifting at the series side. The series side phase shifting mode of Phase Angle Regulator (PAR) type is achieved according to the guidelines provided in subsection III.4.D. The γ-loop is controlled to keep the UPFC bus voltage angle difference Θ_{ij} equal to the referent value Θ_{ijREF}, whereas the r-loop is driven to equalise the UPFC bus voltage magnitudes V_i and V_j.

The time constants and gains of the series and shunt side feedback are given as: V_j-feedback, K_{rpst}=1.50 and T_{rpst}=1.50 s, Θ_{ij}-feedback, K_{gpst}=0.20 and T_{gpst}=0.04 s, and V_i-feedback, K_{ivi}=0.50, T_{ivi}=0.02 s, T_{vis}=0.5 s, and ΔV_{SVG}=0, (Fig. III.12). The converter rating powers and the load models are the same as in the previous cases. No overload within the shunt side is allowed.

After initial steady state period, defined by arbitrary values r=0.05 pu, γ=150°, and V_i being uncontrolled, a sequence of steps operates the UPFC in shunt voltage control and series PAR phase shifting mode.

In the step 1, through the r-loop, the UPFC bus voltage magnitudes V_i and V_j are forced to become equal (Fig. VI.49), having the difference (V_i-V_j) set at zero value (Fig. VI.50). Through the γ-loop, the UPFC bus voltage vectors $\overline{V_i}$ and $\overline{V_j}$ are displaced in phase ($\Theta_{ij}=\Theta_i-\Theta_j$) by the value of Θ_{ijREF} equal to -4° (Fig. VI.51). In the same time, the bus voltage magnitude V_i at the UPFC shunt side is controlled to be 0.94 pu. This also makes the magnitude V_j at the UPFC series side to have the same value in this mode. The magnitude of the compensating voltage, V_{comp}, is slightly increased from approximately 0.050 pu to 0.065 pu in order to adjust for introduction of this mode (Fig. VI.52).

In the step 2, at the UPFC series side the PAR phase shifting mode is preserved, but with the opposite phase displacement which now has a value of Θ_{ijREF}=+4°. The bus voltage magnitudes V_i and V_j are still controlled to be constant at 0.94 pu, keeping the voltage difference (V_i-V_j) at zero value. The magnitude of the compensating voltage, V_{comp}, is approximately the same as in the previous step, but with opposite angle direction.

The simulation finishes with the step 3. By setting the referent value of the voltage angle difference Θ_{ijREF} equal to zero, and still keeping the voltage magnitudes V_i and V_j equalised (V_i being additionally controlled at 0.94 pu), the voltage vectors $\overline{V_i}$ and $\overline{V_j}$ become completely equal. It means that not only the magnitudes V_i and V_j are equal (and set at 0.94 pu), but the angles Θ_i and Θ_j are equal as well. The voltage angle difference Θ_{ij}, and the magnitude of the compensating voltage V_{comp}, become equal to zero at the end of the third step.

This analysis shows that a conventional PAR phase shifting mode could be achieved by governing the UPFC series side within pre-determined conditions of the control system. Moreover, in addition to the UPFC conventional PAR phase shifting, it is also possible to control bus voltage magnitude V_i, whenever there is enough remaining reactive capacity of the shunt converter.

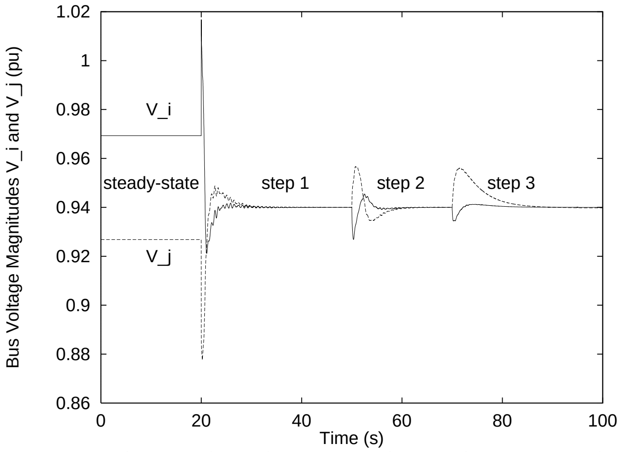

Fig. VI.49 The UPFC bus voltage magnitudes V_i and V_j in PAR mode

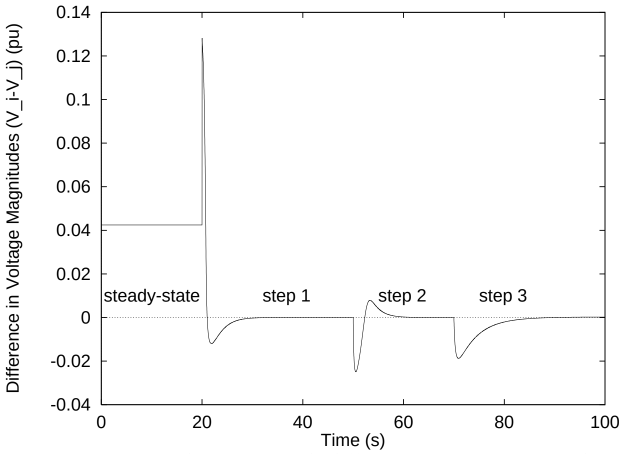

Fig. VI.50 Bus voltage magnitude difference *(V_i-V_j)* in PAR mode

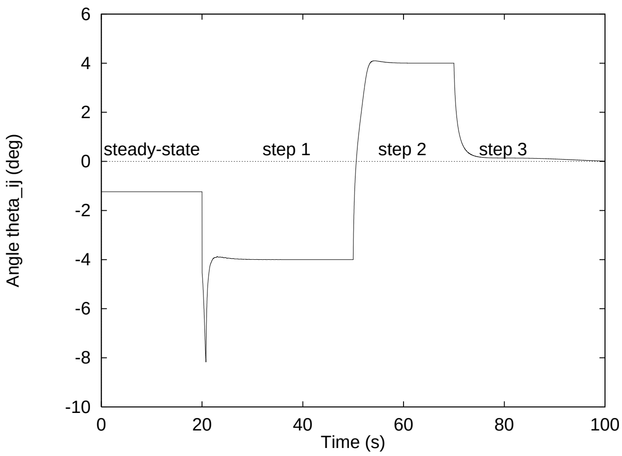

Fig. VI.51 Voltage angle difference *(Θ_i-Θ_j)* in PAR mode

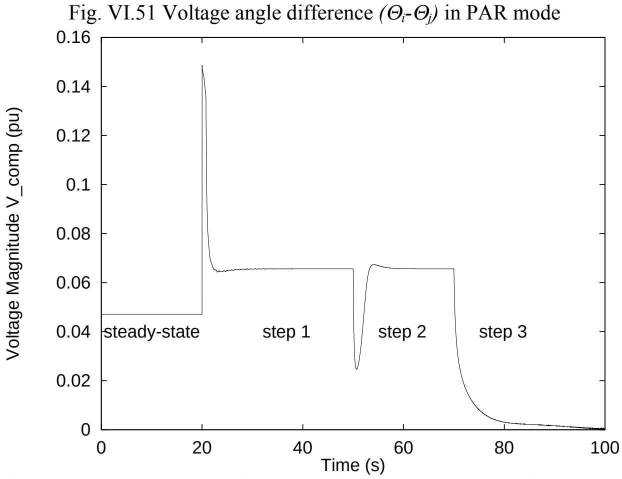

Fig. VI.52 Compensating voltage magnitude V_{comp} in PAR mode

VI.4.D Shunt voltage control and QBT phase shifting

As the second case of the phase shifting mode, the QBT type is analysed. Simultaneous three-parameter control is arranged to achieve voltage control at the shunt side and QBT phase shifting at the series side. The series side phase shifting mode of Quadrature Booster Transformer (QBT) type is achieved according to the guidelines provided in subsection III.4.D. The γ-loop is controlled to keep the compensating voltage angle φ_{comp} equal to the referent value φ_{comp}^{REF} at either 90° or 270°. The r-loop is controlled to keep the compensating voltage magnitude V_{comp} at a pre-determined value.

The time constants and gains of the series and shunt side feedback are given as: V_{comp}-feedback, K_{rpst}=0.01 and T_{rpst}=1.50 s, φ_{comp}-feedback, K_{gpst}=0.20 and T_{gpst}=0.03 s, and V_i-feedback, K_{ivi}=0.50, T_{ivi}=0.02 s, T_{vis}=0.5 s, and ΔV_{SVG}=0, (Fig. III.12). The converter rating powers and the load models are the same as in the previous cases. No overload within the shunt side is allowed.

After initial steady state period, defined by arbitrary values r=0.05 pu, γ=150°, and V_i being uncontrolled, a sequence of steps operates the UPFC in shunt voltage control and series QBT phase shifting mode.

In the step 1, the QBT phase shifting mode is introduced. Through the r-loop, the referent value of the compensating voltage magnitude, V_{comp}^{REF}, is set equal to +0.07 pu (Fig. VI.53). Through the γ-loop, the referent value of the compensating voltage angle, φ_{comp}^{REF}, is set equal to 90° (Fig. VI.54). In the same time, the bus voltage magnitude V_i at the UPFC shunt side is controlled to be 0.94 pu (Fig. VI.55). Within the QBT type, the voltage magnitude V_j at the UPFC series side does not have the same value as V_i due to characteristic perpendicular voltage diagram. Therefore, the difference in the bus voltage magnitudes *(V_i-V_j)* is not equal to zero (Fig. VI.56), whereas the angle difference Θ_{ij} has a value of approximately -4.5°. It means that the UPFC voltage vectors $\overline{V_i}$ and $\overline{V_j}$ are displaced in phase by the value of Θ_{ij}, which is defined by φ_{comp}^{REF}.

In the step 2, the QBT phase shifting mode is preserved at the UPFC series side, but with the opposite phase displacement. The value of φ_{comp}^{REF} is made equal to 270° by setting V_{comp}^{REF} equal to -0.07 pu. The bus voltage magnitude V_i is still controlled to be constant at 0.94 pu. The bus voltage magnitude V_j at the UPFC series side has different value than V_i, and their difference is still less than zero. The angle difference Θ_{ij} has changed its value to opposite direction and is approximately equal to +4.5°.

In the third step, by setting the referent value of the compensating voltage magnitude V_{comp}^{REF} equal to zero, the angle difference Θ_{ij} becomes equal to zero as well. Since the bus voltage magnitude V_i is still controlled at 0.94 pu, the bus voltage magnitude V_j becomes equal to V_i. The UPFC voltage vectors $\overline{V_i}$ and $\overline{V_j}$ become completely equal, in magnitudes and angles. The voltage angle difference, Θ_{ij}, and the magnitude of the compensating voltage, V_{comp}, become equal to zero at the end of the third step.

This analysis shows that a conventional QBT phase shifting mode could be achieved by governing the UPFC series side within pre-determined conditions of the control system. Moreover, in addition to the UPFC conventional PAR phase shifting, it is also possible to control bus voltage magnitude V_i, whenever there is enough remaining reactive capacity of the shunt converter.

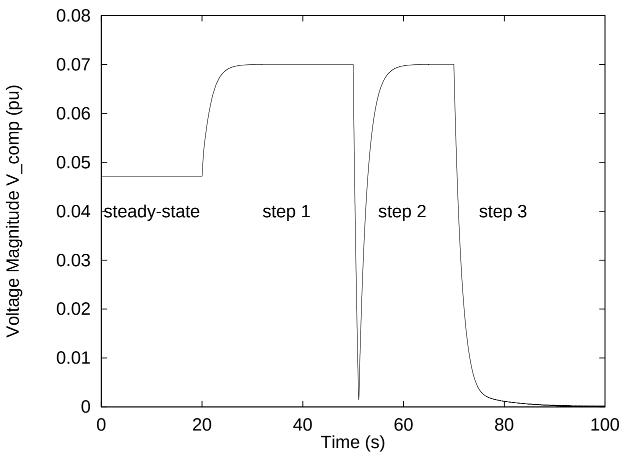

Fig. VI.53 Compensating voltage magnitude V_{comp} in QBT mode

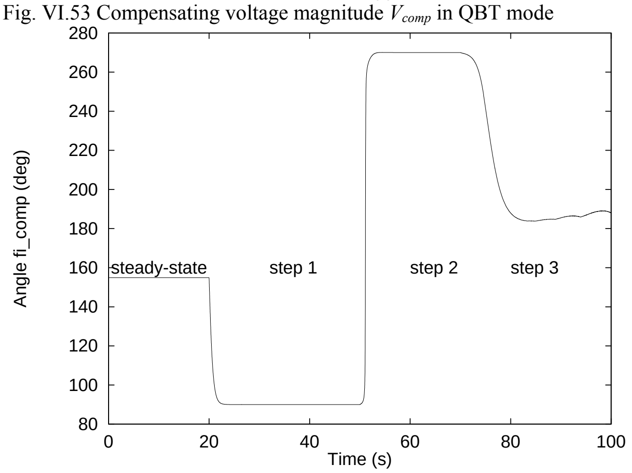

Fig. VI.54 Compensating voltage angle φ_{comp} in QBT mode

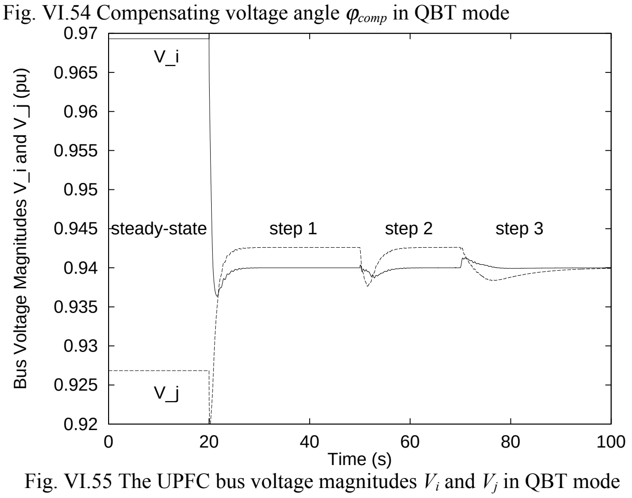

Fig. VI.55 The UPFC bus voltage magnitudes V_i and V_j in QBT mode

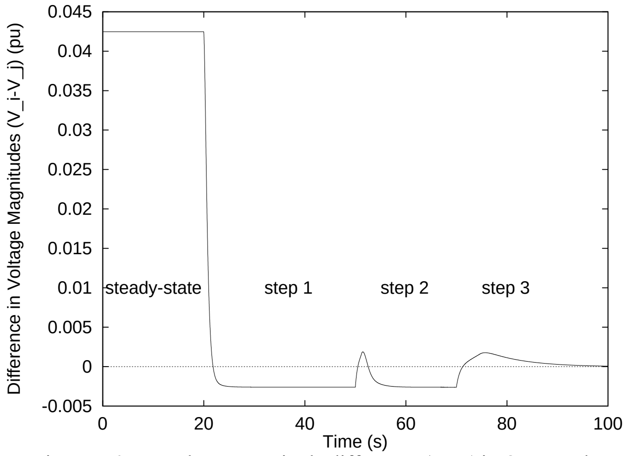

Fig. VI.56 Bus voltage magnitude difference (V_i-V_j) in QBT mode

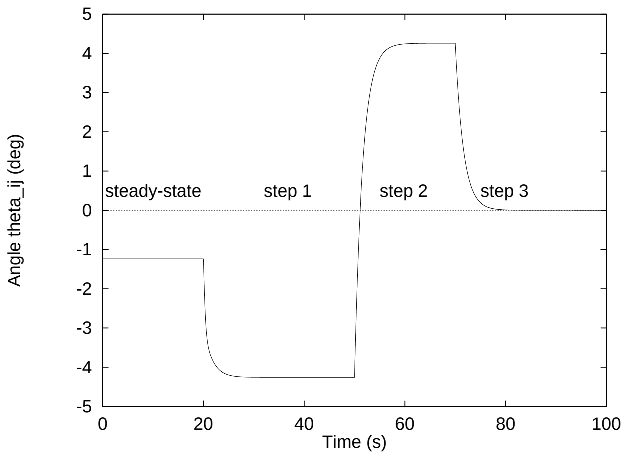

Fig. VI.57 Voltage angle difference $(\Theta_i-\Theta_j)$ in QBT mode

VI.4.E Functional sub-optimisation

As the last case in simultaneous three-parameter control, the functional sub-optimisation is illustrated. The results are provided for the total active power loss P_{loss} being the function for which the minimum is wanted. The functional sub-optimisation is achieved according to the guidelines provided in section V.4. Each of the loops, (r, γ, Q_{conv1}), is controlled by using the sensitivities $(d\ P_{loss}\ /\ d\ p)$. The sensitivities are defined with respect to the set (r, γ, I_{conv1q}) of the UPFC control parameters (V.133).

Analysing steady state behaviour of described functional sensitivities, the results show the ability of the control system to find a point of decreased total active power loss P_{loss} in the system (Figs. VI.58-59).

There are two different ways of reaching the ending point; A) sequential change $\gamma \rightarrow r \rightarrow I_{conv1q}$, and B) simultaneous change of all three parameters. In variant A, after reaching a minimum point using one parameter, the procedure continues with the use of other parameter, but keeping the previous one at its constant value. In variant B, all three parameters experience change in value simultaneously during time span, where after the magnitude r hits zero, the angle γ is shifted for 180° enabling r to be increased, and thereby kept in a non-negative range.

Procedures of finding the minimum point in both variants start from the same point. The starting point is given by r=0.1 pu, γ=350°, and I_{conv1q}= 0 pu. The finish appears in very close points (the ending point). Usually, minimum loss points are located at approximately 180°, where the sensitivity *(dP_{loss} / $d\ \gamma$)* crosses zero. The sensitivity *($d\ P_{loss}$ / $d\ r$)* is displaced nearly 90° apart of it. Since the sensitivity *($d\ P_{loss}$ / $d\ r$)*, at some values of the magnitude r, crosses zero axis at the points that do not correspond to a minimum, it is necessary to prevent its zero-crossing impact in the vector B (V.135). Therefore, some heuristics are applied in the procedure following the value of the power loss and thereby determining the sign of changes in control variables. Similar responses apply for the case study of minimum singular value.

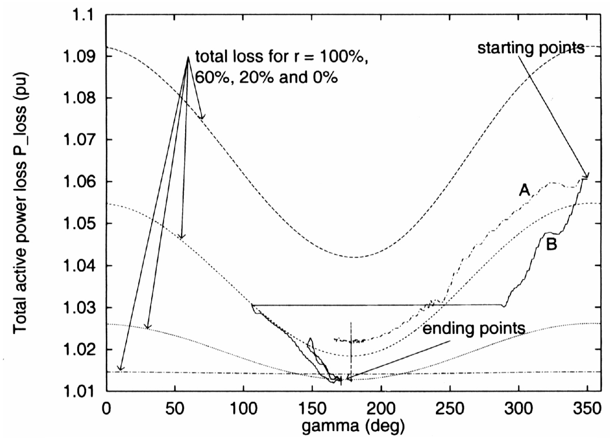

Fig. VI.58 Total active power loss with respect to the angle γ

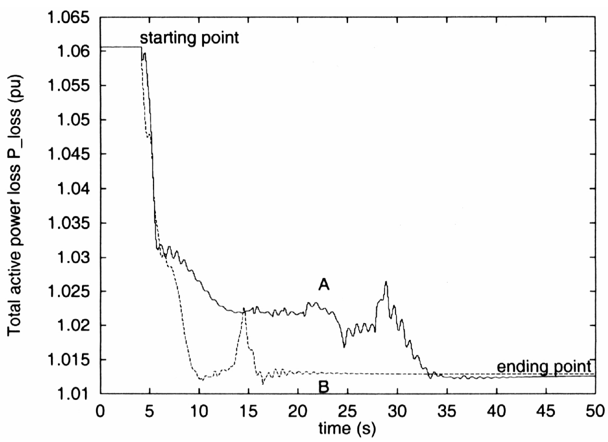

Fig. VI.59 Total active power loss in time domain

VII. NUMERICAL RESULTS ON THE UPFC DAMPING CONTROL

At the second instance, possible benefits of the UPFC injection model are investigated within damping control of electromechanical oscillations in the multi-machine test system. By using appropriate control system of the model it is made possible to damp electromechanical oscillations by simultaneous three-parameter control of the UPFC. Within oscillations damping control, dimensioning procedure is addressed especially from a viewpoint of the series side of the UPFC. By describing achieved results it is shown that the UPFC could be useful transmission system controller not only in steady state operation of power system, but during fast electromechanical transients as well. Furthermore, the injection model with proposed control system has been made to enable damping control of electromechanical oscillations.

VII.1 DAMPING CONTROL

To analyse the UPFC benefits in voltage stability problem, the voltage collapse scenario in the multi-machine test system is established. The scenario is based on a slow dynamics response of the system. It is assumed that the disturbance, which triggers the period of the slow dynamics, appears in the form of a three-phase short circuit. The disturbance occurs on the line L17 closely to the bus BUS15 (Fig. II.1). It is cleared after 220 ms by permanent line L17 outage. Afterwards, the voltage stability problem is demonstrated through a slow dynamics response of the system elements.

Meanwhile, during and shortly after the disturbance, electromechanical oscillations are initiated between the generators. With the UPFC being embedded between buses BUS21 and BUS22 according to a voltage stability criterion, which is given later in the text, this calls for its possible utilisation in a damping control.

Besides the PI regulators being active in steady state and voltage support modes, the control system of the UPFC injection model allows oscillations damping control. The damping control is of take-over type and is based on transient energy function (TEF). The guidelines of the TEF damping control by the UPFC injection model are given in secton III.4.E. Time derivatives of local variables from both sides of the UPFC are used. The shunt part of the TEF block uses information from dV_i/dt, whereas the series part from $d\Theta_{ij}/dt$ (Fig. III.12).

Immediately after the appearance of the disturbance, the TEF block recognises increased values of derivatives dV_i/dt and $d\Theta_{ij}/dt$, and takes over the control. Since the control system allows decoupled usage of the shunt and series part of the TEF block, the achievements are clearly distinguished between them. Usually, the damping level is significantly larger when using the series part (especially in a longitudinal-network case), whereas the shunt part (especially with certain overloading capability) contributes to the damping, but in rather smaller degree.

The converter rating powers S_{conv1n} and S_{conv2n} are set equal to 185 MVA. The shunt converter is allowed to have 35% short-term overload capability (I_{conv1q}^{max}= 1.35 pu) without any slope setting (ΔV_{SVG}= 0 pu). Maximum value of the magnitude r is defined as 0.15 pu. In the period of electromechanical oscillations, the loads are modelled by static ZIP model that has active power part equal to constant current, and reactive one to constant impedance.

Initial steady state period is defined by no-load conditions of the UPFC (r=0.0 pu, γ=0°, and V_i being uncontrolled). The TEF damping control operates the UPFC injection model from the shunt and series side.

During and shortly after the disturbance, electromechanical oscillations appear especially between generators GEN5 and GEN6, influencing also the bus voltage magnitude V_i at the UPFC shunt side. Both parts of the TEF block are used, series and shunt, respectively. The oscillations of the rotor angle difference of the generators (Fig. VII.1), and the shunt side bus voltage magnitude V_i (Fig. VII.2), are damped according to the TEF action described by (III.56-63). Three cases are analysed, namely without any damping control, with series TEF damping control solely, and with series and shunt TEF damping control simultaneously.

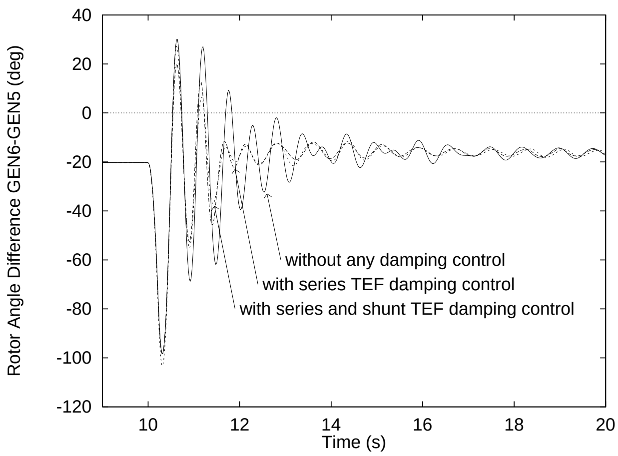

Fig. VII.1 Rotor angle difference (δ_{GEN6}-δ_{GEN5})

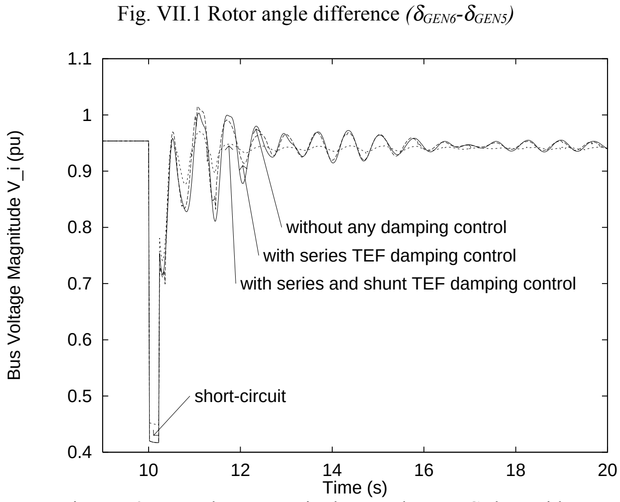

Fig. VII.2 Bus voltage magnitude V_i at the UPFC shunt side

The simulation period concerns the time span between 0 and 20 seconds. At the time instant t=10 s, the disturbance appears, and at t=10.220 s the line is switched off. The responses are shown for the period between 9 and 20 s, neglecting initial steady state period defined by constant values of the variables.

From the responses of the rotor angle difference and the bus voltage magnitude, it is seen that the UPFC damping control is effective within oscillations that arise after large disturbance appeared in the system. Damping level of the rotor angle difference is dominated by the series TEF part, whereas the bus voltage magnitude V_i is better damped by the shunt part (especially with certain overloading capability). Contribution of the shunt TEF part in the rotor angle difference damping is rather modest, as well as it is the case with the series TEF part in the bus voltage magnitude damping.

Damping control is achieved by introducing appropriate changes of the UPFC set of control variables (r, γ, I_{conv1q}).

From the response of the magnitude r, it is seen that the period with the largest engagement of the UPFC series part appears immediately after the disturbance and lasts for approximately 2 s (Fig. VII.3). There is no larger difference in its response between the cases with and without the activity of the shunt part. In the period of the largest engagement, the magnitude r is limited at its maximum value. It leaves some space for considering increase of its value. Toward the end of the simulation period, the magnitude r exhibits decrease in value due to smaller amplitudes of the rotor angle difference oscillations.

From the response of the angle γ, it is seen that the injected series voltage source opposes series active power flow changes by adjusting the angle γ at either *(90° - Θ_{ij})* or *(270° - Θ_{ij})*, (Fig. VII.4). Besides rather small phase lagging, no other difference is noticed between the cases with and without the shunt part being activated. As the oscillations vanish, the angle γ retains its appearance form, but with smaller values of the magnitude r.

From the response of the current I_{conv1q}, it is seen that the period with the largest engagement of the UPFC shunt part appears immediately after the disturbance and lasts for approximately 2 s (Fig. VII.5). In that period, the current I_{conv1q} is limited at its maximum value given by the short-term overload capability (35%). Toward the end of the simulation period, its value is decreased due to smaller amplitudes of the bus voltage magnitude oscillations. The response of the reactive power Q_{conv1} exhibits characteristics similar to the current I_{conv1q}, but in proportionality with the bus voltage magnitude V_i. Due to depressed voltage level immediately after the disturbance, the reactive power is initially decreased as well. This is in contrary with the response of the current I_{conv1q}, which takes maximum value during that initial period.

The UPFC activity is not blocked during the short circuit period. However, its series part has certain initial delay in response, whereas the shunt part is activated immediately.

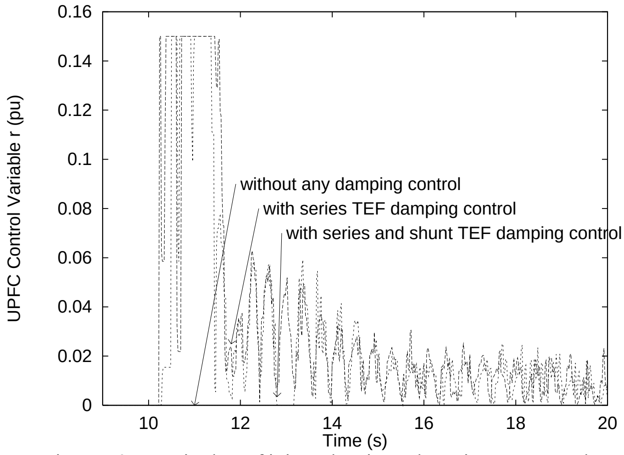

Fig. VII.3 Magnitude r of injected series voltage in TEF control

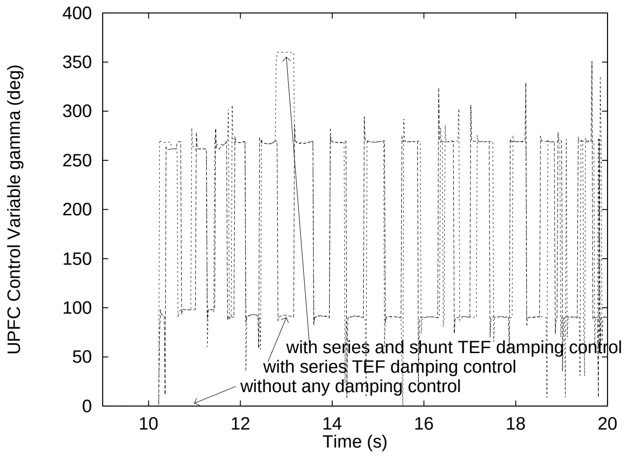

Fig. VII.4 Angle γ of injected series voltage in TEF control

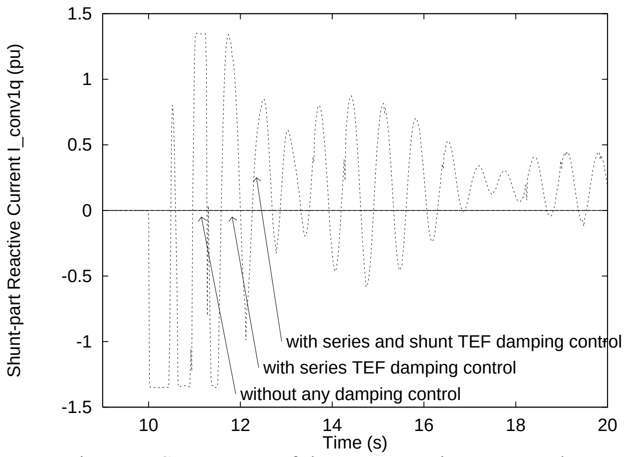

Fig. VII.5 Current I_{conv1q} of shunt converter in TEF control

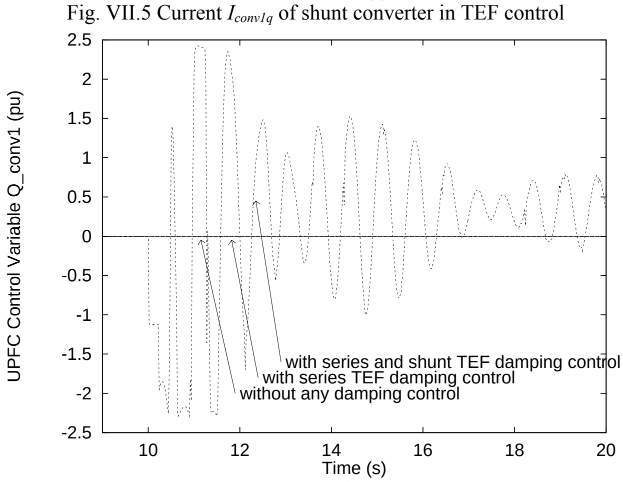

Fig. VII.6 Reactive power Q_{conv1} of shunt converter in TEF control

VII.2 RATING POWERS IN DAMPING CONTROL

The UPFC damping control of electromechanical oscillations depends mostly on the maximum value r_{max} of the magnitude r. The maximum value r_{max} influences the series converter apparent power S_{conv2}. Maximum value of the power S_{conv2} gives an estimate of its nominal rating power S_{conv2n}. Series converter should be adequately dimensioned to enable damping control without possible overloading.

Impact of the maximum value r_{max} to converters dimensioning is analysed by employing two of its values: 0.15 pu and 0.25 pu. Both TEF parts are active in damping control. Other aspects of simulations are kept the same as previous.

From the responses of the rotor angle difference (Fig. VII.7), it is seen that the UPFC damping control is more effective with larger value of r_{max}. This is especially valid for the initial period with the largest oscillations. Later on, as the oscillations become smaller, the impact of increased maximum value of r_{max} is not that pronounced.

From the response of the series converter apparent power S_{conv2} (Fig. VII.8), it is seen that the increased maximum value r_{max} causes larger peak of the power S_{conv2}. For r_{max}=0.25 pu, this peak is approximately equal to 185 MVA, whereas for r_{max}=0.15 pu, it is approximately 120 MVA. Toward the end of the simulation period, the series converter loading is decreased due to smaller amplitudes of the rotor angle oscillations.

In the same time, from the response of the shunt converter apparent power S_{conv1} (Fig. VII.9), it is seen that different values of r_{max} cause just minor changes of the shunt converter loading. Since the current I_{conv1q} is limited at its maximum value given by the short-term overload capability (35%), the peak values in both cases are approximately equal to 245 MVA. Toward the end of the simulation period, its loading level is decreased due to smaller amplitudes of the bus voltage magnitude oscillations.

With the series converter being rated at 185 MVA, the maximum value r_{max} could be set at 0.25 pu during period of oscillations damping. Most probably, in voltage support mode that maximum value would lead to unwanted voltage excursions. Thereby, after oscillations period it should be decreased. The shunt converter could have the same rating power (185 MVA). Its short-term overload capability contributes to the damping control, but in rather smaller degree, which often could be neglected.

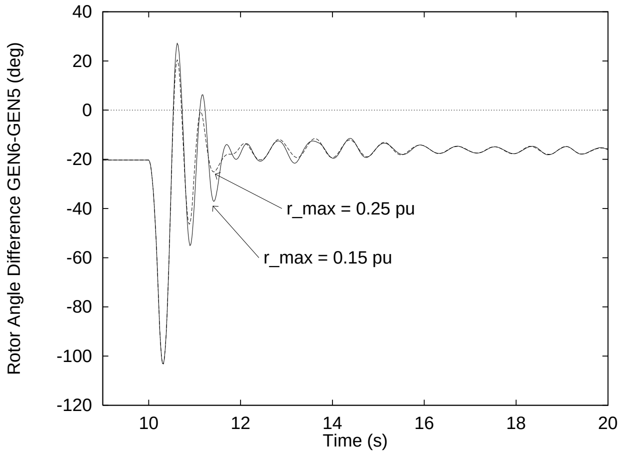

Fig. VII.7 Rotor angle difference (δ_{GEN6}-δ_{GEN5}) with respect to r_{max}

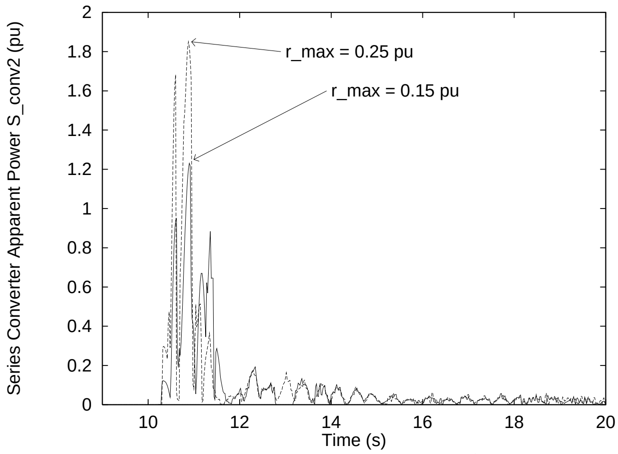

Fig. VII.8 Series converter apparent power S_{conv2} with respect to r_{max}

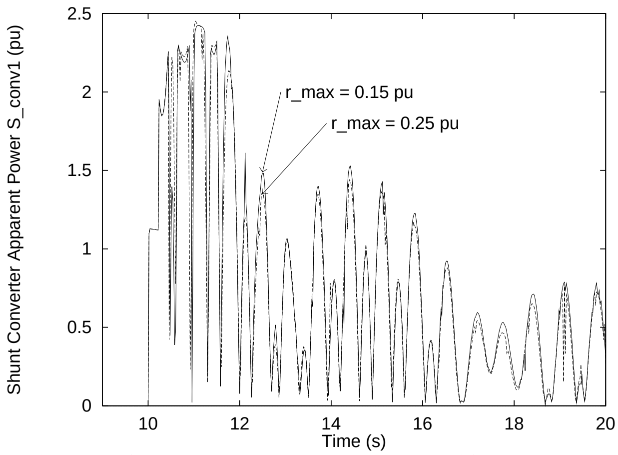

Fig. VII.9 Shunt converter apparent power S_{conv1} with respect to r_{max}

VIII. NUMERICAL RESULTS ON THE UPFC SUPPORT IN VOLTAGE STABILITY

At the third instance, possible benefits of the UPFC injection model and its belonging control system are investigated within voltage stability problem. Characteristics that are recognised in the voltage/power flow regulation and oscillations damping are used to alleviate voltage emergency situation. Two slow dynamics scenarios are assumed in the problem evolving. Different load models are analysed and their contributions to the voltage stability problem are evaluated. Three-parameter control of the UPFC injection model is employed. By describing achieved results it is shown that the UPFC could be useful transmission system controller in slow dynamics period of power system operation. Furthermore, its injection model with proposed control system has a potential for relieving the problem.

VIII.1 VOLTAGE COLLAPSE FROM A VIEWPOINT OF DYNAMIC LOAD MODEL WITH NON-LINEAR RECOVERY

In this section, the voltage stability problem is addressed from a viewpoint of dynamic load model with non-linear recovery. Its guidelines are given in subsection II.3.B. Two of the loads in the multi-machine test system are modelled in this way. The voltage collapse scenario is established first. Then, critical points of power system operation are recognised. Adequate location for the UPFC is defined. At last, the UPFC support is given to the bus voltage magnitudes and power flow regulation in order to alleviate voltage collapse.

VIII.1.A Voltage collapse scenario

In order to analyse possibilities of the UPFC support in voltage stability problem, the voltage collapse scenario in the multi-machine test system is established. The scenario is based on a slow dynamics response of the system given by mid-term recovery of initial load consumption.

The disturbance, which triggers the period of the slow dynamics, is a three-phase short circuit. It occurs on the line L17 closely to the bus BUS15 at time instant t=10 s, and is cleared after 220 ms by line L17 outage (Fig. II.1). The voltage stability problem evolves being dominated by load recovery and insufficient generator voltage control capability.

Loads are located in both of the two main areas (left/right). The two of the loads in the right-hand area, at buses BUS19 and BUS20, are modelled to have a constant active and reactive load power of the first-order dynamic load model with non-linear recovery. The recovery is activated 30 s after the disturbance, allowing for initially longer time of the first LTC tap movement. The rest of the loads are of the ZIP type (active power as constant current and reactive power as constant impedance). The generators are equipped with over-excitation limiters.

The responses of the voltage magnitudes at buses BUS19 and BUS20 clearly indicate that the system undergoes a voltage collapse at t=670 s (Fig. VIII.1). That happens after generators GEN5 and GEN6 (and at the very end GEN4) in the area with two recovery loads lost voltage control capability due to the action of the OELs at t=123 s and 190 s, respectively (Fig. VIII.2). Then, the reactive power demand on the generators exceeded the generator field current limit (Fig. VIII.3).

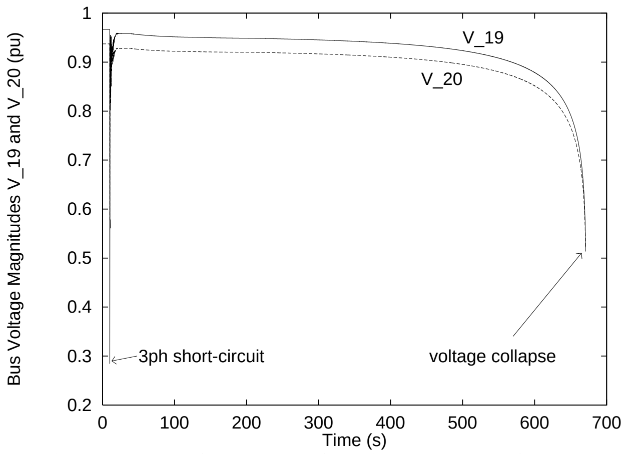

Fig. VIII.1 Bus voltage magnitudes at buses BUS19 and BUS20

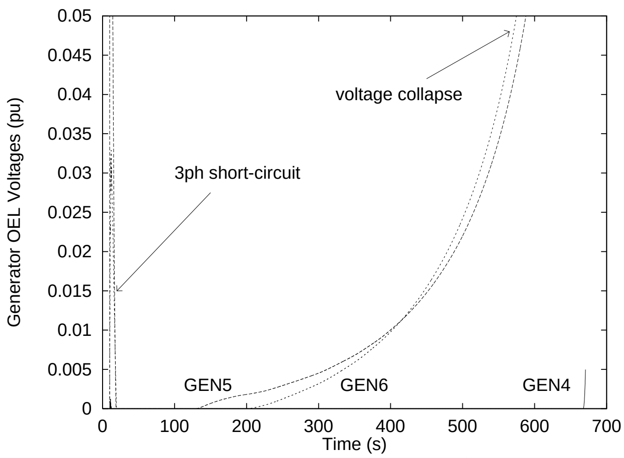

Fig. VIII.2 Generator over-excitation voltages

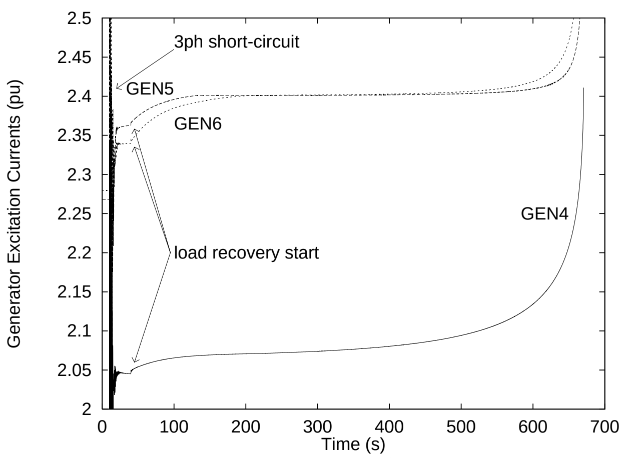

Fig. VIII.3 Generator excitation currents

Time domain responses of dynamic loads clearly depict the voltage collapse mechanism from a load viewpoint (Figs. VIII.4a-d). The responses are given in the ranges that allow non-linear recovery to be best viewed. All of the loads have constant initial power (active and reactive one) set as a recovery objective.

Initially, a three-phase short circuit causes appearance of electromechanical oscillations. Upon line outage, the bus voltage magnitudes are established at new values, which are at a lower level than the initial ones. Being depressed in value, the bus voltage magnitudes cause lower dynamic load consumption for approximately 2% due to a load voltage dependency.

The recovery process starts 30 s after the disturbance appeared. As the loads increase their consumption, the generators are asked to increase excitation current levels and provide more reactive power. The generators become limited by the OELs action, and dynamic loads exhibit changed recovery slopes. The first OEL action (GEN5, at t=123 s) makes somewhat slower recovery, but with its positive slope. The second OEL action (GEN6, at t=190 s) introduces negative slope of recovery process. None of the loads succeeded to achieve the initial value of load consumption. They come close to it, but still the difference exists. By the time passed, the mechanism of the loads that intends to re-establish initial consumption leads the system toward the voltage collapse.

It is seen that the bus voltage magnitudes at BUS19 and BUS20 are rather constant up to the ending part of the scenario. Therefore, it is necessary to establish a reliable index other than value of voltage magnitude to assess the severity of the voltage stability problem well before the actual collapse occurs. From the responses of the dynamic loads, it is seen that a critical point exists in a form of a closest proximity to initial load consumption. Upon recognition of the critical point during time domain simulation period, preventative measures should be applied soon enough to support voltages.

VIII.1.B Critical point recognition

During dynamic time-domain simulations, the extended Jacobi matrix, J_{EXT}, and the state matrix, A_S, are evaluated utilising linearised differential-algebraic model. Guidelines on differential and algebraic equations of system elements are provided in Chapter IV. Sensitivity analysis of the matrices enables recognition of critical points during time domain simulation period. Guidelines on sensitivity analysis are given in Chapter V. The knee-points in well known PV and/or QV curves are recognised denoting one of the possible time instants when voltage support should follow thereafter.

The voltage collapse scenario is followed through the sensitivity analysis taken in time steps of 1 s. Time step for solving differential equations is constant and equal to 0.005 s. Achieved results are written in steps of 0.1 s.

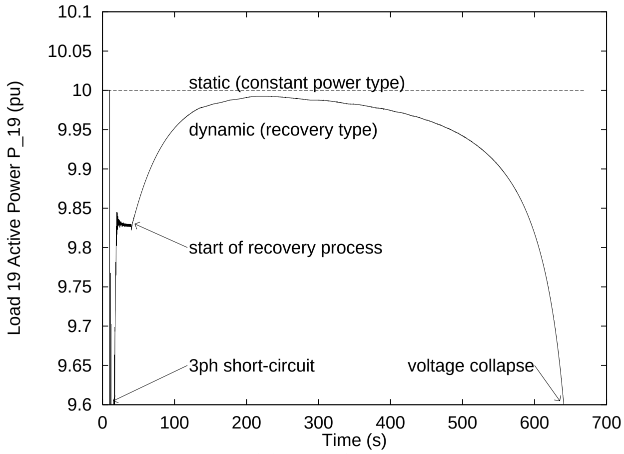

Fig. VIII.4a Response of dynamic load active power at BUS19

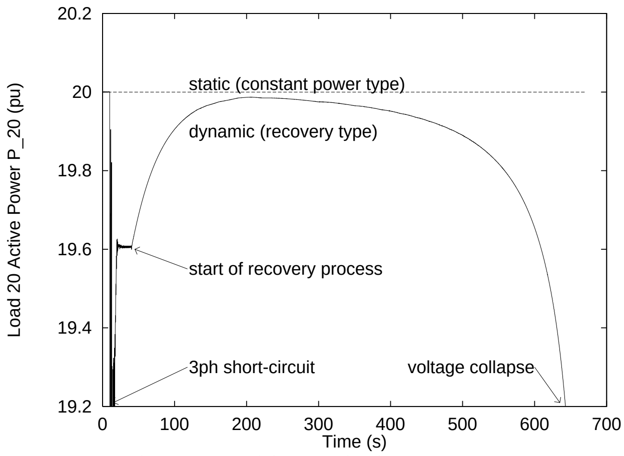

Fig. VIII.4b Response of dynamic load active power at BUS20

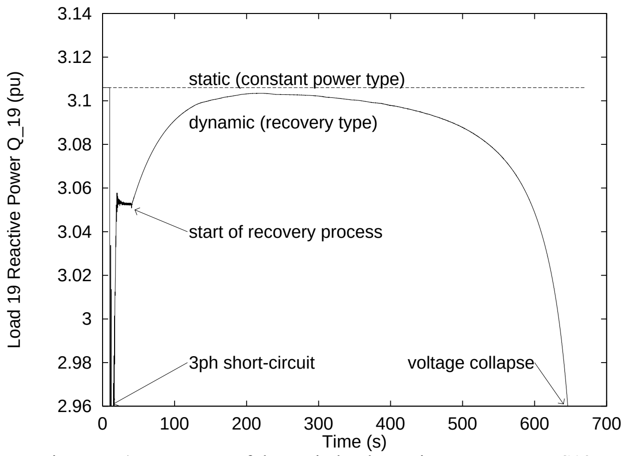

Fig. VIII.4c Response of dynamic load reactive power at BUS19

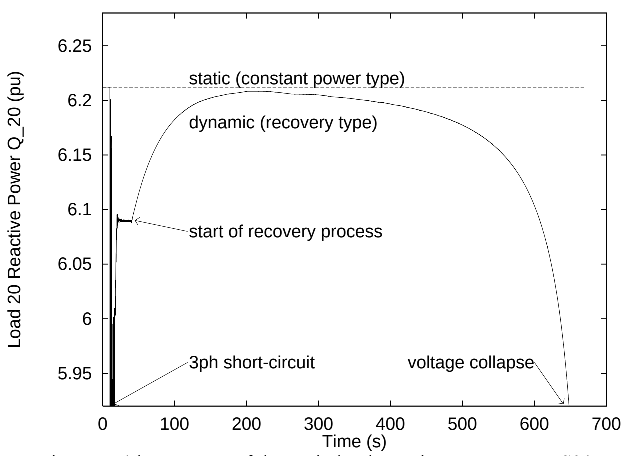

Fig. VIII.4d Response of dynamic load reactive power at BUS20

Particular attention is paid to appearance of the critical point. For that purpose, as a starting point serves a simple idea for finding the knee-point. At that point, the derivative of a PV and/or QV curve changes the sign making recovery slope transferred from positive to negative.

Simple ratio between relative changes of bus voltage magnitude and dynamic load active power is computed for buses BUS19 and BUS20. The ratio is given as $\Delta V_{19}/\Delta P_{19}$ for BUS19 and $\Delta V_{20}/\Delta P_{20}$ for BUS20 (Fig. VIII.5). Similarly, the ratio is computed for dynamic load reactive power at the same buses (Fig. VIII.6). These ratios are obtained in a straightforward manner, simply following values of the variables during time domain simulation.

Time responses of the ratios reveal the change of sign and therefore the knee-point of the load curves. Upon vanishing of initial electromechanical oscillations caused by the disturbance, the load recovery starts at t=40 s. By increasing dynamic load consumption toward the initial one, the voltage magnitudes are decreased. This makes the ratios being negative during that initial period. At t=123 s, generator GEN5 becomes limited by its OEL action. First limiting action causes the ratios and recovery slopes being even more negative. Shortly after generator GEN6 becomes also limited by its OEL action at t=190 s, the critical point occurs and the sign of the ratios is changed. Having critical point passed, actual dynamic load consumption decreases when trying to re-establish initial consumption. The voltages are still decreasing. This makes the sign of the ratios being largely positive. Further intention to reach the initial consumption leads towards the voltage collapse.

Besides following these simple changes, more computationally involved index is used as well. The intention is to match these ratios on the basis of the sensitivity analysis. Thereby, the parametric sensitivity $\partial y/\partial p$ is used being defined as a sensitivity of an algebraic variable with respect to an arbitrary parameter (V.97). As an algebraic variable, the bus voltage magnitude is used, while for an arbitrary parameter, the static part of the dynamic load with non-linear recovery is chosen. The parametric sensitivity is computed for each of the dynamic loads at buses BUS19 and BUS20 given as $\partial V_{19}/\partial(P_{L19}^{0})_{DL}$, $\partial V_{20}/\partial(P_{L20}^{0})_{DL}$, $\partial V_{19}/\partial(Q_{L19}^{0})_{DL}$, and $\partial V_{20}/\partial(Q_{L20}^{0})_{DL}$.

From time responses of these parametric sensitivities, quite similar behaviour to the simple ratios is recognised (Fig. VIII.7). Both instants of the OELs action are identified and the critical point as well. The change of the sign is clearly visible. They differ qualitatively only during steady state periods. While the simple ratios have zero values in these periods, the parametric sensitivities have negative ones indicating position of an operating point at the upper part of PV/QV curves. This position is often referred to as a stable one, but in general its stability depends on a static load characteristic. Having its constant power characteristic, the point is considered as being stable. Therefore, the parametric sensitivity gives some further insights than the simple ratios. Slight difference appears in the final part as well, where the parametric sensitivities end up closer to zero value.

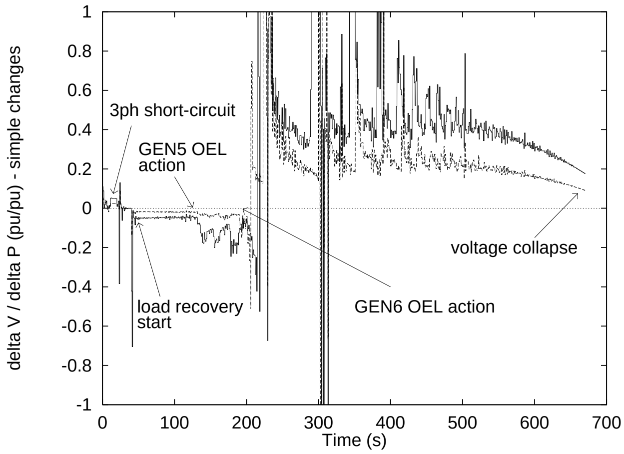

Fig. VIII.5 Time responses of simple changes $\Delta V/\Delta P$ for dynamic loads at buses BUS19 and BUS20

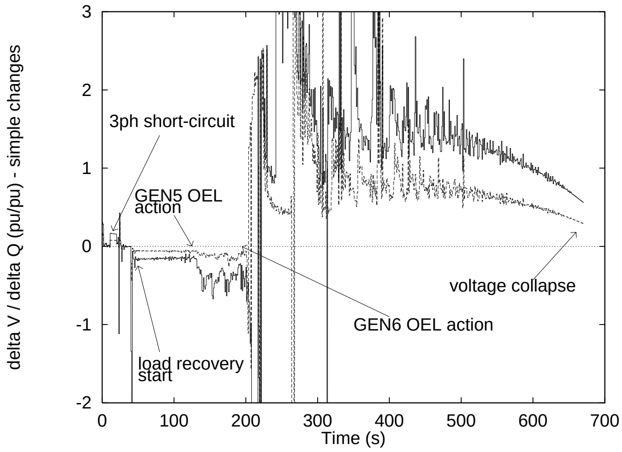

Fig. VIII.6 Time responses of simple changes $\Delta V/\Delta Q$ for dynamic loads at buses BUS19 and BUS20

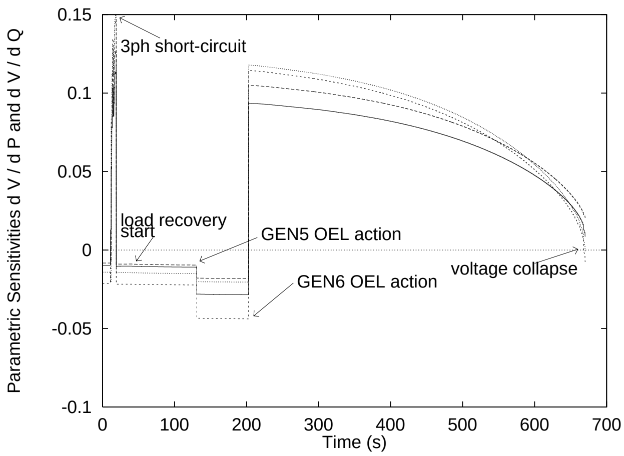

Fig. VIII.7 Time responses of parametric sensitivity $\partial V/\partial P$ and $\partial V/\partial Q$ for dynamic loads at buses BUS19 and BUS20

Besides parametric sensitivities, the sensitivity analysis comprises a functional one as well. The functional sensitivity $\partial\eta/\partial p$ is used here being defined as a sensitivity of a function with respect to an arbitrary parameter (V.123). As a function, the total reactive power production of the generators is used, while for an arbitrary parameter, the static part of the dynamic load with non-linear recovery is chosen again. The functional sensitivity is computed with respect to each of the dynamic loads at buses BUS19 and BUS20 given as $\partial Q_G^{\Sigma}/\partial(P_{L19}^{0})_{DL}$, $\partial Q_G^{\Sigma}/\partial(P_{L20}^{0})_{DL}$, $\partial Q_G^{\Sigma}/\partial(Q_{L19}^{0})_{DL}$, and $\partial Q_G^{\Sigma}/\partial(Q_{L20}^{0})_{DL}$.

From the responses of the functional sensitivities, it is seen that the OELs activation and the critical point are registered again (Fig. VIII.8). The change of the sign is clearly visible. More appropriate responses are achieved for the reactive power being chosen as an arbitrary parameter than the active one. In the last part of the scenario, the functional sensitivity with respect to the active power crosses zero value again and changes the sign once more. Therefore, within functional sensitivity evaluation it could be said that the total reactive power production, as the function, is better related to the reactive power load, as the parameter, than to the active one.

In general, before the occurrence of the critical point, the functional sensitivities have positive values. Afterwards, the values become negative. It means that as the load consumption is increased, the total reactive power production is increased as well resulting with a stable operating point (in general). Having critical point passed, the actual load consumption starts to be decreased, while the total reactive power production stays being increased. Therefore, the same recovery mechanism is reflected with the opposite signs of the parametric and functional sensitivities. As in the previous case of the parametric sensitivity, the functional sensitivity also gives an evaluation for a steady state operating point.

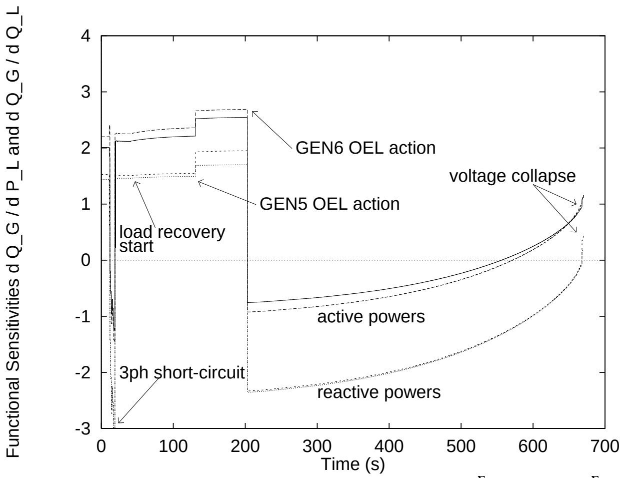

Fig. VIII.8 Time responses of functional sensitivity $\partial Q_G^{\Sigma}/\partial P$ and $\partial Q_G^{\Sigma}/\partial Q$ for dynamic loads at buses BUS19 and BUS20

Each of these sensitivities, which are based on a static load power as a parameter, are considered to be successful in finding the critical point and associated critical events. However, besides them, eigen and singular value decomposition of the matrices result with appropriate indices as well.

Eigenvalue decomposition of the state matrix A_S gives critical eigenvalue with maximum real part (Fig. VIII.9). Its transfer from negative towards positive half-plane happens when generator GEN6 becomes OEL limited (Fig. VIII.10). The plane crossing point appears after the oscillations are damped out, at t=190 s, and only within a real mode. Complex mode is not induced. Thereby, the critical point is again recognised as well as the other events that are associated to. As the voltage collapse becomes closer, the real part of the critical eigenvalue is increased. It also gives certain measure of the proximity to the collapse.

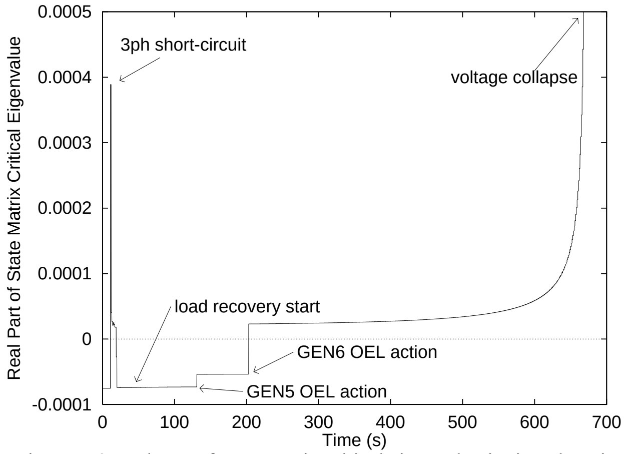

Fig. VIII.9 Real part of state matrix critical eigenvalue in time domain

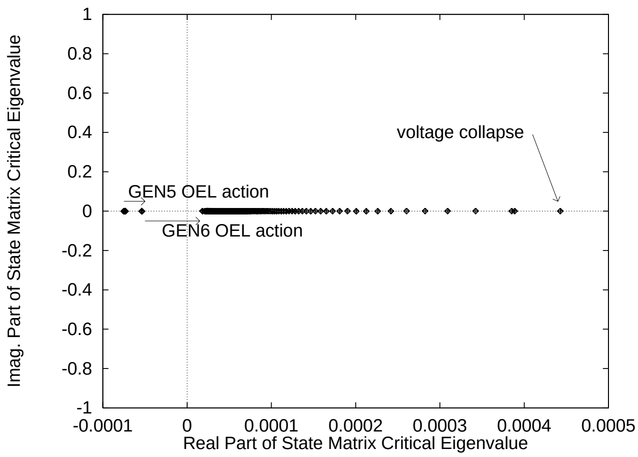

Fig. VIII.10 State matrix critical eigenvalue in complex domain

Singular value decomposition of the state matrix A_S results with the minimum singular value, which is always positive (Fig. VIII.11). As the load recovery starts, the minimum singular value decreases. Generator GEN5 OEL action gives large stress to the system decreasing further minimum singular value. The appearance of the critical point is reflected when the minimum singular value hits zero being ascended afterwards. In this case, generator GEN6 induced discontinuity due to its OEL activation causes the critical point. Therefore, since minimum singular value is always positive, clear point of hitting zero value is not visible, but is reasonably assumed. Having critical point passed, the minimum singular value increases. Minimum singular value also gives certain measure of the proximity to the voltage collapse.

However, it is seen that in cases with discontinuities, it is not clearly visible when the operating point becomes unstable in general. That is a large advantage of eigenvalue decomposition over singular one. In order to enable the minimum singular value being more adequate when recognising critical point, the measure m_{pps} of the projected parametric sensitivity is evaluated (Fig. VIII.12). It is computed with respect to BUS19 and BUS20 static parts of dynamic load, $(P_L^0)_{DL}$ and $(Q_L^0)_{DL}$, respectively (V.99-101). By projecting parametric sensitivities onto the minimum singularsubspace, its measure follows the route of the minimum singular value. But, a significant difference is noticed that it can be negative especially after passing through the critical point.

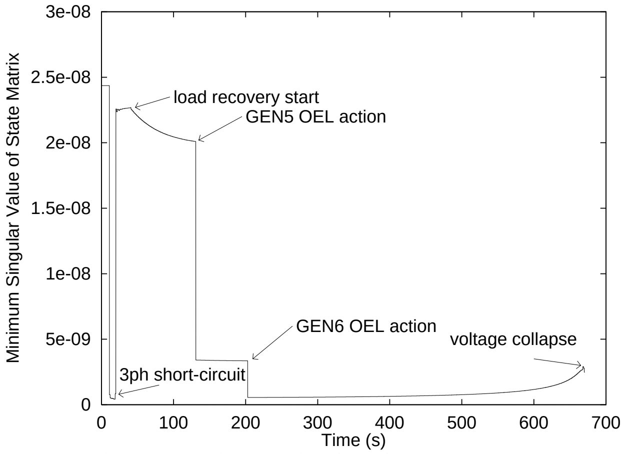

Fig. VIII.11 Minimum singular value of state matrix

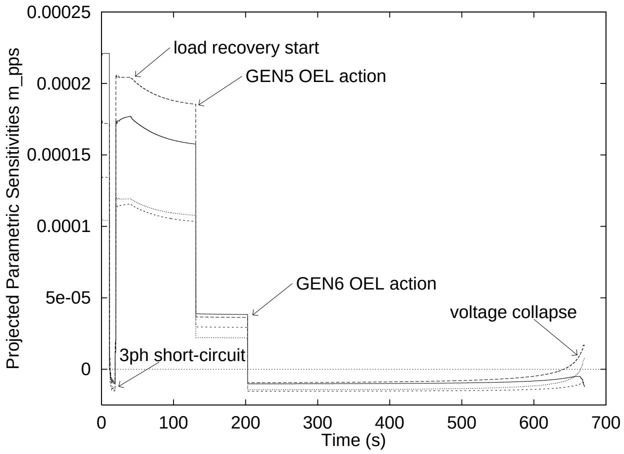

Fig. VIII.12 Measure m_{pps} of projected parametric sensitivities with respect to static parts of dynamic loads at buses BUS19 and BUS20

The indices that are shown in this subsection are successful in critical point recognition. However, the indices based on matrix decomposition have an additional advantage. The participation factors could be evaluated. By correlating bus and branch participation factors to the shunt and series branch of the UPFC, it is concluded about its appropriate location in the system.

VIII.1.C Location of the UPFC

From a viewpoint of static aspects given by matrix decomposition, the participation factors are very helpful in identification of the most critical location in the system. Then, the UPFC could be installed there to introduce the most significant impact during voltage emergency situations.

During time domain simulations, the linearised differential-algebraic model is calculated in steps equal to 1 s. In the voltage collapse scenario, the critical events and critical point are recognised along system trajectory. Thereby, characteristic time snap-shots are identified regarding appearance of the critical events. Before and after each of them, the participation factors are evaluated. The time snap-shots are given in Table VIII.1 concerning initial period of steady state operation, start of the load recovery, generator GEN5 OEL activation, generator GEN6 OEL activation, and final period of impending voltage collapse.

Table VIII.1 Time snap-shots during voltage collapse scenario

No.	time (s)	description
1	5	steady state
2	40	before start of load recovery
3	80	during unconstrained load recovery
4	123	before GEN5 OEL action
5	150	between two of the OEL actions
6	190	before GEN6 OEL action
7	220	after GEN6 OEL action
8	250	final period of impending collapse
9	300	↓
10	350	↓
11	400	↓
12	450	↓
13	500	↓
14	550	↓
15	600	↓
16	640	↓
17	660	↓

The singular value decomposition of the extended Jacobi matrix J_{EXT} is carried out during time domain simulation period. The matrix decomposition results with the right, v_n, and left, u_n, singular vectors associated to the minimum singular value, σ_n. Components of the right singular vector, v_n, related to the sub-matrix g_{y1} of the matrix J_{EXT}, indicate sensitive bus voltage angles and magnitudes (Fig. VIII.13). Components of the left singular vector, u_n, indicate sensitive direction for changes of active and reactive power injections (Fig. VIII.14). Total number of network buses is 22, which makes 44 algebraic variables in sub-matrix g_{y1}.

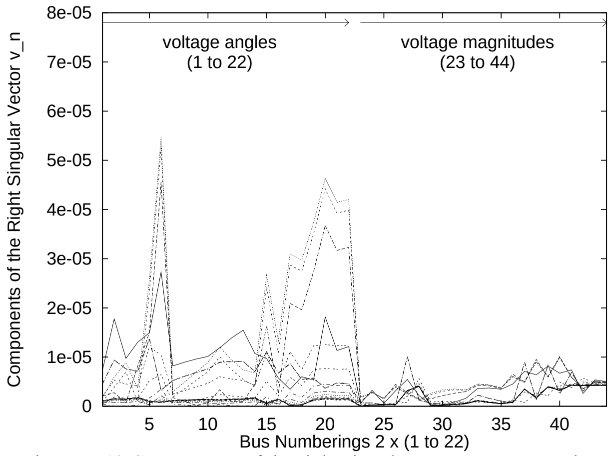

Fig. VIII.13 Components of the right singular vector v_n at snap-shots - decomposition of the extended Jacobi matrix J_{EXT} -

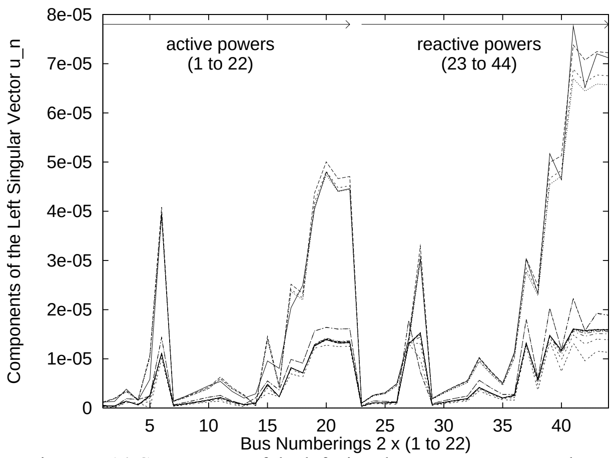

Fig. VIII.14 Components of the left singular vector u_n at snap-shots - decomposition of the extended Jacobi matrix J_{EXT} -

At characteristic time snap-shots, components of the singular vectors clearly depict system area with pronounced voltage stability problem. The right-hand side of the system, between buses BUS17 and BUS22 including generating bus GEN6, has the largest participation during voltage collapse scenario. The left-hand side does not exhibit voltage-related problems. The largest bus participation appears in the area where dynamic loads exhibit non-linear recovery leading to OEL action of nearby generators GEN5 and GEN6.

If the same decomposition is carried out on the state matrix A_S, the results belonging to the generator and load state variables are achieved. Components of the right singular vector, v_n, related to the state matrix A_S, indicate sensitive state variables (Fig. VIII.15). Components of the left singular vector, u_n, indicate sensitive direction for changes of state variable derivatives (Fig. VIII.16). Maximum number of state variables is equal to 59 (53 for generators, 2 for OELs, and 4 for dynamic loads). As the most sensitive state variables are recognised the ones that belong to the dynamic loads. The most sensitive direction, in addition to the state variables of the dynamic loads, is also orientated toward the ones that belong to the generators GEN5, GEN6, and GEN4. Again, the same area is recognised to have the largest participation within state variables during the voltage collapse scenario.

Besides through participation factors of the state variables, synchronous generators are analysed by using their reactive power production as well.

At the snap-shots, the reactive power production of the generators is evaluated (Fig. VIII.17). It is seen, that as generators GEN5 and GEN6 become constrained through the OEL actions, generator GEN4 starts to increase its reactive power production. Its engagement is the largest among the other generators in the system during the scenario.

In addition, generator reactive power, given by (V.125), is linearised with respect to the additional generator algebraic variables V_d, V_q, I_d, and I_q. Then, the set of linearised algebraic variables (ΔV_d, ΔV_q, ΔI_d, ΔI_q) is replaced with a corresponding set obtained from singular value decomposition of extended Jacobi matrix J_{EXT}. As a result, differential change of generator reactive power with respect to the minimum singularsubspace is computed. It is evaluated for each of the generators in the system (Fig. VIII.18). Again, as generators GEN5 and GEN6 become constrained due to the OEL action, generator GEN4 exhibits the largest sensitivity during the scenario.

These results show that not only state variable participation factors serve to recognise critical generators, but their reactive power production is useful as well.

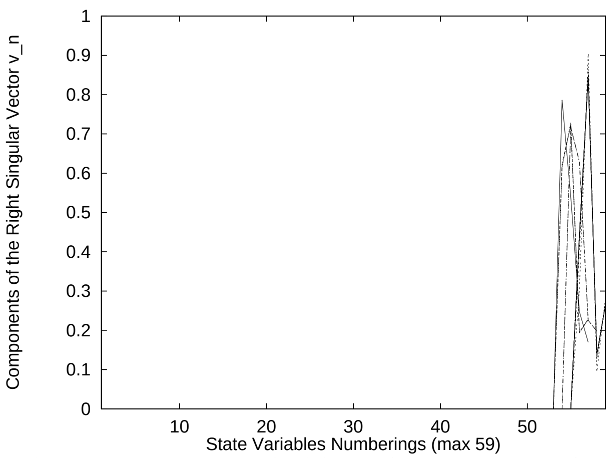

Fig. VIII.15 Components of the right singular vector v_n at snap-shots - decomposition of the state matrix A_S -

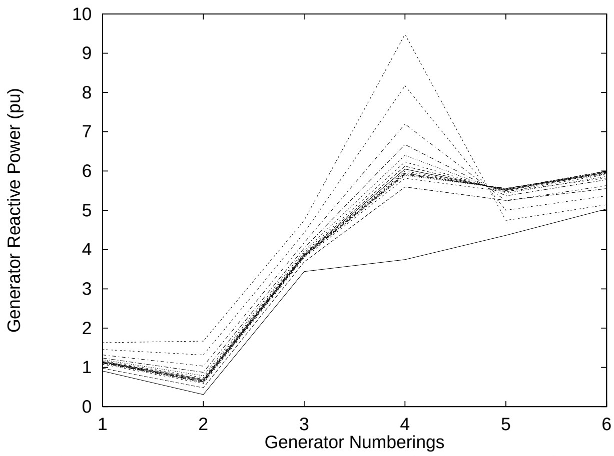

Fig. VIII.17 Generator reactive power production at snap-shots

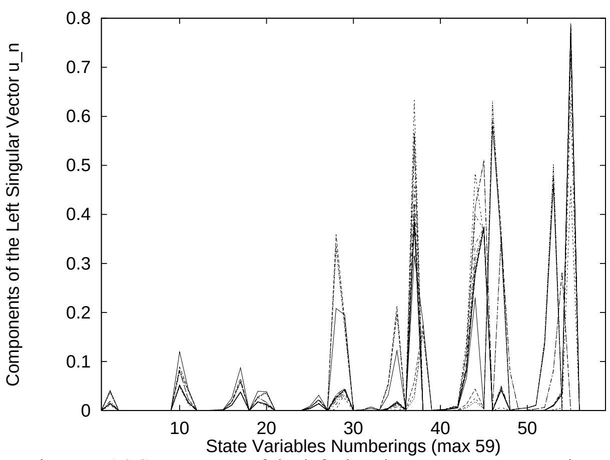

Fig. VIII.16 Components of the left singular vector u_n at snap-shots - decomposition of the state matrix A_S -

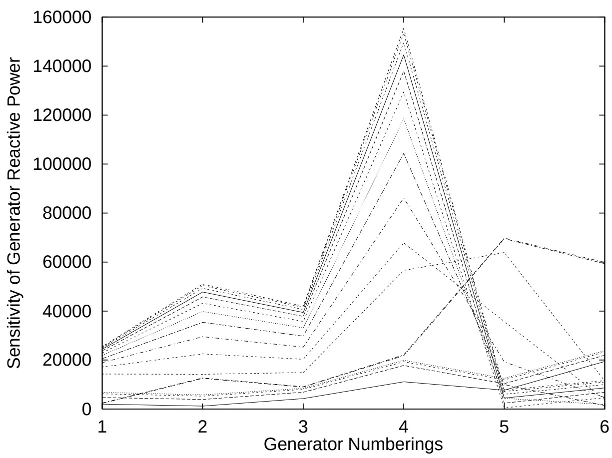

Fig. VIII.18 Sensitivity of generator reactive power at snap-shots

Branch participation factors are used in order to identify transmission network elements (lines and transformers) that have the largest participation in active/reactive power loss. During the scenario, total active power loss is computed according to (V.130), (Fig. VIII.19).

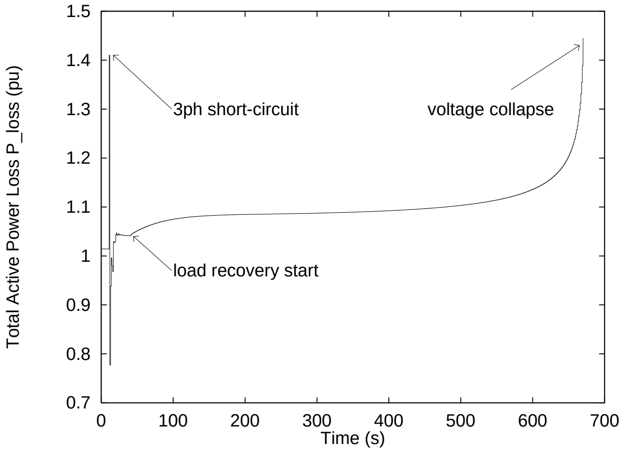

Fig. VIII.19 Total active power loss P_{loss} during voltage collapse scenario

Then, at the snap-shots, total power loss is distributed over network branches in order to be compared mutually (Figs. VIII.20-21). It is seen that lines L18-L25 have large shares of power losses. Lines L26-L27 (originally just L26), are lightly loaded and thereby have lower losses, but they still belong to the same power flow corridor at the right-hand side of the system. Lines L20 and L21 have the largest share of the losses due to their single-line performance.

Branch participation factors are given as differential changes of branch power losses with respect to the minimum singularsubspace of interest (V.74-75, V.81). Concerning them as sensitivities, they indicate which lines consume the most active/reactive power in response to an incremental change in active/reactive load (Figs. VIII.22-23). The right-hand side of the system is again recognised as the critical one. This area, which dominantly includes lines L18-L25, has the largest branch participation factors due to their heavy loading, whereas the lines L26-L27 have low participation factors due to light loading conditions.

The UPFC is based on a power electronic voltage source, and unlike series capacitor, does not need heavily loaded line for efficient power flow regulation. The lines L26-L27 (originally just line L26) make a part of the same corridor (L20 to L25). Therefore, even from the aspect of branch participation factors, the UPFC could be located appropriately at the mid-point between buses BUS19 and BUS20. This causes introduction of two additional new buses BUS21 and BUS22, and lines L26 and L27.

Bus and branch participation factors, accompanied by generator participation factors, denote the area around dynamic loads at buses BUS19 and BUS20 as being appropriate for possible installation of the UPFC. Then, the UPFC voltage support and/or power flow regulation capabilities are utilised in order to alleviate the voltage stability problem.

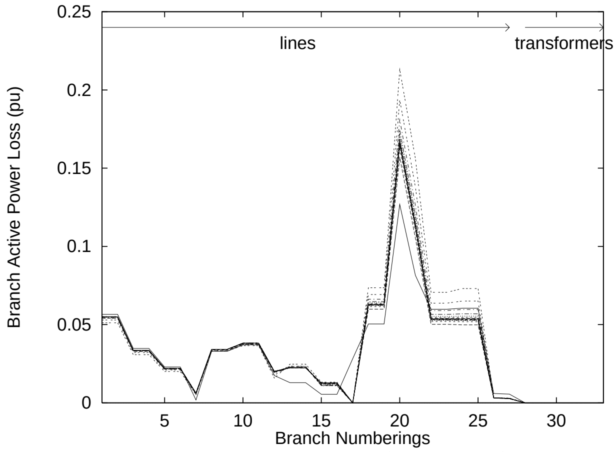

Fig. VIII.20 Branch active power loss at snap-shots

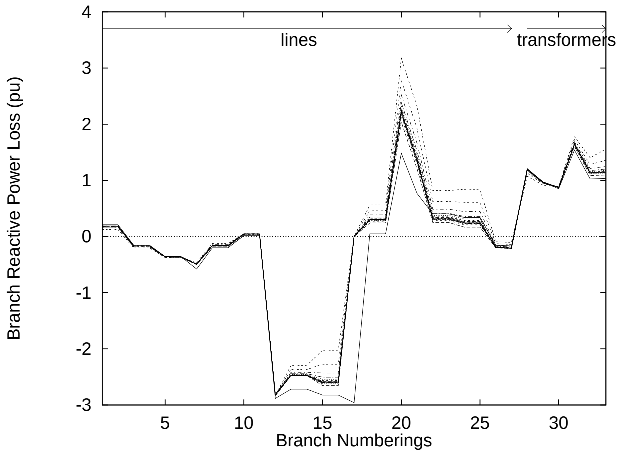

Fig. VIII.21 Branch reactive power loss at snap-shots

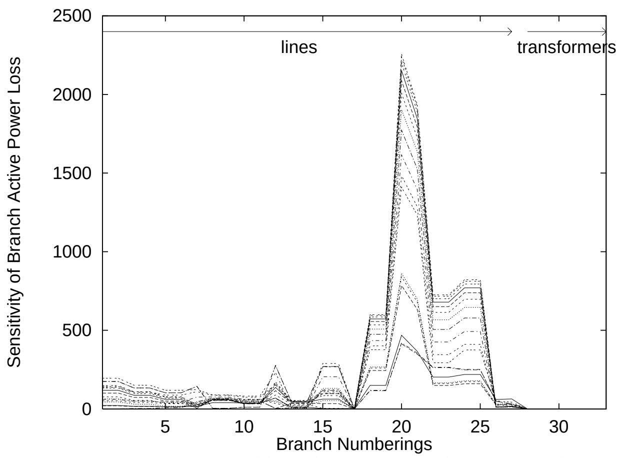

Fig. VIII.22 Sensitivity of branch active power loss at snap-shots

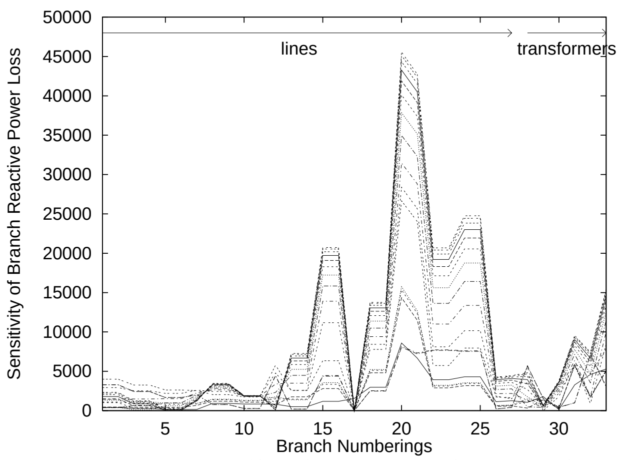

Fig. VIII.23 Sensitivity of branch reactive power loss at snap-shots

VIII.1.D The UPFC support

Having decided upon its location in the system, the UPFC is employed in voltage support and power flow control mode in order to avoid the collapse.

The same voltage collapse scenario is retained. Immediately after the disturbance, the UPFC TEF damping control is applied in take-over mode leaving no room for action of the PI regulators. Thus, upon expiration of the oscillations, the UPFC TEF block is disabled leaving the UPFC control system capable for voltage support. Until activation of the voltage support mode, it is assumed that the UPFC damping control period had expired leaving it at no-load condition.

Having critical point recognised, the UPFC voltage support is applied at several different time instants. They are equal to t=250 s, 400 s, 550 s, 600 s, and 625 s. Upon its activation, the shunt and series bus voltage magnitudes of the UPFC are given as subjects to the change of their referent values. The support is carried out by switching on the regulation modes $V_i \leftrightarrow Q_{conv1}$ and $V_j \leftrightarrow r$ through equal step changes in their PI regulator references. By setting these referent values at 0.95 pu, bus voltage magnitudes from both UPFC sides become equalised in successful cases (Fig. VIII.24). Initially unstable case collapses at t=670 s, whereas in the late case of voltage support (t=625 s) the collapse appears at t=749 s with splitting of the voltage magnitudes at the UPFC sides. In all other cases, the stable operating point is established with more or less dynamics involved. For the successful case applied at t=600 s, dynamics is rather significant, whereas the other cases experience it in a much smaller degree.

Upon establishing stable operating point by two-parameter voltage control, there is the third parameter, the angle γ, to be used as well. At t=750 s, the UPFC load flow control (LF) is applied through the γ-loop, while keeping previous two-parameter voltage support still active. Thereby, the UPFC bus voltage magnitudes are kept constant (Fig. VIII. 25), while the series active power flow is changed to precisely -2.5 pu with γ equal to 92.97° (Fig. VIII.26). The LF control is applied in order to increase minimum singular value and decrease total active power loss, as it is described later on.

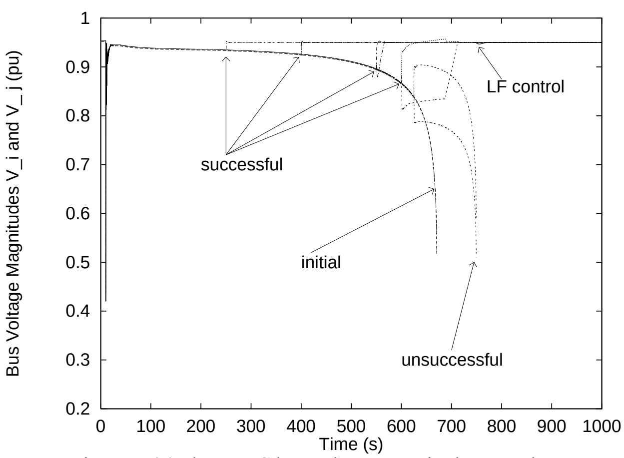

Fig. VIII.24 The UPFC bus voltage magnitudes V_i and V_j

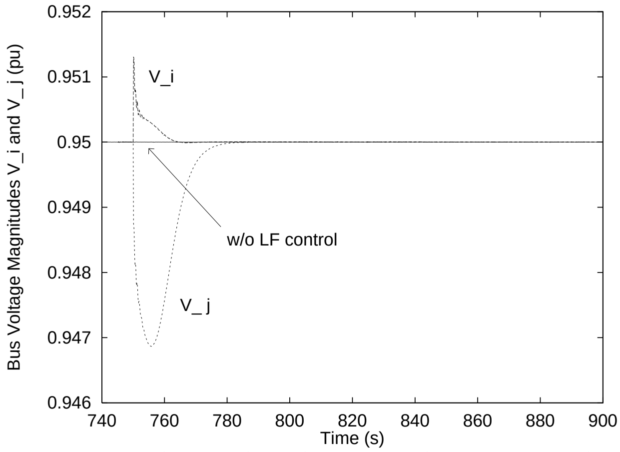

Fig. VIII.25 The UPFC bus voltage magnitudes upon LF control

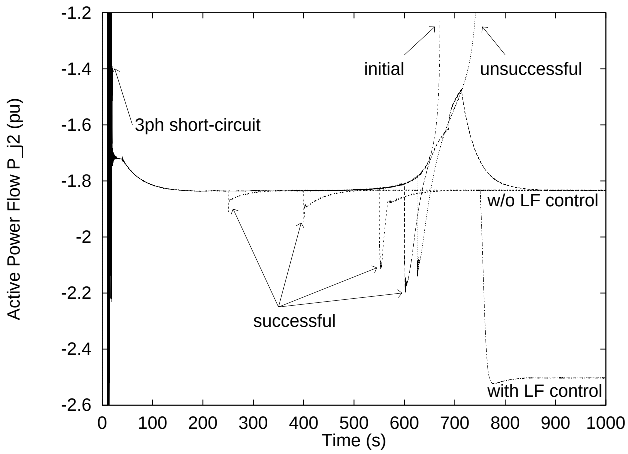

Fig. VIII.26 The UPFC series side active power flow P_{j2}

Activation of the UPFC simultaneous three-parameter control is shown to be very effective in the voltage stability problem. The UPFC set of variables (r, γ, I_{conv1q}) has acceptable responses (Figs. VIII.27-29). From the responses of the magnitude r, it is seen that in successful cases without LF control the UPFC is loaded just transiently in the periods of electromechanical oscillations and upon the step changes. Rather small value of the magnitude r is asked for voltage support solely. If LF control is applied, the magnitude r becomes significantly increased to respond to the power flow change. Besides in the oscillations period, the angle γ has a non-zero value during LF control period as well. During two-parameter voltage support period it is zeroed.

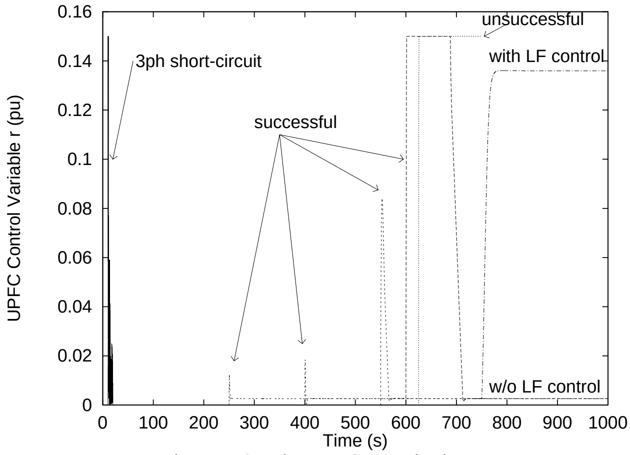

Fig. VIII.27 The UPFC magnitude r

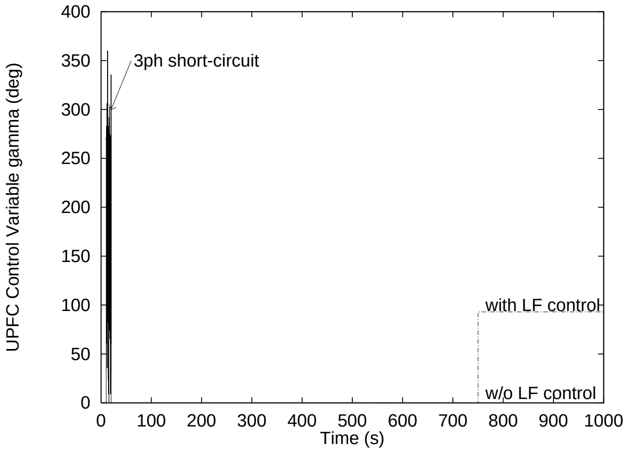

Fig. VIII.28 The UPFC angle γ

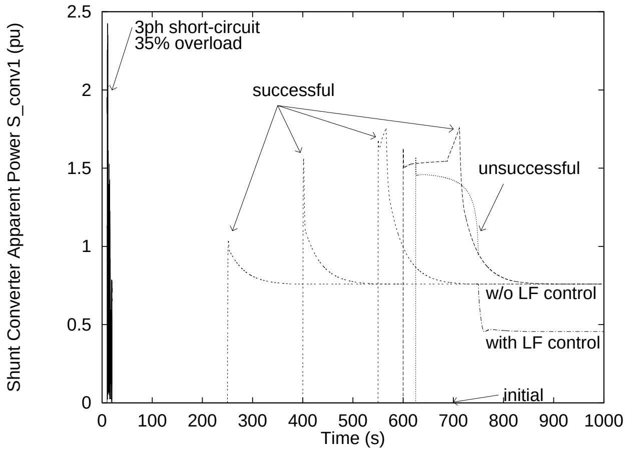

Fig. VIII.30 The UPFC shunt converter apparent power S_{conv1}

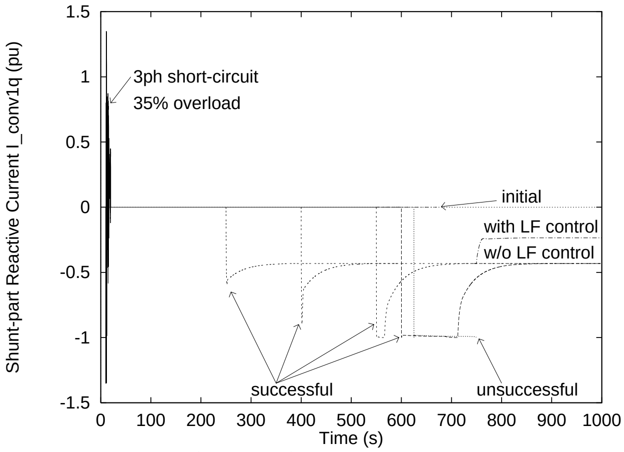

Fig. VIII.29 The UPFC shunt part reactive current I_{conv1q}

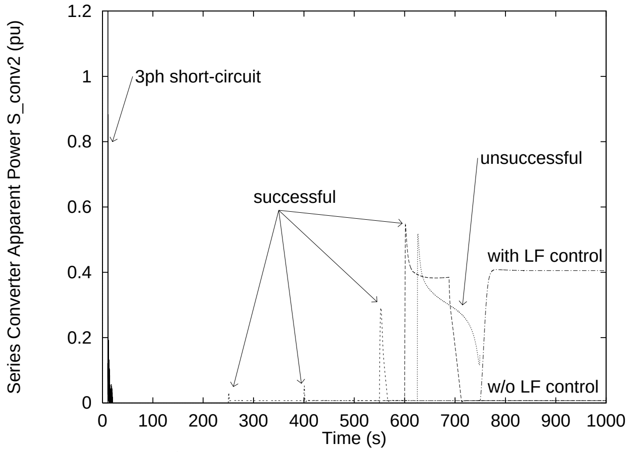

Fig. VIII.31 The UPFC series converter apparent power S_{conv1}

From the responses of the UPFC current I_{conv1q}, it is seen that a capacitive loading of the shunt converter is needed to increase the UPFC shunt side bus voltage magnitude. The loading level stays constant for all successful cases without LF control. If the LF control is applied, the shunt converter reactive current is decreased in absolute value. In damping control mode, the short-term overload is allowed, whereas later on in the voltage support mode it is not. Since the current I_{conv1q} is internal variable of the shunt converter, it is computed on the basis of its nominal rating power S_{conv1n}. Therefore, it is limited at 1 pu in voltage support mode.

Nominal rating powers of the UPFC shunt and series converters, S_{conv1n} and S_{conv2n}, are defined to be equal to 185 MVA (1.85 pu on the system base power 100 MVA). The responses of the converter apparent powers, S_{conv1} and S_{conv2}, show that they are operated within nominal rating limits (Figs. VIII.30-31). The only exception appears in oscillation damping control mode when the shunt converter is allowed to have 35% short-term overload capability.

In successful cases without LF control, loading level of the shunt converter is much larger than the series one. The UPFC shunt side controls bus voltage magnitude V_i, while the series side in that period just adds injected voltage source at the shunt side magnitude. This is the main reason for their disproportionate loading levels. They become approximately equalised after LF control is applied within the series converter.

Responses of the shunt converter apparent power S_{conv1} mostly follow the responses of the current I_{conv1q}. Responses of the series converter apparent power S_{conv2} are rather similar to the ones of the UPFC magnitude r.

Shunt and series converter apparent powers, S_{conv1} and S_{conv2}, are decomposed into active and reactive power parts, Q_{conv1}, P_{conv2}, and Q_{conv2} (Figs. VIII.32-34). Shunt converter active power P_{conv1} is equal to P_{conv2}.

Responses of the UPFC shunt converter reactive power Q_{conv1} are similar to the ones of the current I_{conv1q}. In addition, proportionality to the shunt side bus voltage

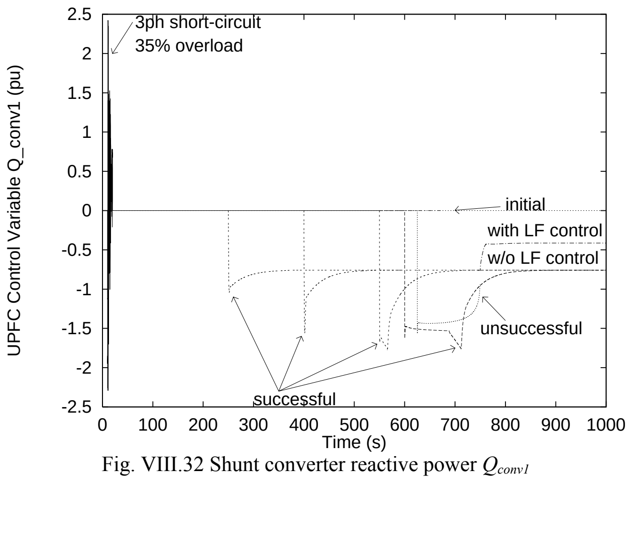

Fig. VIII.32 Shunt converter reactive power Q_{conv1}

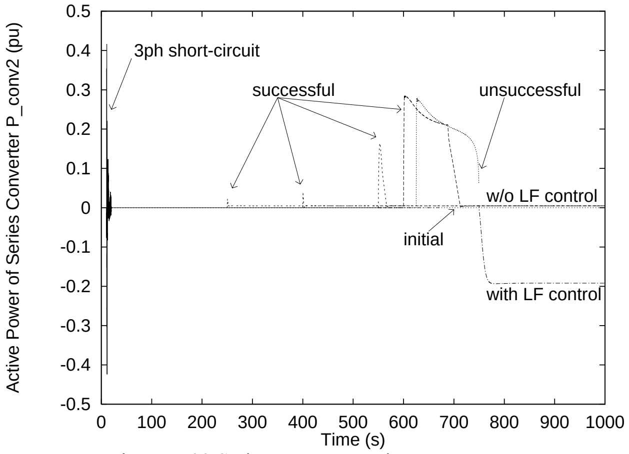

Fig. VIII.33 Series converter active power P_{conv2}

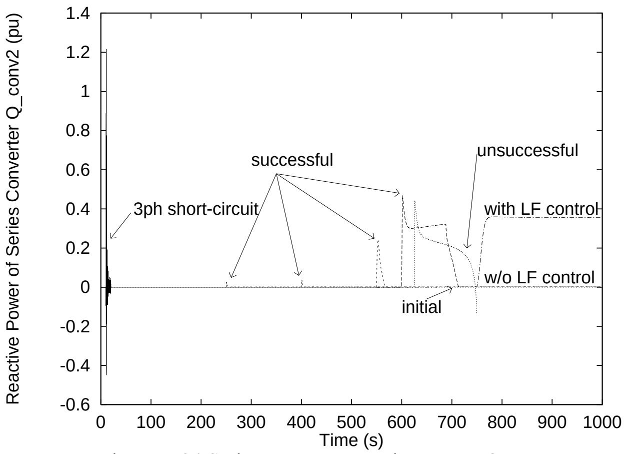

Fig. VIII.34 Series converter reactive power Q_{conv2}

magnitude V_i is recognised, especially during limiting conditions. Loading level in successful cases without LF control is rather high, showing quite small demand for active power. In the case with LF control, reactive power loading level is decreased.

From responses of the series (and shunt) converter active power P_{conv2}, it is seen that a very low demand for active power exists when the LF control is not required. Therefore, in successful cases without LF control, the UPFC shunt converter is loaded dominantly with reactive power. When the LF control is applied, active power demand arises, but shunt converter reactive power Q_{conv1} still has a larger portion in the apparent power S_{conv1}.

Responses of the series converter reactive power Q_{conv2}, denote very low loading level in successful cases without LF control. When the LF control is activated, not only series converter active power P_{conv2} is increased, but the reactive one as well. Upon activation of γ-loop, even larger increase is noticed in series converter reactive power than in the active one. It happens due to increase of the magnitude r aimed to control bus voltage magnitude V_j at the value equal to V_i. Therefore, series converter reactive power Q_{conv2} then represents a larger portion in apparent power S_{conv2} loading level. Change of active power flow at the series side requires increase in series converter reactive power if bus voltage magnitude at the series side should be kept constant and equalised to the shunt one.

Described activity within the UPFC converters and control variables leads to alleviation of the voltage stability problem. Bus voltage magnitudes at buses BUS19 and BUS 20 denote initial case of voltage collapse, unsuccessful case of voltage support due to its late activation, and successful cases with and without LF control (Fig. VIII.35). Upon LF control, the magnitudes are slightly changed due to the change in power flows. Generator OEL voltages are brought to zero value in successful cases of the UPFC voltage support (Fig. VIII.36). Generator excitation currents are decreased in value when the UPFC starts to provide reactive power to the system (Fig. VIII.37). Upon LF control, the excitation currents become changed, with an increase in one and a decrease in the other.

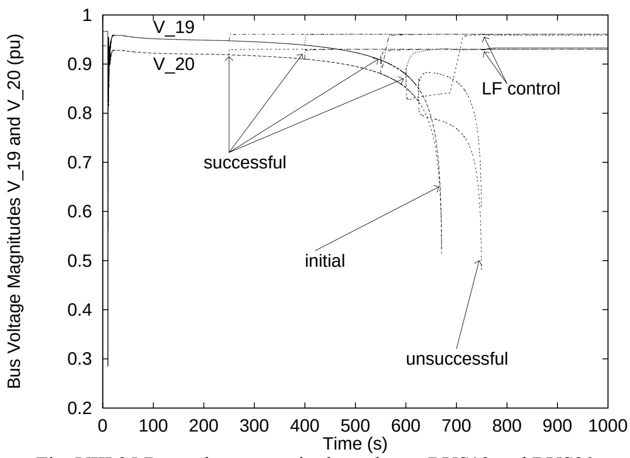

Fig. VIII.35 Bus voltage magnitudes at buses BUS19 and BUS20

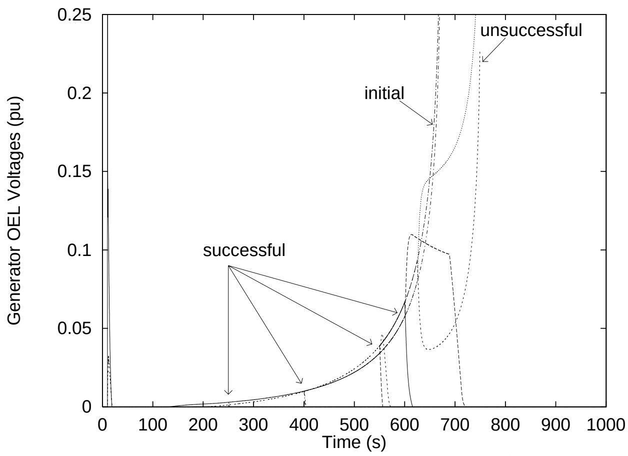

Fig. VIII.36 Generators GEN5 and GEN6 OEL voltages

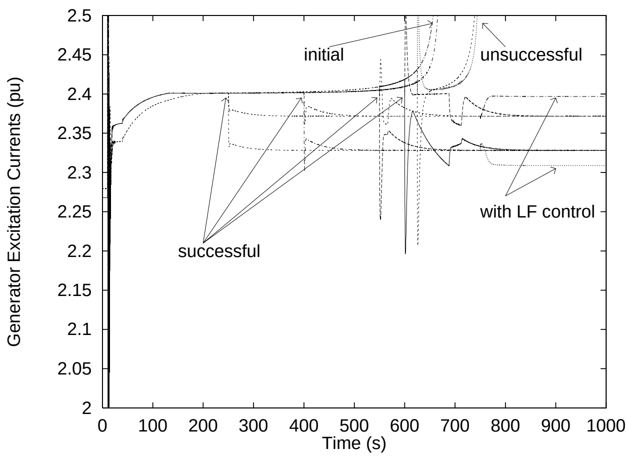

Fig. VIII.37 Generators GEN5 and GEN6 excitation currents

In voltage support mode, obtained responses denote that required engagement of the UPFC in terms of converter loading level is rather constant, whereas a level of overall system dynamics is decreased if the support is given earlier. Preferably, the support should be given upon critical point recognition. Otherwise, overall system dynamics becomes more pronounced as it is seen in generator excitation current responses for the case that is applied at t=600 s. Roots are found in dynamic loads behaviour.

Dynamic loads have non-linear recovery of initial consumption after being disturbed by change of bus voltage magnitude. Example is provided for reactive power load that is connected at bus BUS19 (Figs. VIII.38-39).

In successful cases, increase in bus voltage magnitude appears due to the UPFC voltage support. As the bus voltage magnitude is increased, actual reactive power consumption is initially increased above its steady state value if the voltage support is provided earlier during the scenario. Then, it is decreased toward the initial consumption value along trajectory with constant bus voltage magnitude. If the support is provided earlier, time constant of non-linear recovery process is much longer than the time response of the UPFC voltage magnitudes at both sides. The UPFC bus voltage magnitudes are decoupled in a very short period of time. Therefore, it establishes constant voltage profile much earlier than the load recovers its initial consumption.

If the voltage support is given later on, overall dynamics level is increased. The UPFC needs longer time period to establish constant voltage profile with largely decoupled voltage magnitudes. For the last successful case of the support given at t=600 s, that time period comes into the range of the load recovery time constant. Actually, the load is recovered first, but at the lower voltage magnitude than it is desired by the UPFC step changes. Then, the voltage magnitude is increased due to the UPFC intention to equalise bus voltage magnitudes at both sides. As the UPFC increases bus voltage magnitude, the load is changed again. First, it is increased above steady state value. Then, it recovers initial consumption, but this time at the higher voltage magnitude. The LF control does not impose any significant change in the load behaviour.

The UPFC voltage support has a large impact to the behaviour of the indices aimed for critical point recognition. Example is provided for reactive power dynamic load at bus BUS19. Simple changes $\Delta V/\Delta Q$ for dynamic load at bus BUS19 clearly indicate difference between successful and unsuccessful cases (Fig. VIII.40). When the voltage support is successful, the ratio $\Delta V/\Delta Q$ becomes approximately equal to zero. It means that the load is being recovered at its initial consumption and no further change of bus voltage magnitude appears. Being at zero value, the ratio does not give any estimate of a general stability of an operating point. However, its parametric sensitivity $\partial V/\partial Q$ gives a stability estimate as being brought back to the negative side (Fig. VIII.41).

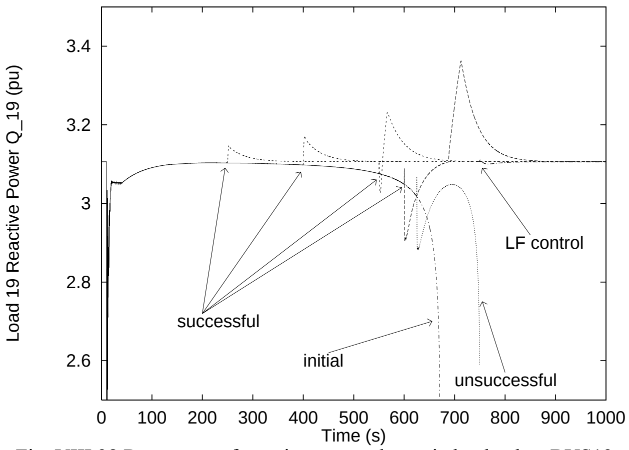

Fig. VIII.38 Responses of reactive power dynamic load at bus BUS19

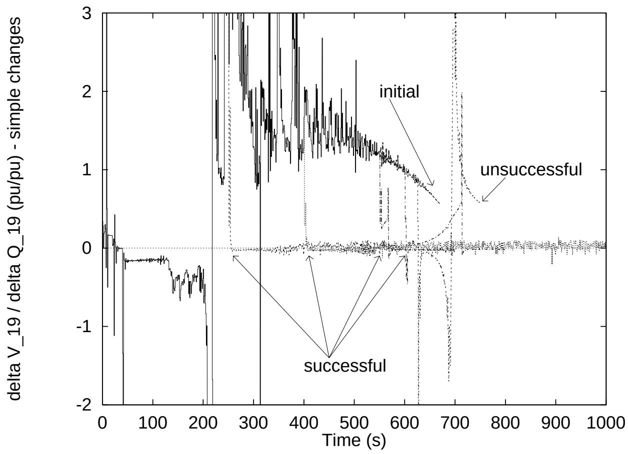

Fig. VIII.40 Simple changes $\Delta V/\Delta Q$ for dynamic load at bus BUS19

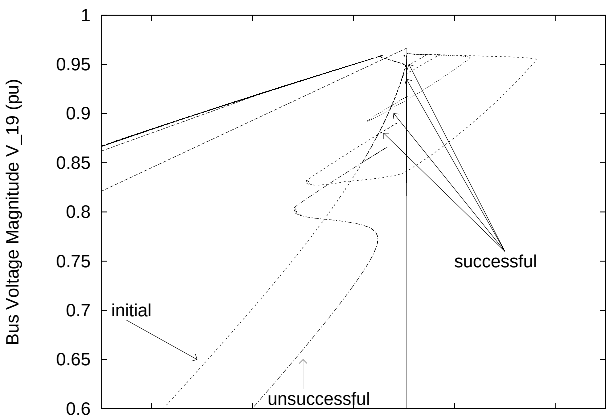

Fig. VIII.39 Voltage magnitude with respect to reactive power at BUS19

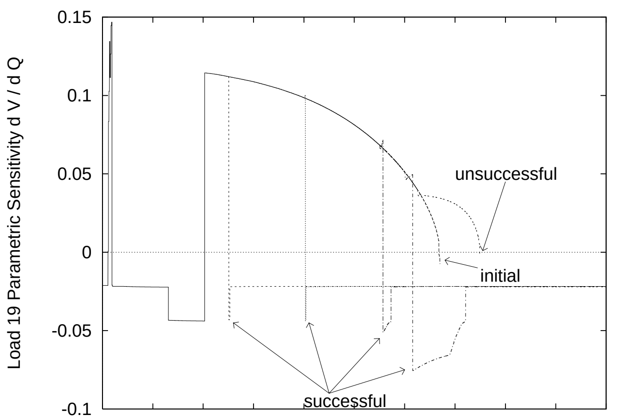

Fig. VIII.41 Parametric sensitivity $\partial V/\partial Q$ for dynamic load at bus BUS19

Increased level of overall system dynamics is visible in responses of the parametric sensitivity as the voltage support is given later on. The same happens with the functional sensitivity of total reactive power production with respect to the static part of the dynamic load (Fig. VIII.42). In successful cases, the UPFC voltage support brings the functional sensitivity at positive value. It also exhibits wanted characteristic of a sensitivity to give a stability estimate of an operating point in steady state. The LF control does not cause any visible impact to the sensitivities.

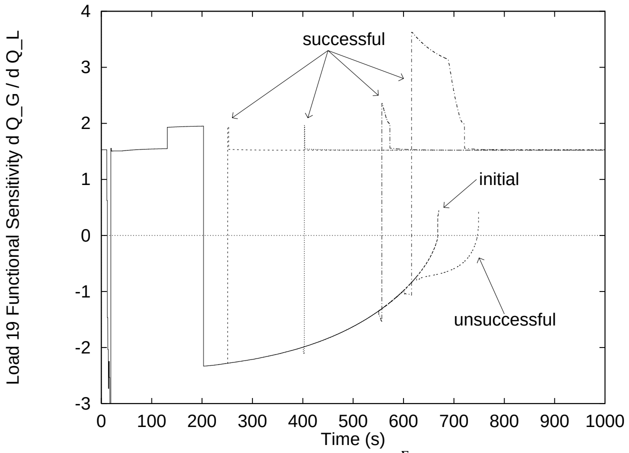

Fig. VIII.42 Functional sensitivity $\partial Q_G^{\Sigma}/\partial Q$ at bus BUS19

Eigenvalue decomposition of the state matrix A_S results with critical eigenvalue with maximum real part. Responses of that variable also clearly show difference between successful and unsuccessful cases (Fig. VIII.43). In successful cases, real part of critical eigenvalue crosses back to the negative half-plane upon timely voltage support. As the support is given later, system dynamics is increased. In the unsuccessful case, the support is provided too late and the system loses stability.

The LF control again does not introduce any significant effect within critical eigenvalue real part. However, if particular time period around its activation is shown, it is noticed that it has a small, but positive impact (Fig. VIII.44). Upon its activation, critical eigenvalue real part is further decreased in negative direction. It makes the system more secure from a voltage stability viewpoint.

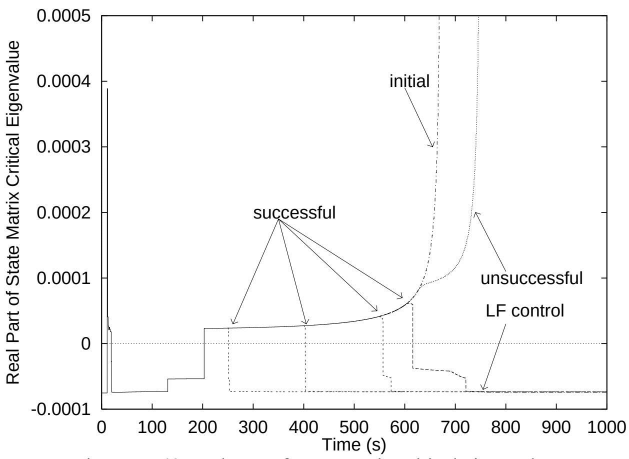

Fig. VIII. 43 Real part of state matrix critical eigenvalue

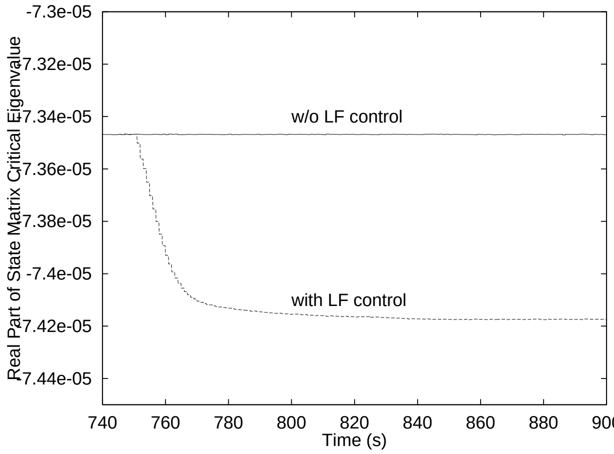

Fig. VIII.44 Real part of state matrix critical eigenvalue upon LF control

Concerning the LF control impact, singular value decomposition exhibits the most sensitive response upon its activation. Minimum singular value becomes largely increased as the voltage support is provided. In each of the successful cases, afterwards it has the same value. Then, with the LF control activated, it is again significantly increased. Its value becomes even larger than in the initial steady state. Similar responses are found within the measure m_{pps} of the projected parametric sensitivity with respect to the static reactive power part of the dynamic load at bus BUS19 (Fig. VIII.46). In each of the successful cases, the UPFC voltage support brings the measure m_{pps} back to a positive value. Later on, the LF control further increases its value denoting operating point as more secure.

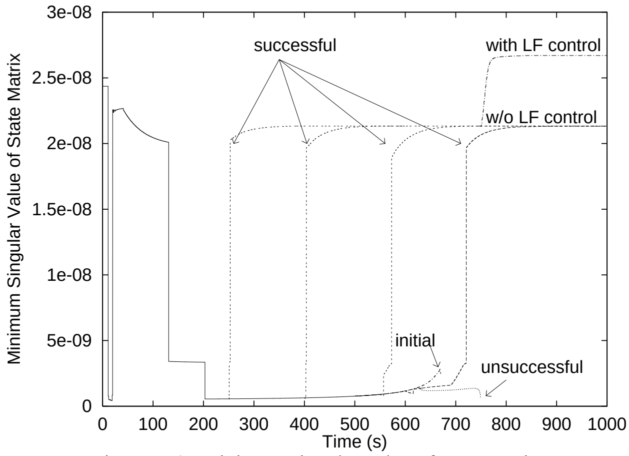

Fig. VIII.45 Minimum singular value of state matrix

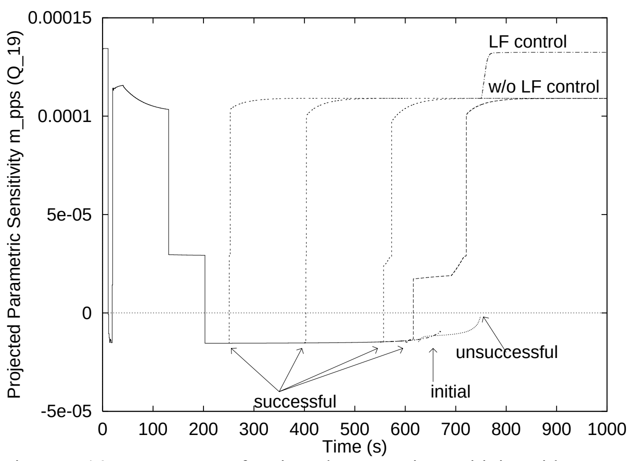

Fig. VIII.46 Measure m_{pps} of projected parametric sensitivity with respect to static reactive power part of dynamic load at BUS19

Total active power loss in the system is also influenced by the UPFC voltage support. In each of the successful cases, the loss is stabilised at the same value with more or less system dynamics induced (Fig. VIII.47). Impact of the LF control is visible only if the period around its activation point (t=750 s) is depicted solely (Fig. VIII.48). It is noticed that after transients the LF control slightly decreases total active power loss.

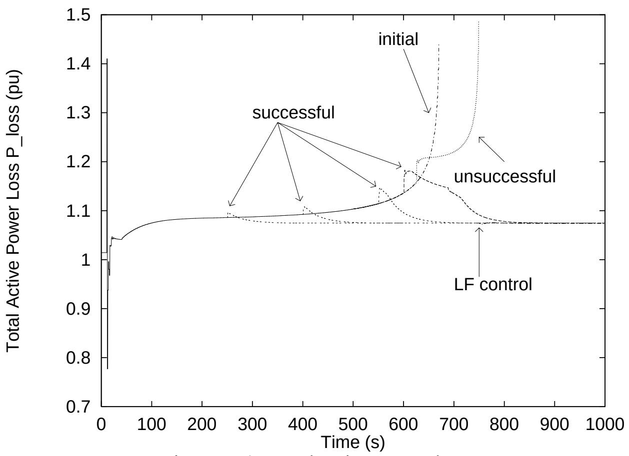

Fig. VIII.47 Total active power loss

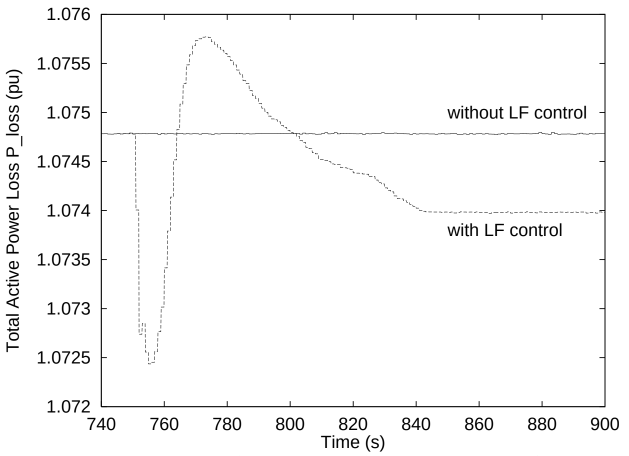

Fig. VIII.48 Total active power loss upon LF control

The analysis of the UPFC voltage support and/or power flow control describes its versatile characteristics that are very useful in simultaneous three-parameter control. The UPFC is very helpful in alleviation of the voltage stability problem. In the same time, it is used to avoid voltage collapse by providing voltage support, and additionally either to increase voltage security index or to decrease total active power loss by control of power flows.

Its versatile characteristics are checked in the voltage stability problem not only from a viewpoint of dynamic load model with non-linear recovery, but from the composite load model as well.

VIII.2 VOLTAGE COLLAPSE FROM A VIEWPOINT OF COMPOSITE LOAD MODEL

In this section, the voltage stability problem is addressed from a viewpoint of the composite load model. Belonging guidelines are provided in subsection II.3.A. Two of the loads in the multi-machine test system are modelled in this way (BUS19 and BUS20). The voltage collapse scenario is established first. Then, critical load parameters are recognised. Critical singularity point is detected. Finally, the UPFC voltage support is given to the bus voltage magnitudes in order to alleviate voltage collapse. The analysis is aimed to indicate similarities and differences in time domain responses of two different load models.

VIII.2.A Voltage collapse scenario

In order to analyse capability of the UPFC to provide support in voltage stability problem, the voltage collapse scenario is established. The scenario is set to be as close to the previous one as it is possible.

In the previous scenario, the loads at BUS19 and BUS20 are modelled as dynamic ones with non-linear recovery of initial consumption. In this one, the composite load model is used instead (Fig. II.9). Buses BUS19 and BUS20 are defined to be the HV buses. Respectively to the loads, additional buses are introduced. Buses BUS23 and BUS25 denote the LV buses, whereas BUS24 and BUS26 denote the LOAD buses. It makes total of 26 buses in this case. Initial load flow computation is carried out in such a way that voltage and power conditions at buses BUS19 and BUS20 do not differ from the ones in the previous scenario. The voltages at BUS19 and BUS20 have very similar values of magnitudes and angles in both cases. The power flows from BUS19 and BUS20 down to the loads have also very similar values to the ones that belong to the dynamic loads in the previous scenario.

Parameters of the individual elements of the composite load model are provided in Appendices. The LTC transformers control bus voltage magnitudes at the LV buses as they are computed within initial load flow procedure. Ratings of the shunt capacitors are defined with respect to the voltage conditions set for the HV buses BUS19 and BUS20 in the previous scenario. Equivalent impedances of distribution feeders are set at values that do not cause voltage magnitude drops larger than 3% for initial load consumption.

At the LOAD buses, the induction motor load, thermostatically controlled load and static load are connected. Parameters of the induction motor loads belong to prone to stall portion of weighted aggregate of residential and industrial motors. Consumed active/reactive power portions of the motors with respect to the total power flowing to the LOAD buses are equal to 20.3/37.7% (BUS24) and 22.2/39.2% (BUS26). Parameters of the thermostatically controlled loads are chosen to initiate recovery of initially consumed power in the time span which is approximately similar to the previous scenario (around 600 s). In reality their values may be even larger, but in this scenario they serve for illustrative purposes rather than for identification ones. Portions of their active power consume amount to 49.3% (BUS24) and 47.3% (BUS26). Parameters of the static loads describe active power load as constant current and reactive one as constant impedance. Portions of their active/reactive power consumes are equal to 30.4/62.3% (BUS24) and 30.5/60.8% (BUS26). In general, the loads at the LOAD buses are defined having the TCL active power consumes approximately equal to half of the total load at the bus. The other two loads (IM and SL) share the rest in approximately equal amounts.

The disturbance, which triggers the period of evolving voltage instability, is the same as in the previous scenario. The three-phase short circuit occurs on the line L17 closely to the bus BUS15 at time instant t=10 s, and is cleared after 220 ms by line L17 outage (Fig. II.1). The voltage stability problem is again dominated by load recovery and insufficient generator voltage control capability. In this scenario, the recovery of the load consumption happens due to the LTCs action and the TCLs control in a longer term, whereas in a short term due to the IM dynamics. The generators are still equipped with over-excitation limiters.

Time domain responses of the voltage magnitudes at buses which belong to the composite load model clearly indicate that the system undergoes a voltage collapse at t=589 s (Figs. VIII.49-50). Voltage collapse appears in the oscillating form.

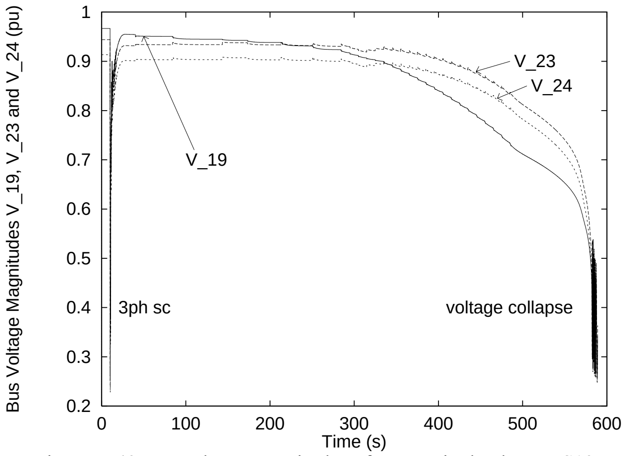

Fig. VIII.49 Bus voltage magnitudes of composite load at BUS19

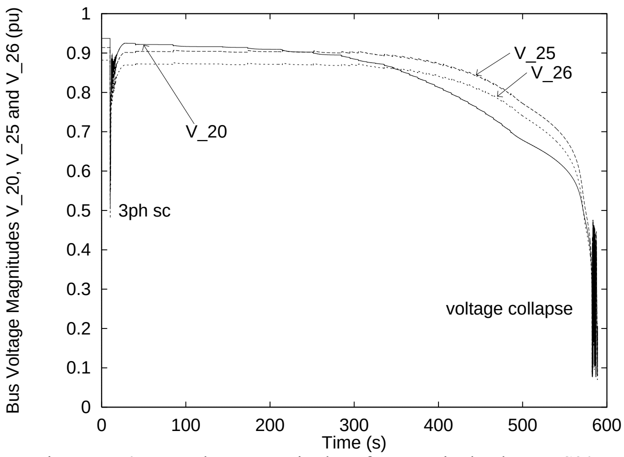

Fig. VIII.50 Bus voltage magnitudes of composite load at BUS20

Bus voltage magnitudes at the HV buses (V_{19} and V_{20}, respectively) have faster rate of the magnitude decrease due to the LTCs action. The LTCs try to keep bus voltage magnitudes at the LV buses (V_{23} and V_{25}, respectively) within pre-specified thresholds at the expense of decrease in bus voltage magnitudes at the HV buses. Bus voltage magnitudes at the LOAD buses (V_{24} and V_{26}, respectively) follow the values of the LV buses with a difference that appears due to the equivalent distribution impedances.

Voltage instability is influenced by a lack of generator reactive power production. Generators GEN5 and GEN6 (and at the very end GEN4) in the area with two composite loads lose voltage control capability due to the action of the OELs at t=84 s and 85 s, respectively (Fig. VIII.51). Upon activation of the OELs, reactive power demands on the generators exceed their field current limits (Fig. VIII.52). Having generators GEN5 and GEN6 limited by the OELs, generator GEN4 takes the role of the reactive power supplier until the very end. After certain time period, the OELs can not stand for demands and the voltages collapse.

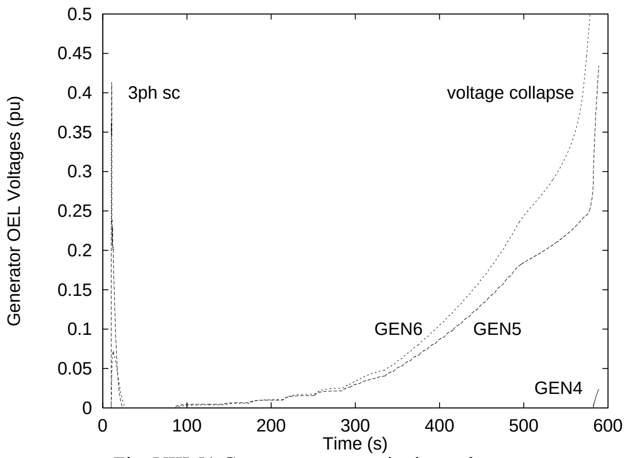

Fig. VIII.51 Generator over-excitation voltages

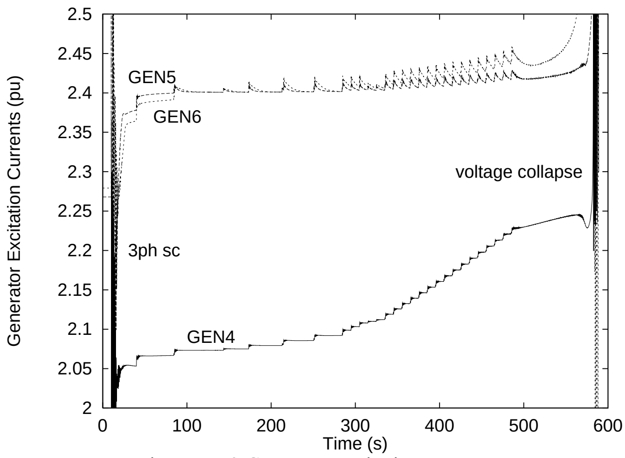

Fig. VIII.52 Generator excitation currents

With each LTC tap change, the burden on the OELs becomes increased. Tap changing starts at t=40 s, after approximately 30 s of initial time span has elapsed (Fig. VIII.53). The initial tap changes happen when the LTC voltage errors become increased above 0.01 pu for pre-defined initial time spans (Fig. VIII.54). Until nearly 300 s, the LTCs succeed to keep the errors within pre-specified threshold. Each time when the error comes within the threshold, the LTC scheme is reset making the initial time span active again. As the error stays out of the threshold, subsequent tap changing appears, but now with smaller time span (10 s). Due to having two different time spans, two periods of the LTCs action are clearly distinguished. The first one is slower, and the second one is faster. The slower period is influenced by longer time span, whereas the faster one by shorter time span. Transfer from one to another appears slightly before t=300 s. The changes of the LTC tap ratio are stopped at approximately t=485 s, when the imposed ±15% regulation limits are reached.

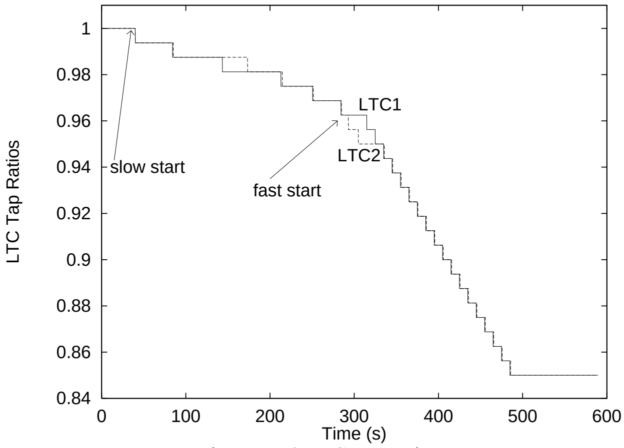

Fig. VIII.53 LTCs tap ratio

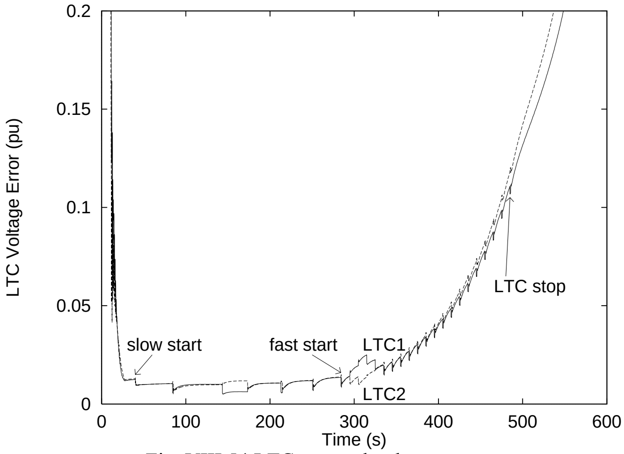

Fig. VIII.54 LTCs control voltage error

Time domain responses of the LTCs active and reactive power flow from the HV bus to the LV bus denote the role of the tap changing mechanism in recovery of initial load consumption. These responses are related to the ones that belong to the dynamic loads with non-linear recovery from the previous scenario (Figs. VIII.4a-d).

Responses of the active power flow show recovery intention followed by fast decrease in load consumption due to collapse mechanism (Fig. VIII.55). Responses of the reactive power flow also exhibit recovery intention (Fig. VIII.56), but in the final part they differ significantly from the responses of the dynamic load model with non-linear recovery. Instead of decrease of reactive load consumption in the final part, the reactive power of the composite load model is first increased and then abruptly decreased followed by oscillations. Overall level of the system dynamics becomes highly pronounced.

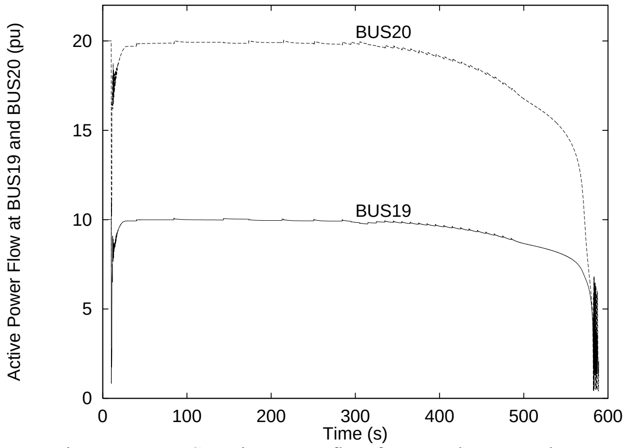

Fig. VIII.55 LTCs active power flow from HV bus to LV bus

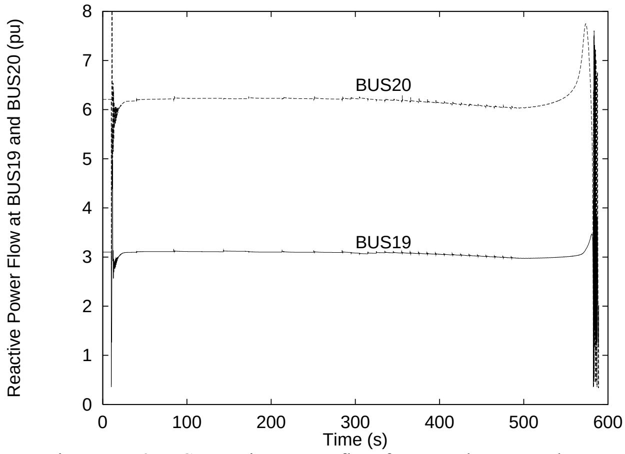

Fig. VIII.56 LTCs reactive power flow from HV bus to LV bus

By decomposing the LTCs power flow, the impact of each individual element of the composite load is recognised. The impacts are mostly concerned with consumed power.

The shunt capacitors, SHUNT1 and SHUNT2, are connected at the LV buses to supply reactive power locally. Index 1 denotes the composite load model at BUS19, whereas index 2 at BUS20. Same notation is used for the other individual elements. Responses of the shunt capacitors reactive power clearly depict its quadratic dependence with respect to bus voltage magnitude. Due to constant value of shunt capacitor susceptance, the reactive power is quadratically decreased when it is most needed.

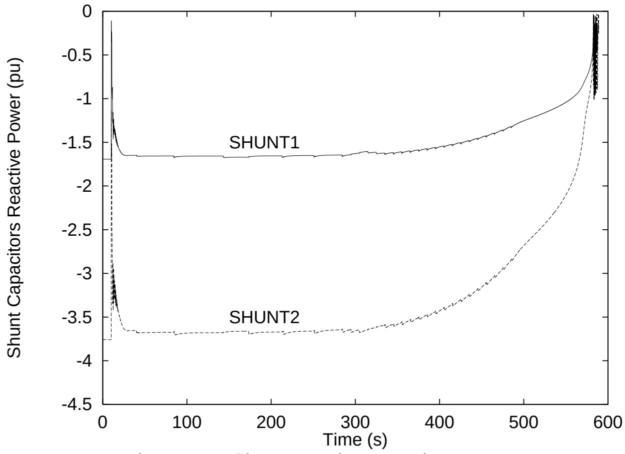

Fig. VIII.57 Shunt capacitors reactive power

Static loads exhibit similar characteristics concerning their dependence on bus voltage magnitudes. As the magnitudes are decreased, active and reactive power of the static loads are decreased as well (Figs. VIII.58-59). Due to constant current type of active power load, it is decreased at somewhat slower pace than the reactive power which has constant impedance type (linear vs. quadratic). In general, constant impedance type of a load has a relieving impact to evolving voltage stability problem. Constant current type imposes more stringent conditions, whereas constant power type has the most stringent ones.

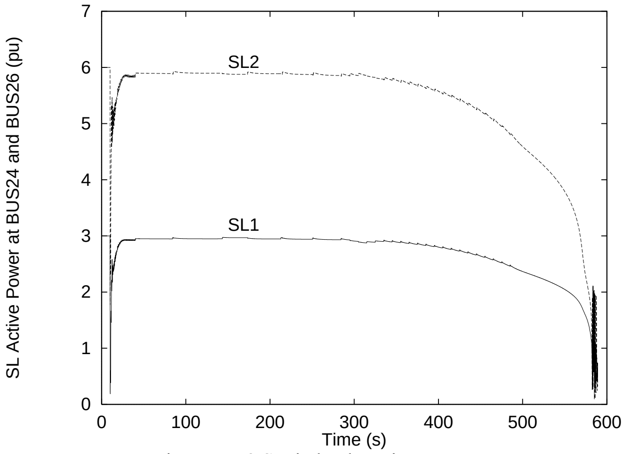

Fig. VIII.58 Static loads active power

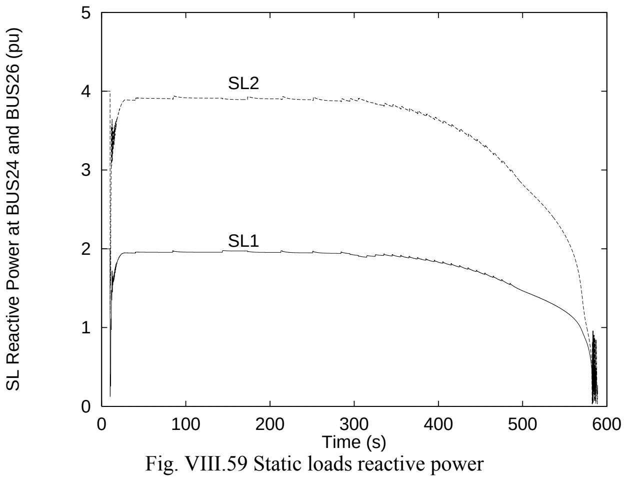

Fig. VIII.59 Static loads reactive power

Responses of characteristic variables belonging to thermostatically controlled loads reveal recovery mechanism of purely resistive heating load.

As the bus voltage magnitudes are decreased due to initial sequence of disturbances, the TCL conductances are first slightly increased. Then, as the magnitudes are further decreased, the conductances become significantly increased (Fig. VIII.60). Being linearly proportional to the conductances and quadratically to the voltage magnitudes, the TCL active power consumptions exhibit recovery characteristics (Fig. VIII.61).

These changes of the TCL conductances are consequences of the TCL control schemes. The control schemes are designated to keep the temperature of the heated area, τ_H, at the pre-specified referent value τ_{REF}. Responses of the temperatures τ_H reveal internal cause of recovery mechanism (Fig. VIII.62). Initial drop of the voltage magnitudes first causes decrease of the temperatures τ_H. Then, by feed-back control, the temperatures τ_H are increased towards the referent ones. Physical background is provided through a fact that the TCLs stay connected to the network within longer periods. After certain time elapsed, the generators in the system become incapable of requested reactive power delivery. The voltage magnitudes are further decreased. The TCL control schemes try to keep the temperatures τ_H at their referent values, but unsuccessfully. The voltages suffer even larger decrease and they finally collapse accompanied with the temperatures.

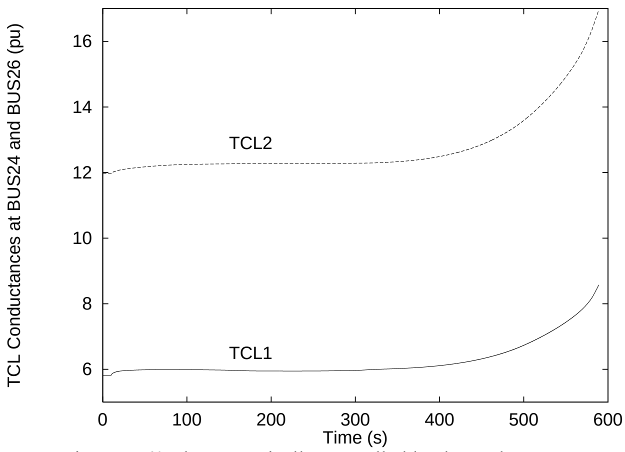

Fig. VIII.60 Thermostatically controlled loads conductance

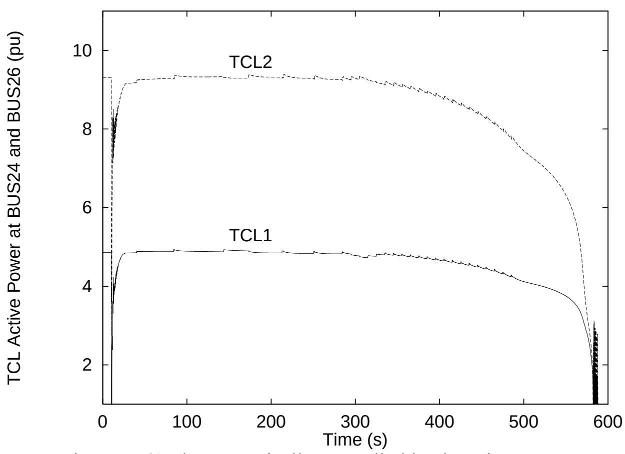

Fig. VIII.61 Thermostatically controlled loads active power

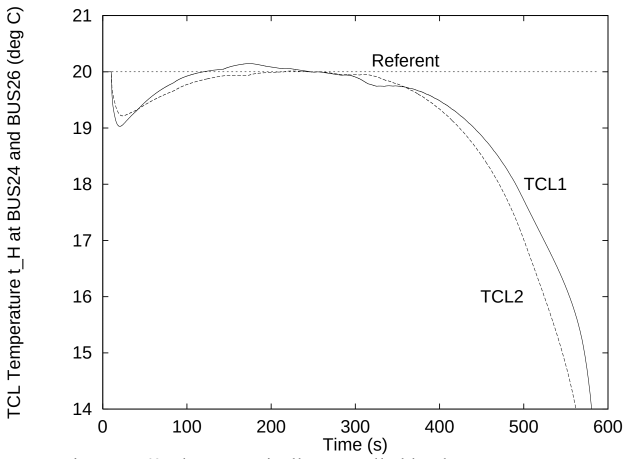

Fig. VIII.62 Thermostatically controlled loads temperatures

Time domain responses of characteristic variables belonging to the induction motors reveal behaviour of the total reactive power in the final part prior to the collapse.

Responses of the induction motors active power show that with chosen parameters they have fairly constant consumption closely up to the collapse (Fig. VIII.63). As the collapse is approached the active power is abruptly decreased and it starts oscillating. Responses of the reactive power exhibit characteristics similar to the ones noted for the LTCs reactive power flow (Fig. VIII.64). As the collapse becomes closer, the reactive power is first increased and then abruptly decreased with induced oscillations. Such responses of the reactive power are caused by the induction motors current drawn from the system (Fig. VIII.65). As the voltage magnitude is decreased, the current is increased to provide enough active power and therefore balance motor mechanical load power. Responses of the speed of the induction motors show its close couplings to the motor active power (Fig. VIII.66). Until the collapse, the motors succeed to keep rotor speed at stable values. As the voltages collapse, the speed is decreased toward lower levels and they finally stall. Stable operating point in a well-known motor speed-torque characteristic domain, (ω_m, T_e), is lost and the oscillations are induced (Fig. VIII.67). Stability of an operating point is lost following motor critical point being passed. Motor critical point is determined by maximum electromagnetic torque that could be developed. Its value is decreased as the voltages are decreased.

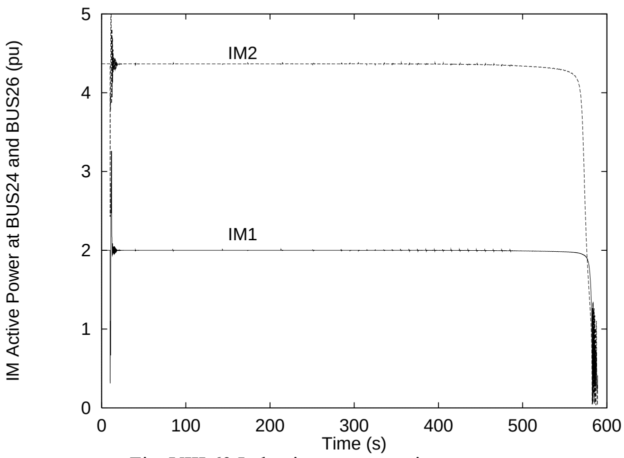

Fig. VIII.63 Induction motors active power

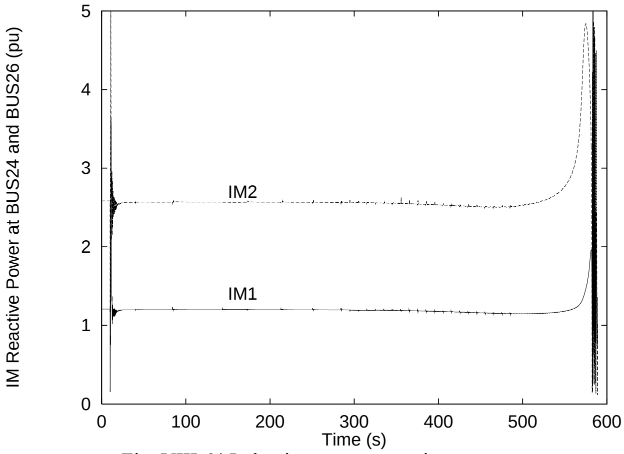

Fig. VIII.64 Induction motors reactive power

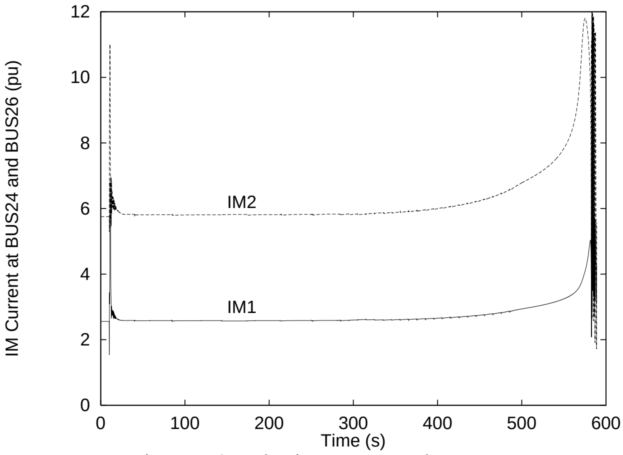

Fig. VIII.65 Induction motors total current

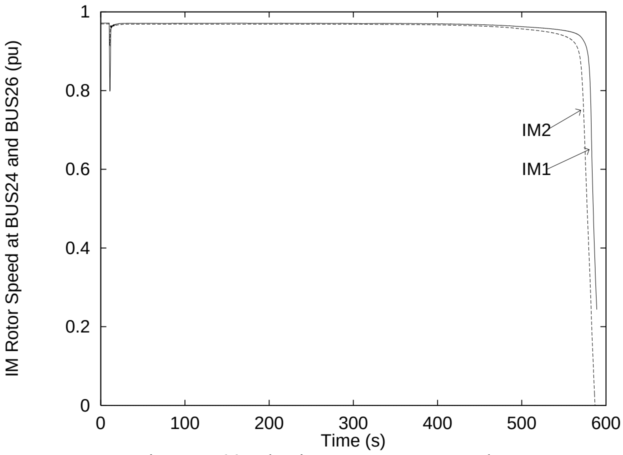

Fig. VIII.66 Induction motors rotor speed

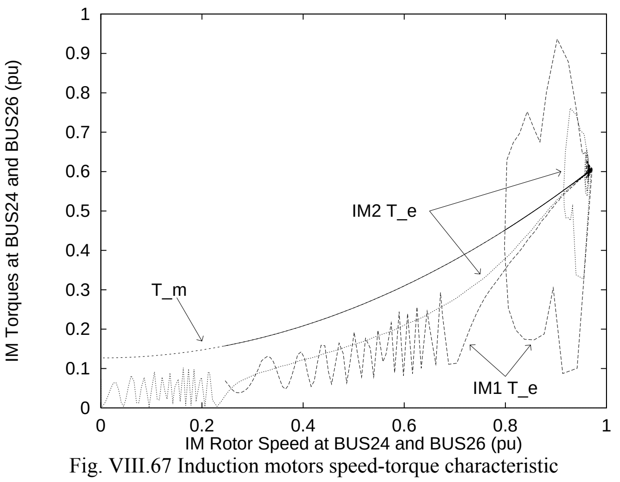

Fig. VIII.67 Induction motors speed-torque characteristic

Analysed impacts of the individual elements within the composite load model denote a need for careful modelling of reactive power recovery process. It is especially pronounced in the final part of voltage stability problem due to the induction motor behaviour.

VIII.2.B Recognition of critical load parameters

Previously, static aspects given by matrix decompositions are used to identify most critical location in the system. Later on, the UPFC is installed at detected location to provide maximum support in the voltage stability problem.

Besides using static aspects for determination of the UPFC location, in this scenario they are used for detection of critical load parameters as well. During time domain simulations, the linearised differential-algebraic model is calculated in steps equal to 1 s. By recognising critical events along system trajectory during voltage collapse scenario, characteristic time snap-shots are identified. Before and after each of them, the participation factors are evaluated. The time snap-shots are given in Table VIII.2. They concern initial period of steady state operation, start of the LTCs slow tap changing, generators GEN5 and GEN6 OEL activation, start of the LTCs fast tap changing, halt of the LTCs tap changing, and final period of impending voltage collapse which involves motor dynamics.

Table VIII.2 Time snap-shots during voltage collapse scenario

No.	time (s)	description
1	5	steady state
2	35	before 1st LTC tap changes
3	80	before GEN5 & GEN6 OEL action
4	90	after GEN5 & GEN6 OEL action
5	130	slow LTCs and both OEL actions
6	170	↓
7	210	↓
8	250	↓
9	275	↓
10	285	fast LTCs and both OEL actions
11	295	↓
12	300	↓
13	310	↓
14	320	↓
15	350	↓
16	390	↓
17	440	↓
18	480	↓
19	500	no LTCs and both OEL actions
20	530	↓
21	560	no LTCs, both OELs, motor instability starts

The singular value decomposition of the state matrix A_S is carried out. The matrix decomposition results with the right, v_n, and left, u_n, singular vectors associated to the minimum singular value, σ_n. Results are obtained for characteristic snap-shots. They belong to the generator and load state variables.

Components of the right singular vector, v_n, related to the state matrix A_S, indicate sensitive state variables (Fig. VIII.68). Components of the left singular vector, u_n, indicate sensitive direction for changes of state variable derivatives (Fig. VIII.69). Multiplied components of the singular vectors, v_n x u_n, combine their corresponding characteristics into overall participation (Fig. VIII.70). Components are given for the snap-shots, which come behind the 4th one. These snap-shots have the same, maximum, number of the state variables, which enables easier comparison. Maximum number of state variables is equal to 65 (1-55 for generators, 56-61 for induction motors, and 62-65 for thermostatically controlled loads). Components of the right singular vector that belong solely to the load state variables (induction motors and TCLs) are given separately for a better overview (Fig. VIII.71).

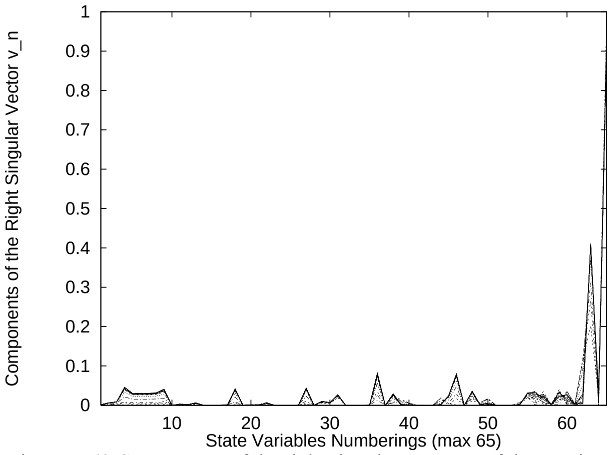

Fig. VIII.68 Components of the right singular vector v_n of the matrix A_S

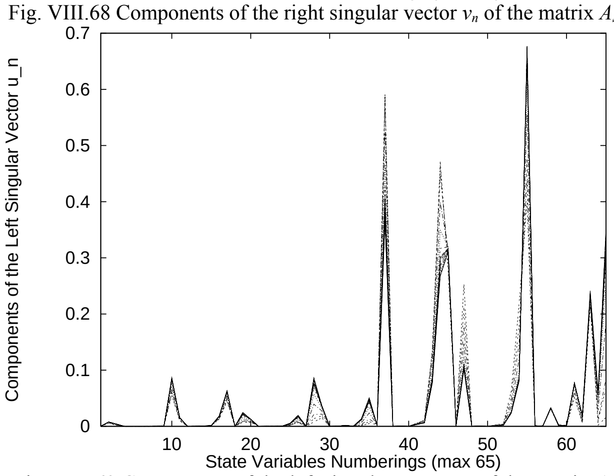

Fig. VIII.69 Components of the left singular vector u_n of the matrix A_S

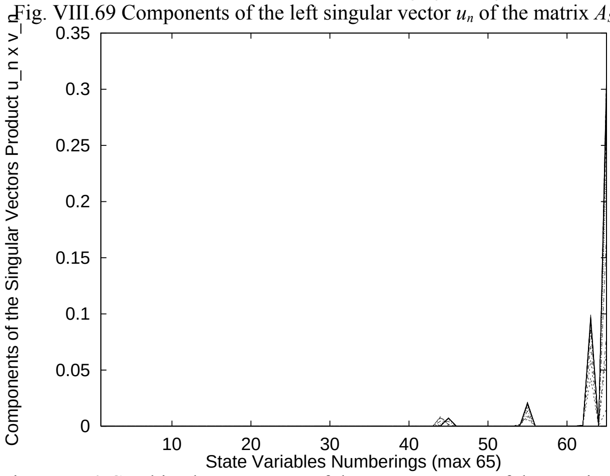

Fig. VIII.70 Combined components of the vectors v_n x u_n of the matrix A_S

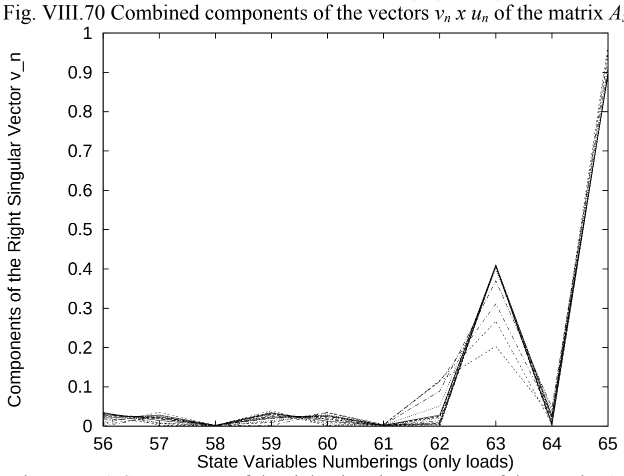

Fig. VIII.71 Components of the right singular vector v_n of the matrix A_S
- load state variables -

As the most sensitive state variables, the ones that belong to the TCLs are recognised. Especially, the TCL conductances are detected to have the largest participation among them. State variables of the induction motors have lower participation. The most sensitive directions, in addition to these of the TCL state variables, are also orientated toward the ones that belong to the generators GEN5, GEN6, and GEN4. Combined components also point out the TCL state variables as most influential in addition to the GEN6 and GEN5 OEL state variables. The same area is recognised to have the largest participation of the state variables during this voltage collapse scenario. The area is characterised as being in close proximity to the generators GEN5, GEN6 and GEN4, and around the composite loads.

Instead of using participation factors of corresponding state variables, highly participating generators are detected by using their reactive power production as well. At the snap-shots, the reactive power production of the generators is evaluated (Fig. VIII.72). It is seen that as generators GEN5 and GEN6 become constrained through the OELs action, generator GEN4 increases its reactive power production. Its engagement is again the largest among the other generators in the system during this scenario. As it is given in the previous scenario, the differential change of generator reactive power with respect to the minimum singularsubspace is computed for each of the generators in the system (Fig. VIII.73). Again, as generators GEN5 and GEN6 become constrained due to the OELs action, generator GEN4 exhibits increased sensitivity.

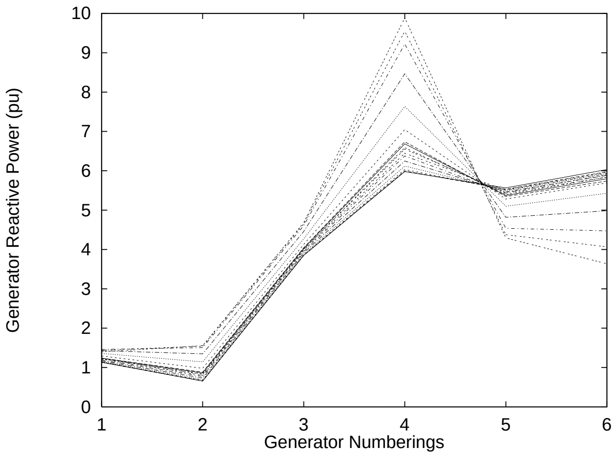

Fig. VIII.72 Generator reactive power production at snap-shots

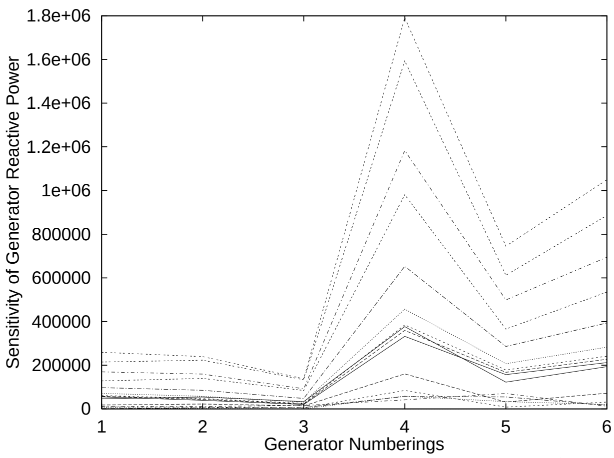

Fig. VIII.73 Sensitivity of generator reactive power at snap-shots

Since the location of the UPFC is retained from the previous scenario, given conclusions are reviewed within following analysis of bus and branch participation factors.

Bus participation factors are evaluated through the singular value decomposition of the extended Jacobi matrix J_{EXT}. This decomposition again results with the singular vectors associated to the minimum singular value. Components of the right singular vector, v_n, related to the sub-matrix g_{y1} of the matrix J_{EXT}, indicate sensitive bus voltage angles and magnitudes (Fig. VIII.74). Components of the left singular vector, u_n, indicate sensitive direction for changes of active and reactive power (Fig. VIII.75). Multiplied components of the singular vectors, $v_n x u_n$, combine their corresponding characteristics into overall bus participation (Fig. VIII.76).

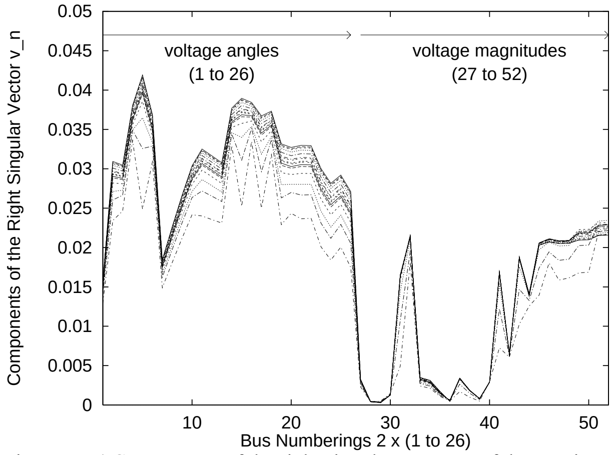

Fig. VIII.74 Components of the right singular vector v_n of the matrix J_{EXT}

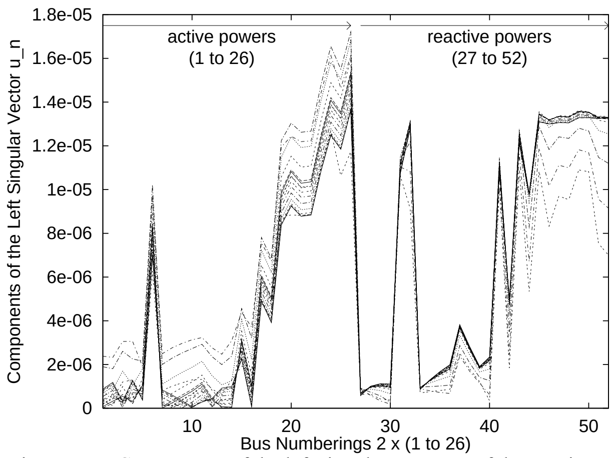

Fig. VIII.75 Components of the left singular vector u_n of the matrix J_{EXT}

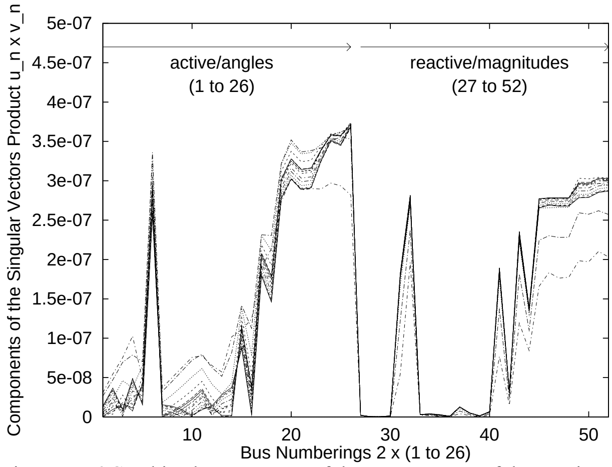

Fig. VIII.76 Combined components of the vectors $v_n x u_n$ of the matrix J_{EXT}

Total number of network buses is now 26, which makes 52 algebraic variables in the sub-matrix g_{y1}. These algebraic variables correspond to the bus voltage angles and magnitudes. In comparison with the previous case, additional 4 buses are included in the system. They belong to the composite loads connected at BUS19 and BUS20. Buses BUS21 and BUS22 belong to the UPFC ones, whereas the new ones are numerically placed behind them.

Computed components of the singular vectors again reveal the same system area with evolving voltage stability problem. The right-hand side of the system, between buses BUS15 and BUS26 including generating buses GEN5 and GEN6, has the largest participation during this voltage collapse scenario. The left-hand side does not exhibit voltage magnitude related problems. The largest bus participation appears in the area where the composite loads exhibit recovery intention. Their behaviour lead to OELs action of nearby generators GEN5 and GEN6. Combined components clearly point out buses in this area as most influential. Buses BUS16 and BUS18 have lower participation in the right-hand side of the system due to their further (upper) location in the branch. Buses BUS15 and BUS17 are located nearer to the composite loads and participate with larger intensity. Generating buses GEN5 and GEN6 join them upon the OELs action. Buses located between BUS19 and BUS26 exhibit the largest participation. They belong to the voltage troubled area with the composite loads being connected to it.

Branch participation factors are computed here to revise transmission network elements (lines and transformers) that have the largest participation in active/reactive power loss.

As in the previous case, the total power loss is distributed over network branches (Figs. VIII.77-78). In addition to the lines L18-L25, there are also two equivalent impedances of the composite loads which have large shares of active power loss. They are placed at 28^{th} and 29^{th} positions. Lines L26-L27 (originally just L26), are rather short and again lightly loaded. Thereby, they have lower active power loss, but they still belong to the same power flow corridor at the right-hand side of the system. Lines L20 and L21 have large shares due to their single-line performance. From a viewpoint of reactive power, there are lines L13-L16, which take significant shares of the loss. Line L12 accompanies them.

Branch participation factors are given as differential changes of branch power losses with respect to the minimum singularsubspace of interest. They are regarded as sensitivities indicating lines where the most active/reactive power is consumed in response to an incremental change in active/reactive load (Figs. VIII.79-80). The equivalent impedances of the composite loads are recognised as the most sensitive from a viewpoint of active power. In addition to the right-hand side of the system (L18-L25), there is an area around generator GEN1, which is indicated to be sensitive as well. Interconnection lines between two of the sides, L13-L16, have also increased sensitivities. Line L12 accompanies them due to nearby generator GEN1, whose step-up transformer has the largest

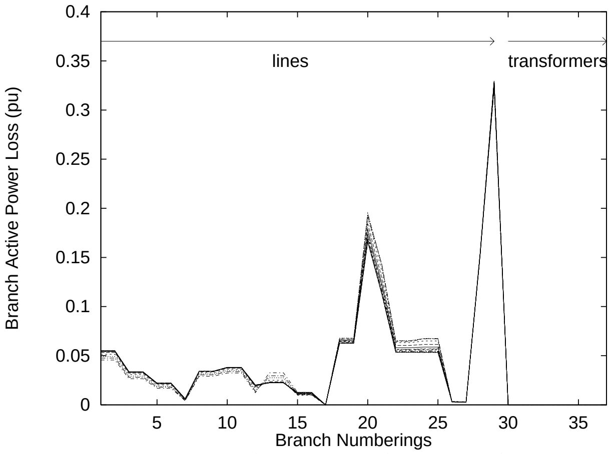

Fig. VIII.77 Branch active power loss at snap-shots

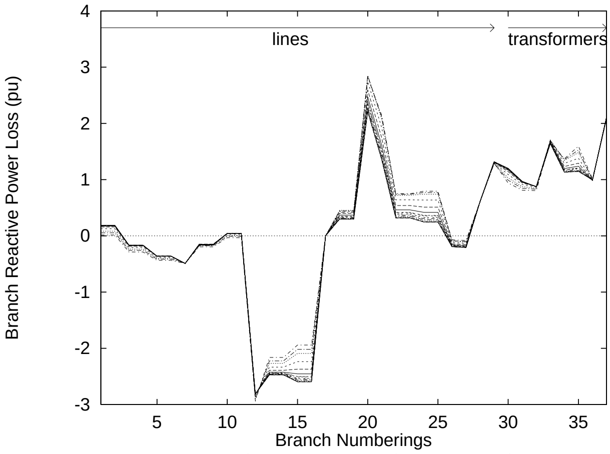

Fig. VIII.78 Branch reactive power loss at snap-shots

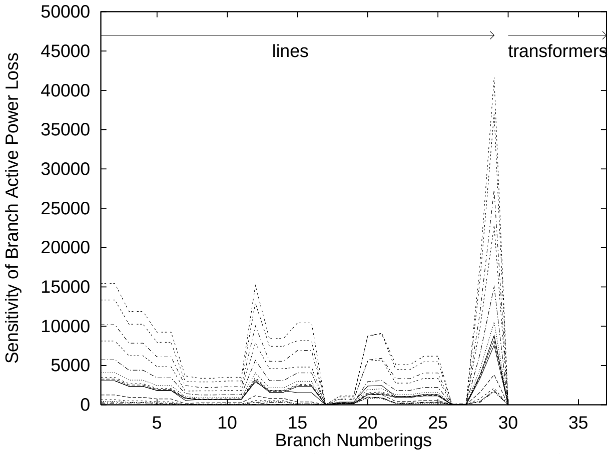

Fig. VIII.79 Sensitivity of branch active power loss at snap-shots

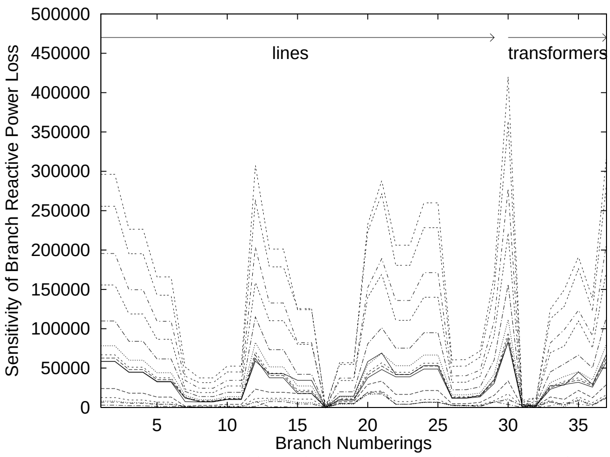

Fig. VIII.80 Sensitivity of branch reactive power loss at snap-shots sensitivity from a viewpoint of reactive power. LTC transformers have also increased sensitivity of branch reactive power loss.

The right-hand side of the system still has rather large branch participation factors (lines L18-L25). The UPFC does not need heavily loaded line for efficient power flow regulation. The lines L26-L27 make a part of the same corridor. The equivalent impedances are nearly situated. Even from the aspect of branch participation factors, the UPFC could be retained at the same location as in the previous scenario. Eventually, its location at a distribution level could be considered. Motivation is found in a need for compensation of the equivalent impedance effects.

The participation factors again point out to the area around buses BUS19 and BUS20 where the composite loads are connected. Thus, the UPFC is retained there. Besides determination of critical load parameters and their location in the system, it is necessary to detect a critical point during this voltage collapse scenario. Upon its detection, voltage support from the UPFC is initiated.

VIII.2.C Critical point recognition

In order to detect a critical point, the static aspects given by matrix decompositions are used in a way that is similar to the previous scenario. During dynamic time-domain simulations, the extended Jacobi matrix, J_{EXT}, and the state matrix, A_S, are evaluated utilising linearised differential-algebraic model. Singular and eigenvalue decompositions are carried out resulting with critical singular and eigenvalues. Sensitivity analysis of the matrices is deployed resulting with parametric and functional sensitivities. Parametric sensitivity of bus voltage magnitude and load state variable is evaluated with respect to characteristic load parameter. Functional sensitivity of total reactive power production of generators is computed with respect to initial load consumption. The sensitivities enable recognition of critical events and critical point during time domain simulation period.

Singular value decomposition results with minimum singular value, which is treated as the critical one. Response of the minimum singular value of the state matrix A_S successfully denotes critical events and critical point (Fig. VIII.81). Minimum singular value is always positive. As the LTCs start tap changing, the minimum singular value first becomes slightly decreased. As soon as generators GEN5 and GEN6 become limited by the OELs action, the system is largely stressed, which is reflected by sharp drop of the minimum singular value. Continued tap changing of the LTCs in combination with the TCLs recovery further decrease the minimum singular value. It hits zero value at t=298 s denoting singularity point. Afterwards, the minimum singular value is increased, but from now on within unstable region. Recovery intentions further lead the system to voltage instability. Shortly before the voltage collapse, the induction motors lose stable operating points and oscillations start. The minimum singular value again exhibit sharp drop.

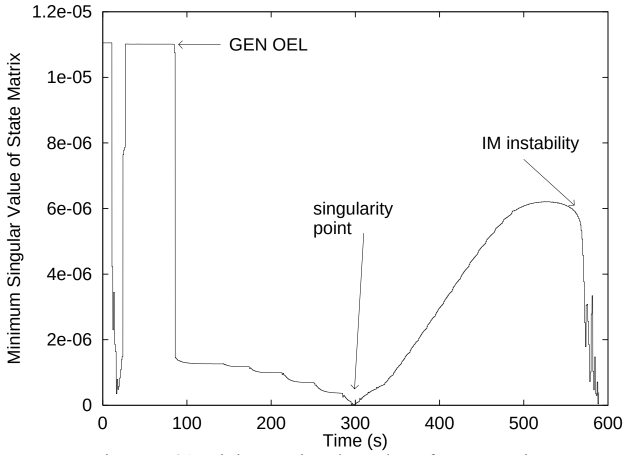

Fig. VIII.81 Minimum singular value of state matrix

In the previous scenario, the critical point appears due to discontinuity, which is induced by the OEL action of generator GEN6 (Fig. VIII.11). In this scenario, the appearance of the critical point is clearly visible due to continuous trajectory. Generators GEN5 and GEN6 are earlier limited by the OELs action. At the critical point, the minimum singular value hits zero being ascended afterwards. The appearance of the critical point corresponds to the change of pace of the LTCs tap changing and to the knee-point of the TCLs temperature τ_H. Around the critical point, the LTCs start tap changing at faster pace (Fig. VIII.53), whereas the TCLs temperatures start decreasing upon reaching maximum (Fig. VIII.62).

Eigenvalue decomposition of the state matrix A_S results with the critical eigenvalue with maximum real part (Fig. VIII.82). Critical events and critical point are detected at the same time instants as within singular value decomposition. The real part of the critical eigenvalue is transferred from negative to positive half-plane at t=298 s when the minimum singular value hits zero. The plane crossing point appears in the continuous part of the trajectory after short-circuit oscillations are vanished and generators GEN5 and GEN6 are limited by the OELs action. Upon the plane crossing point, the real part of the critical eigenvalue is further increased. It finishes in oscillations after the induction motors lose stable operating points. Thereby, the critical point is again recognised as well as the other events that are associated to.

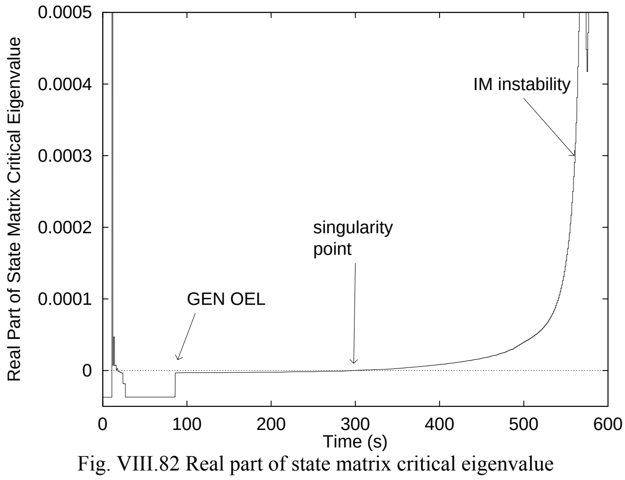

Fig. VIII.82 Real part of state matrix critical eigenvalue

Besides singular and eigenvalue decompositions, the sensitivity analysis is also very helpful in detection of the same critical events and critical point. Parametric and functional sensitivity analysis is used hereafter.

Parametric sensitivity, $\partial x/\partial p$ or $\partial y/\partial p$, is defined as a sensitivity of a state variable or an algebraic variable with respect to an arbitrary parameter. As state variables x, the TCL conductance G and the IM rotor speed ω_m are chosen to provide illustrative examples. As algebraic variable y, the bus voltage magnitude V is used. For arbitrary parameters, the TCL referent temperature τ_{REF} and the IM initial mechanical load torque T_{m0} are chosen. In general, the parametric sensitivity is computed for each individual element of the composite loads, but illustrated just for the mentioned ones.

For the TCL loads, parametric sensitivities $\partial G/\partial \tau_{REF}$ and $\partial V/\partial \tau_{REF}$ are evaluated. Responses of the parametric sensitivity of the state variable with respect to the characteristic load parameter, $\partial G/\partial \tau_{REF}$, clearly depict critical events and critical point (Fig. VIII.83). Generally, around a stable operating point the increase of the temperature τ_{REF} is achieved by the increase of the conductance G, and vice versa. That is the reason for the parametric sensitivity $\partial G/\partial \tau_{REF}$ being positive in the initial steady state. The OELs action induces discontinuity and sharply increases its value. Restorative intentions of the TCLs and LTCs cause further increase. The sensitivity involves the inverse of the state matrix. As the singularity point is approached, the sensitivity becomes very large. At the singularity point, it abruptly changes the sign becoming negative. The singularity point is treated as the critical one. Afterwards, further restorative intentions lead the system toward the voltage collapse. The sensitivity approaches zero value within unstable region. As the induction motors lose stable operating points, the oscillations are induced.

Responses of the parametric sensitivity of the algebraic variable with respect to the characteristic load parameter, $\partial V/\partial \tau_{REF}$, also detect the same critical events and critical point (Fig. VIII.84). Around a stable operating point, the increase of the temperature τ_{REF} is achieved by the increase of the conductance G, which causes increased active power load consumption and therefore bus voltage magnitude drops. The opposite is valid if the temperature is to be decreased. Thus, the parametric sensitivity $\partial V/\partial \tau_{REF}$ is negative in the initial steady state. As the singularity point is approached, the sensitivity becomes largely negative. At the singularity point, it changes the sign and becomes positive. Afterwards, it approaches zero value within unstable region ending with the IM instability.

For the IM loads, parametric sensitivities $\partial \omega_m /\partial T_{m0}$ and $\partial V/\partial T_{m0}$ are evaluated. Responses of the parametric sensitivity of the state variable with respect to the characteristic load parameter, $\partial \omega_m /\partial T_{m0}$, detect the same critical events and critical point (Fig. VIII.85). Within responses of the parametric sensitivity of the algebraic variable with respect to the characteristic load parameter, $\partial V/\partial T_{m0}$, the same is found (Fig. VIII.86).

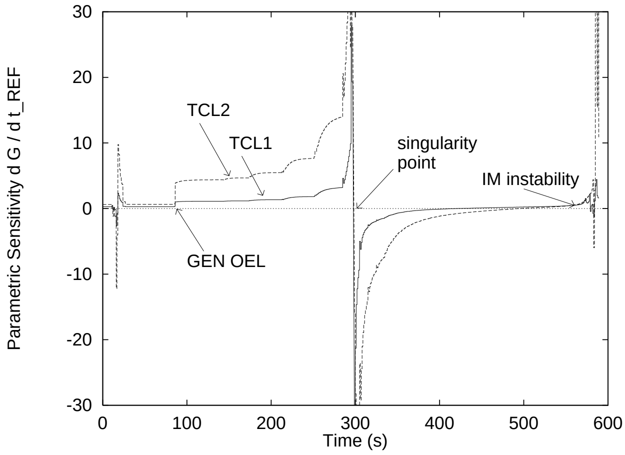

Fig. VIII.83 Parametric sensitivity of TCL loads, $\partial G/\partial \tau_{REF}$

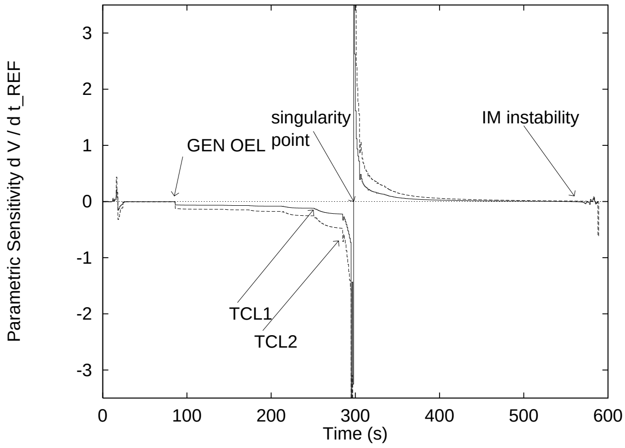

Fig. VIII.84 Parametric sensitivity of TCL loads, $\partial V/\partial \tau_{REF}$

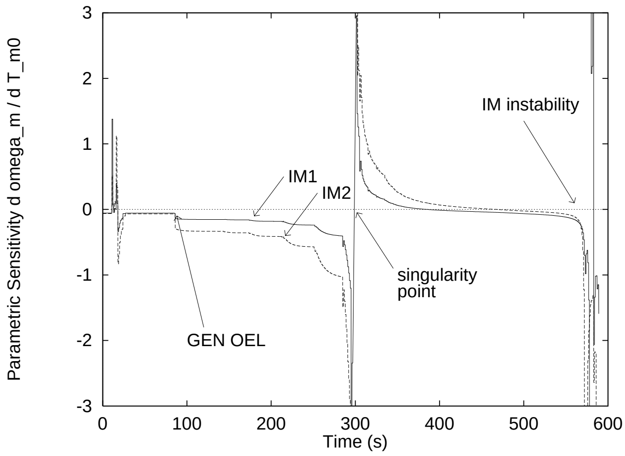

Fig. VIII.85 Parametric sensitivity of IM loads, $\partial \omega_m /\partial T_{m0}$

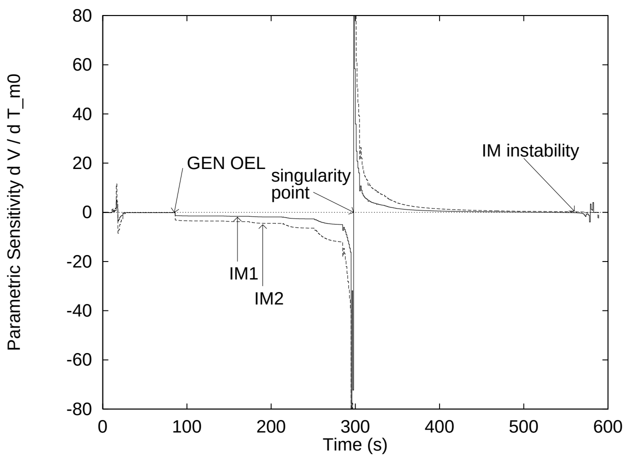

Fig. VIII.86 Parametric sensitivity of IM loads, $\partial V/\partial T_{m0}$

Generally, around a stable operating point the increase of the mechanical torque T_{m0} causes the decrease of the rotor speed ω_m. Due to increased load, the induction motor draws larger current from the network, which causes bus voltage magnitude drop. That is the reason for both of the parametric sensitivities, $\partial\omega_m / \partial T_{m0}$ and $\partial V/\partial T_{m0}$, being negative in the initial steady state. As the singularity point is approached, both sensitivities become largely negative. Having the singularity point passed, they change the sign and become positive. By further load restoration, they approach zero value within unstable region ending with oscillating instability.

Parametric sensitivity $\partial y/\partial p$ is evaluated not only for the loads, but for the LTC transformers as well. The same critical events and critical point are detected within responses of the parametric sensitivity of the LTC bus voltage magnitudes with respect to the tap ratio, $\partial V/\partial t_r$ (Fig. VIII.87). Generally, around a stable operating point the decrease of the tap ratio t_r causes the increase of the LV bus voltage magnitude, and vice versa. That is the reason for the parametric sensitivity $\partial V/\partial t_r$ being negative for the LV buses in the initial steady state. The sensitivity of the HV bus voltage magnitude is significantly smaller and close to zero during that period. It has even opposite sign due to the fact that the increase of the LV bus voltage magnitude is achieved at the expense of the decrease of the HV bus voltage magnitude. As the OELs action induces discontinuity, the sensitivities of both magnitudes (HV and LV) sharply become increased at positive values. After that, the decrease of the tap ratio does not increase the LV bus voltage magnitude. Both magnitudes are decreased due to restorative intentions. As the singularity point is approached, the sensitivity becomes very large. At the singularity point, it abruptly changes the sign becoming negative. Afterwards, by further restorative intentions the sensitivities approach zero value within unstable region. The induction motors lose stable operating points and oscillations appear.

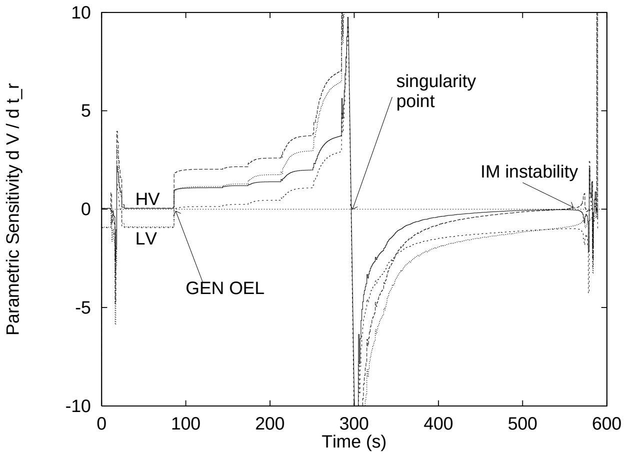

Fig. VIII.87 Parametric sensitivity of LTC transformers, $\partial V/\partial t_r$

Besides parametric sensitivities of state and algebraic variables, the sensitivity analysis is defined as functional one as well. As in the previous scenario, the functional sensitivity $\partial\eta/\partial p$ is defined as a sensitivity of a function with respect to an arbitrary parameter. As a function, the total reactive power production of the generators is used, while for an arbitrary parameter, the initial value of the SL reactive power load is chosen. The functional sensitivity is computed with respect to each of the static loads at the LOAD buses (BUS24 and BUS26) given as $\partial Q_G^{\Sigma}/\partial(Q_{L24}^{0})_{SL}$ and $\partial Q_G^{\Sigma}/\partial(Q_{L26}^{0})_{SL}$.

Generator excitation currents dominantly determine the response of the total reactive power production of the generators in the system Q_G^{Σ} (Fig. VIII.88). After the initial disturbances, the total reactive power Q_G^{Σ} is first sharply increased. Then, the LTCs and TCLs restorative intentions gradually increase the power Q_G^{Σ}. As the LTCs start faster tap changing, the power Q_G^{Σ} also experiences faster increase. As the LTCs are halted, the power Q_G^{Σ} is decreased finishing in oscillations.

In responses of the functional sensitivities (Fig. VIII.89), the critical point is detected again. The change of the sign is clearly visible. Before the occurrence of the critical point, the functional sensitivities have positive values. As the load consumption is increased, the total reactive power production is increased as well resulting with a stable operating point (in general). Afterwards, the functional sensitivities become negative, closely approaching zero within unstable region. Having critical point passed, the actual load consumption starts to be decreased, while the total reactive power production Q_G^{Σ} is still kept increased.

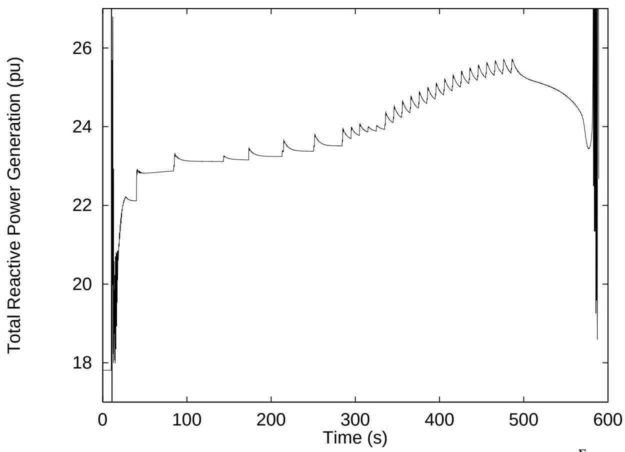

Fig. VIII.88 Total reactive power production of generators Q_G^{Σ}

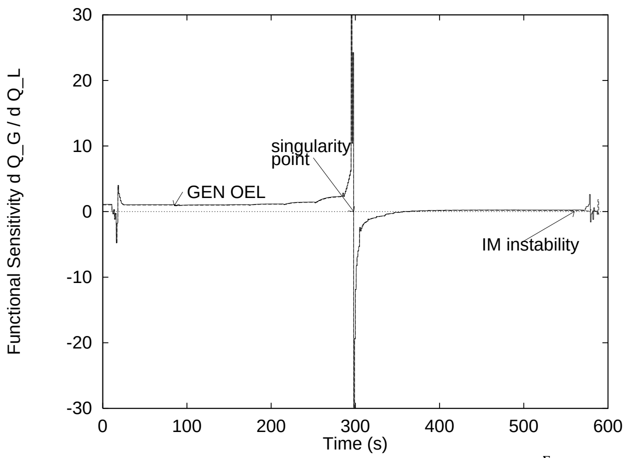

Fig. VIII.89 Time responses of functional sensitivity $\partial Q_G^{\Sigma}/\partial Q$ for static loads at buses BUS24 and BUS26

Singular and eigenvalue decompositions, as well as parametric and functional sensitivities are useful in critical point recognition. Upon its detection, the UPFC voltage support is initiated to alleviate voltage collapse.

VIII.2.D The UPFC support

The UPFC is retained at the same location as in the previous scenario. Upon establishing the new one in subsection VIII.2.A, the location is justified within subsection VIII.2.B. Critical point is detected within subsection VIII.2.C. Upon its detection, the UPFC voltage support is provided in order to avoid the collapse. Since the UPFC is thoroughly analysed in the previous scenario, hereafter the analysis is dominantly orientated toward behaviour of the composite loads. The same initial disturbance is retained. Benefits of the UPFC TEF damping control are shown within previous scenario. Due to simplicity, it is not applied in this one. In the period prior to the UPFC activation, the device is at no-load condition.

During this scenario, the UPFC voltage support is applied at several different time instants with respect to the critical point recognition. The time instants are equal to t=250 s, 310 s, 340 s, and 380 s. Initial voltage collapse scenario (without the UPFC support) is also retained. Upon activation of the UPFC two-parameter support, the shunt and series bus voltage magnitudes of the UPFC are given as subjects to the change of their referent values. The support is again activated by switching on the regulation modes $V_i \leftrightarrow Q_{conv1}$ and $V_j \leftrightarrow r$ through equal step changes in their PI regulator references set at 0.95 pu.

The UPFC bus voltage magnitudes become equalised in the final part of each successful case (Fig. VIII.90). Initially unstable case collapses at t=589 s, whereas in the unsuccessful case of voltage support (t=380 s) the collapse appears at t=781 s with splitting of the voltage magnitudes at the UPFC sides. In successful cases, the stable operating point is established with more or less dynamics involved. For the successful case applied at t=340 s, dynamics is rather significant and it takes approximately 400 s to bring bus voltage magnitude V_i at defined 0.95 pu value. Bus voltage magnitude V_j is regulated significantly faster. The other cases experience dynamics in a much smaller degree.

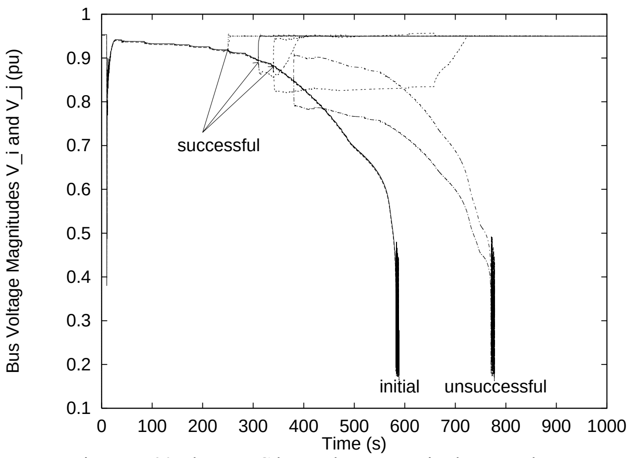

Fig. VIII.90 The UPFC bus voltage magnitudes V_i and V_j

Step changes of the UPFC voltage references lead to alleviation of the voltage stability problem in successful cases. Responses of bus voltage magnitudes at buses belonging to the composite loads connected at BUS19 and BUS 20 clearly denote benefits (Figs. VIII.91-92). The initial case of voltage collapse, three successful cases, and the unsuccessful case of voltage support due to its late activation are illustrated. Bus voltage magnitudes of the composite load connected at BUS19 exhibit larger magnitude excursions than the ones belonging to the composite load at BUS20. Since bus BUS19 is nearly located to the *i*-side of the UPFC, bus voltage magnitude V_i is closely related to the magnitudes of this load. Therefore, the magnitudes of the composite load at BUS19 need longer time to settle down at new steady state values in comparison with those related to BUS20.

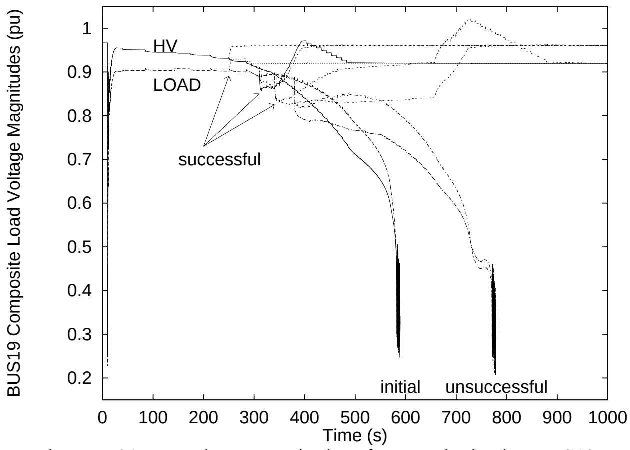

Fig. VIII.91 Bus voltage magnitudes of composite load at BUS19

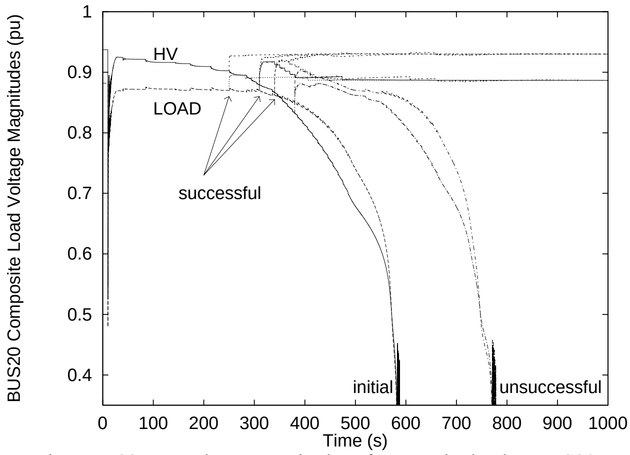

Fig. VIII.92 Bus voltage magnitudes of composite load at BUS20

The other reason for the magnitudes of the load at BUS19 being largely disturbed is found in behaviour of the LTCs tap ratio. Responses of the tap ratio and voltage error of the LTC1, which is related to BUS19, reveal behaviour of the magnitudes of the composite load at BUS19 (Figs. VIII.93-94). Responses of these variables are provided for the LTC2, related to BUS20, as well (Figs. VIII.95-96). By comparing corresponding responses of the LTCs, it is seen that the LTC1 is disturbed largely than the LTC2. Tap ratio of the LTC1 in successful cases exhibits larger and longer changes due to larger voltage error. The changes of the LTC2 are smaller and the variables are settled down faster.

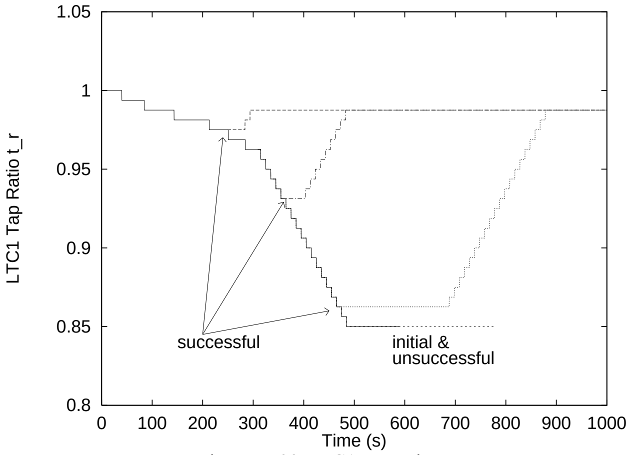

Fig. VIII.93 LTC1 tap ratio

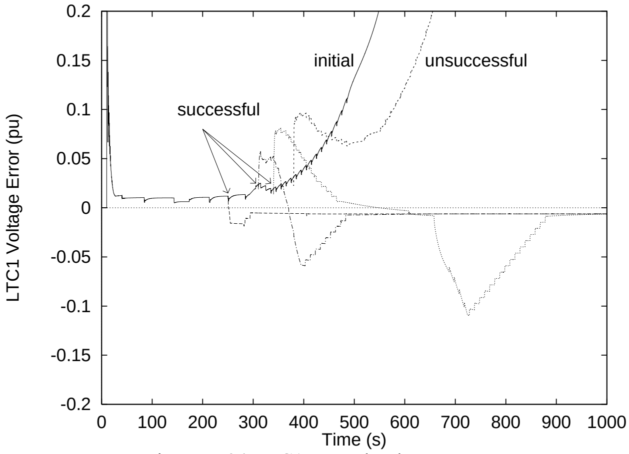

Fig. VIII.94 LTC1 control voltage error

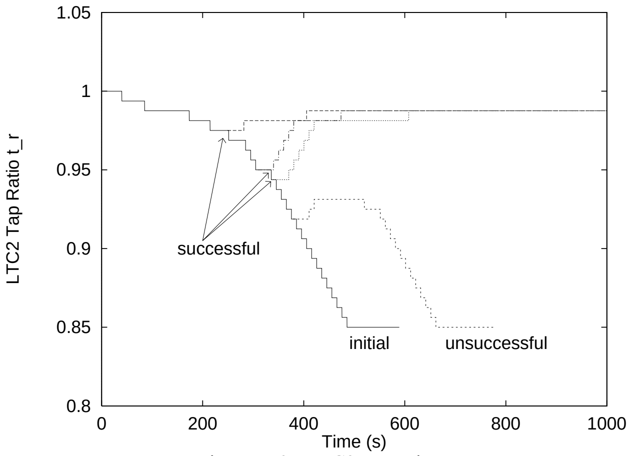

Fig. VIII.95 LTC2 tap ratio

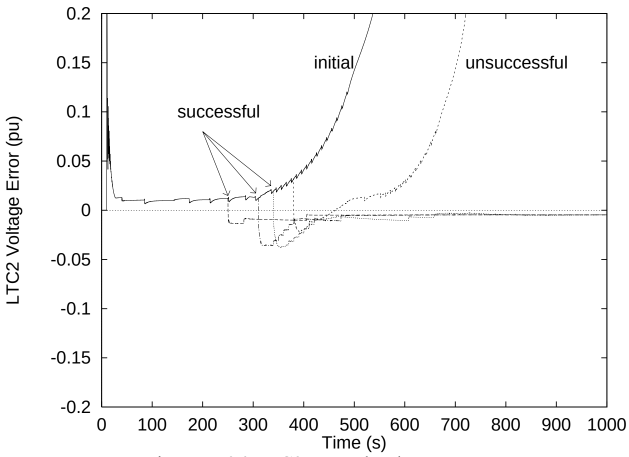

Fig. VIII.96 LTC2 control voltage error

In successful cases, the voltage errors are brought within pre-specified dead-bands equal to ±0.01 pu. New steady state is achieved with the tap ratios two steps smaller than the initial ones due to slightly negative corresponding voltage errors. The initially unstable and unsuccessful cases suffer large changes of the errors leading to instability.

Behaviour of the UPFC and the LTCs influence responses of generator OEL voltages and excitation currents. Generator OEL voltages are brought to zero value in each successful case of the UPFC voltage support (Fig. VIII.97). In the last successful case, the OEL voltage of generator GEN5 has large change prior to settling down due to its near location to the BUS19 and the *i*-side of the UPFC. The OEL voltage of generator GEN6 needs shorter time to achieve zero value.

Generator excitation currents are decreased in value when the UPFC starts to successfully provide reactive power to the system (Fig. VIII.98). Responses are influenced by the LTCs action as well. In each successful case, the final values of the excitation currents are mutually the same for each generator. New steady state value of generator GEN5 excitation current is larger than the one of GEN6. It also needs longer time to be decreased below pre-specified current limit. In the unsuccessful case, the excitation currents are not brought down below the limits, and the collapse appears in oscillating form similarly as in the initially unstable case.

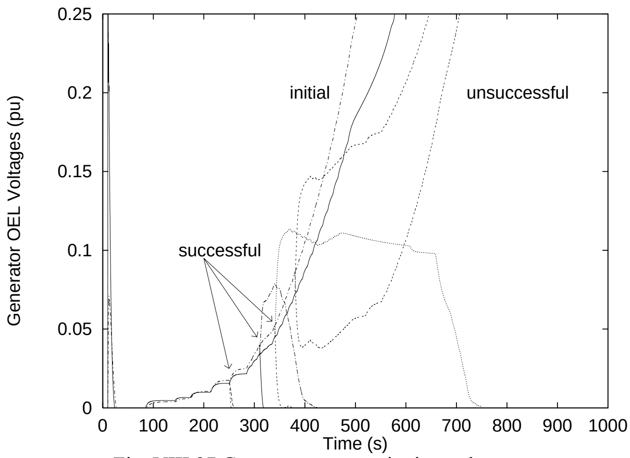

Fig. VIII.97 Generator over-excitation voltages

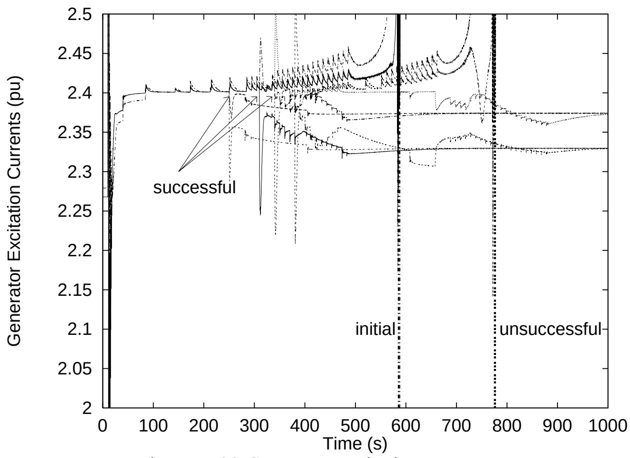

Fig. VIII.98 Generator excitation currents

The UPFC voltage support is proven to be capable to alleviate the voltage stability problem in presence of the composite loads. Responses of the UPFC set of variables (r, γ, I_{conv1q}) is thoroughly analysed within previous scenario (Figs. VIII.27-29). In this one, responses of the UPFC shunt and series converter apparent power, S_{conv1} and S_{conv2}, are provided only to justify already established conclusions. Nominal rating powers of the UPFC shunt and series converters, S_{conv1n} and S_{conv2n}, are the same as previously (185 MVA or 1.85 pu on the system base power 100 MVA).

Responses of the converter apparent powers, S_{conv1} and S_{conv2}, show that they are operated within nominal rating limit (Figs. VIII.99-100). Since the TEF oscillation damping control mode is not activated, the UPFC is at a no-load condition prior to the voltage support activation.

Responses of the UPFC shunt converter apparent power, S_{conv1} (Fig. VIII.99), largely depend on the current I_{conv1q} and, especially during limiting conditions, on the bus voltage magnitude V_i. Upon the voltage support activation, the initially forced loadings of the shunt converter become very high and close to the rated maximum value. As the voltage support is applied later during the scenario, the bus voltage magnitude V_i becomes deeply depressed. Therefore, the forced loading level becomes smaller. The loadings are slightly below rated power. In the last successful case, applied at t=340 s, the shunt converter is forced at maximum value for approximately 400 s. Due to operation at the ceilings, the bus voltage magnitude V_i needs the same time period to achieve referent 0.95 pu value. At the final steady state after the LTCs action, the loading level of the shunt converter is the same for each successful case. It takes rather high value that is approximately twice less than the initial forcing ones.

Responses of the series converter apparent power S_{conv2} are rather similar to the responses of the UPFC magnitude r (Fig. VIII.100). It is seen that the series converter has large loadings upon activation of the voltage support. Later on, the loading level is decreased to a very low value since the γ-loop control of the series active power flow is not currently applied. The loading levels of the series converter are significantly lower than the rating one.

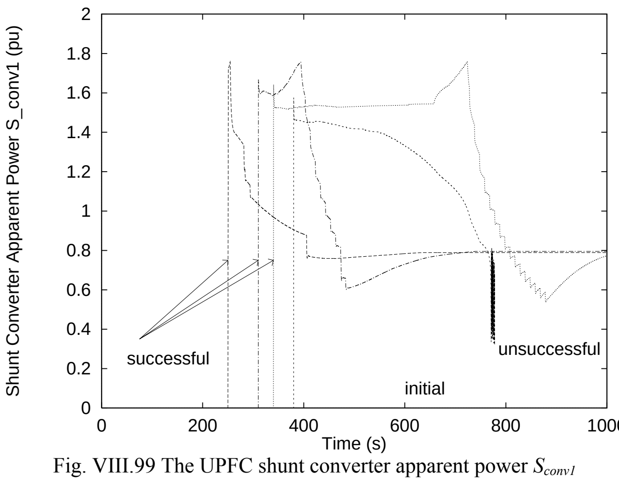

Fig. VIII.99 The UPFC shunt converter apparent power S_{conv1}

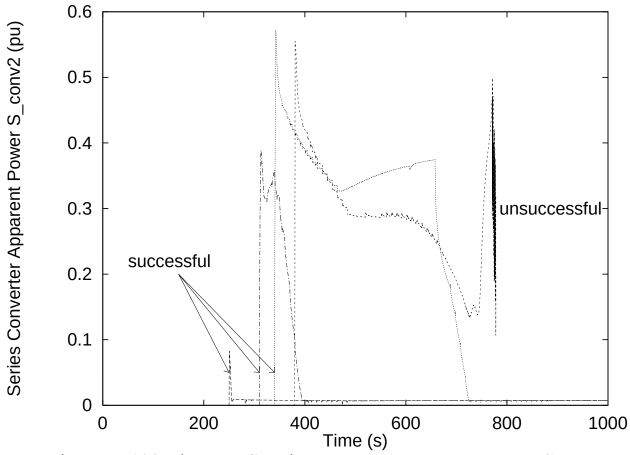

Fig. VIII.100 The UPFC series converter apparent power S_{conv2}

It is seen that the loading level of the shunt converter is significantly larger than the series one. The UPFC shunt side controls bus voltage magnitude V_i, while the series side in that period just adds injected voltage source at the shunt side magnitude. This is the main reason for their disproportionate loading levels.

While establishing this voltage collapse scenario (subsection VIII.2.A), time domain responses of the LTCs active and reactive power flow from the HV bus to the LV bus are provided. They reveal restorative intentions of the composite loads and are related to the dynamic loads with non-linear recovery. Hereafter, they illustrate the impact of the UPFC voltage support to the composite load consumption.

Responses of the active power flow illustrate combined restorative intention of the composite load (Fig. VIII.101). Responses of the reactive power flow also exhibit the same intention (Fig. VIII.102). In the final parts of the initially unstable and unsuccessful cases, they again differ from the responses of the dynamic load model with non-linear recovery. Instead of decrease of reactive load consumption in the final part, the reactive power of the composite load model is first increased and then abruptly decreased ending with oscillations. Overall level of the system dynamics is highly pronounced due to the impact of the induction motors. Since the LTC1 has larger and longer changes of the tap ratio, the power flow that belongs to BUS19 exhibits longer excursions prior to final settling down.

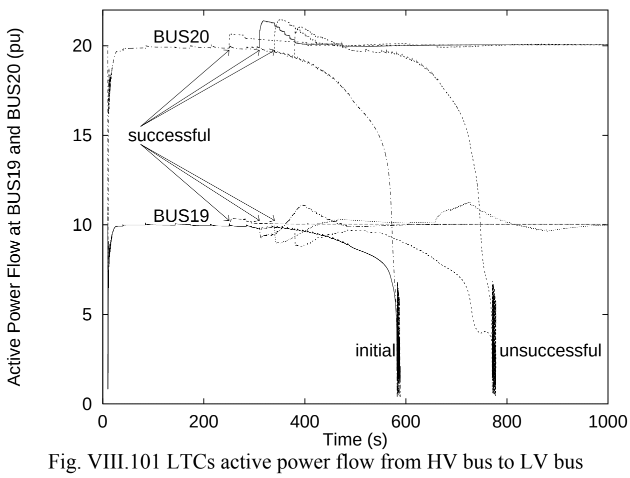

Fig. VIII.101 LTCs active power flow from HV bus to LV bus

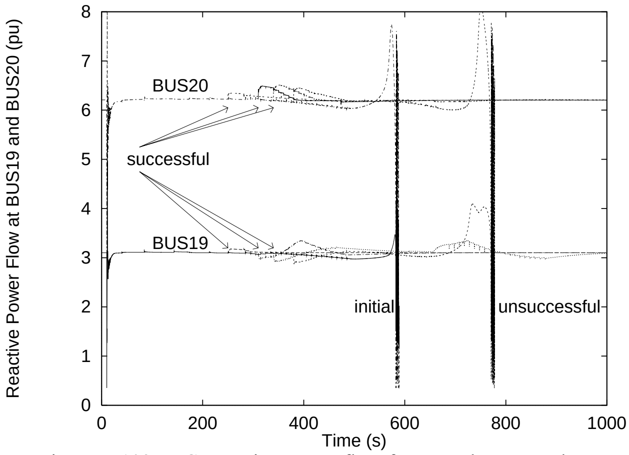

Fig. VIII.102 LTCs reactive power flow from HV bus to LV bus

The LTCs power flow is decomposed in order to recognise dynamic behaviour of each individual element of the composite load when the UPFC voltage support is provided.

The shunt capacitors, SHUNT1 and SHUNT2, are connected to supply reactive power locally at the LV buses, which belong to the composite loads at BUS19 and BUS20, respectively. Responses of the shunt capacitors reactive power illustrate its quadratic dependence with respect to bus voltage magnitude. The reactive power is quadratically decreased when it is most needed. In successful cases, it is recovered nearly to initial value due to the UPFC voltage support. The SHUNT1 is an element of the composite load at BUS19. In the final part, after being regulated the LV bus voltage magnitude of the LTC1 is first increased and then decreased (Fig. VIII.91), due to combined action of the UPFC shunt converter and the LTC1. Therefore, the SHUNT1 reactive power exhibits certain changes in value.

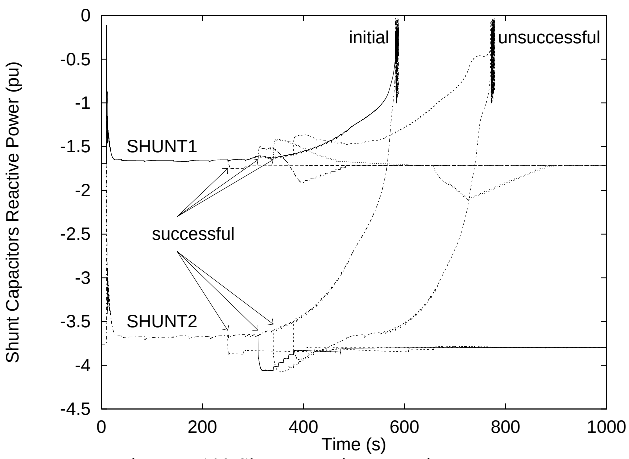

Fig. VIII.103 Shunt capacitors reactive power

The static loads, SL1 and SL2, are similarly related to bus voltage magnitude. Active and reactive power of the static loads are decreased as the magnitudes are decreased (Figs. VIII.104-105). Responses depend on a constant current type of active power load and a constant impedance type of reactive power. The SL1 static load is connected to the LOAD bus of the composite load at BUS19. The LOAD bus voltage magnitude is closely related to the LV one. Therefore, responses of the SL1 active and reactive power become accordingly changed in the final part of the last

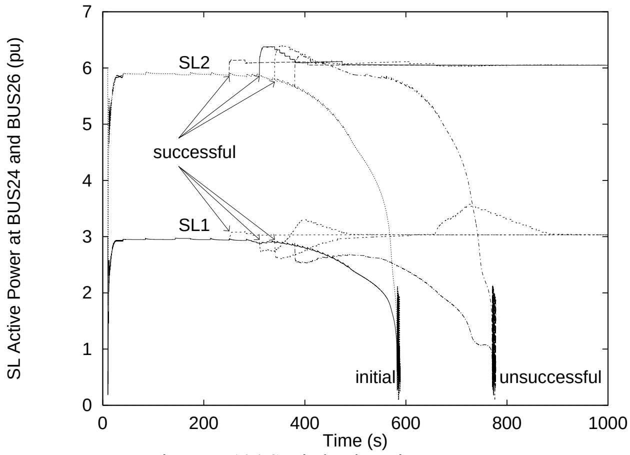

Fig. VIII.104 Static loads active power

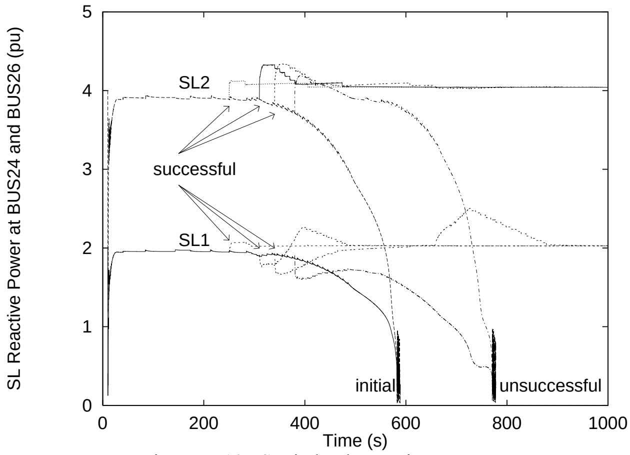

Fig. VIII.105 Static loads reactive power

successful case. This situation is explained within the analysis of the SHUNT1 responses.

Characteristic variables belonging to thermostatically controlled loads are provided to give better insight to the restorative mechanism of resistive heating load.

As the UPFC voltage support is activated, the LOAD bus voltage magnitudes are increased and kept controlled in successful cases. The TCL conductances are brought back to the values similar to the initial ones (Fig. VIII.106). The TCL active power consumptions are linearly proportional to the conductances and quadratically to the LOAD bus voltage magnitudes (Fig. VIII.107). In each successful case, their initial values are closely restored. The TCL control schemes keep the temperature of the heated area, τ_H, at the pre-specified referent value τ_{REF}. In each successful case, the temperature τ_H is successfully controlled (Fig. VIII.108). In the unsuccessful case, the TCL control schemes are incapable to keep the temperatures τ_H at their referent values. The voltages collapse together with the temperatures as in the initially unstable case.

The TCL1 is related to the LTC1 tap changing action. Since its active power consumption is quadratically proportional to the LOAD bus voltage magnitude, large excursions of the active power and the temperature appear in the final part of the last successful case.

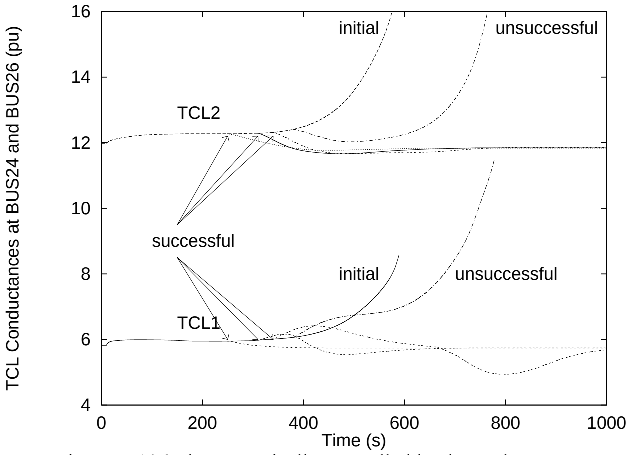

Fig. VIII.106 Thermostatically controlled loads conductance

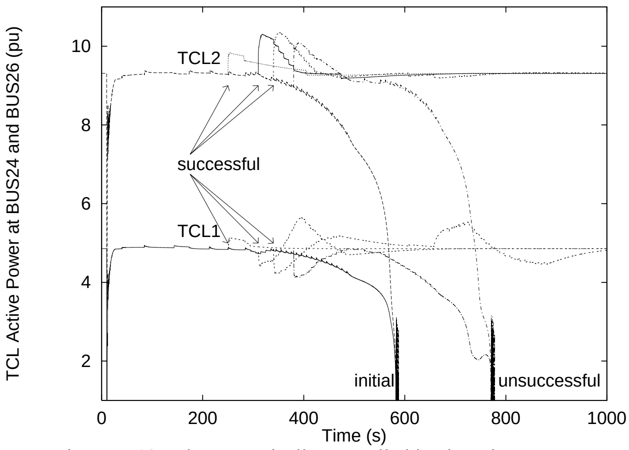

Fig. VIII.107 Thermostatically controlled loads active power

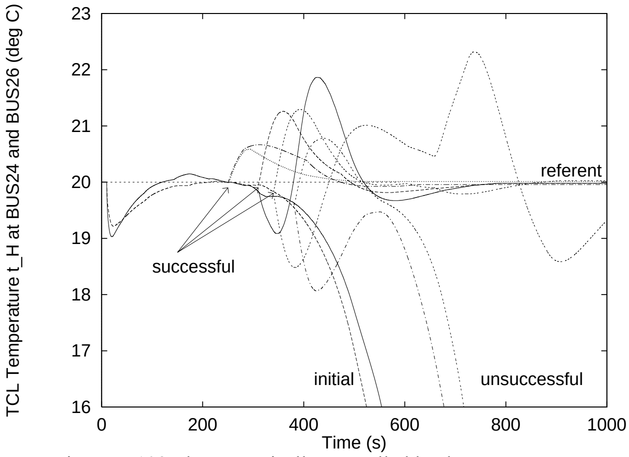

Fig. VIII.108 Thermostatically controlled loads temperatures

Characteristic variables of the induction motors are illustrated as well.

Responses of the induction motors active power again point out to fairly constant consumption closely up to the collapse (Fig. VIII.109). As the collapse is approached, the active power is abruptly decreased ending with oscillations. In successful cases, the active power is preserved. In the unsuccessful case, the UPFC voltage support is given too late and the collapse appears similarly as in the initially unstable one. Responses of the reactive power are similar to the ones noted for the LTCs reactive power flow. As the collapse is approached, the reactive power is first increased and then abruptly decreased ending with oscillations (Fig. VIII.110). By successful support, the reactive power is kept at lower demand. In the final part, the LOAD bus voltage magnitude of the IM1 influences transient behaviour of the reactive power, but it does not introduces visible impact to the active power. The induction motors current that is drawn from the system mainly dominates responses of the reactive power in that final part (Fig. VIII.111). Responses of the speed of the induction motors are closely related to the motors active power (Fig. VIII.112). Up to the collapse, the motors keep the speed at stable values. As the voltages collapse, the motors are stalled. The IM stability is lost passing through the speed-torque critical operating points.

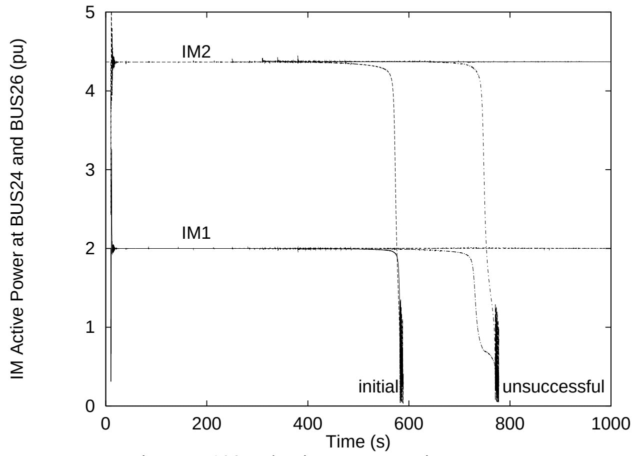

Fig. VIII.109 Induction motors active power

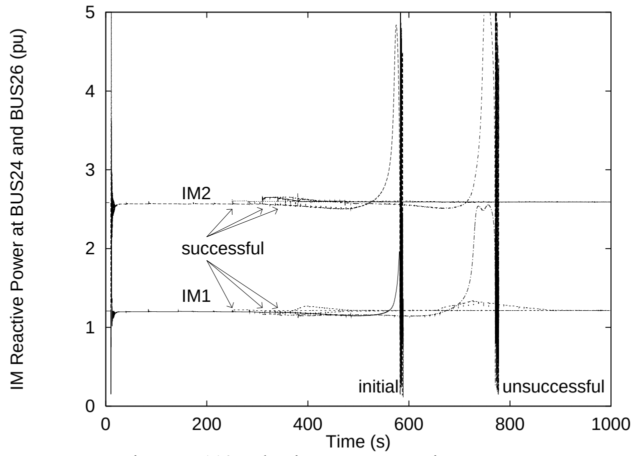

Fig. VIII.110 Induction motors reactive power

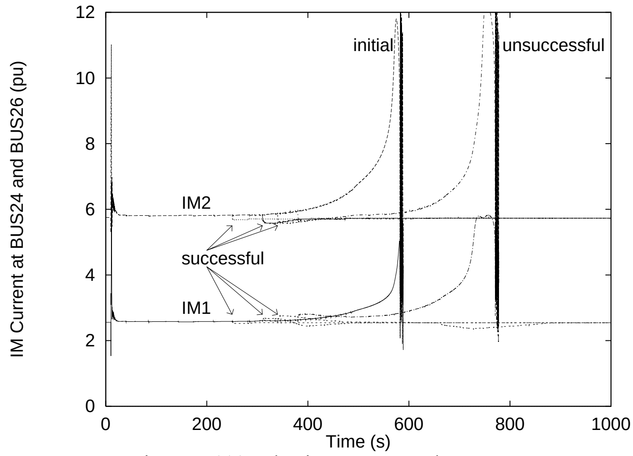

Fig. VIII.111 Induction motors total current

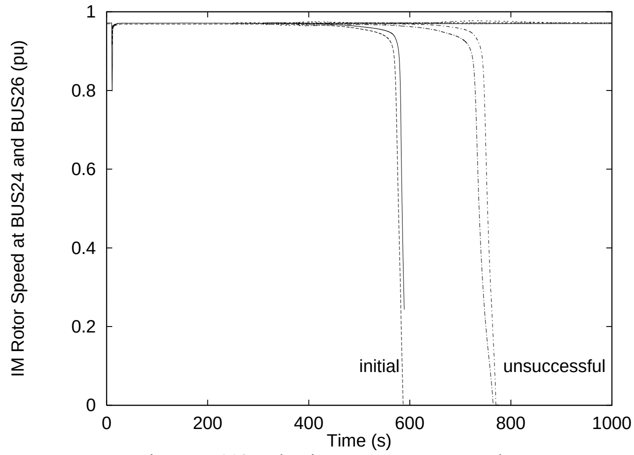

Fig. VIII.112 Induction motors rotor speed

The UPFC voltage support has proven impact to the behaviour of the indices aimed for critical point recognition. Preferably, the support should be given upon its recognition or otherwise overall level of system dynamics becomes more pronounced. Critical singular and eigenvalues, parametric and functional sensitivities are evaluated hereafter. They illustrate benefits of earlier critical point recognition and trigger the voltage support.

Singular value decomposition of the state matrix A_S exhibits sensitive responses upon the voltage support activation. Its minimum singular value, which is regarded as the critical one, becomes largely increased in each successful case as the voltage support is timely provided (Fig. VIII.113). It is essential to activate the UPFC upon critical point recognition or even before it. Later on, it takes significantly longer time to establish stable final steady state due to increased level of overall system dynamics. In the final steady state, the minimum singular value is the same for each successful case. In the unsuccessful case, the support is provided too late. The attempt to restore the minimum singular value is insufficient. The voltages collapse and the motors lose stable operating points.

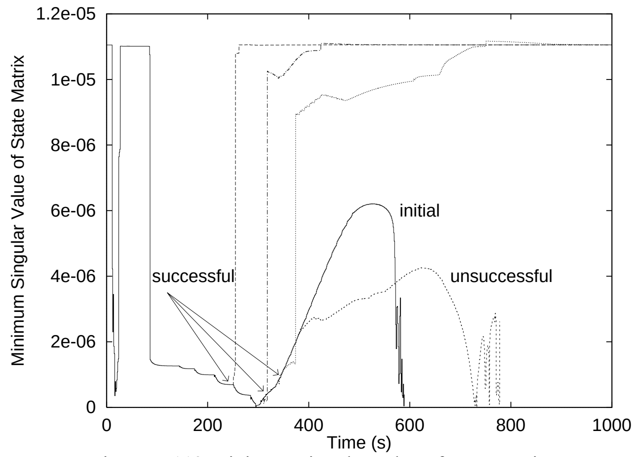

Fig. VIII.113 Minimum singular value of state matrix

Eigenvalue decomposition of the state matrix A_S also results with sensitive responses to the UPFC voltage support. Upon successfully applied support, the real part of the critical eigenvalue is kept within the negative half-plane, which is regarded as the stable one (Fig. VIII.114). Transfer from the positive half-plane to the negative one is made possible if the support is given shortly upon critical point recognition. In the final steady state, the real part is the same for each successful case. As the support is given later on, due to increased level of overall dynamics the system suffers from instability ending in oscillations.

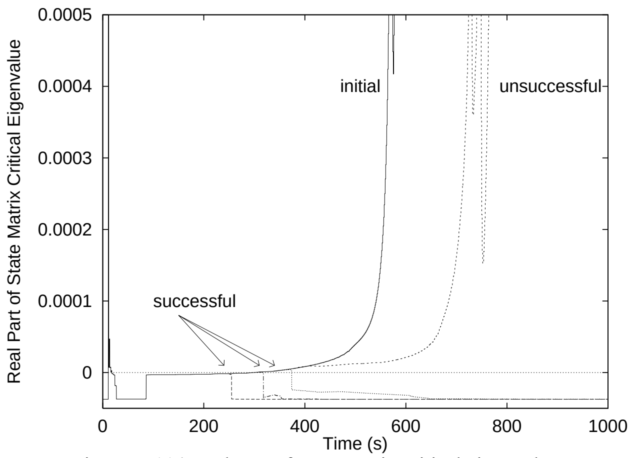

Fig. VIII.114 Real part of state matrix critical eigenvalue

Besides critical singular and eigenvalues, the results of the UPFC voltage support comprise the ones that are achieved by the sensitivity analysis as well. With reference to the previous subsection, VIII.2.C, the parametric sensitivity is illustrated hereafter. The sensitivity involves the inverse of the state matrix. As the singularity point is approached, the sensitivity becomes very large. At the singularity point, it abruptly changes the sign to the opposite one and moves towards zero within unstable region. The singularity point is considered as the critical one.

Parametric sensitivity, $\partial x/\partial p$ or $\partial y/\partial p$, is evaluated for the TCLs and the IM loads. The TCL conductance G, the IM rotor speed ω_m, and the bus voltage magnitude V are retained as state and algebraic variables to provide illustrative examples. The TCL referent temperature τ_{REF} and the IM initial mechanical load torque T_{m0} serve as arbitrary parameters.

For the TCL loads, parametric sensitivities $\partial G/\partial \tau_{REF}$ and $\partial V/\partial \tau_{REF}$ are evaluated with the UPFC voltage support provided at the same time instants. Responses of the parametric sensitivity $\partial G/\partial \tau_{REF}$ illustrate the way of establishing a stable operating point in successful cases (Fig. VIII.115). Around a stable operating point the increase of the temperature τ_{REF} is achieved by the increase of the conductance G, and vice versa. Therefore, the sensitivity $\partial G/\partial \tau_{REF}$ is positive around a stable operating point. As the UPFC voltage support is timely provided in successful cases, the sensitivity $\partial G/\partial \tau_{REF}$ is brought to a small positive value that is close to the initial one. As the support is given later on during the scenario, it takes longer time to achieve new steady state. In the unsuccessful case, the system eventually collapses in oscillations. Responses of the parametric sensitivity $\partial V/\partial \tau_{REF}$ also denote stability of an operating point (Fig. VIII.116). Around a stable operating point, the increase of the temperature τ_{REF} is achieved by the increase of the conductance G, which increases active power load consumption, and therefore bus

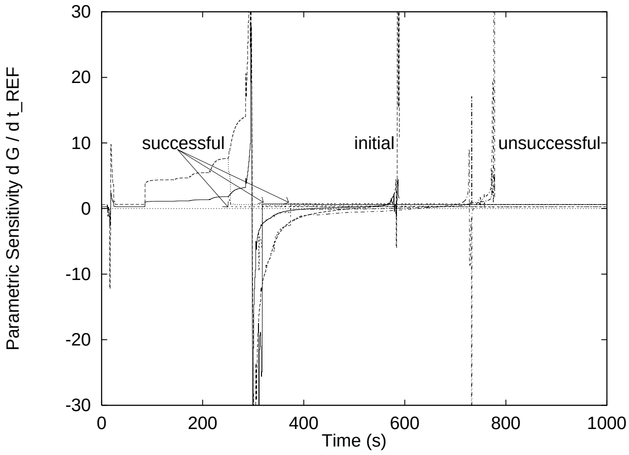

Fig. VIII.115 Parametric sensitivity of TCL loads, $\partial G/\partial \tau_{REF}$

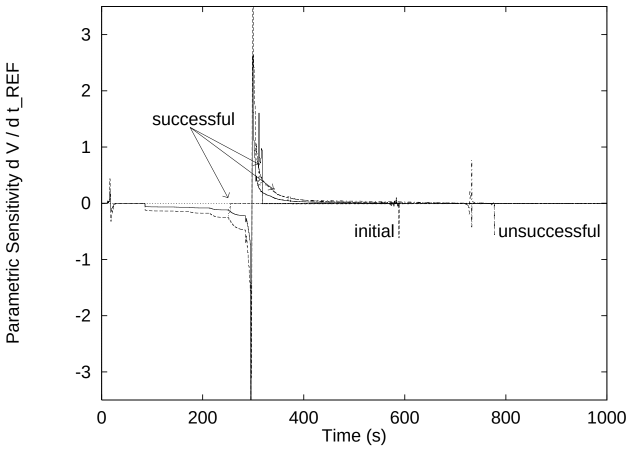

Fig. VIII.116 Parametric sensitivity of TCL loads, $\partial V/\partial \tau_{REF}$

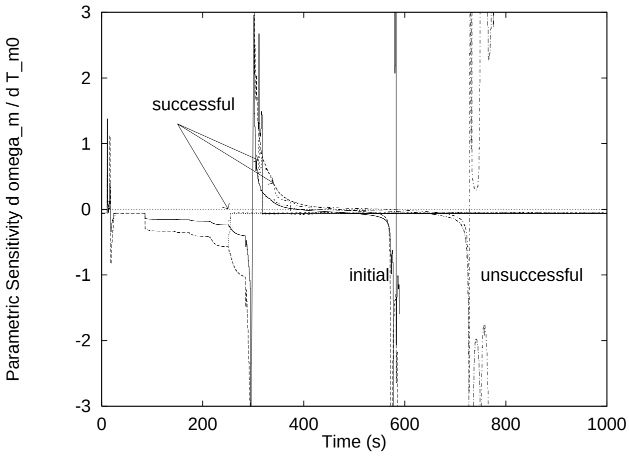

Fig. VIII.117 Parametric sensitivity of IM loads, $\partial \omega_m /\partial T_{m0}$

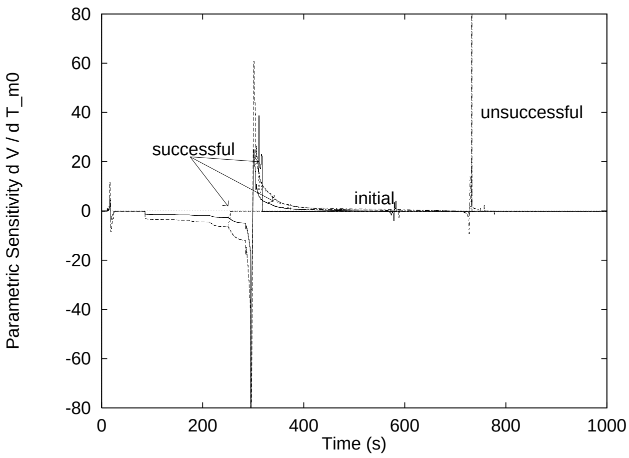

Fig. VIII.118 Parametric sensitivity of IM loads, $\partial V/\partial T_{m0}$

voltage magnitude drops. Thus, the parametric sensitivity $\partial V/\partial \tau_{REF}$ is negative around a stable operating point. In successful cases of the UPFC voltage support, the sensitivity $\partial V/\partial \tau_{REF}$ is brought to a small negative value that is close to the initial one. Giving this support later on in the scenario, new steady state becomes harder to achieve. In the unsuccessful case, the system collapses in oscillations.

For the IM loads, parametric sensitivities $\partial \omega_m /\partial T_{m0}$ and $\partial V/\partial T_{m0}$ are evaluated in presence of the UPFC voltage support. Responses of the parametric sensitivity $\partial \omega_m /\partial T_{m0}$ detect stability of an operating point (Fig. VIII.117). Responses of the parametric sensitivity $\partial V/\partial T_{m0}$ provide the same (Fig. VIII.118). Around a stable operating point, the increase of the mechanical torque T_{m0} causes the decrease of the rotor speed ω_m. The induction motor draws larger current from the network, and its bus voltage magnitude drops. Both of the parametric sensitivities, $\partial \omega_m /\partial T_{m0}$ and $\partial V/\partial T_{m0}$, are negative around a stable operating point. Therefore, in successful cases of the UPFC voltage support, these sensitivities are brought to small negative values that are close to the initial ones. Final values of the sensitivities are the same for each successful case. If the support is given too late as in the unsuccessful case, the system collapses with induced oscillations.

Parametric sensitivity $\partial y/\partial p$ is also illustrated for the LTC1 transformer in presence of the UPFC voltage support. Responses of the parametric sensitivity $\partial V/\partial t_r$ are provided (Fig. VIII.119). Around a stable operating point, the decrease of the tap ratio t_r causes the increase of the LV bus voltage magnitude. The parametric sensitivity $\partial V/\partial t_r$ is negative for the LV bus around a stable operating point. The sensitivity of the HV bus voltage magnitude is significantly smaller. It is close to zero and even has the opposite sign. In successful cases of the UPFC voltage support, the sensitivity $\partial V/\partial t_r$ for the LV bus is brought to a negative value that is close to the initial one. The sensitivity of the HV bus voltage magnitude is brought close to zero with the opposite sign. Final values of the sensitivity are the same for each successful case. By giving the support too late, the system collapses with induced oscillations as in the unsuccessful case.

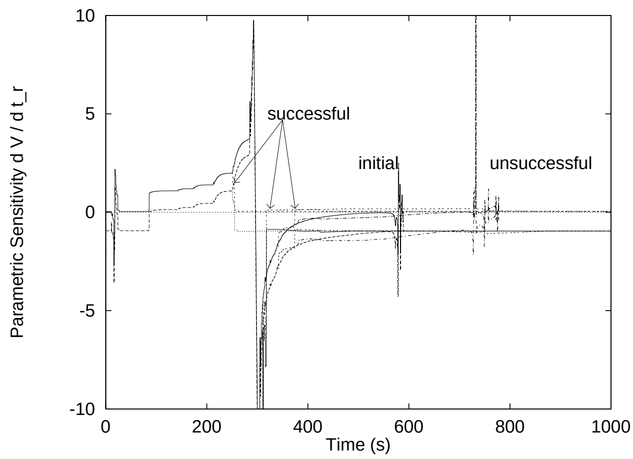

Fig. VIII.119 Parametric sensitivity of LTC1 transformer, $\partial V/\partial t_r$

As the last one among the sensitivities, the functional sensitivity $\partial\eta/\partial p$ is illustrated in presence of the UPFC support. As a function, the total reactive power production of the generators, Q_G^{Σ}, is retained. For an arbitrary parameter, the initial value of the SL reactive power load is kept. The functional sensitivity is computed with respect to each of the static loads at the LOAD buses.

Responses of the total reactive power production Q_G^{Σ} are dominated by generator excitation currents (Fig. VIII.120). As the UPFC successfully provides voltage support, the total reactive power Q_G^{Σ} becomes decreased. It is brought down approximately to a value prior to the first LTCs tap changes. In successful cases, the final value of the power Q_G^{Σ} is the same. If the UPFC support is given earlier, new steady state is achieved faster. In the unsuccessful case, the system ends up in the collapse. Responses of the functional sensitivities also reveal stability of an operating point (Fig. VIII.121). Around a stable operating point, if the load consumption is increased, the total reactive power production is increased as well. Therefore, the functional sensitivities are positive around a stable operating point. If the UPFC voltage support is successfully applied, these sensitivities are brought to small positive values that are close to the initial ones. Final values of the sensitivities are the same for each successful case. Transfer from negative to positive values occurs with more or less dynamics involved, depending on the time instant of applied support. In the unsuccessful case, the support is given too late.

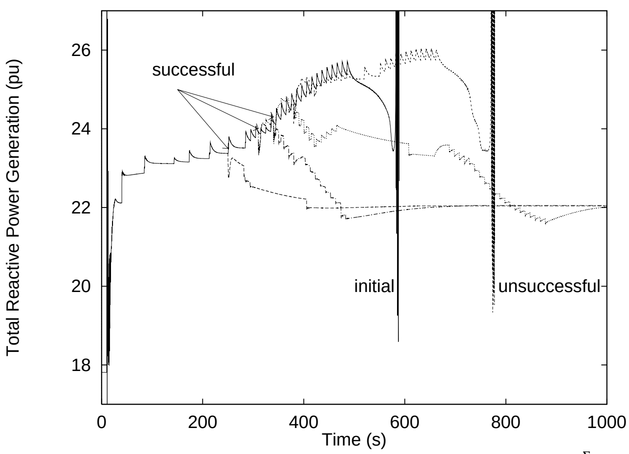

Fig. VIII.120 Total reactive power production of generators Q_G^{Σ}

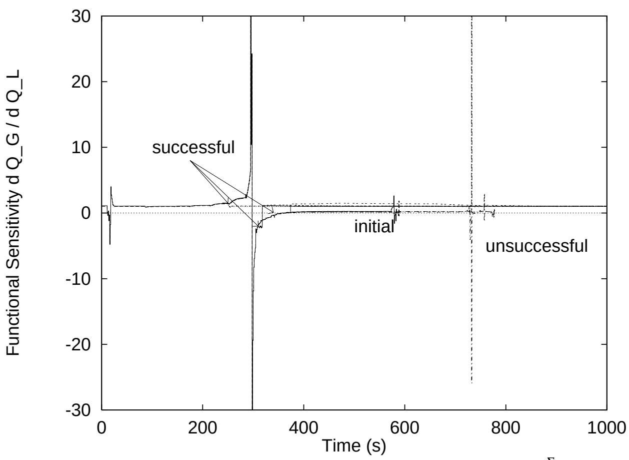

Fig. VIII.121 Time responses of functional sensitivity $\partial Q_G^{\Sigma}/\partial Q$ for static loads at buses BUS24 and BUS26

As the last case, the UPFC three-parameter control is also illustrated in this scenario. The successful case of two-parameter voltage support applied at t=250 s is retained for comparison. It denotes the case without LF control. The third parameter control of the angle γ is applied additionally at t=750 s. Its referent value is changed from 0° to 80°, 85°, and 87.5°. These changes increase the series side active power flow P_{j2} from -1.84 pu to -1.91 pu, -1.97 pu, and -2.05 pu (Fig. VIII.122). The UPFC bus voltage magnitudes are successfully controlled at 0.95 pu (Fig. VIII.123). The third parameter γ control slightly decreases the total active power loss in the network (Fig. VIII.124).

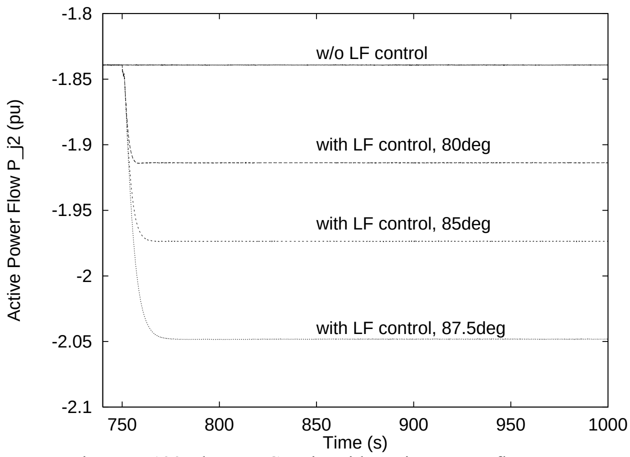

Fig. VIII.122 The UPFC series side active power flow P_{j2}

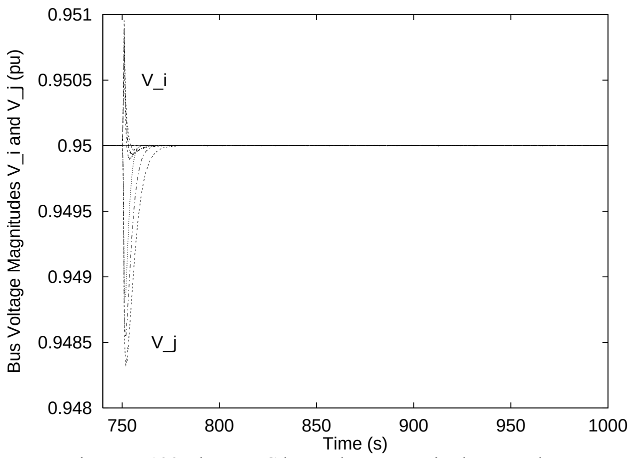

Fig. VIII.123 The UPFC bus voltage magnitudes V_i and V_j

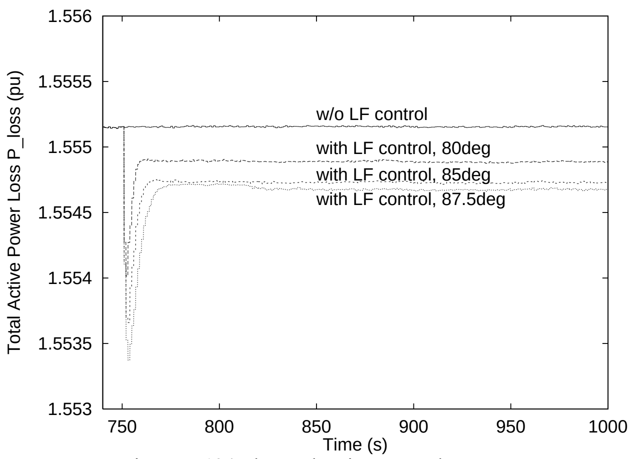

Fig. VIII.124 The total active power loss P_{loss}

IX. CONCLUSIONS

The voltage stability problem, as it is seen from FACTS perspective, represents main concern in this dissertation. In order to deal with the voltage stability problem, solutions with FACTS-controllers must provide voltage support and/or appropriately co-ordinated control actions. The thesis goal is stated as to show how it is possible to alleviate voltage stability problem by using modern, power electronics based FACTS device named the Unified Power Flow Controller (UPFC).

In elaboration of stated thesis, a computer analysis of power system voltage stability has been carried out. Own computer program aimed for mid-term time domain simulation of multi-machine power system is developed. By combining dynamic and static aspects of analysis, it is primarily focused on off-line simulation of voltage emergency situations using differential-algebraic model of power system with the UPFC included.

Findings that have come out from the research work are divided in four main parts, namely, introduction, modelling, numerical results, and conclusions.

In the introductory part, the guidelines are provided for the voltage stability problem and FACTS devices. Current activities in both fields are noted. Their correlation is established. Upon recognition of mutual causalities, the objectives are defined. Sequence of the dissertation is explained along with phases of the thesis elaboration. Main contribution of the dissertation is stated as well.

In the modelling part, the multi-machine test system is described. It contains the model of synchronous generator with excitation system and speed governor - turbine system. Load models are included. Details of the composite load model and the dynamic one with non-linear recovery are clearly separated. An overview of network modelling is provided as it enables key system elements to be connected. The UPFC is embedded in the system. Its injection model is derived along with appropriate control system. Ways to include the UPFC injection model in load flow computation are explained together with nominal rating procedure. Upon embedding the UPFC in the system, the differential-algebraic system model is established. Overall differential and algebraic equations are first combined, and then linearised around an operating point. The state and extended Jacobi matrices are defined enabling analytical procedures to be carried out. Introducing basics of their sensitivities, the modelling part is rounded. Based on singular and eigenvalue decompositions, bus, branch and generator participation factors are defined. Parametric and functional sensitivities are derived. Sub-optimal formulation using sensitivities is set either to maximise minimum singular value or to minimise total active power loss in the network.

In the numerical part, the results are given according to three areas where the UPFC has large impact to the system operation.

In the first area, the results of the UPFC voltage/power flow regulation are described to illustrate capabilities of the UPFC in general steady state operation of the multi-machine test system. By using appropriate control system of the model, it is made possible to control simultaneously three transmission system variables depending on the regulation mode (bus voltage magnitude, power flow, series compensation, and phase shifting). Before tackling voltage/power flow regulation problem, dimensioning procedure is addressed. Rating powers are discussed with respect to the optimal algorithm. Then, independent operation of the UPFC shunt and series branch is analysed. Afterwards, simultaneous three-parameter control of the UPFC injection model is illustrated. By describing achieved results it is shown that the UPFC could be useful transmission system controller in steady state operation of power system. Furthermore, its injection model with proposed control system help in recognising each of the potential operating modes.

In the second area, the results of the UPFC damping control are provided. The voltage collapse scenario is based on a slow dynamics response of the system, which is initiated by a three-phase short circuit. Since the disturbance initially induces electromechanical oscillations, possible utilisation of the UPFC injection model in damping control is analysed. By using appropriate control system of the model, it is made possible to damp electromechanical oscillations by simultaneous three-parameter control of the UPFC. Within oscillations damping control, dimensioning procedure is addressed especially from a viewpoint of the series side of the UPFC. By describing achieved results it is shown that the UPFC could be useful transmission system controller not only in steady state operation of power system, but during fast electromechanical transients as well. Furthermore, the injection model with proposed control system has been made to enable damping control of electromechanical oscillations.

In the third area, the results concerning centrally positioned topic come out after recognising possible regulating actions of the UPFC from previous two areas. More particularly, the role of the UPFC in alleviation of the voltage stability problem is explained by using characteristics that are recognised in the voltage/power flow regulation and oscillations damping. Two slow dynamics scenarios are assumed in the problem evolving. The voltage collapse scenarios are analysed from two aspects given by the dynamic load with non-linear recovery, and by the composite one. Characteristic load parameters are singled out. Critical points of power system operation are recognised. The UPFC is accordingly located and initiated to provide adequate support. Three-parameter control of the UPFC injection model is employed. By describing achieved results, it is shown that the UPFC could be useful transmission system controller in a slow dynamics period of power system operation. Furthermore, its injection model with proposed control system has a potential for relieving the problem.

Conclusions of the dissertation follow two main directions, namely the voltage stability problem and the UPFC model. These main directions are also combined by analysing possible utilisation of the UPFC within each of the established scenarios.

From the viewpoint of the voltage stability problem, the static aspects of the linearised differential-algebraic power system model are shown to be very useful. They concern properties of the state and extended Jacobi matrices according to singular and eigenvalue decomposition, sensitivity analysis, and participation factors. Static aspects are proven to be capable to recognise appearance of the voltage stability problem and the critical point during time domain simulation. Sensitivity analysis of the minimum singular value, total active power loss, and total reactive power generation is carried out to recognise the critical point of power system operation during voltage collapse scenario. Often, the sensitivity involves the inverse of the state or the extended Jacobi matrix. Therefore, it has larger magnitudes as the critical point is approached with abrupt change to opposite sign as it is crossed. The appearance of the critical point represents a reliable sign of impending voltage unstable situation. It gives valuable information on preventative action time instant.

Furthermore, it is shown that the static aspects contribute not only to the determination of preventative action time instant, but also to finding of appropriate location of the UPFC. The UPFC has rather unique capability of simultaneous series control of branch power flow and shunt control of bus voltage magnitude. By correlating that unique capability of the UPFC to branch and bus participation factors obtained from the matrix decompositions, the location of its installation is recognised. At that location, appropriate regulation characteristics of the UPFC are extensively used during voltage emergency situations.

The UPFC characteristics are recognised by using its injection model with appropriate control system. In its general form it can provide simultaneous, real-time control of all basic power system parameters (transmission voltage, impedance and phase angle) and dynamic compensation of ac system. It has been studied concerning its capability to help voltage stability problem solved. It is shown that the model fulfils functions of reactive shunt compensation, voltage regulation, line power flow regulation, series compensation, PAR/QBT phase shifting, and damping control. By analysing each of these functions, it is recognised how it is possible to alleviate the voltage stability problem by using the UPFC. Being established, the multiple control objectives are fulfilled by simultaneous three-parameter control of the UPFC injection model.

The sensitivity analysis is applied with respect to the set of the UPFC control parameters. Since the voltage support capability of the UPFC is achieved by using two of its parameters, there is an additional advantage of its design, which enables simultaneous control of the third parameter as well. By the third parameter being controlled, the voltage support is combined with the power flow regulation that as an objective may either to maximise minimum singular value or to minimise total active power loss.

Special attention is paid to load modelling, since the load is considered to be the driving force of the voltage stability problem. After being shortly disturbed with a consequence of permanently decreased voltage magnitude level, by its mid-term recovery process of re-establishing initial power consumption, the loads could bring generators under over-excitation limiting conditions and/or cause transmission system being incapable of requested power delivery. Therefore, several different load models (static and dynamic) are analysed regarding its contribution to voltage collapse. Besides static ZIP load model, there are included dynamic models of induction motors and thermostatically controlled loads in presence of the LTC transformers, and first order non-linear recovery loads. Besides to the set of the UPFC control parameters, the static aspects and the sensitivity analysis are applied to the characteristic parameters of the load models as well. By analysing load characteristics, the most influential loads that drive the system to the collapse are recognised along with critical parameters.

As for the conclusions, following fundamental characteristics of the dissertation are stated:

- The differential-algebraic model of the multi-machine power system is developed. It is useful in time domain simulation with combined dynamic and static elements of the analysis. The analysis concerns dynamic phenomena of mid-term transient periods of decreased voltage security level.

- The UPFC injection model with adequate control system is developed. The role of the device and its regulation capabilities useful in the voltage stability problem are defined. Methodology of rating, locating and activation timing of the UPFC is established using simultaneous three-parameter control.

- Methodology aimed to recognise critical points of power system operation is established. It uses matrix decompositions and the functions that are characteristic for appearance and evolution of voltage stability problem. The sensitivities are computed with respect to the load parameters and to the UPFC set of control parameters.

By describing these fundamental characteristics of the voltage stability problem and the UPFC, it is shown that the UPFC is useful transmission system controller thanking to its versatile regulation capabilities. Furthermore, the UPFC injection model with proposed control system satisfactorily enables these capabilities to be evaluated. Upon their thorough exploration, the UPFC is proven to be capable to alleviate the voltage stability problem.

X. FUTURE WORK

Future work is seen from the scope of the research work that has led to this dissertation. It is basically determined by the issues resulted from the computer analysis. Field activities are not covered. Only those elements that are in tight connection with the thesis goal are forwarded.

Future prospects basically follow decoupled concerns given on the voltage stability issues and the UPFC (or FACTS in general) ones. Some concerns are raised within their coupled issues as well.

Exploration of the voltage stability problem has been carried out intensively within past decade. Still, there exists strong urge for improving models of relevant power system elements.

It is especially valid for a load modelling. Aggregate load characteristics and mid-term recovery process call for being further investigated. Recovery of the reactive power load needs to be related to recovery of the active power. In the dissertation, they are treated separately in the voltage collapse scenario that employs dynamic load model with non-linear recovery. Their causality should be modelled noticing eventual differences in time responses. Also, the impact of the induction motor should be included in restorative intention of the reactive power.

The other important element of the voltage stability problem is related to generator limiters. Only over-excitation limiter is employed in the dissertation, whereas some voltage collapse scenarios have pointed out the need for combining it with generator stator current limiter. It can also have certain impacts to time domain responses.

Proper identification of parameters is of large concern. Well-defined parameters should be provided to relevant models.

Besides improving single models, further methods are sought for analysis of a large system. By making transfer from a rather small test system towards larger real power system configuration, some answers of practical value could be obtained. Perhaps, numerical problems could be associated with the matrix decompositions of a large system and clustering formulation could be considered. Indices that need less computational involvement and are less demanding to an operator still deserve attention. Not only detection of a critical point is important, but its prediction is as well. Indices that predict proximity to a critical point are sought for.

From the FACTS viewpoint, future prospects are mostly dependable on a number of practical applications of the FACTS-controllers. Expecting increased number of their installations, raised concern appears within their co-ordination in overall planning and operational procedures. Systems with several FACTS devices are to be analysed. Possible overlapping or interactions between control systems are to be investigated. Value-added increase of transmission capacity by using FACTS device is to be compared with other solutions. In the dissertation, control system of the UPFC injection model is made to enable regulating capabilities of the device. Advanced approach is needed in determination of the parameters that belong to each individual proportional-integral regulator. In this case, for each operating mode of the UPFC, a different set of gains and time constants is needed. More robust solution is to be found, which could be effective for wider spectrum of the UPFC operation. The UPFC injection model is to be compared with the other existing models.

Being embedded in the multi-machine system, the UPFC needs adequate position in the overall differential-algebraic model. In this dissertation, the UPFC is included only in its algebraic part. By including differential equations of the UPFC control system in the differential part of overall system, more advanced analysis of its control system could be enabled. The voltage collapse within analysed scenarios is avoided by using the UPFC, which provided voltage support and at the end power flow control to increase voltage security index. The analysis has not resulted with any scenario where a voltage collapse would be avoided by redistribution of power flows solely. Perhaps some other test systems exhibit that property of the UPFC operation. Generally, other test systems are sought for, especially the ones that are adequate to reveal other problems, which could be solved by using the UPFC. Other problems concern loop flows, line overloading, cable compensation, corridor of power transmission…

It is seen that many other questions still need answers even within such a narrowly stated field of research. A lot of work is still out there to be done. Further technology development will certainly bring us new surprises.

APPENDICES. TEST SYSTEM DATA

Table A.1 Synchronous generator data

generator	GEN1	GEN2	GEN3	GEN4	GEN5	GEN6
S_n (MVA)	2100	1200	1200	2100	1200	1200
U_n (kV)	25	26	26	25	26	26
$cos\varphi_n$	0.9	0.9	0.9	0.9	0.9	0.9
r (pu)	0.0021	0.0010	0.0010	0.0021	0.0010	0.0010
x_l (pu)	0.228	0.135	0.135	0.228	0.135	0.135
x_d (pu)	1.693	1.79	1.79	1.693	1.79	1.79
x_q (pu)	1.636	1.715	1.715	1.636	1.715	1.715
x_d' (pu)	0.346	0.22	0.22	0.346	0.22	0.22
x_q' (pu)	0.346	0.40	0.40	0.346	0.40	0.40
H (s)	2.00	2.00	2.00	2.00	2.00	2.00
τ_{d0}' (s)	6.58	4.30	4.30	6.58	4.30	4.30
τ_{q0}' (s)	1.50	0.90	0.90	1.50	0.90	0.90

Table A.2 Excitation system data

excitation	GEN1	GEN2	GEN3	GEN4	GEN5	GEN6
K_A (pu/pu)	10	10	10	15	15	15
τ_A (s)	0.05	0.05	0.05	0.05	0.05	0.05
V_{AMAX} (pu)	4.62	4.80	4.80	4.62	4.80	4.80
V_{AMIN} (pu)	-4.16	-4.32	-4.32	-4.16	-4.32	-4.32

Table A.3 Over-excitation limiter data

over-exc	GEN1	GEN2	GEN3	GEN4	GEN5	GEN6
I_{FLM1} (pu)	3.7	3.84	3.84	3.7	3.84	3.84
I_{FLM2} (pu)	2.31	2.40	2.40	2.31	2.40	2.40
$LM2$ (pu)	-3.85	-3.85	-3.85	-3.85	-3.85	-3.85
T_{OEL} (s)	10	5	5	10	5	10
K_2	0.248	0.2	0.2	0.248	0.2	0.248
K_3	2	2	2	2	2.5	2

Table A.4 Speed governor - turbine system data

gov-tur	GEN1	GEN2	GEN3	GEN4	GEN5	GEN6
R	0.04	0.05	0.05	0.04	0.05	0.05
P_{MAX} (MW)	1890	1085	1085	1890	1085	1085
τ_1 (s)	0.18	0.10	0.10	0.18	0.10	0.10
τ_2 (s)	0.0	0.0	0.0	0.0	0.0	0.0
τ_3 (s)	0.04	0.20	0.20	0.04	0.20	0.20
τ_4 (s)	0.20	0.10	0.10	0.20	0.10	0.10
τ_5 (s)	5.00	8.72	8.72	5.00	8.72	8.72
F	0.3	0.3	0.3	0.3	0.3	0.3

Table A.5 Generator step-up transformer data

generator	GEN1	GEN2	GEN3	GEN4	GEN5	GEN6
FROM	BUS7	BUS13	BUS10	BUS14	BUS15	BUS20
TO	GEN1	GEN2	GEN3	GEN4	GEN5	GEN6
t_r	1.050	1.050	1.050	1.063	1.063	1.013
b_T (pu)	-210	-120	-120	-210	-120	-120
S_n (MVA)	2100	1200	1200	2100	1200	1200
U_{B1} (kV)	400	400	400	400	400	400
U_{B2} (kV)	25	26	26	25	26	26
U_{n2} (kV)	25	26	26	25	26	26
$U_{n1}^{(0)}$ (kV)	420	420	420	425	425	405

Table A.6 Data of dynamic load with non-linear recovery

load	BUS19	BUS20
P_L^0 (pu)	10	20
K_{pp}	1	1
T_P (s)	30	30
k_P	350	700
Q_L^0 (pu)	3.106	6.212
K_{qq}	1	1
T_Q (s)	30	30
k_Q	110	220
α	2	2
V_{n0} (pu)	0.96667	0.93722
Θ_{n0} (°)	-44.01	-47.41

Table A.7 LTC transformer data

transformer	LTC1	LTC2
FROM	BUS19	BUS20
TO	BUS23	BUS25
t_r	1	1
b_T (pu)	-120	-240
S_n (MVA)	1200	2400
U_{B1} (kV)	400	400
U_{B2} (kV)	35	35
$U_{n1}^{(0)}$(kV)	400	400
U_{n2} (kV)	35	35
$P_{FR\text{-}TO}$ (pu)	10.008	20.005
$Q_{FR\text{-}TO}$ (pu)	3.100	6.208
DB (pu)	0.01	0.01
T_{d1} (s)	27.5	27.5
T_{d2} (s)	7.5	7.5
T_m (s)	2.5	2.5
n_0	0	0
n_{max}	+24	+24
n_{min}	-24	-24
Δu (%)	5/8	5/8

Table A.8 Shunt capacitor data

shunt	SHUNT1	SHUNT2
BUS	BUS23	BUS25
V_{SHU} (pu)	1.00	1.00
Q_{SHn} (pu)	-1.90	-4.5
V_{n0} (pu)	0.94389	0.91396
Q_{SH0} (pu)	-1.693	-3.759

Table A.9 Equivalent impedance data

impedance	Y_{eq1}	Y_{eq2}
FROM	BUS23	BUS25
TO	BUS24	BUS26
$P_{TO\text{-}FR}$ (pu)	10.008	20.005
$Q_{TO\text{-}FR}$ (pu)	3.814	7.886
$P_{FR\text{-}TO}$ (pu)	-9.857	-19.679
$Q_{FR\text{-}TO}$ (pu)	-3.208	-6.583
g_{eq} (pu)	50	100
b_{eq} (pu)	-200	-400

Table A.10 Static load data

load	SL1	SL2
BUS	BUS24	BUS26
P_L^0 (pu)	3	6
K_{pi}	1	1
k_P	350	700
Q_L^0 (pu)	2	4
K_{qz}	1	1
V_{n0} (pu)	0.91352	0.88201

Table A.11 Thermostatically controlled load data

load	TCL1	TCL2
BUS	BUS24	BUS26
P_0 (pu)	5.82	11.97
V_0 (pu)	1.00	1.00
P_{eTCL0} (pu)	4.857	9.312
V_{n0} (pu)	0.91352	0.88201
K_P	0.1	0.1
K_I	0.5	0.75
T_C (s)	138	138
T_I (s)	50	50
τ_A (°C)	-5	-5
τ_{REF} (°C)	20	20

Table A.12 Induction motor data

motor	IM1	IM2
BUS	BUS24	BUS26
V_{n0} (pu)	0.91352	0.88201
S_{nmot} (MVA)	320	700
$S_{nmot}^{(0)}$(MVA)	233.6	507.4
P_{emot} (pu)	2.000	4.367
Q_{emot} (pu)	1.208	2.583
X_{mag} (pu)	3.08	3.08
H (s)	0.833	0.833
X_S (pu)	0.087	0.087
X_r (pu)	0.162	0.162
R_S (pu)	0.029	0.029
R_r (pu)	0.034	0.034
A	0.8	0.8
C	0.2	0.2
T_{m0} (pu)	0.635	0.635
ω_{m0} (pu)	1.00	1.00

NOTATION

ABREVIATIONS

AC alternating current
AC/DC alternating current/direct current
BUS bus
CONV1 shunt converter of the UPFC
CONV2 series converter of the UPFC
E external
FACTS flexible ac transmission system
GEN generator
HV high voltage
I internal
IM induction motor
L line
LOAD load
LTC load tap changer
LV low voltage
MOT motor
OEL over-excitation limiter
PAR phase angle regulator
PI proportional-integral
PST phase shifting transformer
QBT quadrature booster transformer
SC series compensation
SL static load
SNRM2 second norm of vector
TCL thermostatically controlled load
TEF transient energy function
TEF-(r, γ) series part damping control
TEF-I_q shunt part damping control
UPFC unified power flow controller
ZIP static load model (impedance/current/power)

VARIABLES

GENERATOR

$\overline{V}_n$ generator terminal bus voltage vector
V_n magnitude of voltage vector $\overline{V}_n$
Θ_n angle of voltage vector $\overline{V}_n$
$\overline{V}_n = V_d + jV_q$ generator terminal voltage with d and q-axis components
$\overline{E}'_i$ voltage vector behind generator admittance
$\overline{E}'_{gen} = E'_d + jE'_q$ corrected generator internal voltage with d and q-axis components
$\overline{E}$ generator induced voltage vector
$\overline{E}_I$ q-axis component of induced voltage $\overline{E}$
E_I magnitude of generator q-axis component $\overline{E}$
$\overline{I}_{gen} = I_d + jI_q$ terminal current with d and q-axis components
P_n, Q_n generator nominal active and reactive power
δ angle between referent and generator q-axis
ω generator rotor speed
D generator damping coefficient
τ_j constant proportional to generator inertia
τ'_{d0} transient time constants of open circuits in d-axis
τ'_{q0} transient time constants of open circuits in q-axis
r stator resistance
x_d d-axis synchronous reactance
x_q q-axis synchronous reactance
x'_d d-axis transient reactance
x'_q q-axis transient reactance
$1/(r+jx'_d)$ generator internal admittance

EXCITATION SYSTEM

E_{FD} generator excitation voltage
K_A regulator gain in excitation system
τ_A regulator time constant in excitation system
V_{AMAX} r regulator maximum output value
V_{AMIN} regulator minimum output value
V_{REF} excitation referent voltage
V_{OEL} output voltage of over-excitation limiter
OFF1 offset value
I_{FD} generator excitation current
I_{FLM1} short term operation limit of excitation current
I_{FLM2} continuos operation limit of excitation current
K_2, K_3 gains in over-excitation limiter
T_{OEL} time constant in over-excitation limiter

SPEED GOVERNOR - TURBINE SYSTEM

T_m generator mechanical torque
GOV1, *GOV4*, *GOV5*, T_m state variables of speed governor - turbine system
P_{m0} referent power
ω_{REF} referent rotor speed
R droop
P_{MAX}, P_{MIN} turbine power limits
τ_1 to τ_5 time constants
F constant determining aggregate type (hydro/turbo)

TRANSFORMER

t_r transformer tap ratio
$\overline{y}_T$ transformer series admittance
u_k transformer short circuit voltage
$\overline{y}_0$ transformer shunt admittance
i_0 transformer no-load current
$\overline{I}_t$ current behind ideal transformer
$\overline{I}_i$, $\overline{I}_j$ currents at *i* and *j* sides of transformer
$\overline{V}_i$, $\overline{V}_j$ voltages at *i* and *j* sides of transformer
$\overline{I}_{Ti}$, $\overline{I}_{Tj}$ injected currents at *i* and *j* sides

$\overline{S}_{Ti}$, $\overline{S}_{Tj}$ injected apparent powers at *i* and *j* sides

P_{Ti} , Q_{Ti} , P_{Tj} , Q_{Tj} injected active and reactive powers at *i* and *j* sides of transformer

LTC SCHEME

$V^{(TO)}$ voltage magnitude of transformer secondary *j* side
ΔV voltage difference
DB dead-band
ε directional sensitivity tolerance
e output of measuring element
T_d (T_{d1}>T_{d2}) time delay constants of time delay element
b output of time delay element
T_m time constant of motor drive unit and tap changer mechanism
Δn output of motor drive unit and tap changer mechanism
n_i tap position in next step
Δn_i tap change
$n_{(i-1)}$ current tap position
Δu per unit voltage change
$n\ \Delta u$ requested tap position
U_{B1}, U_{B2} primary and secondary side base voltages
U_{n1}, U_{n2} primary and secondary side nominal voltages

SHUNT CAPACITOR

Q_{SHn} nominal reactive power of shunt capacitor bank
b_{SH} shunt susceptance

DISTRIBUTION FEEDER

Z_{eq} equivalent impedance of distribution feeder

INDUCTION MOTOR

$\overline{V}_n = V_d - jV_q$ motor terminal voltage vector with d and q-axis components
$\overline{E}'_{mot} = E'_d - jE'_q$ motor internal voltage vector with d and q-axis components
$\overline{I}_{mot} = I_d - jI_q$ motor terminal current with d and q-axis components
$\overline{V}_e$ equivalent voltage vector
$\overline{I}_S$, $\overline{I}_r$ stator and rotor currents of motor
S_{nmot} motor nominal power
S_B system base power
P_{emot} , Q_{emot} electrical active and reactive powers
ΔP_{emot}, ΔQ_{emot} power changes between two consecutive iterations
ε_P, ε_Q pre-established thresholds of powers
P_{sh} motor shaft power
P_{ag} motor air-gap power
P_{rloss} rotor power loss
s motor slip
ω_{0S} per unit value of stator frequency
ω_m per unit value of rotor speed
T_e, T_m electromagnetic and mechanical torques
s_{Temax} maximum point slip
T_{emax} maximum point torque
a, b, c quadratic equation coefficients
T_{m0} load torque at speed ω_{m0}
A, B, and C coefficients of quadratic, linear and constant terms
D, am factors of initial torque.
$R_m(s)+jX_m(s)$ initial equivalent impedance
R_S, R_r stator and rotor resistances
X_S, X_r stator and rotor leakage reactances
X_{mag} magnetising reactance
R_e equivalent series resistance
X_e equivalent series reactance
g_1+jb_1 admittance between external and internal bus
R_S+jX' motor impedance
R_S stator resistance
X' derived reactance
X reactance
T_0' constant
H motor inertia constant

TCL LOAD

G conductance of TCL
V_n bus voltage magnitude of TCL
P_{eTCL} active load power of TCL
K_P, K_I gains of proportional-integral leading TCL branch
T_C integral time constant of proportional-integral leading TCL branch
G_{MAX} maximum conductance value
τ_{REF} referent temperature
τ_H temperature of heated space
T_I lag term time constant
τ_A ambient temperature
$K_1GV_n^2$ term proportional to active power consumption
K_1 gain

STATIC LOAD

V_n bus voltage magnitude of static load
Δf bus frequency change of static load
V_{n0} bus voltage magnitude at initial steady state
P_L^0 active power demand at V_{n0}
K_{pz}, K_{pi},, K_{pp} proportionality coefficients for voltage dependent part of power
K_{p1}, n_{pv1}, and n_{pf1} proportionality coefficients of voltage/frequency dependent parts
$(P_L^0)_{SL}$ and $(Q_L^0)_{SL}$ static parts of initial active and reactive power demands of static loads.

DYNAMIC LOAD MODEL WITH NON-LINEAR RECOVERY

P_d consumed dynamic active power

T_P	time constant of recovery process
P_S	static active power characteristic
V_n	bus voltage magnitude
$k_P(V_n)$	voltage dependable function
x_P	state variable of load active power
$P_t(V)$	active power transient function
dx_P/dt	derivative of state variable
ΔP_{d0}	initial change of consumed active power
V_{n0-}, V_{n0+}	bus voltage magnitude before and immediately after disturbance
$\Delta P_{d\infty}$	final change of consumed active power
V_{n0-}, $V_{n\infty}$	initial and final values of bus voltage magnitude V_n
$(P_L^0)_{DL}$, $(Q_L^0)_{DL}$	static parts of initial active and reactive power demands of dynamic loads with non-linear recovery

NETWORK

n_{BUS}	number of network buses
n_{GEN}, n_{MOT}	number of internal generator/motor buses
n	total number of network and internal generator/motor buses
$[Y]=[G]+j[B]$	bus admittance matrix
G_{km}, B_{km}	elements of bus admittance matrix
P_{EI} , Q_{EI}	active and reactive power flows from external to internal bus

UPFC

x_S	reactance seen from terminals of series transformer
x_k	series transformer reactance
b_S	series branch susceptance
$\overline{V}_S$	injected series voltage vector
r	magnitude of injected voltage vector
r_{max}	maximum per unit value of injected voltage magnitude
γ	angle of injected voltage vector
$\overline{S}_{conv1}$	apparent power of shunt converter
S_{conv1n}	nominal rating power of shunt converter
S_{conv1}	actual value of shunt converter apparent power
P_{conv1}	active power of shunt converter
Q_{conv1}	reactive power of shunt converter
$\overline{S}_{conv2}$	apparent power of series converter
S_{conv2n}	nominal rating power of series converter
S_{conv2}	actual value of series converter apparent power
P_{conv2}	active power of series converter
Q_{conv2}	reactive power of series converter
S_S	initial estimation for series converter rating power
$\overline{S}_{iS}$, $\overline{S}_{jS}$	series voltage source apparent power injections into buses
P_{Si} , Q_{Si} , P_{Sj} , Q_{Sj}	active and reactive power injections out of buses
P_{i1} , Q_{i1}	active and reactive power flow into i bus
P_{j2} , Q_{j2}	active and reactive power flow into j bus
$\overline{I}_S$	Norton equivalent current
$\overline{I}_{conv1} = I_{conv1p} + jI_{conv1q}$	total current of shunt converter with active and reactive parts
I_{conv1n}	nominal rating current
$I_{conv1q}^{\max}$	maximum reactive current capability of shunt converter
$\overline{I}_{ij}$	current flowing through the injected voltage source
I_{ij} , φ	magnitude and angle of current $\overline{I}_{ij}$
Θ and V	voltage angles and magnitudes
$\overline{V}_i$	shunt side network bus voltage
V_i	shunt side bus voltage magnitude
Θ_i	shunt side bus voltage angle
$\overline{V}_j$	series side network bus voltage
V_j	series side bus voltage magnitude,
Θ_j	series side bus voltage angle
Θ_{ij}	angle difference between Θ_i and Θ_j
$\overline{V}_i'$	voltage vector behind voltage source
$\overline{V}_{comp}$	compensating voltage vector
V_{comp}	compensating voltage magnitude
φ_{comp}	compensating voltage angle
$I_{conv1qREF}$	reference value of shunt reactive current
ΔV_{SVG}	voltage change of full range shunt reactive power compensation
V_{LOW} and V_{UPP}	voltage limits
V_{inom}	nominal shunt side bus voltage magnitude
x	current overload level
x_{cont}	continuous operation limit
x_{max}	maximum short-term limit
t	time variable
T_1, T_2, T_3	time spans
K_{ivi}	gain of shunt proportional-integral regulator
T_{ivi}	time constant of shunt proportional-integral regulator
T_{vis}	lagging time constant of shunt feedback
k_c	proportionality factor
Θ_{ijREF}	referent angle difference of Θ_{ij}-feedback
φ_{comp}^{REF}	referent value of angle φ_{comp}
V_{comp}^{REF}	referent value of voltage V_{comp}
K_r, T_{ir}	gain and time constant of V_j-feedback
V_{jREF}	referent voltage magnitude of V_j-feedback
K_γ, $T_{i\gamma}$	gain and time constant of P_{j2}-feedback
P_{j2REF}	referent active power flow of P_{j2}-feedback
K_Q, T_{iQ}	gain and time constant of Q_{j2}-feedback
Q_{j2REF}	referent reactive power flow of Q_{j2}-feedback
K_{zQ}, T_{zQ}	gain and time constant of Q_{conv2}-feedback
K_{zp}, T_{zp}	gain and time constant of P_{conv2}-feedback
K_{rpst}, T_{rpst}	gain and time constant of PST feedback
K_{gpst}, T_{gpst}	gain and time constant of PST feedback
V_i-V_j	voltage magnitude difference at i and j-side
dV_i/dt	derivative of shunt side bus voltage magnitude
$d\Theta_{ij}/dt$	derivative of bus voltage angle difference
$\dot{\nu}_{sh}$	shunt part damping control function

k_l, k_k shunt damping factors
ΔI_{qTEF} shunt reactive current damping output
$\dot{v}_{ser}$ series part damping control function
k_j, k_i series damping factors
Δr_{TEF} series magnitude damping output
$\Delta\gamma_{TEF}$ series angle damping output

DIFFERENTIAL-ALGEBRAIC MODEL

x state variables
y algebraic variables
p arbitrary parameters
f differential equations
g algebraic equations
$\frac{dx}{dt}$ state variable derivative
$\Delta\frac{dx}{dt}$ differential of state variable derivative
Δx , Δy , Δp differentials of state, algebraic and parameter variables
$\frac{\partial x}{\partial p}$, $\frac{\partial y}{\partial p}$ parametric sensitivities of state and algebraic variables with respect to arbitrary parameters
f_x , f_y , f_p partial derivatives of differential equations with respect to state, algebraic and parameter variables
g_x , g_y , g_p partial derivatives of algebraic equations with respect to state, algebraic and parameter variables
J_{EXT} extended Jacobian matrix
g_{y1}, g_{y2}, g_{y3} , g_{y4} minor sub-matrices of g_y
g_{y1} ordinary Jacobian load flow matrix
$[J]_{LF}$ sub-matrix of ordinary steady state Jacobian matrix
A_S state matrix
σ_n and λ_n critical singular and eigenvalues
u_n, v_n, f_n, e_n associated left and right critical vectors
σ_n minimum singular value.
U matrix of left singular vectors u_i,
V matrix of right singular vectors v_i,
Σ diagonal matrix of singular values σ_i
$\frac{\partial\sigma_n}{\partial p}$ sensitivity of minimum singular value with respect to parameter p
$\partial\sigma_n/\partial r$, $\partial\sigma_n/\partial\gamma$ sensitivities of minimum singular value with respect to magnitude r and angle γ
$\partial J_{EXT}/\partial p$ partial derivative of extended Jacobi matrix with respect to parameter p
λ_n critical singular value.
E matrix of right eigenvectors e_i
F matrix of left eigenvectors f_i
Λ diagonal matrix of eigenvalues λ_i
$\frac{\partial\lambda_n}{\partial p}$ sensitivity of critical eigenvalue with respect to parameter p
g_l+jb_l transmission line series admittance
$jb_c/2$ transmission line shunt half-admittance
$\overline{S}_{SE}$ sending end apparent power
Θ_{SE} sending end bus voltage angle
Θ_{RE} receiving end bus voltage angle
Θ_{SR} bus voltage angle difference (Θ_{SE} - Θ_{RE})
V_{SE} sending end bus voltage magnitude
V_{RE} receiving end bus voltage magnitude
$\overline{S}_{RE}$ receiving end apparent power
P_{loss}^{line} , Q_{loss}^{line} line active and reactive power losses
ΔP_{loss}^{line} , ΔQ_{loss}^{line} differentials of line active and reactive power loss
m_{pps} measure of projected parametric sensitivity
(g_r, g_γ, $g_{Iconv1q}$) three-column matrix g_p
$g_r^{(P_i)}$, $g_r^{(P_j)}$, $g_r^{(Q_i)}$, $g_r^{(Q_j)}$ non-zero entries of column vector g_r
$g_\gamma^{(P_i)}$, $g_\gamma^{(P_j)}$, $g_\gamma^{(Q_i)}$, $g_\gamma^{(Q_j)}$ non-zero entries of column vector g_γ
$g_{Iconv1q}^{(Q_i)}$ non-zero entry of column vector $g_{Iconv1q}$
$\eta(x,y)$ scalar quantity
$\frac{\partial\eta}{\partial p}$ sensitivity of scalar quantity
$\partial\eta/\partial x$, $\partial\eta/\partial y$ partial derivatives of scalar function with respect to state and algebraic variables
Q_G^{Σ} total reactive power production of generators
P_{loss} total active power loss
$(d P_{loss} / d p)$ sensitivity of total active power loss with respect to parameter p
dP_{loss}/dr, $dP_{loss}/d\gamma$ sensitivities of total active power loss with respect to magnitude r and angle γ
F_{loss} objective function in power loss case
P_{loss}^{0} base case loss
P_{loss}^{set} desired value of power loss
Δ^{max} maximum permitted deviation of variable
p_k (k = 1, 2, 3) one of the UPFC control parameters
w_{pk} participation factor
A_{kk} , A_{kl} entries of matrix A in power loss case
B_k entries of vector B in power loss case
F_{σ_n} objective function in σ_n case

REFERENCES

[1] Abe S., Hamada N., Isono A., Okuda K., “Load flow convergence in the vicinity of a voltage stability limit,” *IEEE Trans. Power Systems*, vol. PAS-97, no. 6, November 1978, pp. 1983-1993

[2] Agee J., Vu H., "Overexcitation limiter testing and modeling," *Proceedings of the IEEE PES Winter Meeting,* New York, USA, February 1999, pp. 162-165

[3] Ainsworth J., Davies M., Fitz P., Owen K., Trainer D., “Static VAr compensator (STATCOM) based on single-phase chain circuit converters,” *IEE Proc. - Gener. Transm. Distrib.*, vol. 145, no. 4, July 1998, pp. 381-386

[4] Ajjarapu V., Christy C., “The continuation power flow: a tool for steady state voltage stability analysis,” *IEEE Trans. Power Systems*, vol. 7, no. 1, February 1992, pp. 416-423

[5] Ajjarapu V., Lee B., “Bibliography on voltage stability,” *IEEE Trans. Power Systems,* vol. 13, no. 1, February 1998, pp. 115-125

[6] Ajjarapu V., Lee B., “Bifurcation theory and its application to nonlinear dynamical phenomena in an electrical power system,” *IEEE Trans. Power Systems*, vol. 7, no. 1, February 1992, pp. 424-431

[7] Ambriz-Perez H., Acha E., Fuerte-Esquivel C., Dela Torre A., “Incorporation of a UPFC in an optimal power flow using Newton’s method,” *IEE Proc. - Gener. Transm. Distrib.*, vol. 145, no. 3, May 1998, pp. 336-344

[8] Anderson P. M., *Analysis of faulted power systems*, IEEE Press, ISBN 0-7803-1145-0, 1995

[9] Anderson P., “A stability taxonomy,” *Proceedings of the IEEE PES Winter Meeting, Panel Session on Stability Terms and Definitions*, New York, USA, February 1997

[10] Anderson P., Fouad A., *Power system control and stability*, Revised Printing, IEEE Press, ISBN 0-7803-1029-2, 1994

[11] Arabi S., Kundur P., “A versatile FACTS device model for power flow and stability simulations,” *IEEE Trans. Power Systems,* vol. 11, no. 4, November 1996, pp. 1944-1950

[12] Arabi S., Kundur P., Adapa R., “Innovative techniques in modeling UPFC for power system analysis,” *IEEE Trans. Power Systems,* vol. 15, no. 1, February 2000, pp. 336-341

[13] Arnborg S., Andersson G., “Dynamic and static aspects of undervoltage load shedding,” *Proceedings of the 12th Power System Computation Conference*, Dresden, Germany, August 1996, pp. 515-520

[14] Arnborg S., Andersson G., Hill D., Hiskens I., “On influence of load modelling for undervoltage load shedding studies,” *IEEE Trans. Power Systems*, vol. 13, no. 2, May 1998, pp. 395-400

[15] Arnborg S., Andersson G., Hill D., Hiskens I., “On undervoltage load shedding in power systems,” *Electrical Power & Energy Systems*, vol. 19, no. 2, February 1997, pp. 141-149

[16] Arnborg S., *Emergency control of power systems in voltage unstable conditions*, Ph. D. Thesis, TRITA-EES-9701, ISSN 1100-1607, Electric Power Systems, Royal Institute of Technology, Stockholm, Sweden, 1997

[17] Arnborg S., *Undervoltage load shedding in power systems - as a means of emergency control during voltage unstable situations*, Tech. Lic. Thesis, TRITA-EES-9403, ISSN 1100-1607, Electric Power Systems, Royal Institute of Technology, Stockholm, Sweden, 1994

[18] Arrillaga J., *Computer modelling of electrical power systems*, John Wiley & Sons, ISBN 0-471-10406-X, 1983

[19] Avramović B., Fink L., “Energy management systems and control of FACTS,” *Electrical Power & Energy Systems*, vol. 17, no. 3, June 1995, pp. 195-198

[20] Ayasun S., Nwankpa C., and Kwatny H., "Numerical issues in the location of singularity-induced bifurcation points," *Proceedings of the IEEE PES Winter Meeting,* New York, USA, February 1999, pp. 707-712

[21] Baker M., Thanawala H., Young D., Erinmez I., “Static Var compensators enhance a meshed transmission system,” *Proceedings of the CIGRÉ Joint Session 14/37/38 - Technology and benefits of Flexible AC Transmission Systems*, 14/37/38-03, Paris, France, 1992

[22] Balanathan R., Pahalawaththa N., Annakkage U., “Comparative evaluation on the use of UPFC and SVC for voltage control,” *Proceedings of the International Power Engineering Conference IPEC’97*, Singapore, May 1997, pp. 442-447

[23] Barbier C., Barret J., “An analysis of phenomena of voltage collapse on a transmission system,” *Revue Générale de L’Électricité*, tome 89, no. 10, October 1980, pp. 672-690

[24] Begović M., Mills R., “Load identification and voltage stability monitoring,” *IEEE Trans. Power Systems*, vol. 10, no. 1, February 1995, pp. 109-116

[25] Begović M., Phadke A., “Control of voltage stability using sensitivity analysis,” *IEEE Trans. Power Systems*, vol. 7, no. 1, February 1992, pp. 114-123

[26] Begović M., Phadke A., “Dynamic simulation of voltage collapse,” *IEEE Trans. Power Systems*, vol. 5, no. 4, November 1990, pp. 1529-1534

[27] Begović M., Phadke A., “Power system emergency control near voltage instability,” *Proceedings of the 28th Conference on Decision and Control*, Tampa, FL, USA, December 1990, pp. 2179-2180

[28] Begović M., Phadke A., “Voltage stability assessment through measurement of a reduced state vector,” *IEEE Trans. Power Systems,* vol. 5, no. 1, February 1990, pp. 198-203

[29] Berizzi A., Faranda R., Marannino P., Silvestri A., "Optimal control of power flows using FACTS devices," *Proceedings of the 13th Power System Computation Conference - PSCC'99,* Trondheim, Norway, June 1999, pp. 1285-1291

[30] Berizzi A., Finazzi P., Dosi D., Marannino P., Corsi S., “First and second order methods for voltage collapse

assessment and security enhancement," *IEEE Trans. Power Systems*, vol. 13, no. 2, May 1998, pp. 543-551

[31] Berizzi A., Zeng Y.-G., Marannino P., Vaccarini A., Scarpellini P., "A second order method for contingency severity assessment with respect to voltage collapse," *IEEE Trans. Power Systems,* vol. 15, no. 1, February 2000, pp. 81-87

[32] Bertoldi O., Demartini G., Innorta M., Scarpellini P., Mocenigo M., Delfino B., Denegri G., Invernizzi M., "New issues in optimisation and control methods in open access transmission environment," *Proceedings of the CIGRÉ Session*, 38-205, Paris, France, 1998

[33] Bian J., Ramey D., Nelson R., Edris A., "A study of equipment sizes and constraints for a Unified Power Flow Controller," *IEEE Trans. Power Delivery*, vol. 12, no. 3, July 1997, pp. 1385-1391

[34] Bian J., Rastgoufard P., "Power system voltage stability and security assessment," *Electric Power Systems Research*, vol. 30, 1994, pp. 197-201

[35] Bompard E., Carpaneto E., Chicco G., Napoli R., "A dynamic interpretation of the load-flow Jacobian singularity for voltage stability analysis," *Electrical Power & Energy Systems*, vol. 18, no. 6, August 1996, pp. 385-395

[36] Bompard E., Carpaneto E., Chicco G., Napoli R., "Analysis and modelling of thermostatically-controlled loads," *Proceedings of the 8th Mediterranean Electrotechnical Conference MELECON'96*, May 1996, Bari, Italy, pp. 730-734

[37] Bompard E., Carpaneto E., Chicco G., Napoli R., "Asynchronous motor models for voltage stability analysis," *Proceedings of the International Seminar on Bulk Power System Voltage Phenomena - III, Voltage Stability, Security and Control*, Davos, Switzerland, August 1994, pp. 489-499

[38] Borghetti A., Caldon R., Mari A., Nucci C., "Modelling of generic dynamic loads for voltage collapse numerical simulations," *Proceedings of the 32nd Universities Power Engineering Conference UPEC'97*, Manchester, UK, September 1997, pp. 971-974

[39] Borghetti A., Caldon R., Mari A., Nucci C., "On dynamic load models for voltage stability studies," *IEEE Trans. Power Systems,* vol. 12, no. 1, February 1997, pp. 293-303

[40] Bourgin F., Testud G., Heilbronn B., Verseille J., "Present practices and trends on the French power system to prevent voltage collapse," *IEEE Trans. Power Systems*, vol. 8, no. 3, May 1993, pp. 778-788

[41] Caldon R., Mari A., Paolucci A., Turri R., "An efficient modular model for static and dynamic analysis of FACTS performances on electric power systems," *Proceedings of the IEEE Power Tech'99 Conference - BPT'99,* Budapest, Hungary, August 1999, paper BPT99-138-44

[42] Cañizares C., "On bifurcations, voltage collapse and load modelling," *IEEE Trans. Power Systems*, vol. 10, no. 1, February 1995, pp. 512-522

[43] Cañizares C., Faur Z., "Analysis of SVC and TCSC controllers in voltage collapse," *IEEE Trans. Power Systems,* vol. 14, no. 1, February 1999, pp. 158-165

[44] Cañizares C., Rosehart W., "Bifurcation analysis of induction motor loads for voltage collapse studies," *Proceedings of the 28th North American Power Symposium NAPS'96*, M.I.T., MA, USA, November 1996, pp. 559-565

[45] Cañizares C., Souza A., Quintana V., "Comparison of performance indices for detection of proximity to voltage collapse," *IEEE Trans. Power Systems,* vol. 11, no. 3, August 1996, pp. 1441-1450

[46] Carbone F., Castellano G., Moreschini G., "Coordination and control of tap changers under load at different voltage level transformers," *Proceedings of the 8th Mediterranean Electrotechnical Conference MELECON'96*, May 1996, Bari, Italy, pp. 1646-1648

[47] Chen A., Nwankpa C., Kwatny H., Yu X., "Voltage stability toolbox: an introduction and implementation," *Proceedings of the 28th North American Power Symposium NAPS'96*, M.I.T., MA, USA, November 1996, pp. 343-349

[48] Chen H., Andersson G., "A versatile approach for the control of FACTS equipment in multimachine power systems," *Electrical Power & Energy Systems*, vol. 17, no. 3, June 1995, pp. 215-222

[49] Chiang H., Jean-Jumeau R., "Toward a practical performance index for predicting voltage collapse in electric power systems," *IEEE Trans. Power Systems,* vol. 10, no. 2, May 1995, pp. 584-592

[50] Chiang H., Jean-Jumeau R., "A more efficient formulation for computation of the maximum loading points in electric power systems," *IEEE Trans. Power Systems*, vol. 10, no. 2, May 1995, pp. 635-646

[51] Chiang H., Jean-Jumeau R., "Toward a practical performance index for predicting voltage collapse in electric power systems," *IEEE Trans. Power Systems*, vol. 10, no. 2, May 1995, pp. 584-592

[52] Choi S., Jiang F., Shrestha G., "Suppression of transmission system oscillations by thyristor-controlled series compensation," *IEE Proc. - Gener. Transm. Distrib.*, vol. 143, no. 1, January 1996, pp. 7-12

[53] Chow J., Fischl R., Yan H., "On the evaluation of voltage collapse criteria," *IEEE Trans. Power Systems*, vol. 5, no. 2, May 1990, pp. 612-620

[54] Christensen J., "New control strategies for utilizing power system network more effectively," *ÉLECTRA*, no. 173, August 1997, pp. 5-16

[55] Christl N., Hedin R., Sadek K., Lützelberger P., Krause P., McKenna S., Montoya A., Torgerson D., "Advanced series compensation (ASC) with thyristor controlled impedance," *Proceedings of the CIGRÉ Joint Session 14/37/38 - Technology and benefits of Flexible AC Transmission Systems*, 14/37/38-05, Paris, France, 1992

[56] CIGRÉ TF 11 WG38.02, *Indices predicting voltage collapse including dynamic phenomena*, Report, 1994

[57] CIGRÉ TF 14/37/38/39.24, *FACTS technology for open access*, Report, 2001

[58] CIGRÉ TF 14-19, *Static synchronous compensator (STATCOM)*, Report, 1999

[59] CIGRÉ TF 14-27, *Unified Power Flow Controller (UPFC)*, Report, 2000

[60] CIGRÉ TF 34-08, *Protection against voltage collapse*, Report, 1998

[61] CIGRÉ TF 38-01-03, *Planning against voltage collapse*, Report, 1986

[62] CIGRÉ TF 38-01-06, *Load flow control in high voltage power systems using FACTS controllers*, Report, 1996

[63] CIGRÉ TF 38-01-07, *Analysis and control of power system oscillations*, Report, 1996

[64] CIGRÉ TF 38-02-10, *Modelling of voltage collapse including dynamic phenomena*, Report, 1993

[65] CIGRÉ TF 38-02-12, *Criteria and countermeasures for voltage collapse*, Report, 1995

[66] CIGRÉ TF 38-02-16, *Impact of interactions among power system controls*, Report, 2000

[67] CIGRÉ TF 39.02, "Voltage and reactive control," *ÉLECTRA*, no. 173, August 1997, pp. 115-141

[68] CIGRÉ WG 39.04, "Coordination of protective relays and controls of generating sets under abnormal voltage conditions on the network," *Proceedings of the CIGRÉ Symposium*, 3A-03, Montréal, Canada, 1991

[69] Cinieri E., Carrus A., Gatta F.M., "Improving the system security in a weak HV grid by means of coordinated FACTS," *Proceedings of the IASTED International Conference - Power and Energy Systems,* Las Vegas, Nevada, USA, November 1999, pp. 94-100

[70] Clark H. K., "New challenge: voltage stability," *IEEE Power Engineering Review*, April 1990, pp. 33-37

[71] Clerici A., Di Manici G., Testi G., Valfre L., Paris L., "Means to enhance the capability of existing transmission facilities*," Proceedings of the CIGRÉ Joint Session 14/37/38 - Technology and benefits of Flexible AC Transmission Systems*, 14/37/38-06, Paris, France, 1992

[72] Concordia C., "Voltage instability," *Electrical Power & Energy Systems*, vol. 13, no. 1, 1991, pp. 14-20

[73] Costi A., Shu L., Schlueter R., "Power system voltage stability and controllability*," Proceedings of the IEEE International Symposium on Circuits and Systems*, San Jose, California, USA, 1986, pp. 1023-1027

[74] Criado R., Rouco L., Rodriguez J., Noroozian M., "Improvement of the dynamic performance of the Spanish power system with FACTS devices," *Proceedings of the CIGRÉ Session*, 14-109, Paris, France, 1998

[75] Crow M., Chen J., "The multirate simulation of FACTS devices in power system dynamics*," IEEE Trans. Power Systems*, vol. 11, no. 1, February 1996, pp. 376-382

[76] Ćalović M., "Modeling and analysis of under-load tap-changing transformer control systems," *IEEE Trans. Power Systems*, vol. PAS-103, no. 7, July 1984, pp. 1909-1915

[77] Daniel D., Le Du A., Poumarede C., Therond P., Langlet B., Taisne J., Collet-Billon V., "Power electronics: an effective tool for network development? An Electricité de France answer based on the development of a prototype Unified Power Flow Controller," *Proceedings of the CIGRÉ Symposium*, 520-02, Tokyo, Japan, 1995

[78] Davy R., *Energy functions for power systems with load dynamics*, M. S. Thesis, Department of Electrical and Computer Engineering, The University of Newcastle, Newcastle, Australia, September 1996

[79] De Oliveira M., Ekström Å., "Performance of a real-time model of a Unified Power Flow Controller under unbalanced conditions," *Proceedings of the 3rd International Conference on Digital Power System Simulators - ICDS'99,* Vasteras, Sweden, May 1999

[80] De Oliveira M., *Theoretical analysis and real-time simulator studies of an advanced Static Var Compensator*, Tech. Lic. Thesis, TRITA-EHE-9602, ISSN 1100-1615, High Power Electronics, Royal Institute of Technology, Stockholm, Sweden, 1996

[81] De Souza A., Cañizares C., Quintana V., "Critical bus and point of collapse determination using tangent vectors," *Proceedings of the 28th North American Power Symposium NAPS'96*, M.I.T., MA, USA, November 1996, pp. 329-333

[82] Delfino B., Denegri G., Invernizzi M., Morini A., "Voltage stability of power systems: Links between static and dynamic approaches," *Proceedings of the 8th Mediterranean Electrotechnical Conference MELECON'96*, May 1996, Bari, Italy, pp. 854-858

[83] DeMarco C., Overbye T., "An energy based security measure for assessing vulnerability to voltage collapse*," IEEE Trans. Power Systems*, vol. 5, no. 2, May 1990, pp. 419-427

[84] Deuse J., Stubbe M., "Dynamic simulation of voltage collapses," *IEEE Trans. Power Systems*, vol. 8, no. 3, August 1993, pp. 894-904

[85] Deuse J., Stubbe M., Meyer B., Panciatici P., "Modelling of FACTS for power system analysis," *Proceedings of the CIGRÉ Symposium*, 320-04, Tokyo, Japan, 1995

[86] Dobson I., Lu L., "New methods for computing a closest saddle node bifurcation and worst case load power margin for voltage collapse," *IEEE Trans. Power Systems*, vol. 8, no. 3, August 1993, pp. 905-913

[87] Dwyer A., Nielsen R., Stangl J., "Load to voltage dependency tests at B. C. Hydro," *IEEE Trans. Power Systems*, vol. 10, no. 2, May 1995, pp. 709-715

[88] Edris A., "FACTS technology development: an update," *IEEE Power Engineering Review*, vol. 20, no. 3, March 2000, pp. 4-9

[89] Edris A., Mehraban A., Rahman M., Gyugyi L., Arabi S., Reitman T., "Controlling the flow of real and reactive power," *IEEE Computer Application in Power*, vol. 11, no. 1, January 1998, pp. 20-25

[90] Edris A.A., "Challenges and benefits in developing and applying FACTS technology in the USA," *Proceedings of the IEEE Power Tech'99 Conference - BPT'99,* Budapest, Hungary, August 1999, paper BPT99-376-44

[91] Edström A., Walve K., "A highly interactive fast simulator covering transient stability and long term

dynamics in large power systems," *Proceedings of the CIGRÉ Session*, 38-204, Paris, France, 1994

[92] Ejebe G., Irisari G., Mokhtari S., Obadina O., Ristanovic P., and Tong J., "Methods for contingency screening and ranking for voltage stability analysis of power systems," *IEEE Trans. Power Systems,* vol. 11, no. 1, February 1996, pp. 350-356

[93] El-Kateb M., Abdelkader S., Kandil M., "Linear indicator for voltage collapse in power systems*," IEE Proc. - Gener. Transm. Distrib.,* vol. 144, no. 2, March 1997, pp. 139-146

[94] Erche M., Lerch E., Povh D., Mihalič R., "Improvement of power system performance using power electronic equipment," *Proceedings of the CIGRÉ Joint Session 14/37/38 - Technology and benefits of Flexible AC Transmission Systems*, 14/37/38-02, Paris, France, 1992

[95] Fardanesh B., Henderson M., Shperling B., Zelingher S., Gyugyi L., Schauder C., Lam B., Mountford J., Adapa R., Edris A., "Convertible static compensator application to the New York transmission system," *Proceedings of the CIGRÉ Session*, 14-103, Paris, France, 1998

[96] Faur Z., *Effects of FACTS devices on static voltage collapse phenomena*, M. S. Thesis, University of Waterloo, Waterloo, Ontario, Canada, 1996

[97] Feng Z., Ajjarapu V., Maratukulam D., "A comprehensive approach for preventive and corrective control to mitigate voltage collapse," *IEEE Trans. Power Systems,* vol. 15, no. 2, May 2000, pp. 791-797

[98] Flatabø N., Fosso O., Ognedal R., Carlsen T., Heggland K., "A method for calculation of margins to voltage instability applied on the Norwegian system for maintaining required security level," *IEEE Trans. Power Systems*, vol. 8, no. 3, August 1993, pp. 920-928

[99] Flatabø N., Ognedal R., Carlsen T., "Voltage stability in a power transmission system calculated by sensitivity methods," *IEEE Trans. Power Systems*, vol. 5, no. 4, November 1990, pp. 1286-1293

[100] Fuerte-Esquivel C. R., Acha E., Ambriz-Perez H., "A comprehensive Newton-Raphson UPFC model for the quadratic power flow solution of practical power networks," *IEEE Trans. Power Systems,* vol. 15, no. 1, February 2000, pp. 102-109

[101] Fuerte-Esquivel C., Acha E., "Unified power flow controller: a critical comparison of Newton-Raphson UPFC algorithms in power flow studies," *IEE Proc. - Gener. Transm. Distrib.*, vol. 144, no. 5, September 1997, pp. 437-444

[102] Galiana F., Zeng Z., "Analysis of the load flow behaviour near a Jacobian singularity," *IEEE Trans. Power Systems,* vol. 7, no. 3, August 1992, pp. 1362-1369

[103] Gampenrieder R., Gick B., Wess T., Häusler M., Rittiger J., Glaunsinger W., Zimmermann U., "Load-flow control in EHV networks - Feasibility study on the possibilities of Facts application in Germany," *Elektrizitatswirtschaft*, Jg. 97, 1998, pp. 14-20

[104] Gampenrieder R., Gick B., Wess T., Hausler M., Rittiger J., Glaunsinger W., Zimmermann U., "Load-flow control in EHV networks - Feasibility study on the possibilities of application of FACTS elements in the German power system," *Proceedings of the CIGRÉ Session*, 14-110, Paris, France, 1998

[105] Gao B, Morison G., Kundur P., "Towards the development of a systematic approach for voltage stability assessment of large-scale power systems," *IEEE Trans. Power Systems*, vol. 11, no. 3, August. 1996, pp. 1314-1324

[106] Gao B., Morison G., Kundur P., "Voltage stability evaluation using modal analysis," *IEEE Trans. Power Systems*, vol. 7, no. 4, November 1992, pp. 1529-1542

[107] Ge S.Y., Chung T.S., "Optimal active power flow incorporating power flow control needs in flexible AC transmission systems," *IEEE Trans. Power Systems*, vol. 14, no. 2, May 1999, pp. 738-744

[108] Gebreselassie A., Chow J., "Investigation of the effects of load models and generator voltage regulators on voltage stability," *Electrical Power & Energy Systems*, vol. 16, no. 2, 1994, pp. 83-89

[109] Ghandhari M., Andersson G., "Two various control laws for controllable series capacitor (CSC)," *Proceedings of the IEEE Power Tech'99 Conference - BPT'99,* Budapest, Hungary, August 1999, paper BPT99-181-12

[110] Ghandhari M., *Control Lyapunov Functions: a control strategy for damping of power oscillations in large power systems*, Ph.D. Thesis, TRITA-EES-0004, ISSN 1100-1607, Electric Power Systems, Royal Institute of Technology, Stockholm, Sweden, 2000

[111] Ghandhari M., *Control of power oscillations in transmission systems using controllable series devices*, Lic. Thesis, TRITA-EES-9705, ISSN 1100-1607, Electric Power Systems, Royal Institute of Technology, Stockholm, Sweden, 1997

[112] Gjerde J., Flølo R., Gjengedal T., "Use of HVDC and FACTS-components for enhancement of power system stability," 1996, pp. 802-808

[113] Godhwani A., Kim K., and Basler M., "An under and over excitation limiter implementation in a digital excitation system for synchronous generators," *Proceedings of the IEEE PES Winter Meeting,* New York, USA, February 1999, pp. 193-195

[114] Gotham D., Heydt G., "Power flow control and power flow studies for systems with FACTS devices," *IEEE Trans. Power Systems*, vol. 13, no. 1, February 1998, pp. 60-65

[115] Grainger J., *Power system analysis*, McGraw-Hill, ISBN 0-07-061293-5, 1994

[116] Greene S., *Margin and sensitivity methods for security analysis of electric power systems*, Ph. D. Thesis, University of Wisconsin - Madison, Madison, Wisconsin, USA, 1998

[117] Griffin J., Atanacković D., Galiana F., "A study of the impact of FACTS on the secure-economic operation of power systems," *Proceedings of the 12th Power Systems Computation Conference PSCC'96*, Dresden, Germany, August 1996, pp. 1077-1082

[118] Gronquist J., Sethares W., Lasseter R., "Power swing damping control strategies for FACTS devices based upon locally measurable information," *Proceedings of the CIGRÉ Symposium*, 520-05, Tokyo, Japan, 1995

[119]Gubina F., Grgič D., Strmčnik B., "An alternative approach to voltage instability assessment*," Proceedings of the CIGRÉ Session*, 39-110, Paris, France, 1998

[120]Gubina F., Strmčnik B., "A simple approach to voltage stability assessment in radial networks," *IEEE Trans. Power Systems*, vol. 12, no. 3, August 1997, pp. 1121-1128

[121]Gubina F., Strmčnik B., "Voltage collapse proximity index determination using voltage phasors approach," *IEEE Trans. Power Systems*, vol. 10, no. 2, May 1995, pp. 788-794

[122]Gustafsson M., Krantz N., Daalder J., "Voltage stability: significance of load characteristics and current limiters," *IEE Proc. - Gener. Transm. Distrib*., vol. 144, no. 3, May 1997, pp. 257-262

[123]Gustafsson M., Krantz N., *Voltage collapse in power systems - Analysis of component related phenomena using a power system model*, Tech. Lic. Thesis, Technical Report no. 215L, Department of Electrical Power Engineering, School of Electrical and Computer Engineering, Chalmers University of Technology, Göteborg, Sweden, 1995

[124]Gyugyi L., "Dynamic compensation of AC transmission lines by solid-state synchronous voltage source*," IEEE Trans. Power Delivery*, vol. 9, no. 2, April 1994, pp. 904-911

[125]Gyugyi L., "Unified power-flow control concept for Flexible AC Transmission Systems," *IEE Proc. - C*, vol. 139, no. 4, July 1992, pp. 323-331

[126]Gyugyi L., Schauder C., Sen K., "Static Synchronous Series Compensator: a solid-state approach to the series compensation of transmission lines," *IEEE Trans. Power Delivery*, vol. 12, no. 1, January 1997, pp. 406-417

[127]Gyugyi L., Schauder C., Williams S., Rietman T., Torgerson D., Edris A., "The Unified Power Flow Controller for independent p and q flow control in transmission lines," *Proceedings of the Conference on Flexible AC Transmission Systems (FACTS 3): The Future in High-voltage Transmission*, Baltimore, MD, USA, October 1994

[128]Gyugyi L., Schauder C., Williams S., Rietman T., Torgerson D., Edris A., "The Unified Power Flow Controller: a new approach to power transmission control," *IEEE Trans. Power Delivery*, vol.10, no. 2, April 1995, pp. 1085-1097

[129]Gyugyi L., *Solid-state synchronous voltage sources for dynamic compensation and real-time control of AC transmission lines***,** IEEE Emerging Practices in Technology, IEEE Standards Press, 1993

[130]Hajagos L., Danai B., "Laboratory measurements and models of modern loads and their effect on voltage stability studies," *IEEE Trans. Power Systems,* vol. 13, no. 2, May 1998, pp. 584-592

[131]Hammad A., "Comparing the voltage control capabilities of present and future Var compensating techniques in transmission systems," *IEEE Trans. Power Delivery*, vol. 11, no. 1, January 1996, pp. 475-484

[132]Hanson A., Grigsby L., "Current source modeling of FACTS devices for power flow studies," *Proceedings of the 28th North American Power Symposium NAPS'96*, M.I.T., MA, USA, November 1996, pp. 173-178

[133]Hatziadoniu C., Funk A., "Development of a control scheme for a series-connected solid-state synchronous voltage source," *IEEE Trans. Power Delivery*, vol. 11, no. 2, April 1996, pp. 1138-1144

[134]Herbig A., Andersson G., "Control of power flows in transmission systems*," Proceedings of the International Power Engineering Conference IPEC'97*, Singapore, May 1997, pp. 431-435

[135]Herbig A., *On load flow control in electric power systems*, Ph. D. Thesis, TRITA-EES-0001, ISSN 1100-1607, Electric Power Systems, Royal Institute of Technology, Stockholm, Sweden, 2000

[136]Herbig A., *On load flow control using TCSC and PAR,* Technical report, Royal Institute of Technology, Stockholm, Sweden, November 1997

[137]Hill D., "Nonlinear dynamic load models with recovery for voltage stability studies," *IEEE Trans. Power Systems*, vol. 8, no. 1, February 1993, pp. 166-176

[138]Hill D., Hiskens I., "Modelling, stability and control of voltage behaviour in power supply systems," Invited paper, *Proceedings of the IV Symposium of Specialists in Electric Operational and Expansion Planning*, Foz do Iguacu, Brazil, May 1994

[139]Hill D., Hiskens I., "On definitions for power system stability," *Proceedings of the IEEE PES Winter Meeting*, *Panel Session on Stability Terms and Definitions*, New York, USA, February 1997

[140]Hill D., Hiskens I., Popović D., "Stability analysis of power system loads with recovery dynamics," *Electrical Power & Energy Systems*, vol. 16, no. 4, 1994, pp. 277-286

[141]Hill D., Löf P.-A., Andersson G., "Analysis of long-term voltage stability*," Proceedings of the 10th Power System Computation Conference PSCC'90*, Graz, Austria, 1990, pp. 1252-1259

[142]Hingorani N., "Flexible AC transmission ," *IEEE Spectrum*, vol. 30, no. 4, April 1993, pp. 40-45

[143]Hingorani N., "High power electronics and Flexible AC Transmission System," *IEEE Power Engineering Review*, July 1988, pp. 3-4

[144]Hingorani N., "Power electronics in AC power transmission systems," *Proceedings of the CIGRÉ Session - Panel 1*, P1-00, Paris, France, 1996

[145]Hingorani N., Gyugyi L., *Understanding FACTS: Concepts and Technology of Flexible AC Transmission Systems,* IEEE Press, ISBN 0-7803-3455-8, 2000

[146]Hingorani N., Stahlkopf K., "High-power electronics," *Scientific American*, vol. 269, no. 5, November 1993, pp. 52-59

[147]Hiskens I., Chakrabarti B., "Direct calculation of reactive power limit points," *Electrical Power & Energy Systems*, 1995, pp. 121-129

[148]Hitzeroth H.V., Braisch D., Herold G., Povh D., "Compensation, stability and losses in the presence of wheeling transactions with use of FACTS devices," *Proceedings of the IEEE Power Tech'99 Conference - BPT'99,* Budapest, Hungary, August 1999, paper BPT99-397-12

[149]Hojo M., "Power system stabilization based on power swing linearization controlled by UPFC," *Proceedings of the IEEE Power Tech'99 Conference - BPT'99,* Budapest, Hungary, August 1999, paper BPT99-377-12

[150]Hu L., Morrison R., "Simulation study of a transmission system containing two unequally rated parallel lines and UPFC," *Proceedings of the IEE AC and DC Power Transmission Conference*, Conference Publication no. 423, April 1996, pp. 346-350

[151]Huang Z., Ni Y.., Shen C., Wu F., Chen S., Zhang B., "Application of Unified Power Flow Controller in interconnected power systems - modelling, interface, control strategy, and case study," *IEEE Trans. Power Systems,* vol. 15, no. 2, May 2000, pp. 817-824

[152]Hubbi W., Takashi H., "Placement of static VAR compensators to minimize power system losses," *Electric Power System Research*, vol. 47, 1998, pp. 95-99

[153]IEEE FACTS Terms & Definition Task Force, "Proposed terms and definitions for flexible AC transmission system (FACTS)," *IEEE Trans. Power Delivery*, vol. 12, no. 4, October 1997, pp. 1848-1853

[154]IEEE Power Electronics Modeling Task Force & Digital Simulation Working Group, "Guidelines for modeling power electronics in electric power engineering applications," *IEEE Trans. Power Delivery*, vol. 12, no. 1, January 1997, pp. 505-514

[155]IEEE PSRC WG K12, *Voltage collapse mitigation*, Draft 4.0, IEEE Power System Relaying Committee, 1996

[156]IEEE Task Force on Excitation Limiters, "Recommended models for overexcitation limiting devices," *IEEE Trans. Energy Conversion*, vol. 10, no. 4, December 1995, pp. 706-713

[157]IEEE Task Force on Load Representation for Dynamic Performance, "Bibliography on load models for power flow and dynamic performance simulation," *IEEE Trans. Power Systems*, vol. 10, no. 1, February 1995, pp. 523-538

[158]IEEE Task Force on Load Representation for Dynamic Performance, "Standard load models for power flow and dynamic performance simulation," *IEEE Trans. Power Systems*, vol. 10, no. 3, August 1995, pp. 1302-1313

[159]IEEE, *FACTS Application*, IEEE catalogue number 96TP116-0, 1996

[160]IEEE, *IEEE Guide for synchronous generator modeling practices in stability analyses*, IEEE Std 1110-1991

[161]IEEE, *IEEE Recommended practice for excitation system models for power system stability studies*, IEEE Std 421.5-1992

[162]IEEE, *Suggested techniques for voltage stability analysis*, IEEE catalogue number 93TH0620-5 PWR, 1993

[163]IEEE, *System protection and voltage stability*, Report, ISBN 0-7803-9981-1, June 1993

[164]IEEE, *Voltage stability of power systems: concepts analytical tools, and industry experience*, IEEE catalogue number 90TH0358-2-PWR, 1990

[165]Ilić M., "A survey of the present state-of-the-art voltage control with emphasis on potential role of FACTS devices," *Proceedings of the Bulk Power System Voltage Phenomena II - Voltage Stability and Security*, Deep Creek Lake, MD, USA, August 1991, pp.379-394

[166]Ilić M., "Fundamental engineering problems and opportunities in operating power transmission grids of the future," *Electrical Power & Energy Systems*, vol. 17, no. 3, June 1995, pp. 207-214

[167]Ingelsson B., Lindström P.-O., Karlsson D., Runvik G., Sjödin J.-O., "Special protection scheme against voltage collapse in the south part of the Swedish grid," *Proceedings of the CIGRÉ Session*, 38-105, Paris, France, 1996

[168]Jiang Y., Ekström Å., "A comparison study between UPFC and back-to-back stations," *Proceedings of the International Power Engineering Conference IPEC'97*, Singapore, May 1997, pp. 343-350

[169]Johansson S., Daalder J., "Maximum thermal utilization of generator rotors to avoid voltage collapse," *Proceedings of the International Power Engineering Conference IPEC'97*, Singapore, May 1997, pp. 234-239

[170]Johansson S., Sjögren F., *Voltage collapse in power systems - The influence of generator current limiters, on-load tap changers, and load dynamics*, Tech. Lic. Thesis, Technical Report no. 192L, Department of Electrical Power Systems, School of Electrical and Computer Engineering, Chalmers University of Technology, Göteborg, Sweden, 1995

[171]Jovanović S., Fox B., Hogg B., "Fast decoupled transient load flow," *Electrical Power & Energy Systems*, vol. 17, no. 5, 1995, pp. 301-304

[172]Ju P., Handschin E., Rehtanz C., "A comparative study on the nonlinear dynamic load models," *Proceedings of the 12th Power System Computation Conference PSCC'96*, Dresden, Germany, August 1996, pp. 1069-1074

[173]Ju P., Handschin, Wei Y., Schlücking U., "Sequential parameter estimation of a simplified induction motor load model," *IEEE Trans. Power Systems*, vol. 11, no. 1, February 1996, pp. 319-324

[174]Kannan S., Jayaram S., Salama M., "Application of fuzzy logic for real and reactive power flow control using UPFC," *Proceedings of the 28th North American Power Symposium NAPS'96*, M.I.T., MA, USA, November 1996, pp. 437-444

[175]Kao W., Huang C., "Dynamic load modeling in Tai power system stability studies," *IEEE Trans. Power Systems*, vol. 10, no. 2, May 1995, pp. 907-914

[176]Karlsson D., *Voltage stability simulations using detailed models based on field measurements*, Ph. D. Thesis, Technical Report no. 230, Department of Electrical Power Systems, School of Electrical and Computer Engineering, Chalmers University of Technology, Göteborg, Sweden, 1992

[177]Kataoka Y., "State variable description of dynamic load models in electrical power system analysis," *IEEE Trans. Power Systems*, vol. 10, no. 1, February 1995, pp. 149-157

[178]Keri A., Mehraban A., Lombard X., Elriachy A., Edris A.A., "Unified Power Flow Controller (UPFC): modeling and analysis," *IEEE Trans. Power Delivery*, vol. 14, no. 2, April 1999, pp. 648-654

[179]Keri A., Ware B. J., Byron R. A., Mehraban A. S., Chamia M., Halvarsson P., Ängquist L., "Improving transmission system performance using controlled series capacitors," *Proceedings of the CIGRÉ Joint Session 14/37/38 - Technology and benefits of Flexible AC Transmission Systems*, 14/37/38-07, Paris, France, 1992

[180]Kessel P., Glavitsch H., "Estimating the voltage stability of a power system," *IEEE Trans. Power Delivery*, vol. PWRD-1, no. 3, July 1986, pp. 346-354

[181]Kim T.-H., Seo J.-C., Lim J.-U., Moon S.-I., Park J.-K., and Han B.-M., "A decoupled Unified Power Flow Controller model for power flow considering limit resolution," *Proceedings of the IEEE PES Winter Meeting,* New York, USA, February 1999, pp. 1190-1195

[182]Klump R., Overbye T., "A transmission-based voltage stability measure for available transfer capability (ATC) calculations," *Proceedings of the 28th North American Symposium NAPS'96*, M.I.T., MA, USA, November 1996, pp. 351-357

[183]Knight R., Young D., Trainer D., "Relocatable GTO-based static VAr compensator for NGC substations," *Proceedings of the CIGRÉ Session*, 14-106, Paris, France, 1998

[184]Koessler R., Feltes J., "Time-domain simulation investigates voltage collapse," *IEEE Computer Applications in Power*, vol. 6, no. 4, October 1993, pp. 18-22

[185]Kohno H., Yokoyama A., "Control system design of UPFC for power system damping enhancement taking into account rating of converter during oscillation," *Proceedings of the IEEE Power Tech'99 Conference - BPT'99,* Budapest, Hungary, August 1999, paper BPT99-085-12

[186]Kosterev D., "Modeling synchronous voltage source converters in transmission system planning studies," *IEEE Trans. Power Delivery*, vol. 12, no. 2, April 1997, pp. 947-952

[187]Kundur P., "Evolving techniques for voltage stability analysis," *Proceedings of the IEEE PES Winter Meeting, Panel Session on Recommended Techniques for Voltage Stability Analysis*, New York, USA, February 1994

[188]Kundur P., Morison G., "A review of definitions and classification of stability problems in today's power systems," *Proceedings of the IEEE PES Winter Meeting, Panel Session on Stability Terms and Definitions*, New York, USA, February 1997

[189]Kundur P., Morison G., Balu N., "A comprehensive approach to power system analysis," *Proceedings of the CIGRÉ Session*, 38-106, Paris, France, 1994

[190]Kundur P., Morison K., Gao B., "Practical considerations in voltage stability assessment," *Electrical Power & Energy Systems*, vol. 15, no. 4, 1993, pp. 205-215

[191]Kundur P., *Power system stability and control*, EPRI McGraw-Hill, ISBN 0-07-035958-X, 1994

[192]Löf P.-A., Andersson G., Hill D., "Voltage dependent reactive power limits for voltage stability studies," *IEEE Trans. Power Systems*, vol. 10, no. 1, February 1995, pp. 220-228

[193]Löf P.-A., Andersson G., Hill D., "Voltage stability indices for stressed power systems," *IEEE Trans. Power Systems*, vol. 8, no. 1, February 1993, pp. 326-335

[194]Löf P.-A., Hill D., Arnborg S., Andersson G., "On the analysis of long-term voltage stability," *Electrical Power & Energy Systems*, vol. 15, no. 4, 1993, 229-237

[195]Löf P.-A., *On static analysis of long-term voltage stability in electric power systems*, Ph. D. Thesis, TRITA-EES-9501, ISSN 1100-1607, Electric Power Systems, Royal Institute of Technology, Stockholm, Sweden, 1995

[196]Löf P.-A., Smed T., Andersson G., Hill D., "Fast calculation of a voltage stability index," *IEEE Trans. Power Systems*, vol. 7, no. 1, February 1992, pp. 54-64

[197]Löf P.-A., *Study of long-term voltage stability in electric power systems*, Tech. Lic. Thesis, TRITA-EES-9101, ISSN 1100-1607, Electric Power Systems, Royal Institute of Technology, Stockholm, Sweden, 1991

[198]Lachs W., "Voltage collapse in EHV systems," *Proceedings of the IEEE PES Winter Meeting*, A 78 057-2 PWRS, New York, USA, January 1978

[199]Lachs W., Sutanto D., "Different types of voltage instability," *IEEE Trans. Power Systems*, vol. 9, no. 2, May 1994, pp. 1126-1134

[200]Lachs W., Sutanto D., "Rotor heating as an indicator of system voltage instability," *IEEE Trans. Power Systems*, vol. 10, no. 1, February 1995, pp. 175-181

[201]Lachs W., Sutanto D., "Voltage instability in interconnected power systems: a simulation approach," *IEEE Trans. Power Systems*, vol. 7, no. 2, May 1992, pp. 753-761

[202]Lachs W., Sutanto D., Logothetis D., "Power system control in the next century," *IEEE Trans. Power Systems*, vol. 11, no. 1, February 1996, pp. 11-18

[203]Lagonotte P., "The different electrical distances," *Proceedings of the 10th Power Systems Computation Conference PSCC'90*, Graz, Austria, August 1990, pp. 543-550

[204]Lanyin L., Xiaoyan L., Zuo L., Shousun C., Baolin Z., "Study on prototype Unified Power Flow Controller and its coordinated control," *Proceedings of the IFAC Control of Power Systems and Power Plants*, Beijing, China, August 1997, pp. 197-202

[205]Larsen E., Bowler C., Damsky B., Nilsson S., "Benefits of thyristor controlled series compensation," *Proceedings of the CIGRÉ Joint Session 14/37/38 - Technology and benefits of Flexible AC Transmission Systems*, 14/37/38-04, Paris, France, 1992

[206]Larsen E., Miller N., Nilsson S., Lindgren S., "Benefits of GTO-based compensation systems for electric utility applications," *IEEE Trans. Power Delivery*, vol. 7, no. 4, October 1992, pp. 2056-2064

[207]Lasseter R., Wang R., "The impact of generation mix on placement of static VAr compensators," *IEEE PES Winter Meeting paper PE-105-PWRD-0-10-1998,* New York, USA, February 1999

[208]Le Dous G., Daalder J., Karlsson D., "Dynamic load measurements in a 2000 MW system in order to operate

power systems closer to their limits," *Proceedings of the CIGRÉ Session*, 39-107, Paris, France, 1998

[209]Le Du A., Tontini G., Winfield M., "Which FACTS equipment for which need? Identification of the technology developments to meet the needs of Electricité de France (EDF), Ente per l'Energia Elettrica (ENEL) and National Grid Company (NGC*)," Proceedings of the CIGRÉ Joint Session 14/37/38 - Technology and benefits of Flexible AC Transmission Systems*, 14/37/38-08, Paris, France, 1992

[210]Lee B., Ajjarapu V., Invariant subspace parametric sensitivity (ISPS) of structure-preserving power system models," *IEEE Trans. Power Systems,* vol. 11, no. 2, May 1996, pp. 845-850

[211]Lee B., Lee K., "Dynamic and static voltage stability enhancement of power systems," *IEEE Trans. Power Systems*, vol. 8, no. 1, February 1993, pp. 231-238

[212]Lei X., Lerch E., Povh D., Renz K., "Power electronic equipment for increasing capability of transmission links in interconnected power systems," *Proceedings of the IFAC Control of Power Systems and Power Plants*, Beijing, China, August 1997, pp. 235-240

[213]Lemaître C., Paul J., Tesseron J., Harmand Y., Zhao Y., "An indicator of the risk of voltage profile instability for real-time control applications," *IEEE Trans. Power Systems*, vol. 5, no. 1, February 1990, pp. 154-161

[214]Lemay J., "Meeting the real needs of power transmission networks with FACTS devices (a planner's point of view)," *Proceedings of the Conference on Flexible AC Transmission Systems (FACTS 3): The Future in High-voltage Transmission*, Baltimore, MD, USA, October 1994

[215]Lerch E. Povh D., Witzmann R., Hlebčar B., Mihalič R., "Simulation and performance analysis of Unified Power Flow Controller," *Proceedings of the CIGRÉ Session*, 14-205, Paris, France, 1994

[216]Lerm A., Lemos F., Silva A., "Indices for voltage stability analysis based on eigenvalue sensitivity*," Proceedings of the 29th North American Power Symposium NAPS'97*, Laramie, WY, October 1997, pp. 582-587

[217]Li C., Wang Z., Ma X., Xiu L., "Physical experiments on a ± 10 Kvar STATCOM model," *Proceedings of the IEEE PES Winter Meeting,* New York, USA, February 1999, pp. 1184-1189

[218]Li N., Xu Y., Chen H., "FACTS-based power flow control in interconnected power systems," *IEEE Trans. Power Systems,* vol. 15, no. 1, February 2000, pp. 257-262

[219]Liang Y., Nwankpa C., Fischl R., De Vito A., Readinger S., "Dynamic reactive load model*," IEEE Trans. Power Systems*, vol. 13, no. 4, November 1998, pp.1365-1372

[220]Lima E., Fernandes L., "Assessing eigenvalue sensitivities," *IEEE Trans. Power Systems,* vol. 15, no. 1, February 2000, pp. 299-306

[221]Limyingcharoen S., Annakkage U., Pahalawaththa N., "Effects of unified power flow controllers on transient stability*," IEE Proc. - Gener. Transm. Distrib*., vol. 145, no. 2, March 1998, pp. 182-188

[222]Limyingcharoen S., Annakkage U., Pahalawaththa N., "Fuzzy logic based Unified Power Flow Controllers for transient stability improvement," *IEE Proc. - Gener. Transm. Distrib*., vol. 145, no. 3, May 1998, pp. 225-232

[223]Litzenberger W., Varma R., Flanagan J., "An annotated bibliography of HVDC transmission and FACTS devices 1996-1997," *Bonneville Power Administration - EPRI,* IEEE Working Group 15.05.07 on HVDC and FACTS Bibliography and Records, June 1998

[224]Liu J., Song Y., Foss A., "Digital simulations of the PWM UPFC using EMTP*," Proceedings of the IEE AC and DC Power Transmission Conference*, Conference Publication no. 423, April 1996, pp. 351-356

[225]Liu J., Song Y., Foss A., "Power flow control and voltage support in a meshed power system using Unified Power Flow Controllers," *Proceedings of the 32nd Universities Power Engineering Conference UPEC'97*, Manchester, UK, September 1997, pp. 531-534

[226]Liu J., Song Y.., Mehta P., "Strategies for handling UPFC constraints in steady-state power flow and voltage control," *IEEE Trans. Power Systems,* vol. 15, no. 2, May 2000, pp. 566-571

[227]Liyi C., Tianjiao P., Linchuan L., Lei D., Xi K., "Load flow calculation for Flexible AC Transmission Systems," *Proceedings of the IFAC Control of Power Systems and Power Plants*, Beijing, China, August 1997, pp. 203-206

[228]Lombard X., Therond P., "Control of Unified Power Flow Controller: comparison of methods on the basis of a detailed numerical model," *IEEE Trans. Power Systems*, vol. 12, no. 2, May 1997, pp. 824-830

[229]Lombard X., Therond P., Giard A., Vitet S., "Unified Power Flow Controller impact on the relays in a power system," *Proceedings of the IFAC Control of Power Systems and Power Plants*, Beijing, China, August 1997, pp. 213-218

[230]Long B., Ajjarapu V., "The sparse formulation of ISPS and its application to voltage stability margin sensitivity and estimation," *IEEE Trans. Power Systems,* vol. 14, no. 3, August 1999, pp. 944-957

[231]Long B., Ajjarapu V., "Voltage stability sensitivity and transfer margin estimation*," Proceedings of the 29th North American Power Symposium NAPS'97*, Laramie, WY, October 1997, pp. 588-594

[232]Machowski J., Bialek J., Bumby J., *Power system dynamics and stability*, John Wiley & Sons, ISBN 0 471 97174 X (PPC), 1997

[233]Makarov Y., Popović D., Hill D., "Stabilization of transient processes in power systems by an eigenvalue shift approach," *IEEE Trans. Power Systems*, vol. 13, no. 2, May 1998, pp. 382-388

[234]Maliszewski R., Pasternack B., Chamia M., Frank H., Paulsson L., "Power flow control in a highly integrated transmission network," *Proceedings of the CIGRÉ Session*, 37-303, Paris, France, 1990

[235]Mansour Y., Xu W., Alvarado F., Rinzin C., "SVC placement using critical modes of voltage instability*," IEEE Trans. Power Systems*, vol. 9, no. 2., May 1994, pp. 757-763

[236]Matsuno K., Taniguchi H., Egawa M., Fujita H., Konishi H., Irokawa S., Akamatsu M., “Analogue simulation studies with actual controllers for FACTS equipment,” *Proceedings of the CIGRÉ Session*, 14-104, Paris, France, 1998

[237]Mehraban A., Keri A., Gernhardt M., Schauder C., Stacey E., Edris A., “Application of the world’s first UPFC on the AEP system,” *Proceedings of the EPRI Future of Power Delivery Conference*, Washington, DC, USA, April 1996

[238]Mehraban B., Kovalsky L., "Unified Power Flow Controller on the AEP system: commissioning and operation," *Proceedings of the IEEE PES Winter Meeting,* New York, USA, February 1999, pp. 1287-1292

[239]Mihalič R., Žunko P., Povh D., “Improvement of transient stability using Unified Power Flow Controller*,” IEEE Trans. Power Delivery*, vol. 11, no. 1, January 1996, pp. 485-491

[240]Mihalič R., “System aspects of GTO-controlled series compensation*,” Proceedings of the 31st Universities Power Engineering Conference UPEC’96*, Iraklio, Crete, Greece, September 1996, pp. 433-436

[241]Mihalič R., *Določitev obratovalnih parametrov prečnega transformatorja za izboljšanje obratovalnih razmer in povečanje prenosne zmogljivosti elektoenergetskega sistema,* Ph. D. Thesis, Faculty of Electrical Engineering and Computing, University of Ljubljana, Ljubljana, Slovenia, 1993 (in Slovenian)

[242]Mihalič R., Papič I., "Mathematical models and simulation of a static synchronous series compensator," *Proceedings of the IEEE Power Tech'99 Conference - BPT'99,* Budapest, Hungary, August 1999, paper BPT99-315-42

[243]Mihalič R., Papič I., “Power flow control using static synchronous series compensator*,” Proceedings of the 32nd Universities Power Engineering Conference UPEC’97*, Manchester, UK, September 1997, pp. 174-177

[244]Mihalič R., Papič I., “Power transmission control using UPFC*,” Proceedings of the 31st Universities Power Engineering Conference UPEC’96*, Iraklio, Crete, Greece, September 1996, pp. 285-288

[245]Mihalič R., Povh D., Žunko P., “Increased loadability of long transmission lines by insertion of FACTS devices,” *Electrotechnical Review*, Ljubljana, Slovenia, vol. 60, no. 1, 1993, pp. 7-12 (in Slovenian)

[246]Mihalič R., Žunko P., Povh D., “Modeling of Unified Power Flow Controller and its impact on power oscillation damping,” *Proceedings of the CIGRÉ Symposium*, 320-01, Tokyo, Japan, 1995

[247]Milanović J., Hiskens I., “Effects of dynamic load model parameters on damping of oscillations in power systems,” *Electric Power Systems Research*, vol. 33, 1995, pp. 53-61

[248]Miller N., D’Aquila R., Jimma K., Sheehan M., Comegys G., “Voltage stability of the Puget Sound system under abnormally cold weather conditions,” *IEEE Trans. Power Systems*, vol. 8, no. 3, August 1993, pp. 1133-1142

[249]Miller N., Price W., “Influence of load modeling assumptions on the dynamics of large system voltage collapse simulations,” *Proceedings of the International Seminar on Bulk Power System Voltage Phenomena - III, Voltage Stability, Security and Control*, Davos, Switzerland, August 1994, pp. 635-641

[250]Miller N., Price W., “Planning and operations benefits of high fidelity voltage collapse simulations*,” Electrical Power & Energy Systems*, vol. 15, no. 4, 1993, pp. 245-250

[251]Modlitba P., Pavlinec P., Vyskočil V., Kozak F., Kalousek V., “Analytical method for evaluating power system transfer capability with regard to voltage stability,” *Proceedings of the CIGRÉ Session*, 38-06, Paris, France, 1986

[252]Morioka Y., Mishima Y., Nakachi Y., Asada M., Tokuhara K., “Implementation of Unified Power Flow Controller and verification for transmission capability improvement,” *IEEE Trans. Power Systems*, vol. 14, no. 2, May 1999, pp. 575-581

[253]Mummert R., "Excitation system limiter models for use in system stability studies," *Proceedings of the IEEE PES Winter Meeting,* New York, USA, February 1999, pp. 187-192

[254]Murdoch A., Lawson R., and Venkataraman S., "Excitation system protective limiters - modeling and testing," *Proceedings of the IEEE PES Winter Meeting,* New York, USA, February 1999, pp. 182-186

[255]Mutale J., Strbac G., “Transmission network reinforcement versus FACTS: an economic assessment,” *IEEE Trans. Power Systems,* vol. 15, no. 3, August 2000, pp. 961-967

[256]Nabavi-Niaki A., Iravani M., “Steady-state and dynamic models of Unified Power Flow Controller (UPFC) for power system studies,” *IEEE Trans. Power Systems,* vol. 11, no. 4, November 1996, pp. 1937-1943

[257]Nagao T., Tanaka K., Takenaka K., “Development of static and simulation programs for voltage stability studies of bulk power system,” *IEEE Trans. Power Systems*, vol. 12, no. 1, February 1997, pp. 273-281

[258]Nam H., Kim Y., Shim K., Lee K., “A new eigen-sensitivity theory of augmented matrix and its applications to power system stability analysis,” *IEEE Trans. Power Systems,* vol. 15, no. 1, February 2000, pp. 363-369

[259]Nam H., Song C., Kim D., Moon Y., and Lee K., "A new efficient unified strategy to compute voltage collapse point and voltage stability enhancement by generation shift," *Proceedings of the IEEE PES Winter Meeting,* New York, USA, February 1999, pp. 640-645

[260]Nedwick P., Mistr A., Croasdale E., “Reactive management - a key to survival in the 1990s*,” IEEE Trans. Power Systems*, vol. 10, no. 2, May 1995, pp. 1036-1043

[261]Nelson R., “Transmission planning application guidelines for the Unified Power Flow Controller (UPFC),” *Proceedings of the American Power Conference APC’97*, Chicago, IL, USA, April 1997, pp. 1257-1262

[262]Nelson R., “Transmission power flow control: electronic vs. electromagnetic alternatives for steady-state operation,” *IEEE Trans. Power Delivery*, vol. 9, no. 3, July 1994, pp. 1678-1684

[263]Nelson R., Bian J., Williams S., "Transmission series power flow control," *IEEE Trans. Power Delivery*, vol. 10, no. 1, January 1995, pp. 504-510

[264]Nilsson S., "Security aspects of flexible AC transmission system controller applications," *Electrical Power & Energy Systems*, vol. 17, no. 3, June 1995, pp. 173-180

[265]Noroozian M., Ängquist L., Ghandhari M., Andersson G., "Improving power system dynamics by series-connected FACTS devices," *IEEE Trans. Power Delivery*, vol. 12, no. 4, October 1997, pp. 1635-1641

[266]Noroozian M., Ängquist L., Ghandhari M., Andersson G., "Use of UPFC for optimal power flow control," *IEEE Trans. Power Delivery*, vol. 17, no. 4, October 1997, pp. 1629-1634

[267]Noroozian M., Ängquist L., Ghandhari M., Andersson G., "Use of UPFC for optimal power flow control," *Proceedings of the Stockholm Power Tech Conference*, Stockholm, Sweden, June 1995, pp. 506-511

[268]Noroozian M., Ängquist L., Petterson Å., Chamia M., Ghandhari M., Andersson G., "Series-connected FACTS devices control strategy for damping of electromechanical oscillations," *Proceedings of the 12th Power Systems Computation Conference PSCC'96*, Dresden, Germany, August 1996, pp. 1090-1096

[269]Noroozian M., Ängquist L., Petterson Å., Chamia M., Ghandhari M., Andersson G., "Improving power systems dynamics by series-connected FACTS devices," *IEEE Trans. Power Delivery*, vol. 12, no. 4, October 1997, pp. 1635-1641

[270]Noroozian M., Andersson G., "Damping of inter-area and local modes by use of controllable components," *IEEE Trans. Power Delivery*, vol. 10, no. 4, October 1995, pp. 2007-2012

[271]Noroozian M., Andersson G., "Damping of power system oscillations by use of controllable components," *IEEE Trans. Power Delivery*, vol. 9, no. 4, October 1994, pp. 2046-2054

[272]Noroozian M., Andersson G., Tomsović K., "Robust, near time-optimal control of power system oscillations with fuzzy logic," *IEEE Trans. Power Delivery*, vol. 11, no. 1, January 1996, pp. 393-400

[273]Noroozian M., *Exploring benefits of controllable series compensators in power systems*, Ph. D. Thesis, TRITA-EES-9402, ISSN 1100-1607, Electric Power Systems, Royal Institute of Technology, Stockholm, Sweden, 1994

[274]O'Kane P., Fox B., O'Hara D., Morrow J., "Enhanced power system load relief via control of embedded generator voltage," *Proceedings of the 32nd Universities Power Engineering Conference UPEC'97*, Manchester, UK, September 1997, pp. 979-982

[275]O'Keefe R., Schuly R., Bhatt N., "Improved representation of generator and load dynamics in the study of voltage limited power system operations," *IEEE Trans. Power Systems,* vol. 12, no. 1, February 1997, pp. 304-314

[276]Ognedal R., Carlsen T., "Voltage stability condition in a power transmission system calculated by sensitivity methods," *IEEE Trans. Power Systems*, vol. 5, no. 4, November 1990, pp. 1286-1293

[277]Ohtsuki H., Yokoyama A., Sekine Y., "Reverse action of on-load tap changer in association with voltage collapse," *IEEE Trans. Power Systems*, vol. 6, no. 1, February 1991, pp. 300-306

[278]Omata T., Uemura K., "Effects of series impedance on power system load dynamics," *Proceedings of the IEEE PES Winter Meeting*, PE-489-PWRS-0-01-1997, New York, USA, February 1997

[279]Ooi B., Kazerani M., Marceau R., Wolanski Z., Galiana F., McGillis D., Joos G., "Mid-point siting of FACTS devices in transmission lines," *IEEE Trans. Power Delivery*, vol. 12, no. 5, October 1997, pp. 1717-1722

[280]Østrup T., "Capability chart for a turbo-generator," *Internal Paper, ELKRAFT Power Company*, Ballerup, Denmark, January 1990

[281]Østrup T., "QU-diagrams for generators," *Internal Paper, ELKRAFT Power Company*, Ballerup, Denmark, May 1992

[282]Østrup T., "Reactive power production capability of a turbo-generator," *Internal Paper, ELKRAFT Power Company*, Ballerup, Denmark, September 1991

[283]Padiyar K. R., Uma Rao K., "Discrete control of series compensation for stability improvement in power systems," *Electrical Power & Energy Systems*, vol. 19, no. 5, June 1997, pp. 311-319

[284]Padiyar K., Kulkarni A., "Control design and simulation of Unified Power Flow Controller," *IEEE Trans. Power Delivery*, vol. 13, no. 4, October 1998, pp. 1348-1354

[285]Pagola L., Perez-Arriaga J., Verghese G., "On sensitivities, residues, and participations: application to oscillatory stability analysis and control," *IEEE Trans. Power Systems*, vol. 4, no. 1, February 1989, pp. 278-285

[286]Pai M., Sauer P., Lesieutre C., "Static and dynamic nonlinear loads and structural stability in power systems," *Proceedings of the IEEE*, vol. 83, no. 11, November 1995, pp. 1562-1572

[287]Pai M., Sauer P., Lesieutre R., Adapa R., "Structural stability in power systems - effects of load models," *IEEE Trans. Power Systems*, vol. 10, no. 2, May 1995, pp. 609-615

[288]Pal M., "Assessment of corrective measures for voltage stability considering load dynamics," *Electric Power & Energy Systems*, vol. 17, no. 5, June 1995, pp. 325-334

[289]Pal M., "Voltage stability conditions considering load characteristics," *IEEE Trans. Power Systems*, vol. 7, no. 1, February 1992, pp. 243-249

[290]Pal M., "Voltage stability: analysis needs, modelling requirement, and modelling adequacy," *IEE Proc. - C*, vol. 140, no. 4, July 1993, pp. 279-286

[291]Panvini A., Yohn T. J., "Field assessment of generators reactive capability," *IEEE Trans. Power Systems*, vol. 10, no. 1, February 1995, pp. 288-296

[292]Papič I., Žunko P., Povh D., Weinhold M., "Basic control of Unified Power Flow Controller," *IEEE Trans. Power Systems*, vol. 12, no. 4, November 1997, pp. 1734-1739

[293]Parniani M., Iravani M. R., "Voltage control stability and dynamic interaction phenomena of static Var

compensators," *IEEE Trans. Power Systems*, vol. 10, no. 3, August 1995, pp. 1592-1597

[294]Pilotto L., Ping W., Carvalho A., Wey A., Long W., Alvarado F., Edris A., "Determination of needed FACTS controllers that increase asset utilization of power systems," *IEEE Trans. Power Delivery*, vol. 12, no. 1, January 1997, pp. 364-371

[295]Pinto H., Martins N., Vieira X., Bianco A., Gomes P., Dos Santos M., "Modal analysis for voltage stability: application at base case and point of collapse," *Proceedings of the International Seminar on Bulk Power System Voltage Phenomena - III, Voltage Stability, Security and Control*, Davos, Switzerland, August. 1994, pp. 215-228

[296]Popović D., Hiskens I., Hill D., "Investigations of load-tap changer investigation," *Electric Power & Energy Systems*, vol. 18, no. 2, February 1996, pp. 81-97

[297]Popović D., Hiskens I., Hill D., "Stability analysis of induction motor networks," *Electrical Power & Energy Systems*, vol. 20, no. 7, 1998, pp. 475-487

[298]Popović D., *Modelling, stability and control of voltage behavior in power supply systems*, Ph. D. Thesis, Department of Electrical and Computer Engineering, University of Newcastle, Newcastle, Australia, October 1995

[299]Povh D., Mihalič R., Papič I., "FACTS equipment for load flow control in high voltage systems," *Proceedings of the CIGRÉ Symposium*, 310-06, Tokyo, Japan, 1995

[300]Povh D., Renz K., Teltsch E., Witzmann R., "Integrated operation of HVDC and FACTS," *Proceedings of 12th Conference on the Electric Power Supply Industry 12CEPSI*, Pattaya, Thailand, November 1998, pp. 64-71, 34-09

[301]Prasad D., Al-Mulhim M., "Performance evaluation of dynamic load models for voltage stability analysis," *Electrical Power & Energy Systems*, vol. 19, no. 8, November 1997, pp. 533-540

[302]Prasad D., Al-Mulhim M., Ray G., Gopichand B., "Comparative assessment of the effect of dynamic load models on voltage stability," *Electrical Power & Energy Systems*, vol. 19, no. 5, June 1997, pp. 305-309

[303]Rahim A., Nassimi S., "Synchronous generator damping enhancement through coordinated control of exciter and SVC," *IEE Proc. - Gener. Transm. Distrib*., vol. 143, no. 2, March 1996, pp. 211-218

[304]Rahman M., Ahmed M., Gutman R., O'Keefe R., Nelson R., Bian J., "UPFC application on the AEP system: Planning considerations," *IEEE Trans. Power Systems*, vol. 12, no. 4, November 1997, pp. 1695-1701

[305]Rahman M., O' Keefe R., Mehraban A., Hanneton V., Daniel D., Lombard X., Vitet S., Edris A., "Two application cases of UPFC on EDF's and AEP's networks," *Workshop EPRI*, San Diego, November 1997

[306]Rajagopalan C., Lesieutre B., Sauer P., Pai M., "Dynamic aspects of voltage/power characteristics," *IEEE Trans. Power Systems*, vol. 7, no. 3, August 1992, pp. 990-1000

[307]Rajaraman R., Alvarado F., Maniaci A., Camfield R., Jalali S., "Determination of location and amount of series compensation to increase power transfer capability," *IEEE Trans. Power Systems*, vol. 13, no. 2, May 1998, pp. 294-300

[308]Ramar K., Raviprakasha M., "Design of compensation schemes for long AC transmission lines for maximum power transfer limited by voltage stability," *Electrical Power & Energy Systems*, vol. 17, no. 2, February 1995, pp. 83-89

[309]Ramey D., "Application of the Unified Power Flow Controller to create a virtual generation bus," *Proceedings of the 61st American Power Conference - APC'99,* Chicago, IL, USA, May 1999, Vol. 61-1999-08 Interconnected Operations paper d.

[310]Reason J., "Controlling network power flow," *Electrical T&D World - Special Report: New York State acts to relieve growing network congestion*, vol. 213, no. 1, January / February 1999, pp. 12-22

[311]Reason J., "New York State acts to relieve growing network congestion - Controlling network power flow," *Electrical T&D World - Special Report*, vol. 213, no. 1, January 1999, pp. 12-19

[312]Renz B., "Implementing the world's first Unified Power Flow Controller," *Power Industry Development - Sterling Publications Ltd.*, Spring 1999, pp. 9-12

[313]Renz B., Keri A., Mehraban A., Kessinger J., Schauder C., Gyugyi L., Kovalsky L., Edris A., "World's first Unified Power Flow Controller on the AEP system," *Proceedings of the CIGRÉ Session*, 14-107, Paris, France, 1998

[314]Roa-Sepulveda C., Knight U., "Experience in the dynamic analysis of voltage phenomena," *Proceedings of the International Seminar on Bulk Power System Voltage Phenomena - III, Voltage Stability, Security and Control*, Davos, Switzerland, August 1994, pp. 605-616

[315]Rouco L., Pagola F., "An eigenvalue sensitivity approach to location and controller design of controllable series capacitors for damping power system oscillations," *IEEE Trans. Power Systems*, vol. 12, no. 4, November 1997, pp. 1660-1666

[316]Round S., Yu Q., Norum L., Undeland T., "Performance of a Unified Power Flow Controller using a d-q control system," *Proceedings of the IEE AC and DC Power Transmission Conference*, Conference Publication no. 423, April 1996, pp. 357-362

[317]Rousseaux P., Van Cutsem T., "Fast small-disturbance analysis of long term voltage stability," *Proceedings of the 12th Power System Computation Conference PSCC'96*, Dresden, Germany, August 1996, pp. 295-302

[318]Ruiz D., Asiain T., Olguin D., "Improvement of induction motors models for power system transient stability studies," *Proceedings of the IEEE Power Tech'99 Conference - BPT'99,* Budapest, Hungary, August 1999, paper BPT99-051-12

[319]Söder L., "Estimation of reduced electrical distribution losses depending on dispersed small scale energy production," *Proceedings of the 12th Power*

Systems Computation Conference PSCC'96, Dresden, Germany, August 1996, pp. 1229-1234

[320]Samuelsson J., Wilk-Wilczynski A., "New innovative tools in AC transmission to serve the deregulated energy market," *Proceedings of the IASTED International Conference - Power and Energy Systems,* Las Vegas, Nevada, USA, November 1999, pp. 77-83

[321]Sanchez-Gasca J., D'Aquila R., Paserba J., Price W., Klapper D., Hu I., "Extended-term dynamic simulation using variable time step integration," *IEEE Computer Application in Power*, vol. 6, no. 4, October 1993, pp. 23-28

[322]Sandberg L., Roudén K., Ekstam L., "Security assessment against voltage collapse based on real-time data including generator reactive capacity," *Proceedings of the CIGRÉ Session*, 39/11-03, Paris, France, 1994

[323]Schauder C., Gernhardt M., Stacey E., Lemak T., Gyugyi L., Cease T. W., Edris A., "Development of a ±100 Mvar static condenser for voltage control of transmission systems," *IEEE Trans. Power Delivery*, vol. 10, no. 3, July 1995, pp. 1486-1496

[324]Schauder C., Gernhardt M., Stacey E., Lemak T., Gyugyi L., Cease T. W., Edris A., "Operation of ±100 Mvar TVA STATCON," *IEEE Trans. Power Delivery*, vol. 12, no. 4, October 1997, pp. 1805-1811

[325]Schauder C., Gyugyi L., Lund M., Hamai D., Rietman T., Torgerson D., Edris A., "Control and protection studies for the Unified Power Flow Controller (UPFC)," *Proceedings of the EPRI Future of Power Delivery Conference*, Washington, DC, USA, April 1996

[326]Schauder C., Gyugyi L., Lund M., Hamai D., Rietman T., Torgerson D., Edris A., "Operation of the Unified Power Flow Controller (UPFC) under practical constraints," *IEEE Trans. Power Delivery,* vol. 13, no. 2, April 1998, pp. 630-639

[327]Schauder C., Mehta H., "Vector analysis and control of advanced Static Var Compensators," *IEE Proc. - C*, vol. 140, no. 4, July 1993, pp. 299-306

[328]Schauder C., Stacey E., Lund M., Gyugyi L., Kovalsky L., Keri A., Mehraban A., Edris A., "AEP UPFC project: Installation, commissioning, and operation of the ±160 MVA STATCOM (phase I)," *IEEE Trans. Power Delivery*, vol. 13, no. 4, October 1998, pp. 1530-1535

[329]Schlueter R., "A voltage stability security assessment method," *IEEE Trans. Power Systems,* vol. 13, no. 4, November 1998, pp. 1423-1431

[330]Schlueter R., Hu I., "Types of voltage instability and the associated modeling for transient/mid-term stability simulation," *Electric Power Systems Research*, vol. 29, 1994, 131-145

[331]Schlueter R., Hu I., Chang M., Lo J., Costi A., "Methods for determining proximity to voltage collapse*,*" *IEEE Trans. Power Systems*, vol. 6, no. 1, February 1991, pp. 285-292

[332]Sekine Y., Ohtsuki H., "Cascaded voltage collapse," *IEEE Trans. Power Systems*, vol. 5, no. 1, February 1990, pp. 250-256

[333]Sekine Y., Takahashi K., Hayashi T., "Application of power electronics technologies to the 21st century's bulk power transmission in Japan," *Electrical Power & Energy Systems*, vol. 17, no. 3, June 1995, pp. 181-194

[334]Semlyen A., Gao B., Janischewskyj W., "Calculation of the extreme loading condition of a power system for the assessment of voltage stability," *IEEE Trans. Power Systems*, vol. 6, no. 1, February 1991, pp. 307-315

[335]Sen K., "STATCOM - STATic synchronous COMpensator: theory, modeling, and applications," *Proceedings of the IEEE PES Winter Meeting,* New York, USA, February 1999, pp. 1177-1183

[336]Sen K., Stacey E., "UPFC - Unified Power Flow Controller: Theory, modeling, and applications*,*" *IEEE Trans. Power Delivery*, vol. 13, no. 4, October 1998, pp. 1453-1460

[337]Senyu T., Shiroma T., Uezato K., "The control concept of Unified Power Flow Controller in power systems for improving transient stability and damping of synchronous generators," *Proceedings of the CIGRÉ Symposium*, 510-02, Tokyo, Japan, 1995

[338]Smed T., *Interactions between high voltage AC and DC systems*, Ph. D. Thesis, TRITA-EES-9004, ISSN 1100-1607, Electric Power Systems, Royal Institute of Technology, Stockholm, Sweden, 1991

[339]Smith K., Ran L., Penman J., "Dynamic modelling of a Unified Power Flow Controller*,*" *IEE Proc. - Gener. Transm. Distrib*., vol. 144, no. 1, January 1997, pp. 7-12

[340]Song Y., Liu J., "Electromagnetic transient simulation studies of sinusoidal PWM Unified Power Flow Controllers," *European Transactions on Electric Power*, vol. 8, no. 3, May/June 1998, pp. 187-192

[341]Sonnenmoser A., Lehn P., "Line current balancing with a Unified Power Flow Controller," *IEEE PES Winter Meeting paperPE-438-PWRD-0-10-1998,* New York, USA, February 1999

[342]Srivastava K., Srivastava S., "Effect of generation rescheduling on voltage stability margin*,*" *Electrical Power & Energy Systems*, vol. 19, no. 1, January 1997, pp. 11-17

[343]Stahlkopf K., Budney W., Renz B., Cerdan J., Humphries M., "Stretching transmission capacity by technology deployment," *IEEE Power Engineering Review*, vol. 16, no. 11, November 1996, pp. 4-12

[344]Stahlkopf K., Wilhelm M., "Tighter controls for busier systems," *IEEE Spectrum*, vol. 34, no. 4, April 1997, pp. 48-52

[345]Steimer P., Grüning H., Werninger J., Dähler P., Linhofer G., Boeck R., "Series connection of GTO thyristors for high-power static frequency converters," *ABB Review*, no. 5, 1996, pp. 14-20

[346]Strmčnik B., Gubina F., "Voltage phasors approach to voltage instability in distribution systems*,*" *Electrotechnical Review*, Ljubljana, Slovenia, vol. 61, no. 1-2, 1994, pp. 13-17

[347]Stubbe M., Bihain A., Deuse J., "Simulation of voltage collapse," *Electrical Power & Energy Systems*, vol. 15, no. 4, 1993, pp. 239-243

[348]Sun Y., Proske D., "Stability enhancement using ASVG nonlinear control*," Proceedings of the 32nd Universities Power Engineering Conference UPEC'97*, Manchester, UK, September 1997, pp. 983-986

[349]Tare R., Bijwe P., "A new index for voltage stability monitoring and enhancement," *Electrical Power & Energy Systems*, vol. 20, no. 5, June 1998, pp. 345-351

[350]Tasić D., Rajaković N., Stajić Z., Vukić Đ., "The analysis of load influence on appearance of voltage collapse in transmission networks," *Proceedings of the 32nd Universities Power Engineering Conference UPEC'97*, Manchester, UK, September 1997, pp. 77-80

[351]Taylor C., "Concepts of undervoltage load shedding for voltage stability," *IEEE Trans. Power Delivery*, vol. 7, no. 2, April 1992, pp. 480-488

[352]Taylor C., "Improving grid behavior," *IEEE Spectrum*, vol. 36, no. 6, June 1999, pp. 40-45

[353]Taylor C., "Survey of effective and practical solutions for longer-term voltage stability*," Electrical Power & Energy Systems*, vol. 15, no. 4, 1993, pp. 217-220

[354]Taylor C., Comegys G., Nassief F., Elwood D., Kundur P., "Simulation and implementation of undervoltage load shedding for Pacific Northwest voltage stability," *Proceedings of the CIGRÉ Session*, 38-103, Paris, France, 1994

[355]Taylor C., Erickson D., "Recording and analyzing the July 2 cascading outage*," IEEE Computer Application in Power*, vol. 10, no. 1, January 1997, pp. 26-30

[356]Taylor C., *Power system voltage stability*, EPRI McGraw-Hill, ISBN 0-07-063184-0, 1994

[357]Taylor C., *Reactive power compensation and voltage stability: removing transmission limitations*, Seminar Book, February 1997

[358]Taylor C., Van Leuven A., "CAPS: improving power system stability using the time-overvoltage capability of large shunt capacitor banks," *IEEE Trans. Power Delivery*, vol. 11, no. 2, April 1996, pp. 783-792

[359]Teshome A., Esiyok E., "Distance to voltage collapse through second-order eigenvalue sensitivity technique," *Electrical Power & Energy Systems*, vol. 17, no. 6, 1995, pp. 425-431

[360]Tewardson R., *Sparse matrices*, Academic Press, 1973

[361]Thomas R., "A systems approach to controlling the onset of voltage collapse*," Proceedings of the International Seminar on Bulk Power System Voltage Phenomena - III, Voltage Stability, Security and Control*, Davos, Switzerland, August 1994, pp. 527-540

[362]Tiranuchit A., Ewerbring L., Duryea R., Thomas R., Luk F., "Towards a computationally feasible on-line voltage instability index," *IEEE Trans. Power Systems*, vol. 3, no. 3, May 1988, pp. 669-675

[363]Tiranuchit A., Thomas R., "A posturing strategy against voltage instabilities in electric power systems," *IEEE Trans. Power Systems*, vol. 3, no. 1, February 1988, pp. 87-93

[364]Toufan M., Annakkage U.D., "Simulation of the Unified Power Flow Controller performance using PSCAD/EMTDC," *Electric Power Systems Research*, vol. 46, no. 1, July 1998, pp. 67-75

[365]Tripathy S., Indulkar C., Viswanatha B., "Voltage collapse at the load end of a series compensated EHV transmission line," *Electrical Power & Energy Systems*, vol. 15, no. 4, 1993, pp. 251-253

[366]Urbanek J., Piwko R., Larsen E., Damsky B., Furumasu B., Mittlestadt W., Eden J., "Thyristor controlled series compensation prototype installation at the Slatt 500 kV substation," *IEEE Trans. Power Delivery*, vol. 8, no. 3, July 1993, pp. 1460-1469

[367]Uzunović E., Cañizares C., Reeve J., "Fundamental frequency model of Unified Power Flow Controller," *Proceedings of the 30th North American Power Symposium NAPS'98*, October 1998, Cleveland, OH, USA, pp. 294-299

[368]Van Cutsem T., "A comprehensive analysis of mid-term voltage stability," *IEEE Trans. Power Systems*, vol. 10, no. 3, August 1995, pp. 1173-1182

[369]Van Cutsem T., "A method to compute reactive power margins with respect to voltage collapse*," IEEE Trans. Power Systems*, vol. 6, no. 1, February 1991, pp. 145-156

[370]Van Cutsem T., "An approach to corrective control of voltage instability using simulation and sensitivity"*, Trans. Power Systems*, vol. 10, no. 2, May 1995, pp. 616-622

[371]Van Cutsem T., "Dynamic and static aspects of voltage collapse," *Proceedings of the International Workshop on Bulk Power System Voltage Phenomena: Voltage Stability and Security*, Potosi, Missouri, USA, 1988

[372]Van Cutsem T., Karlsson D., "Tutorial on voltage stability*," Proceedings of the 12th Power Systems Computation Conference PSCC'96*, Dresden, Germany, August 1996

[373]Van Cutsem T., Mailhot R., "Validation of a fast voltage stability analysis method on the Hydro-Quebec system," *IEEE Trans. Power Systems*, vol. 12, no. 1, February 1997, pp. 282-292

[374]Van Cutsem T., Moisse C., Mailhot R., "Determination of secure operating limits with respect to voltage collapse," *IEEE Trans. Power Systems,* vol. 14, no. 1, February 1999, pp. 327-335

[375]Van Cutsem T., Vournas C., "Voltage stability analysis in transient and mid-term time scales*," IEEE Trans. Power Systems*, vol. 11, no. 1, February 1996, pp. 146-154

[376]Van Cutsem T., Vournas C., *Voltage stability of electric power systems*, Kluwer Academic Publishers, ISBN 0-7923-8139-4, 1998

[377]Veera Raju V., Kuppurajulu A., "A closed-loop reactive power margins with respect to voltage collapse," *Electrical Power & Energy Systems*, vol. 19, no. 3, March 1997, pp. 153-164

[378]Venikov V. A., *Electrical network performance calculations and analysis*, English Translation, Mir Publishers Moscow, 1985

[379]Venikov V. A., *Transient phenomena in electrical power systems - problems and illustrations*, English Translation, Pergamon Press, 1965

[380]Venikov V. A., *Transient processes in electrical power systems*, English Translation, Mir Publishers Moscow, 1980

[381]Venkatasubramanian V., Schättler H., Zaborszky J., "Voltage dynamics: Study of a generator with voltage control, transmission and matched MW load," *IEEE Trans. Automatic Control*, vol. 37, no. 11, November 1992, pp. 1717-1733

[382]Vournas C., "Voltage stability and controllability indices for multimachine power systems," *IEEE Trans. Power Systems*, vol. 10, no. 3, August 1995, pp. 1183-1194

[383]Vournas C., Manos G., "Modelling of stalling motors during voltage stability studies," *IEEE Trans. Power Systems*, vol. 13, no. 3, August 1998, pp. 775-781

[384]Vournas C., Sauer P., Pai M., "Relationships between voltage and angle stability of power systems," *Electrical Power & Energy Systems*, vol. 18, no. 8, November 1996, pp. 493-500

[385]Vu K., Liu C., Taylor C., Jimma K., "Voltage instability: mechanisms and control strategies," *Proceedings of the IEEE*, vol. 83, no. 11, November 1995, pp. 1442-1455

[386]Walve K., "Modelling of power system components at severe disturbances," *Proceedings of the CIGRÉ Session*, 38-18, Paris, France, 1986

[387]Wan H., Song Y., Johns A., "Effective control for power system voltage stability enhancement," *Proceedings of the 28th North American Symposium NAPS'96, M.I.T.*, MA, USA, November 1996, pp. 257-263

[388]Wang H., "A unified model for the analysis of FACTS devices in damping power system oscillations - part III: Unified Power Flow Controller," *IEEE Trans. Power Delivery,* vol. 15, no. 3, July 2000, pp. 978-983

[389]Wang H., Swift F., "A unified model for the analysis of FACTS devices in damping power system oscillations part I: single-machine infinite-bus power system," *IEEE Trans. Power Delivery,* vol. 12, no. 2, April 1997, pp. 941-946

[390]Wang H.F., "Effect of multi-functional UPFC upon power system oscillation stability," *Proceedings of the IEEE Power Tech'99 Conference - BPT'99,* Budapest, Hungary, August 1999, paper BPT99-026-12

[391]Wang H.F., "Modelling Unified Power Flow Controller into multi-machine power systems for stability study," *Proceedings of the 3rd International Conference on Digital Power System Simulators - ICDS'99,* Vasteras, Sweden, May 1999

[392]Wang K., Chung C., Tse C., Tsang K., "Multimachine eigenvalue sensitivities of power system parameters," *IEEE Trans. Power Systems,* vol. 15, no. 2, May 2000, pp. 741-747

[393]Wilkinson J., *The algebraic eigenvalue problem*, Oxford Science Publications, ISBN 0 19 853418 3, Reprint 1996

[394]Wong K., "Simple rules for the application of series voltage sources in power transmission systems," *IEEE Trans. Power Delivery*, vol. 13, no. 4, October 1998, pp. 1488-1493

[395]Wu Q., Popović D., Hill D., and Parker C., "System security enhancement against voltage collapse via coordinated control," *Proceedings of the IEEE PES Winter Meeting,* New York, USA, February 1999, pp. 755-760

[396]Xin Z., Vilathgamuwa M., "A robust H_∞ control of a Unified Power Flow Controller," *Proceedings of the International Power Engineering Conference IPEC'97*, Singapore, May 1997, pp. 397-402

[397]Xu W, Mansour Y., "Voltage stability analysis using generic dynamic load models," *IEEE Trans. Power Systems*, vol. 9, no. 1, February 1994, pp. 479-493

[398]Xu W., Mansour Y., Harrington P., "Planning methodologies for voltage stability limited power systems," *Electrical Power & Energy Systems*, vol. 15, no. 4, 1993, pp. 221-228

[399]Xu W., Vaahedi E., Mansour Y., Tamby J., "Voltage stability load parameter determination from field tests on B.C. Hydro's system," *IEEE Trans. Power Systems,* vol. 12, no. 3, August 1997, pp. 1290-1297

[400]Xue Y., Xu T., Han Z., Li Y., "A criterion and margin for transient voltage stability considering induction motors," *Proceedings of the International Power Engineering Conference IPEC'97*, Singapore, May 1997, pp. 217-222

[401]Yan X., Naihu L., Wang H., Heng C., "Analysis of power flow control based on Flexible AC Transmission Systems," *Proceedings of the IFAC Control of Power Systems and Power Plants*, Beijing, China, August 1997, pp. 207-212

[402]Yorino N., Danyoshi M., Kitagawa M., "Interaction among multiple controls in tap change under load transformers," *IEEE Trans. Power Systems,* vol. 12, no. 1, February 1997, pp. 430-436

[403]Yorino N., Sasaki H., Masuda Y., Tamura Y., Kitagawa M., Oshimo A., "An investigation of voltage instability problems," *IEEE Trans. Power Systems*, vol. 7, no. 2, May 1992, pp. 600-611

[404]Young D., Hanson D., Baker M., Knight R., "A 225 Mvar transmission SVC for the UK incorporating a 150 Mvar STATCOM," *Proceedings of 12th Conference on the Electric Power Supply Industry 12CEPSI*, Pattaya, Thailand, November 1998, pp. 31-38, 34-05

[405]Zaborszky J., "On the road towards FACTS," *Electrical Power & Energy Systems*, vol. 17, no. 3, June 1995, pp. 165-172

[406]Zadeh K., Meyer R., Cauley G., "Practices and new concepts in power system control," *IEEE Trans. Power Systems,* vol. 11, no. 1, February 1996, pp. 3-10

[407]Zambroni de Souza A., "Tangent vector applied to voltage collapse and loss sensitivity studies," *Electric Power Systems Research*, vol. 47, 1998, pp. 65-70

[408]Zhu T., Tso S., Lo K., "An investigation into the OLTC effects on voltage collapse," *IEEE Trans. Power Systems,* vol. 15, no. 2, May 2000, pp. 515-521

RESUME

Nijaz Dizdarević was brought up in Kutina, Croatia, in 1966. There he completed elementary and secondary school of mathematical specialisation with honours as excellent pupil. In 1985 he passed qualification exam at Faculty of Electrical Engineering and Computing - University of Zagreb, Croatia, and after one year of compulsory military service, in September 1986, started with classes.

In December 1990, after nine semesters of enrolment in the regular program, he received a B.Sc. degree in the field of power system engineering with specialisation in power system design and operation. During his undergraduate studies he achieved excellent grades (GPA 4.55/5.00) and was awarded three times from the Faculty (two annual awards and one bronze medal "Josip Lončar" for the entire undergraduate studies). His total graduation mark was excellent (5). It was obtained upon the basis of GPA for the entire study (4.55), and of a mark (5) earned for the B.Sc. thesis work. The title of the thesis was "Transient Stability of Synchronous Generator - A Computer Representation," and it was done under supervision of Professor Srđan Babić.

Since May 1991 he has been employed at the same Faculty - Department of Power Systems. As a research assistant, he started attending M.Sc. graduate studies in the field of power systems dynamics and control. Besides the field of transient analysis, his activities have also comprised the analysis of steady state mode of power system operation. Having completed the studies by passing the exams with excellent grades (GPA 5.0), and defending the thesis work named "Contingency Selection and Analysis Algorithms in Electrical Power Networks," he received M.Sc. degree in February 1994 under supervision of Professor Srđan Babić.

Afterwards he has been enrolled in a Ph.D. study program at the same Faculty under supervision of Professor Sejid Tešnjak. His scientific research topics concern the impact of the FACTS-controllers (especially Unified Power Flow Controller) in solving the problem of the power system voltage stability by combining dynamic and static analytical aspects. The greatest motivation in choosing such an interesting field came from his 15-month scholarship period spent at the Royal Institute of Technology in Stockholm, Sweden, during 1996 and 1997. Under the sponsorship of The Swedish Institute he had privilege to work in a team of Professor Göran Andersson (later affiliated to ETH Zurich). Fruitful co-operation resulted with several papers published at international conferences.

Mr Dizdarević is author of several scientific and professional papers and project studies.

ŽIVOTOPIS

Nijaz Dizdarević rođen je 1966. godine u Kutini, Hrvatska, gdje je završio osnovnu i srednju školu matematičko-informatičkog smjera kao odličan učenik uz brojne nagrade i priznanja. Prijamni ispit na Fakultetu elektrotehnike i računarstva, Sveučilište u Zagrebu, položio je 1985. godine. Nakon jednogodišnjeg obvezatnog služenja vojnog roka, u rujnu 1986. godine, započinje s redovitim pohađanjem studija.

U prosincu 1990. godine, nakon devet semestara pohađanja redovitog studija, stječe titulu diplomiranog inženjera elektrotehnike, smjer Elektroenergetika, usmjerenje Izgradnja i pogon elektroenergetskog sustava. Tijekom dodiplomskog studija istaknuo se izvrsnim ocjenama (ukupni prosjek 4.55), a bio je tri puta nagrađivan od strane znanstveno-nastavnog vijeća Fakulteta (dvije godišnje nagrade i jedna brončana medalja "Josip Lončar" za izvrstan uspjeh na cijelom dodiplomskom studiju). Ukupna ocjena studija bila je izvrstan (5). Dobivena je na temelju ukupnog prosjeka svih ocjena na dodiplomskom studiju (4.55), i izvrsne ocjene (5) dobivene za diplomski rad. Diplomski rad pod nazivom "Prijelazna stabilnost ees-a na PC računalu" napravio je pod mentorstvom profesora Srđana Babića.

Od svibnja 1991. godine djelatnik je Zavoda za visoki napon i energetiku, Fakultet elektrotehnike i računarstva, Sveučilište u Zagrebu. Kao znanstveni novak sudjelovao je u radu znanstveno-istraživačkih projekata Ministarstva znanosti i tehnologije RH br. 2-05-279 (1991-1996) "Planiranje, pogon i eksploatacija elektroenergetskog sustava" i br. 036016 (od 1996. godine) "Planiranje i vođenje srednje razvijenih elektroenergetskih sustava". Pohađao je poslijediplomski studij u području dinamike i upravljanja elektroenergetskim sustavom. Osim u području analize prijelaznih stanja, njegove aktivnosti bile su izražene i u analizi stacionarnih stanja pogona ees-a. Nakon što je položio sve ispite na poslijediplomskom studiju s izvrsnim ocjenama (ukupni prosjek 5.00) i pod mentorstvom profesora Srđana Babića obranio magistarski rad pod nazivom "Algoritmi za analize slučajnih ispada elemenata elektroenergetske mreže", u veljači 1994. godine stječe titulu magistra znanosti u području Energetika.

Po svršetku poslijediplomskog magistarskog studija, uz mentorstvo profesora Sejida Tešnjaka upisuje se na doktorski studij gdje polaže sve ispite s ocjenom izvrstan (5). Temu njegovog znanstvenog istraživanja predstavlja utjecaj FACTS naprava (osobito UPFC) na izbjegavanje problema nestabilnosti napona ees-a uz kombiniranje dinamičkih i statičkih aspekata analize. Najveći dio motivacije pri izboru ovog područja istraživanja pojavio se tijekom 15-mjesečne znanstveno-istraživačke specijalizacije koju je proveo na The Royal Institute of Technology, Stockholm, Sweden, tijekom 1996. i 1997. godine. Zahvaljujući stipendiji dobivenoj od zaklade The Swedish Institute, uspostavio je plodonosnu međunarodnu suradnju s profesorom Anderssonom (sada na ETH Zurich) koja je rezultirala objavljivanjem više radova na inozemnim konferencijama.

Nijaz Dizdarević je autor više znanstvenih i stručnih članaka te studijskih radova.

ABSTRACT AND KEYWORDS

Unified Power Flow Controller in alleviation of voltage stability problem

ABSTRACT: The problem of voltage stability with voltage collapse as its final consequence is an emerging phenomenon in planning and operation of modern power systems. The increase in utilisation of existing power systems may get the system operating closer to voltage stability boundaries making it subject to the risk of voltage collapse. This possibility in association with several incidents throughout the world have given major impetus for analysing this problem with increased interest in modelling of generation, transmission and distribution/load levels of electric power systems.

Since the rapid development of power electronics has made it possible to design power electronic equipment of high rating for high voltage systems, the problem resulting from transmission system may be, at least partly, improved by use of the well-known FACTS-controllers. The de-regulation (restructuring) of power networks will probably imply new loading conditions and new power flow situations. This is an additional reason to face the FACTS.

In order to deal with the voltage stability problem, the solutions with FACTS-controllers must provide voltage support and/or appropriately co-ordinated control actions. Apart from several larger rating prototypes of Static Var Generator, as an improved version of Static Var Compensator, no other modern FACTS-controller application has been considered to help solve the voltage stability problem. This is considered to be a new impetus, since the most often the analyses are concentrated only on a power flow regulation and damping methods of electromechanical oscillations.

Therefore, a work on this dissertation has been launched aiming to fulfil following general objectives:

- set a comprehensive explanation of voltage stability problem and mechanism of voltage collapse in a multi-machine power system,
- develop analytical methods useful in the problem solving by early recognition of impending voltage collapse within combined dynamic and static approach, and
- develop preventative measures and actions using adequate FACTS-controllers (especially Unified Power Flow Controller, UPFC) to alleviate the problem and increase transmission throughput.

The thesis goal is stated as to show how it is possible to alleviate voltage stability problem by using modern, power electronics based, FACTS device named UPFC. In the elaboration of the thesis, a computer analysis of power system voltage stability has been taken. In order to analyse dynamic phenomena, a FORTRAN computer program for mid-term time domain simulation of multi-machine power system is developed. By combining dynamic and static aspects of analysis, its prime focus is in off-line simulation of voltage emergency situations using differential-algebraic model of power system. In-house developed program is tested and verified on the basis of other commercially available software. Eventually, it could be installed in a control centre serving for voltage security evaluation of a power system.

There have been several phases in the thesis elaboration.

In the first phase of its development, the program for time domain simulation has been made. It has featured different generator models with generic excitation and speed governor - turbine control systems, models of static and dynamic loads, induction motors, LTCs, transmission lines and buses... Computational methods that have been included have comprised fast de-coupled transient load flow along with Gauss-Seidel and Jacobi load flows, sparse matrix techniques, and 4th-order Runge-Kutta method of solving differential equations by using constant step-size integration.

In the second phase, the static aspects of linearised differential-algebraic power system model have been included, concerning properties of state and extended Jacobi matrices that are useful in general stability analysis (singular and eigenvalue decomposition, sensitivity analysis, and participation factors). Static aspects are very helpful in recognition of voltage stability problem, while modern means of voltage support are sought for should it be applied thereafter.

Thus, the third phase of the thesis elaboration has been initiated turning out the need for modelling of the FACTS device. The UPFC injection model has been set up along with its control structure. The UPFC in its general form can provide simultaneous, real-time control of all basic power system parameters (transmission voltage, impedance and phase angle) and dynamic compensation of ac system.

While the static aspects help the voltage stability problem being recognised through the matrix decompositions, the UPFC, heart and soul of the thesis, represents source of voltage support and power flow control. The UPFC has been studied concerning its possibilities to help voltage stability problem solved. Combined static and dynamic approach is used to analyse the control system of the UPFC injection model. It fulfils functions of reactive shunt compensation, voltage regulation, line power flow regulation, series compensation and PAR/QBT phase shifting meeting multiple control objectives. The injection model enables three parameters to be simultaneously controlled, namely the shunt reactive power, Q_{conv1}, and the magnitude, r, and angle, γ, of the injected series voltage.

The control system is of de-coupled single-input single-output type. The selection of input/output signals depends

on the predetermined control mode, which could be changed during simulation. At external level, following locally measured variables of the UPFC are controlled:

- shunt side bus voltage magnitude, V_i, (by changing Q_{conv1}),
- series side bus voltage magnitude, V_j,
- reactive power flow into series side bus, Q_{j2},
- reactive power requirement of the series converter, Q_{conv2}, or
- compensating voltage magnitude, V_{comp}, (by changing r), and
- active power flow into the series side bus, P_{j2},
- active power requirement of the series converter, P_{conv2},
- bus voltage angle difference, Θ_{ij}, or
- compensating voltage angle, φ_{comp}, (by changing γ).

In the model, the shunt side is controlled only in the voltage mode $V_i \leftrightarrow Q_{conv1}$, emphasising that Q_{conv1} represents reactive power loading of the shunt converter. The series side is controlled through the $r \Leftrightarrow \gamma$ pair in several different modes: bus voltage and active power flow $V_j \Leftrightarrow P_{j2}$, reactive and active power flow $Q_{j2} \Leftrightarrow P_{j2}$, series compensation $Q_{conv2} \Leftrightarrow P_{conv2}(=0)$, phase shifting of Phase Angle Regulator (PAR) type $V_j\,(=V_i) \Leftrightarrow \Theta_{ij}$, and phase shifting of Quadrature Boosting Transformer (QBT) type $V_{comp} \Leftrightarrow \varphi_{comp}(=\pi/2)$. The variables are chosen satisfying general $V \leftrightarrow Q$ and $\Theta \leftrightarrow P$ decoupling. Damping of electromechanical oscillations based on transient energy function is implemented in the model as well. The strategy is of take-over type using time derivatives of local variables from both sides of the UPFC. The shunt part of TEF block uses information from dV_i/dt, whereas the series part from $d\Theta_{ij}/dt$.

The sensitivity analysis, applied in more general sense, contributes to find appropriate location and action of the UPFC. The UPFC has rather unique capability of simultaneous series control of branch power flow and shunt control of bus voltage magnitude. By correlating branch and bus participation factors obtained from the matrix decompositions, it is possible to recognise location of its installation where appropriate regulation characteristics could be extensively used during voltage emergency situations. Since the voltage support capability of the UPFC is usually achieved by using two of its parameters, there is an additional advantage of its design, which enables simultaneous control of the third parameter as well.

Sensitivity analysis of the minimum singular value, total active power loss, and total reactive power generation is carried out to recognise critical points of power system during voltage collapse scenario. It serves to show capability of having all three UPFC parameters controlled simultaneously. Often, sensitivity involves the inverse of the state and the extended Jacobi matrix. Therefore, it has larger magnitudes as the critical point is approached with abrupt change to opposite sign as it is crossed. The appearance of the critical point represents a reliable sign of impending voltage unstable situation and could trigger voltage support from the UPFC. Therefore, if the sensitivity analysis is applied with respect to the set of the UPFC control parameters it is possible to define its adequate regulating action.

Within the thesis, special attention is paid to load modelling, since the load is considered to be the driving force of the voltage stability problem. After being shortly disturbed with a consequence of permanently decreased voltage magnitude level, by its mid-term recovery process of re-establishing initial power consumption, the loads could bring generators under over-excitation limiting conditions and/or cause transmission system being incapable of requested power delivery. Therefore, several different load models (static and dynamic) are analysed regarding its contribution to voltage collapse. Besides static ZIP load model, there are included dynamic models of induction motors and thermostatically controlled loads in presence of the LTC transformers, and first order non-linear recovery loads. Besides to the set of the UPFC control parameters, the static aspects and the sensitivity analysis are applied to the characteristic parameters of the load models as well. This helps to conclude about the most influential loads and their critical parameters that drive the system to the collapse.

Benefits of the proposed methodology are explored by analysing a multi-machine test system using in-house developed computer program. According to the established general objectives, it is possible to point out the main contribution and achievements of the thesis as follows:

- development of the differential-algebraic model of the multi-machine power system useful in time domain simulation with combined dynamic and static elements of analysis in order to study dynamic phenomena of mid-term transient periods of decreased voltage security level,
- development of the UPFC injection model with adequate control system in order to define the role of the device and its regulation capabilities useful in the voltage stability problem, as well as to define the methodology of rating, locating and timing of the UPFC action with simultaneous three-parameter control, and
- development of the methodology aimed to recognise critical points of power system operation using matrix decompositions and functions characteristic for appearance and evolution of voltage stability problem, as well as to compute their sensitivities with respect to the load parameters and the UPFC set of control parameters.

Future prospects are mostly dependable on a number of practical applications of the FACTS-controllers. Expecting increased number of their installations, the analysis could be very important in overall planning and operational procedures. By making transfer from the test-system towards larger real power system configuration, the answers of practical value could be given. To achieve that, the proposed analysis should be implemented on a regular basis within EMS paradigms in a control centre.

KEYWORDS: power system voltage stability, load modelling, FACTS, UPFC, sensitivity analysis

SAŽETAK I KLJUČNE RIJEČI

Objedinjeni regulator toka snage u izbjegavanju nestabilnosti napona

SAŽETAK: Problemi prijenosa električne energije i stabilnosti napona elektroenergetskog sustava među glavnim su izazovima pri planiranju i pogonu ees-a. Jedan od osnovnih uzroka povećanog zanimanja za probleme stabilnosti napona nalazi se u opasnom približavanju mnogih sustava granicama stabilnosti napona uslijed povećanog opterećenja sustava koje nije praćeno odgovarajućim povećanjem prijenosne moći. Globalna pojava više slomova napona ees-a uspostavila je problem stabilnosti napona kao jednu od najznačajnijih i najzanimljivijih grana istraživanja u području analize ees-a.

Problem stabilnosti napona prijenosnog sustava moguće je ublažiti korištenjem suvremenih FACTS naprava zasnovanih na energetskoj elektronici, koje posljednjih godina pored teorijskih razmatranja doživljavaju i svoje prve praktične primjene. Liberalizacija tržišta električnom energijom vjerojatno će utjecati na pojavu novih uvjeta i tokova snaga u prijenosnom sustavu. To je svakako dodatni razlog potrebe za suočavanjem s FACTS napravama.

U svrhu izbjegavanja stanja nestabilnog napona, rješenja koja uključuju korištenje FACTS naprava trebaju pružiti podršku naponu i/ili odgovarajuće koordinirano upravljačko djelovanje. Osim nekoliko većih prototipova statičkog generatora jalove snage kao poboljšane izvedbe statičkog kompenzatora jalove snage, ostale FACTS naprave do sada nisu razmatrane u rješavanju problema stabilnosti napona. Budući da su do sada najčešće razmatrani problemi vezani uz regulaciju toka snage i prigušenje elektromehaničkih oscilacija, izbjegavanje stanja nestabilnog napona svakako predstavlja novi poticaj.

Stoga su u okviru rada na ovoj disertaciji postavljeni slijedeći općeniti ciljevi:

- objasniti problem stabilnosti napona i mehanizam sloma napona u višestrojnom ees-u,
- razviti analitičke metode korisne pri rješavanju problema kako bi se ranije prepoznao nadolazeći slom napona korištenjem kombiniranog dinamičkog i statičkog pristupa, i
- razviti preventivne mjere i upravljačka djelovanja korištenjem odgovarajućih FACTS naprava (posebice objedinjenog regulatora toka snage, UPFC) u svrhu izbjegavanja problema i povećanja prijenosne moći.

Osnovna teza disertacije mogućnost je izbjegavanja problema stabilnosti napona korištenjem UPFC-a, suvremene FACTS naprave. U razradi postavljene teze koristi se računalna analiza stabilnosti elektroenergetskog sustava. U razmatranju dinamičkih pojava u uvjetima dužih prijelaznih perioda smanjene razine sigurnosti, koristi se vlastiti računalni FORTRAN program za simulaciju višestrojnog sustava u vremenskoj domeni. Kombiniranjem dinamičkog i statičkog aspekta analize, provodi se off-line simulacija stanja snižene sigurnosti napona korištenjem diferencijalno-algebarskog modela ees-a. Program je testiran i verificiran usporedbom s ostalim tržišno dobavljivim programima. U konačnici, program može biti primijenjen u dispečerskom centru u svrhu procjene sigurnosti napona sustava.

Razrada postavljene teze podijeljena je u nekoliko faza.

U prvoj fazi, različiti modeli generatora s generičkim upravljačkim sustavima uzbude i brzine vrtnje povezani su s proračunima tokova snaga. Uključeni su statički i dinamički tereti, asinkroni motori, LTC transformatori, prijenosni vodovi i čvorišta... Među metodama proračuna, uz proračune tokova snaga prema Gauss-Seidel i Jacobi metodama, nalazi se i brzi neulančeni proračun prijelaznih tokova snaga, metoda rada s rijetko popunjenim matricama i Runge-Kutta metoda 4. reda za rješavanje diferencijalne jednadžbe korištenjem konstantnog koraka integracije.

U drugoj fazi razrade, statički aspekti lineariziranog diferencijalno-algebarskog modela ees-a uključeni su u svrhu razmatranja svojstava matrice stanja i proširene Jacobi matrice. Statički aspekti su vrlo korisni u općoj analizi stabilnosti (dekompozicija po singularnim i vlastitim vrijednostima i vektorima, analiza osjetljivosti, faktori participacije…). Dekompozicija matrica od velike je pomoći u prepoznavanju problema stabilnosti napona. Nakon prepoznavanja, napori su usmjereni prema definiranju poželjnih svojstava i modeliranju suvremenih naprava za regulaciju napona i toka snage.

Stoga je u trećoj fazi razrade iniciran postupak modeliranja UPFC-a. Postavljen je nadomjesni model s injektiranim snagama i odgovarajući upravljački sustav. UPFC, u svom općem obliku, omogućava istodobno upravljanje sa svim osnovnim varijablama sustava (iznosom napona, impedancijom i faznim kutem) te dinamičku kompenzaciju izmjeničnog sustava.

Dok statički aspekti analize pomažu prepoznavanju problema stabilnosti napona putem dekompozicije matrica, UPFC, kao osnova disertacije, podržava napon i regulira tok snage. Definirane su potencijalne mogućnosti UPFC-a u rješavanju problema stabilnosti napona. Kombinirani dinamički i statički pristup koristi se u analizi upravljačkog sustava modela UPFC-a. Upravljački sustav omogućava poprečnu kompenzaciju jalove snage, regulaciju napona, regulaciju toka snage u vodu, serijsku kompenzaciju i PAR/QBT regulaciju kuta prijenosa uz istodobno zadovoljavanje višestrukih ciljeva upravljanja. Time je omogućena istodobna regulacija sa sva tri njegova glavna parametra; s poprečnom jalovom snagom Q_{conv1}, te iznosom r i kutem γ injektiranog serijskog napona.

Upravljački sustav UPFC-a neulančenog je oblika i tipa "jedan ulaz-jedan izlaz". Izbor ulaznih/izlaznih signala

ovisan je o vrsti upravljanja koju je moguće promijeniti tijekom simulacije. Na vanjskoj se razini upravlja sa slijedećim lokalno dostupnim varijablama UPFC-a:

- iznos napona čvorišta poprečne strane, V_i, (promjenom Q_{conv1}),
- iznos napona čvorišta serijske strane, V_j,
- tok jalove snage prema čvorištu serijske strane, Q_{j2},
- potrebita jalova snaga konvertera na serijskoj strani, Q_{conv2}, ili
- iznos napona kompenzacije, V_{comp}, (promjenom r), i
- tok djelatne snage prema čvorištu serijske strane, P_{j2},
- potrebita djelatna snaga konvertera na serijskoj strani, P_{conv2},
- razlika kuteva napona čvorišta poprečne i serijske strane, Θ_{ij}, ili
- kut napona kompenzacije, φ_{comp}, (promjenom γ).

Na poprečnoj strani modela upravljanje se izvodi samo u obliku regulacije iznosa napona $V_i \leftrightarrow Q_{conv1}$, pri čemu je potrebno naglasiti da je Q_{conv1} jalova snaga konvertera poprečne strane. Na serijskoj strani, upravljanje putem para varijabli $r \Leftrightarrow \gamma$ izvodi se na nekoliko različitih načina; iznos napona i tok djelatne snage $V_j \Leftrightarrow P_{j2}$, tok djelatne i jalove snage $Q_{j2} \Leftrightarrow P_{j2}$, serijska kompenzacija $Q_{conv2} \Leftrightarrow P_{conv2}(=0)$, fazni PAR zakret $V_j\ (=V_i) \Leftrightarrow \Theta_{ij}$, i fazni QBT zakret $V_{comp} \Leftrightarrow \varphi_{comp}(=\pi/2)$. Varijable su odabrane u skladu s uvjetima opće $V \leftrightarrow Q$ i $\Theta \leftrightarrow P$ neulančenosti. Prigušenje elektromehaničkog njihanja u modelu je zasnovano na funkciji prijelazne energije (TEF). Odabran je oblik potpunog preuzimanja regulacijskog sustava korištenjem derivacija po vremenu lokalnih varijabli s obje strane UPFC-a. Na poprečnoj strani koristi se derivacija dV_i/dt, a na serijskoj strani $d\Theta_{ij}/dt$.

Analiza osjetljivosti, primijenjena u općem obliku, doprinosi pronalaženju odgovarajuće lokacije i djelovanja UPFC-a. UPFC ima jedinstvenu mogućnost istodobne uzdužne regulacije toka snage kroz prijenosni element i poprečne regulacije napona u čvorištu. Statički pristup prema matričnim dekompozicijama rezultira s faktorima participacije uzdužnih i poprečnih prijenosnih elemenata (vodovi i čvorišta). Korištenjem sličnosti prepoznatih osobina UPFC-a i statičkog pristupa, uvelike se doprinosi postupku dimenzioniranja, lociranja i djelovanja UPFC-a u stanjima poremećenog napona. Budući da se regulacija napona s obje strane UPFC-a postiže korištenjem dva parametra, otvorena je mogućnost istodobnog korištenja i njegovog trećeg parametra.

Analiza osjetljivosti minimalne singularne vrijednosti, ukupnih gubitaka djelatne snage i ukupne proizvodnje jalove snage generatora u sustavu provodi se u svrhu prepoznavanja kritičnih točaka u tijekom scenarija sloma napona. Razmatraju se radi pronalaženja mogućnosti istodobnog korištenja sva tri regulacijska parametra UPFC-a. Osjetljivost često uključuje inverziju matrice stanja ili proširene Jacobijeve matrice te stoga poprima veće iznose u blizini kritične točke uz naglu promjenu predznaka nakon njezinog prolaska. Pojava kritične točke predstavlja pouzdan znak nadolazećeg stanja nestabilnog napona i poticaj je za uključivanje naponske podrške UPFC-a. Analizom osjetljivosti obzirom na skup UPFC-ovih upravljačkih parametara moguće je definirati odgovarajuće regulacijsko djelovanje.

U okviru disertacije, osobita je pozornost povećena modeliranju opterećenja obzirom na njihov doprinos scenariju sloma napona. Nakon početnog poremećaja koji za posljedicu ima trajno sniženje iznosa napona, oporavak tereta i ponovno uspostavljanje početne potrošnje mogu približiti generatore područja naduzbudnog ograničenja i/ili smanjiti prijenosnu moć sustava. Stoga je analiziran utjecaj nekoliko različitih modela tereta (statičkih i dinamičkih) obzirom na scenarij sloma napona. Osim statičkog ZIP modela, razmotreni su dinamički modeli asinkronog motora i termostatički upravljanog tereta čiji se naponi reguliraju transformatorom s promjenjivim prijenosnim omjerom pod opterećenjem. Analiziran je i nelinearni model prvog reda oporavljajućeg tereta. Osim obzirom na skup UPFC-ovih varijabli, statička analiza te analiza osjetljivosti primijenjene su i obzirom na karakteristične parametre tereta. Osjetljivost obzirom na njihove parametre od velike je pomoći u prepoznavanju onih tereta koji u najvećoj mjeri vode sustav prema slomu napona.

Iskoristivost predložene metodologije istražena je analizom na višestrojnom test-sustavu korištenjem vlastitog računalnog programa. Prema postavljenim ciljevima, moguće je istaknuti slijedeća glavna postignuća disertacije:

- razvoj diferencijalno-algebarskog modela višestrojnog sustava korisnog za provođenje simulacija u vremenskoj domeni kombiniranjem dinamičkog i statičkog aspekta analize, a u svrhu razmatranja dinamičkih pojava u uvjetima dužih prijelaznih perioda smanjene razine sigurnosti napona,
- razvoj nadomjesnog modela i upravljačkog sustava UPFC-a u svrhu definiranja uloge i regulacijskih svojstava, metodologije dimenzioniranja i određivanja lokacije i vremena djelovanja naprave uz istodobnu regulaciju sva tri upravljačka parametra obzirom na analizu problema stabilnosti napona,
- razvoj metodologije prepoznavanja kritičnih točaka pogona korištenjem matričnih dekompozicija i funkcija ees-a karakterističnih za nastanak i razvoj problema stabilnosti napona te proračuna njihovih osjetljivosti obzirom na parametre modela tereta i UPFC-a.

Mogućnosti nastavka istraživanja uvelike ovise o broju i vrsti praktičnih primjena FACTS naprava. Očekujući povećani broj njihovih instalacija, predložena analiza vrlo je značajna sa stajališta planiranju i pogona sustava. Prijelazom s manjeg test-sustava na neku od većih konfiguracija mreže postigli bi se vrlo praktični odgovori na stvarne probleme pogona. U tu bi svrhu predloženu metodologiju trebalo primijeniti u okviru rada dispečerskog centra na vođenju ees-a.

KLJUČNE RIJEČI: stabilnost napona elektroenergetskog sustava, modeliranje opterećenja, FACTS, UPFC, analiza osjetljivosti